e-ISSN: 2602-277X

International Journal of Chemistry and Technology

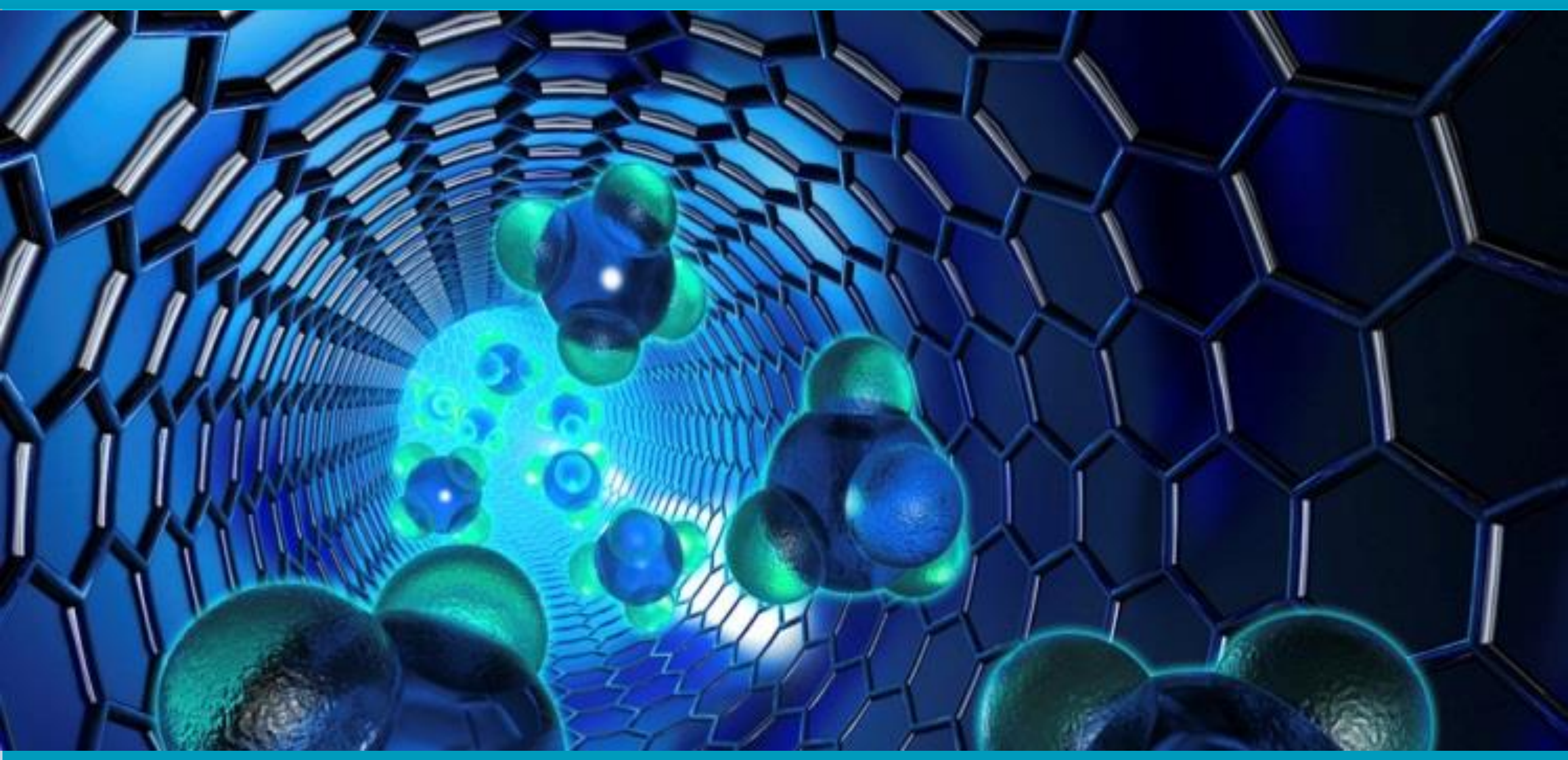

Volume: 6, Issue: 2 31 December 2022

E - Journal http://dergipark.org.tr/pub/ijct

e-ISSN: 2602-277X

International Journal of Chemistry and Technology

JOURNAL INFO

Journal Name	International Journal of Chemistry and Technology
Journal Initial	IJCT
Journal Abbreviation	Int. J. Chem. Technol.
ISSN (Online)	2602-277X
Year of Launching	2017, August
Editor-in-Chief and Managing Editor	Prof. Dr. İbrahim Demirtaş
Manager of Publication	Dr. Oğuzhan Koçer
Scope and Focus	Chemistry, Material Science, Technology
Review Type	Peer Review Double-Blinded
Ethical Rules	Plagiarism check, copyright agreement form, conflict of interest, ethics committee report
Access Type	Open Access
Publication Fee	Free
Article Language	English
Frequency of Publication	Biannualy
Publication Issue	June, December
Publisher	Prof. Dr. İbrahim DEMİRTAŞ
Web Page	http://dergipark.org.tr/pub/ijct
Contact E-mail address	ijctsubmission@gmail.com, ijctsubmission@yahoo.com
Contact Address and Executive address	Kilis 7 Aralik University, Faculty of Science and Arts, Department of Chemistry, 79000, Kilis
Contact Telephone	90 5535983054 (Editor-in-Chief), 90 530 3645222 (Manager of Publication), 90 532 233 17 38 (Secretary)
Publication Date	28/12/2018
Technical Editor	Assist. Prof. Dr. Evrim BARAN AYDIN
Spelling Editor	Dr. Oğuzhan Koçer, MSc. Rabia Acemioğlu
Language (Grammar) Editor	Assist. Prof. Dr. Muhammet KARAMAN, Assist. Prof. Dr. Muhittin KULAK, Dr. Lawali YABO DAMBAGI
Secretary	Dr. Oğuzhan KOÇER, MSc. Rabia ACEMIOĞLU

All detailed information including instructions for authors, aim and scopes, ethical rules, manuscript evaluation, indexing info, and manuscript template etc. can be found on the main web page of IJCT (http://dergipark.gov.tr/ijct).

e-ISSN: 2602-277X

International Journal of Chemistry and Technology

Volume: 6, Issue: 2, 31 December 2022

e-ISSN: 2602-277X

International Journal of Chemistry and Technology

Advisory Editorial Board

e-ISSN: 2602-277X

International Journal of Chemistry and Technology

Advisory Editorial Board

International Journal of Chemistry and Technology

Issue Reviewers

Order	Reviewer	Article	E-mail	Institution	Additional Subjects	Subjects
1	Adile AKPINAR	Contributions to the fauna of Türkiye Geometridae	aozdemir@gantep.edu.tr	gaziantep üniversitesi		Mathematics and Science, Biology
2	Ahmet İYİGÖR	Structural transition of LiBeH3 under high pressure	ahmetiyigor@ahievran.edu.tr	Kırşehir Ahi Evran University		Condensed Matter Physics, Material Physics, Physics
3	Anton FİCAİ	Polymer – flufenamic acid delivery systems for injured skin	anton_ficai81@yahoo.com			
4	Ayşegül İYİDOĞAN	The investigation of the effect of chalcones with benzoic acid on xanthine oxidase activity	aysgliyidogan@gmail.com			
5	Cihan KÜRKÇÜ	Structural transition of LiBeH3 under high pressure	ckurkcu@ahievran.edu.tr			Physics
6	Falah Saleh MOHAMMED	Some pharmacological properties of Alyssum stylare (Boiss. & Balansa) Boiss	falah.sindy@uoz.edu.krd	Zahko University		Biology
7	Haşim BAĞCI	An overlook on the relationship between green finance and the environment	hasimbagci1907@hotmail.com	AKSARAY ÜNİVERSİTESİ, SAĞLIK BİLİMLERİ FAKÜLTESİ, SAĞLIK YÖNETİMİ BÖLÜMÜ		Investment and Portfolio Management, Finance, Banking, Behavioural Finance, Financial Markets and Institutions, Financial Risk Management, Financial Forecast and Modelling, Gayrimenkul Değerleme ve Finansmanı, Finance of Islam, International Finance
8	Jale GÜLEN	Effect of phosphogypsum use as a waste recycling on GHG emissions by mineral carbonisation method	gulenj@yildiz.edu.tr			Environmental and Sustainable Processes
9	Mahfuz ELMASTAŞ	The comparison of chemical content and bioactive capacity of domestic and import Hypericum perforatum aqueous extracts	mahfuzelm@gmail.com	SAĞLIK BİLİMLERİ ÜNİVERSİTESİ, ECZACILIK FAKÜLTESİ		Medical Biochemistry
10	Mehmet SÖNMEZ	Structural characterization and DNA binding properties of a phenanthrene based Schiff base compound	msonmez@gantep.edu.tr	GAZİANTEP ÜNİVERSİTESİ		Inorganic Chemistry
11	Mehmet ÖTEN	Effect of Different Salt Concentrations on Germination of Forage Pea	mehmetoten@subu.edu.tr	Sakarya Uygulamalı Bilimler Üniversitesi		Tarla Bitkileri Yetiştirme ve Islahı
12	Muhammet KARAMAN	Attachment of Idarubicin to Glutaraldehyde-coated Magnetic Nanoparticle and Investigation of its Effect in HL-60 Cell Line	mhmmtkaraman@gmail.com	KILIS 7 ARALIK UNIVERSITY		Biochemistry, Molecular Biology
13	Mustafa SEVİNDİK	Some pharmacological properties of Alyssum stylare (Boiss. & Balansa) Boiss	sevindik27@gmail.com	OSMANIYE KORKUT ATA UNIVERSITY		Mathematics and Science
14	Mustafa SEVİNDİK	Contributions to the fauna of Türkiye Geometridae	mustafasevindik@osmaniye.edu.tr	OSMANIYE KORKUT ATA UNIVERSITY		Biology

Order	Reviewer	Article	E-mail	Institution	Additional Subjects	Subjects
15	Nafiz ÇELİKTAŞ	Polymer – flufenamic acid delivery systems for injured skin	nafizcel@hotmail.com			
16	Nalan ÖZDEMİR	Attachment of Idarubicin to Glutaraldehyde-coated Magnetic Nanoparticle and Investigation of its Effect in HL-60 Cell Line	ozdemirn@erciyes.edu.tr	ERCİYES ÜNİVERSİTESİ, FEN FAKÜLTESİ		Biochemistry
17	Ramazan ERENLER	The comparison of chemical content and bioactive capacity of domestic and import Hypericum perforatum aqueous extracts	rerenler@gmail.com	Gaziosmanpasa University		Chemistry
18	Recep ÖZEN	Effect of phosphogypsum use as a waste recycling on GHG emissions by mineral carbonisation method	rozen@mersin.edu.tr			Chemistry
19	Rizvan İMAMOĞLU	A new approach to breast cancer therapy: targeted nanocarrier systems	rimamoglu@bartin.edu.tr	BARTIN ÜNİVERSİTESİ		Mathematics and Science
20	Salih ÖKTEN	Cytotoxic, apoptotic, and necrotic effects of silver nanoparticles biosynthesized using Origanum majorana extract	sokten@gmail.com	Kırıkkale Üniversitesi		Pharmaceutical Chemistry, Chemistry Education, Chemistry, Organic Chemistry, Pharmacy, Medicinal Chemistry
21	Sema BİLGİN	A new approach to breast cancer therapy: targeted nanocarrier systems	sema.bilgin@gop.edu.tr	TOKAT GAZİOSMANPAŞA ÜNİVERSİTESİ		Biochemistry
22	Sultan ERKAN	Structural characterization and DNA binding properties of a phenanthrene based Schiff base compound	sultanerkan58@gmail.com	Chemistry and Chemical Processing Technology, Yıldızeli Vocational High School, Cumhuriyet University, Sivas/TURKEY		Chemistry
23	Tevfik OZEN	Cytotoxic, apoptotic, and necrotic effects of silver nanoparticles biosynthesized using Origanum majorana extract	tevfikoz@omu.edu.tr	ONDOKUZ MAYIS ÜNİVERSİTESİ		Biochemistry
24	Yavuz ERDEN	Nutritive value, antimicrobial and antioxidant activities of tchihatchewia isatidea boiss	yerden@bartin.edu.tr	Bartın University		Cell Biology, Biology, Molecular Biology, Physiology
25	Yusuf SICAK	The investigation of the effect of chalcones with benzoic acid on xanthine oxidase activity	yusufsicak@mu.edu.tr	Mugla Sıtkı Kocman University		Chemistry
26	Yusuf TEPELİ	An overlook on the relationship between green finance and the environment	yusuftepeli@mu.edu.tr	MUĞLA SITKI KOÇMAN ÜNİVERSİTESİ, İKTİSADİ VE İDARİ BİLİMLER FAKÜLTESİ		Financial Accounting, Financial Statement Analysis, Financial Risk Management
27	İbrahim ERTEKİN	Effect of Different Salt Concentrations on Germination of Forage Pea	ibrahim.ertkn@hotmail.com	Hatay Mustafa Kemal Üniversitesi Ziraat Fakültesi Tarla Bitkileri Bölümü		Agriculture Science, Pasture-Meadow Forage Plants
28	Şemsettin CİVELEK	Nutritive value, antimicrobial and antioxidant activities of tchihatchewia isatidea boiss	scivelek@firat.edu.tr	Fırat Üniversitesi, Fen Fakültesi, Biyoloji Bölümü		Plant Morphology and Anatomy, Plant Systematics, Biology

TABLE OF CONTENTS

DOI: http://dx.doi.org/10.32571/ijct.1139627 **E-ISSN: 2602-277X**

International Journal of Chemistry and Technology

http://dergipark.org.tr/ijct

Research Article

A new approach to breast cancer therapy: targeted nanocarrier systems

Nazan GÖKŞEN TOSUN[1,*], Özlem KAPLAN[2], Seçil ERDEN TAYLAN[3], Cemil ALKAN[4], İsa GÖKÇE[5]

[1] *Department of Biomaterial and Tissue Engineering, Faculty of Engineering and Architecture, Tokat Gaziosmanpaşa University, Tokat, Türkiye*

[2] *Department of Molecular Biology and Genetic, Faculty of Science, Istanbul University, İstanbul, Türkiye*

[3] *Department of Pharmaceutical Biotechnology, Faculty of Pharmacy, Tokat Gaziosmanpaşa University, Tokat, Türkiye*

[4] *Department of Chemistry, Faculty of Science and Literature, Tokat Gaziosmanpaşa University, Tokat, Türkiye*

[5] *Department of Biochemistry, Faculty of Pharmacy, Tokat Gaziosmanpaşa University, Tokat, Türkiye*

Received: 2 July 2022; Revised: 3 July 2022; Accepted: 18 July 2022

*Corresponding author e-mail: nazan_goksen@hotmail.com

Citation: Gökşen, Tosun, N.; Kaplan, Ö.; Erden, Taylan, S.; Alkan, C.; Gökçe, İ. *Int. J. Chem. Technol.* **2022**, 6 (2), 81-92.

ABSTRACT

Cancer is one of the most prevalent diseases in the world. Breast cancer is the second most deadly cancer type after lung cancer. Surgical intervention, chemotherapy, and radiotherapy are the most used conventional methods in the treatment of breast cancer. The non-targeted approach of conventional treatments causes serious side effects in healthy cells and tissues, and often mortality is due to the side effects of these conventional treatments. In recent years, nano-sized particles called drug delivery systems targeting cancer cells have attracted attention as a new approach to cancer treatment. The fact that these nanocarrier systems target tumor cells without damaging healthy tissues has been a hope for breast cancer. Moreover, nanocarriers are unique biomaterials that may exhibit low toxicity, high biocompatibility, biodegradability, ease of use, high dose drug loading, and adjustable surface functionalities. In the present study, we summarize recent studies of nanocarriers that offer a critical review of an alternative strategy to breast cancer therapy.

Keywords: Drug delivery systems, breast cancer, nanocarriers, nanoparticles.

Meme kanseri tedavisinde yeni bir yaklaşım: hedefe özgü nanotaşıyıcı sistemler

ÖZ

Kanser, dünyadaki en yaygın hastalıklardan biridir. Meme kanseri, akciğer kanserinden sonra ikinci en ölümcül kanser türüdür. Cerrahi müdahale, kemoterapi ve radyoterapi meme kanseri tedavisinde en çok kullanılan geleneksel yöntemlerdir. Konvansiyonel tedavilerin hedefe yönelik olmayan yaklaşımı, sağlıklı hücrelerde ve dokularda ciddi yan etkilere neden olur ve mortalite genellikle bu geleneksel tedavilerin yan etkilerinden dolayı gerçekleşmektedir. Son yıllarda kanser hücrelerini hedef alan ilaç taşıyıcı sistemler adı verilen nano boyutlu partiküller kanser tedavisinde yeni bir yaklaşım olarak dikkatleri üzerine çekmektedir. Bu nanotaşıyıcı sistemlerin sağlıklı dokulara zarar vermeden tümör hücrelerini hedef alması meme kanseri tedavisi için umut verici bir yaklaşımdır. Ayrıca nanotaşıyıcılar, düşük toksisite, yüksek biyouyumluluk, biyobozunurluk, kullanım kolaylığı, yüksek doz ilaç yükleme ve ayarlanabilir yüzey işlevleri gösterebilen benzersiz biyomalzemelerdir. Bu çalışmada, meme kanseri tedavisine alternatif bir yaklaşım sunan nanotaşıyıcıların son çalışmalarını eleştirel bir analizle özetledik.

Anahtar Kelimeler: İlaç taşıyıcı sistemler, meme kanseri, nanotaşıyıcılar, nanopartiküller.

DOI: http://dx.doi.org/10.32571/ijct.1139627 E-ISSN: 2602-277X

1. INTRODUCTION

Cancer is a complicated disease resulting from the uncontrolled division and proliferation of malignant cells under the influence of genetic and environmental factors, potentially spreading to or invading various parts of the body. The World Health Organization estimates 18 million new cancer cases worldwide in 2018, and 10 million cancer deaths are expected. It is estimated that the number of new cases will be 29-37 million, nearly double the global burden for 2040.

Lung cancer is the most diagnosed cancer type (11.6%) and has the highest mortality rate, followed by breast cancer (11.6%), mostly seen in women, followed by colorectal cancer (10%). Relative to both sexes, the incidence of breast cancer, the second most common cancer, is only 1% in men (Figure 1). The survival rate of breast cancer, which has a higher incidence in women, depends on early diagnosis, and it is estimated that this rate will be 5 years after the diagnosis in advanced breast cancer cases, in the light of research.[1]

Age, gender, hormone therapy[2], environmental conditions, hereditary variables, and consuming habits[3–5] are all risk factors for the development and spread of breast cancer. Breast cancer incidence increases with age, it is less common in developed than in developing countries,[5] and the risk are higher in people who consume alcohol[6] and cigarettes, considering their consumption habits. Some studies reveal a link between hormone therapy and an increased risk of breast cancer. Therefore, hormone therapy has a higher possibility of having breast cancer. Statistical data show that the survival rate is still below 25 percent in the last 5 years of breast cancer treatment.[4,7]

Surgical intervention, chemotherapy, and radiotherapy, the so-called conventional methods of treatment, or a combination of these methods have been preferred for many years in the treatment of breast cancer. Surgical resection, i.e., removal of the entire breast to remove the tumor, is stressful for the patient both physically (due to the loss of the existing organ or tissue) and psychologically and aesthetically. Chemotherapeutic agents used in conventional chemotherapy cause controlled death of rapidly growing and proliferating cancer cells through different pathway mechanisms, including the destruction of the cell membrane, damage to cell integrity, inhibition of DNA synthesis, and impairment of mitosis.[8] The main disadvantage of the agents used in chemotherapy is that they have toxic effects on healthy cells and tissues due to their non-selectivity. They can also cause unexpected and undesirable negative side effects such as nausea and loss of appetite.[9] Serious side effects of chemotherapeutic drugs on healthy tissues and organs increase the death rate in cancer. Because of the low absorption of these medications at the tumor site, greater doses are required, resulting in increased toxicity and multidrug resistance in normal healthy tissues and cells. As a result, it is preferable to create chemotherapeutic drugs that target cancer cells to minimize adverse side effects.[9]

Over the past two decades, work in nanotechnology has profoundly impacted clinical therapeutics in general. Nanoscale drug delivery systems have the potential to solve some of these issues by reducing toxicity in normal cells and increasing therapeutic efficacy due to features such as active cellular uptake, increased permeability, and retention effect.[10] Cancer chemoresistance is a phenomenon that occurs when cancer cells that were originally inhibited by an anticancer agent develop resistance to that drug after some time. Therefore, there is a need for new, more targeted drugs to prevent cancer development, suppress side effects, and relieve pain caused by chemotherapy.[11]

Nanocarriers (NCs) or drug carriers are currently being prepared from organic and inorganic compounds, proteins, lipids, and synthetic polymers for the improvement of cancer therapeutics. When compared to direct delivery of chemotherapeutic drugs, medication encapsulation in a carrier has various advantages, such as circulatory disruption protection, improved drug solubility, increased drug stability, targeted drug delivery, and reduced toxic side effects.[12] Liposomes, mesoporous silica NCs, viral NCs, polymer-, metal-, or carbon-based NCs have been explored in breast cancer therapy to date.[13,14] Various techniques such as encapsulation, covalent or electrostatic bonding, and adsorption are used to load drugs into NCs, again depending on the NCs.[15] NCs enable easy transport of poorly soluble, hydrophobic drugs in the blood and make cancer therapeutics biocompatible.[16] At the same time, they are nanoscale particles that enable slow release of the drug, target cancer cells, increase permeability, and are nontoxic and biodegradable.[17]

In in vitro breast cancer studies, many targeted NC systems were investigated using breast cancer cell lines with different characteristics.[18] At the same time, doxorubicin (Dox), which is highly chosen in the treatment of many cancers, has been widely used as a reference agent and therapeutic agent in drug delivery systems. The other chemotherapeutics (trastuzumab, cisplatin, paclitaxel (PTX), carboplatin, anastrozole, fulvestrant, etc.) have been studied in phase 2 phase 3 clinical trials. In addition, combination studies have investigated the synergistic effects of these chemotherapeutic agents against breast cancer when used together.[19–23]

Concentrations of drugs used in the treatment of breast cancer without the use of a drug delivery system require pharmacologically higher doses than concentrations of

DOI: http://dx.doi.org/10.32571/ijct.1139627 E-ISSN: 2602-277X

drugs loaded into targeted drug delivery systems. The usage of targeted drug carriers could greatly reduce the side effects and serious damages caused by non-targeted chemotherapeutic drugs in healthy cells and tissues. Therefore, combination therapy and NCs have the potential to reduce damage to healthy tissue and cells. NCs are also important in combination therapies, where different drugs are used together, or in treatments that use oligonucleotides, as they respond to the need to transport drugs to the target without degradation.[24]

2. BIOMARKERS

A biomarker is a valuable tool for disease diagnosis and treatment in the clinic. Cancer cells are targeted by utilizing molecular recognition markers in breast cancer treatment. The use of biomarkers to target drug delivery can increase the target specificity of therapies for cancer cells by reducing toxicity to healthy cells. Moreover, several biomarkers have been linked to the beginning and progression of BC. Progesterone receptor (PR), estrogen receptor (ER), and human epidermal growth factor receptor (HER2/ERBB2) are the most common BC biomarkers. While ER overexpression is found in most breast tumors, HER2 overexpression is found in about a quarter of them.[25] Triple-negative breast cancer (TNBC) is a tumor that does not express ER, PR, or HER2.[26,27] As a result, these biomarkers have been used in the classification of BC and the development of novel treatments based on target ligands.

2.1. HER 2

HER2 is a transmembrane glycogen protein with three distinct regions. HER1, HER2, HER3, and HER4 are the four proteins that constitute the HER family. HER2 is the only receptor without a known ligand, yet it aids cell proliferation by dimerizing with three other members of the family.[28] N-terminal extracellular domain, which is separated into subdomains, makes up the majority of HER2 (I-IV). Homo-dimerization and heterodimerization are controlled by cysteine-rich subdomains II and IV.[28] Subdomain II's dimerization arm emits dimerization. Pertuzumab and trastuzumab, both monoclonal antibodies, have been found as dimerization inhibitors. They attach to HER2's dimerization arm and inhibit signaling, preventing dimerization with other family members, which slows cell proliferation.[29]

2.2. ER

ERs can be found both intracellularly and in the membrane of BC cells. Most breast tumors are ER+, and ER+ type BC can affect both premenopausal and postmenopausal women. For ER+ breast cancers, tamoxifen is the most prescribed antagonist. Tamoxifen does not directly target adipose tissues, so targeted drug release of NPs is critical.[30] Dreaden et al. revealed the delivery of tamoxifen-conjugated NPs to ERs.[31] The nanoparticles increased the efficacy of tamoxifen 2.7 times compared to the free drug. Li and colleagues demonstrated a polymer-based NP-based tamoxifen delivery system into ER+ BC cells with dramatically lower cytotoxicity than healthy cells.[32]

2.3. PR

PR is a steroid hormone receptor that mediates progesterone. PR plays a role in lobuloalveolar differentiation.[33] They are used in clinical practice to identify patients with invasive BC who may benefit from various types of endocrine therapy. It is employed as a predictor for all therapy phases, including adjuvant and neoadjuvant.[34]

2.4. TNBC

Targeted drug delivery is more difficult because 15% of breast cancers lack ER, PR, or HER2. 2. Although basal type cancers account for 85 percent of TNBC, not all basal type tumors are triple-negative. TNBC-like tumors with no ER, PR, or HER2 expression are known as basal-type cancers.[35] However, specific protein alterations may occur in basal-type cancers not seen in TNBC. Many solid tumors, including breast cancer, express folic acid, transferrin, arginylglycylase particulate acid (RGD), and epidermal growth factor receptors (EGFR). Wu et al. devised a drug delivery system mediated by RGD ligand-conjugated NPs that exhibited better cellular absorption in MDA-MB-231 cells than the untargeted system.[36] Furthermore, treating TNBC with a combination of therapeutic drugs at the same time has been demonstrated to be more effective. Both in vitro and in vivo, the approach has shown effectiveness in suppressing cell growth.[37,38]

3. TARGETING LIGANDS FOR BREAST CANCER THERAPY

For active targeting of breast cancer cells, various approaches and techniques are currently available monoclonal antibodies were previously used to target cell surface epitopes. The number of possible ligands for targeted BC therapy has significantly increased due to additional research and comprehensive screening of peptide and aptamer archives.[39] Antibodies, peptides, aptamers, oligosaccharides, and small molecules are among the ligands now in use.[40–43] This new targeting strategy includes a form of chemical recognition that triggers the binding of ligand receptors. The NPs can be selectively fixed to the tumor cell's surface thanks to this conjugation.

Previous research has also demonstrated this potential binding and the efficacy of these NPs in vitro and in vivo.[44–46] For example, when NPs connect to a targeted

DOI: http://dx.doi.org/10.32571/ijct.1139627 E-ISSN: 2602-277X

ligand, they often internalize more quickly and undergo receptor-mediated endocytosis.[47,48] The binding affinity of the ligand is raised because of definite conjugation, resulting in more effective receptor-mediated endocytosis. Monoclonal antibodies conjugated with complete NP families like superparamagnetic iron oxide nanoparticles[49] quantum dots,[50] and liposomes[51] have been used in numerous investigations to contribute to BC-specific targeting.

Monoclonal antibodies regulate redundant parts of single-chain variable segments via bioengineering, lowering size and immunogenicity compared to the original antibody. This modified T cell with a chimeric antigen receptor is a promising approach applied to the therapy of various malignancies, such as B-cell leukemia and lymphoma[52] Aptamers and peptides are two more notable ligands, both of which are characterized by practical targeting approaches[53,54].

4. NANOCARRIERS SYSTEMS in BREAST CANCER

Nanoparticles (NPs) are small particles with sizes between 1-100 nm. Although NPs in drug delivery systems are not yet widely employed in clinical treatments, various research studies are underway to explore the potential benefits of NPs in drug delivery systems for cancer treatment. Because of their biocompatibility, water dispersion, and biodegradability, NPs have become popular as nanocarriers. The use of nanoparticles in cancer therapy increases drug solubility and half-life, boosting the bioavailability of many chemotherapy medicines.[55] Furthermore, through improved permeability and retention (EPR), NPs might increase medication accumulation in cancer tissues.[56] Furthermore, by targeting particular cancer sites with target ligands and decreasing side effects, the NPs-anti-cancer drug combination can improve therapeutic efficacy.[57,58] NPs are employed in the BC targeted drug delivery system in various ways. Polymer, liposomal, carbon, metal, protein-based, and mesoporous silica NPs are some of the available NPs (Figure 2).

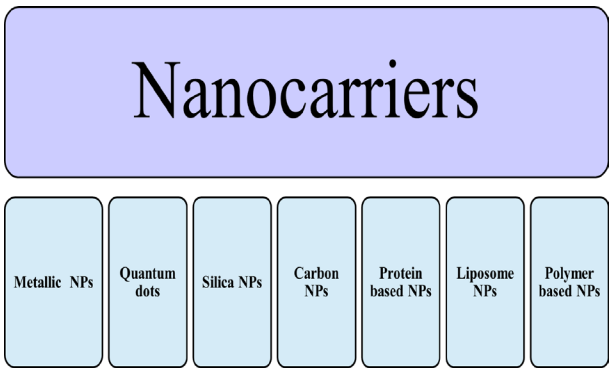

Figure 2. Types of nanocarriers for treatments of breast cancer

4.1. Metallic Nanoparticles

Researchers are interested in metal or metal oxide-based nanoparticles because of their potential applications in cancer diagnostics and treatment.[59] Photodynamic therapy (PDT), photothermal therapy (PTT), immunotherapy, and chemotherapy are cancer treatment techniques that use metallic nanoparticles.[60] Because of their magnetic, optical, thermal, and electrical capabilities, metallic nanoparticles have many applications in cancer therapy and detection. Metallic nanoparticles (NPs), including Au, Ag, Pt, Zn, and TiO, show promise for anticancer treatments and diagnostics. Magnetic nanoparticles (MNPs), such as gold nanoparticles (AuNPs) and Fe_3O_4, show promise in anticancer therapy and diagnostic imaging of breast cancers.[61,62]

Several metal-based nanoparticles use chemical processes to induce intracellular ROS production, oxidative stress, and tumor cell apoptosis.[63] Silver nanoparticles (AgNPs) have anti-proliferative, pro-apoptotic, and anti-angiogenic action on cancer cells.[64] ZnO nanoparticles can modify the micronucleus within tumor cells, speeding mitotic and interphase apoptotic cell death, acting as genotoxic medicines for anticancer therapy.[65] Nanoparticles of CuO, Fe_2O_3, silica, CeO_2, and TiO2 have been studied in the diagnosis and therapy of BC.[66] Through a DNA-damage mechanism, CeO_2 nanoparticles induce apoptotic cell death and oxidative stress.[67]

The remarkable properties of gold nanoparticles make them worthy of investigation. These nanoparticles' size, shape, and surface activity can be easily adjusted to improve circulation time, targeting ability, biocompatibility, and tumor cell attraction.[68] To enable active targeting, gold nanoparticles are typically coated with organic compounds.[69] In various investigations, gold nanoparticles targeting EGFR were found to inhibit breast cancer cells. Surface conjugation considerably stabilizes gold nanoparticles compared to unconjugated nanoparticles.

Kardani et al. prepared gold nanoparticles loaded with anti-miR-155 and examined their activity on the MCF-7 cell line. To facilitate tumor-targeted dispersion, the nanoparticles were modified with the AS1411 aptamer, which binds to the nucleus of cancer cells. Zhao et al. used positron emission tomography (PET) to detect primary cancer cells and lung metastases in a mouse with breast cancer.[70] The primary disadvantage of employing gold nanoparticles is their low biodegradability.

The magnetic core of magnetic iron oxide nanoparticles is maghemite (Fe_2O_3) or magnetite (Fe_3O_4). Maghemite, rather than magnetite, is recommended as the core material for magnetic nanoparticles because the Fe (III)

DOI: http://dx.doi.org/10.32571/ijct.1139627 E-ISSN: 2602-277X

released from maghemite is less hazardous than the Fe (II) emitted from magnetite.[71] Due to the hydrophobicity of these nanoparticles, direct use causes them to aggregate in the plasma. Coating the magnetic core with a hydrophilic material can help overcome this disadvantage. PEG, polysaccharides, PLA, and dextran are biopolymers that can be employed as coating materials.[72,73] Hyperthermia is a treatment method in which heat reduces tumor growth. Because tumor cells are heat sensitive, magnetic hyperthermia employing superparamagnetic iron oxide nanoparticles (SPIONS) can reduce tumor size.[74]

To increase the stability of iron oxide nanoparticles, PEG is often coated on them. Furthermore, functional groups on the surface of PEG-coated nanoparticles facilitate ligand conjugation. The drug can be loaded by sticking to the surface or sealing it within the core. There are various studies in the literature on nanoparticles of iron oxide for targeted treatment. Jeon et al. produced paclitaxel-loaded SPIONs and coated the nanoparticles' surfaces with folic acid (FA). FA conjugation increased nanoparticle absorption by tumor cells.[75] Methotrexate-conjugated arginine functionalized magnetic nanoparticles and their targeting abilities were investigated by Attari et al. These nanoparticles effectively delivered the drug to the tumor site.[76] Soleimani et al. produced a folate-conjugated iron oxide nanoparticle technology and examined its targetability.[77]

4.2. Quantum Dots

Quantum dots (QDs) are semiconductors that are widely used in cancer imaging and range in size from 2 to 10 nm[78]. They are very promising for cancer imaging due to their high surface/volume ratio, resistance to photobleaching, high brightness, and tunable optics. PEGylation is commonly performed on QDs to increase water solubility and reduce RES formation.[79] QDs emitting multiple wavelengths have been studied in breast cancer. This study combined QDs with complementary antibodies to detect quantitative biomarkers such as EGFR, ER, HER2, and PR.[80] QDs have two significant disadvantages; the first is that they contain heavy metals that are hazardous to our bodies in their inner core. The second is the hydrophobicity of metallic QDs and their difficulties in using them in vivo. Researchers have recently turned to studies on carbon-based QDs in cancer therapy. It was shown that carbon QDs synthesized by conjugating quinic acid as a targeting agent and loading it with Gemcitabine charge have good light properties and can be used as theranostic agents.[81] Graphene quantum dots (GQDs) are used in photodynamic therapy (PDT). PDT is a non-invasive procedure that irradiates GQDs to inhibit tumor growth. Because conventional PDT drugs are bombarded with UV-Visible light, their use in deeper tissue malignancies is limited. Furthermore, GQDs are more efficient PDT agents because they can be irradiated at longer wavelengths.[82]

4.3. Silica Nanoparticles

Mesoporous silica nanoparticles have a porous surface and high drug loading capacity. Furthermore, researchers have chosen it for therapeutically targeted distribution due to its easily replaceable surface, the potential for pore size modification, and vast surface.[83] Tsai et al. discovered that anti-HER2 monoclonal antibodies linked to silica nanoparticles could be used to effectively target breast cancer cells. To target HER2-positive breast cancer cells, they coupled mesoporous silica nanoparticles with Herceptin. Nanoparticles with a high concentration of Herceptin were highly effective at targeting BT-474 cell lines. Internalization of Herceptin-conjugated nanoparticles in BT-474 cells has been demonstrated.[84] Meng et al. developed silica nanoparticles containing doxorubicin and siRNA coupled with PEI and PEG on their surface. According to the findings, there was improved permeability at the tumor location and decreased nanoparticle aggregation in the RES. It has also been discovered that a lower dosage of doxorubicin can be supplied using this nanoparticulate method, which helps to minimize doxorubicin's cardiovascular toxicity.[85] When it comes to toxicity and biocompatibility, mesoporous silica nanoparticles outperform metallic nanoparticles. However, their inability to penetrate the tumor mass is a significant disadvantage. In vitro targeting of mesoporous nanoparticles conjugated with Herceptin was investigated by Milgroom et al. As a result, researchers discovered that silica nanoparticles are biocompatible, stable, and excellent drug carriers. It has also been demonstrated that antibody-conjugated silica nanoparticles can stay in the bloodstream for an extended period, overcoming half-life difficulties.[86]

Fortuni et al. revealed doxorubicin-loaded mesoporous nanoparticles and coupled them with HA. The data indicated increased anti-tumor efficacy and anticancer cell selectivity.[87] In another study, PEG- and chitosan-functionalized mesoporous silica nanoparticles were employed to transport doxorubicin to the MCF-7 cell line. These nanoparticles revealed increased medicine effectiveness as well as drug loading and release capacities.[88]

4.4. Carbon Nanoparticles

Carbon nanoparticles such as fullerenes, nanotubes, and graphene are extensively employed in cancer therapy. Carbon nanoparticle features such as shape, size, structure, surface charge, aggregation, and chemical composition can influence how they interact with cells and biomolecules.[89] These nanoparticles were supposed to be superior to metal-based nanoparticles in terms of

DOI: http://dx.doi.org/10.32571/ijct.1139627 E-ISSN: 2602-277X

focused and regulated medication administration. Carbon nanotubes are long, hollow, cylindrical structures made of graphene sheet walls. Based on the number of graphene sheet coverings, the fullerene allotropes are classed as single-walled or multi-walled nanotubes. It is remarkable due to its chemical stability, tunable surfaces, and unique thermal and electrical properties.[90] HER2 immunoglobulin 'Y' conjugated nanotubes were used to identify and destroy tumors in an in vivo model of HER2-expressing breast cancer cells.[91] Drug loading into nanotubes can be accomplished in filament loading and direct surface loading.[92] Nanotubes have a lower drug loading capacity, but it has been discovered that employing copolymers on the surface can improve the loading capacity of tiny hydrophobic medicines.[93] However, for bulky pharmaceuticals, only a limited amount of space is accessible on the surface of the polymers, restricting drug loading and subsequent ligand conjugation.[94] Paclitaxel was combined with docosanol and then conjugated to the surface of nanotubes by Shao et al. In addition, in the same study, folic acid was conjugated to the surface of nanotubes to target breast cancer tissue and increase treatment efficacy.[95] Carbon-based nanoparticles can be used effectively in the targeted release of drugs in cancer.[96] Docetaxel-loaded fullerene was found to have 4.2-fold higher bioavailability than free drug and enhanced cytotoxicity in breast cancer cells.[97]

Carbon nanoparticles have recently been studied for their potential usefulness in photodynamic treatment. Carbon nanoparticles can aggregate late at the tumor site and absorb infrared radiation, generating heat and cytotoxicity.[96] Carbon nanoparticles are substantially less soluble in aqueous media, causing agglomeration in biological fluids, and they are highly resistant to enzymatic oxidation because they are not removed from the body.[98]

4.5. Protein-Based NPs

Protein-based NPs are a group of viral NPs that resemble viruses' protein envelopes or capsids. In the absence of the virus genome, these viral NPs are not contagious. In the production of viral NPs, plant tissues can be used, and recombinant proteins produced in plants can then be commercially increased to appropriate production levels.[99] The surface of viral NPs is suitable for drug conjugation and is emerging as a highly favorable method for targeted drug delivery. For example, trastuzumab is carried by viral NPs as a targeted therapy in patients with HER2+ cancer. Esfandiari et al. potato virus X (PVX) has been identified and reported to cause increased mortality of BC cells. Esfandiari et al. achieved selective targeting of BC by combining PVX with the trastuzumab monoclonal antibody that can suppress proliferation and signal transduction of BC cells.[100] Le et al. revealed that PVX-Dox treatment of MDA-MB-231 BC xenografts in athymic mice resulted in reduced tumor growth.[101] In a murine BC model, glycophosphatidylinositol and HER2 antigen conjugated to influenza virus NPs and HER2-expressing inhibited tumor growth.[102] Viral NPs are evolving, and viral NPs are predicted to play an important clinical role very soon.

4.6. Liposome-Based NPs

Liposomal NPs (LNPs) are spherical vesicles that contain one or more phospholipid bilayers and can reach diameters of several hundred nanometers. LNPs consist of a hydrophilic inner core and a hydrophobic layer covering that. The unique morphology of LNPs makes them important for the delivery of hydrophobic medicine. LNPs are one of the most favored drug carrier systems that allow hydrophobic agents to be encapsulated in the outer layer while simultaneously encapsulating hydrophilic agents in the inner core. In this way, they also reduce the side effects of drugs that are not targeted in the body. Encapsulation of a drug can greatly reduce its toxicity, as it greatly inhibits its release until it reaches the target. Several studies have shown that some chemotherapeutic drugs, such as DOX and Vincristine[103], were encapsulated in the inner core of LNPs, reducing their cardio cytotoxicity [104]. The efficacy of the PTX agent encapsulated with LNPs and the efficacy of these encapsulated forms on breast cancer cell lines were studied by Marcial et al.[105]

LNPs tend to infiltrate and accumulate in the bilayer of the tumor cell membrane. Pegylation of LNPs renders them with longer half-lives and higher target activity.[106] As carrier systems in passive targeting, pegylated LNPs have shown effective targeting both in vitro and in vivo. Wong and Chiu encapsulated vincristine and quercetin into the pegylated liposome. It showed prolonged plasma residence time and controlled release in vivo by pegylation. Also, compared to the two drugs, liposomal encapsulation has been shown to be the more effective approach.[107,108]

LNPs have been recognized as important carriers in the siRNA, peptide, and oligonucleotide-based gene therapy approach. Encapsulation of genetic material such as siRNA and peptides, which are rapidly degradable in the vascular environment, with LNPs protects them from degradation and allows them to be targeted using surface ligands.[109,110] LNPs, surface modified with A7R-cysteine peptide, were designed by Cao et al. as carrier systems for PTX delivery and tested in vitro and in vivo. In this study, increased cytotoxicity and accumulation were reported in BC xenografts, as more modified LNPs were vesiculated by BC cells due to the A7R-cysteine peptide; These results put frothed the importance of the peptide as a targeting ligand in the PTX-loaded targeted delivery system.[111] The novel drug delivery system produced by loading siRNA onto chitosan-coated LNPs was presented

DOI: http://dx.doi.org/10.32571/ijct.1139627 E-ISSN: 2602-277X

by Salva et al for the in vitro delivery of siRNA. This study provides evidence for the theory that co-administration of siHIF1-a (hypoxia-inducible factors) and siVEGF (vascular endothelial growth factors) will produce lower cytotoxicity and higher silencing efficiency. When the expressions of the relevant mRNAs were examined, it was reported that the proliferation of MCF-7 and MDA-MB-435 BC cells was significantly inhibited. In addition, stability analysis indicated that overnight serum treatment reported that chitosan-coated LNPs were able to protect siRNAs from serum degradation.[112] A bio-nanocarrier produced with the antigen located on the surface of hepatitis B virus and liposomes was loaded with siRNA to deliver HER2-expressing BC. This system successfully realized the gene silencing and protein knockdown through.[113] In this study, in which siRNA and a chemotherapeutic agent, Dox, were used together to overcome BC's multi-drug resistance (MDRChen et al. described a liposomal approach that used cationic and anionic liposomes in conjunction with polycation-DNA (LPD). A new capsule was produced to encapsulate both agents with this technique. Cellular uptake of Dox has been observed to be increased when combined with siVEGF in targeted passive metastatic BC. It has been observed that the entrapment efficiency of Dox was higher in anionic-LPD NCs through modification to overcome Pgp-mediated drug efflux.[114] Consequently, LNPs, one of the nanocarriers that have been needed for easily biodegradable therapeutic agents, especially peptides and siRNAs, to reach target cells without degradation, have become very popular. Also, LNPs have been often coated with polymers for better biocompatibility but this coating makes increases their size. Depending on the polymer used in the coating, the drug release process may also vary.

4.7. Polymer-Based NPs

Polymer-based nanoparticles (PNPs) are nanometer-sized colloidal nanoparticles. Typically, these NPs are created by attaching one copolymer to another polymer matrix.[115] Polymer-based nanocarriers can be produced from natural polymers such as cellulose and chitosan or synthetic polymers, which are more demanding in the biotechnological field with high biocompatibility.[116] Common techniques used in the chemical synthesis of PNPs are nanoprecipitation, emulsification, and salting. These chemical methods can be modified so that PNPs are specific to the drug they will carry, target to be transported, and lipophilicity, charge, and biocompatibility. Drugs can be carried by adsorbing to the surface of PNPs, forming chemical conjugation with PNPs, or loading into the core for active or passive delivery to the target site. PNPs have been a solution and advantage for hydrophobic anticancer agents.[117] The high solubility and permeability of PNPs facilitate the delivery of hydrophobic drugs in vivo, making them soluble. In addition to solubility, it also provides controlled release and long-term stability of the drug, thereby freeing the hydrophobic drug from its handicaps.[118] In addition, an extra coating on PNPs, PEG-phospholipid, has been reported to reduce toxicity by increasing the encapsulation efficiency of the drug.[119] PNPs have become important drug delivery systems for combination studies such as DOX and PTX or trastuzumab and cis-platin where anti-cancer agents are used together, and there are many studies in the literature on this subject.[120] NPs produced using poly(ε-caprolactone) have been reported to be targeted in breast cancer by loading tamoxifen into their PEG-modified and non-PEG-modified forms. Poly(ε-caprolactone) NCs modified with PEG demonstrated higher accumulation in breast cancer cells compared to the unmodified forms.[121,122] In addition, different studies have been presented in which not only chemotherapeutic agents but also photosensitizers have been preferred for cancer treatment. Photodynamic therapy using PNPs for the treatment of triple-negative breast cancer was reported by Jin et al.[123] In this study, it was revealed that PNPs conjugated with a luminescent substance when irradiated with light, produce ROS and lead to cell inhibition. PNPs conjugated with a cyclic arginine-glycine-aspartic acid peptide-modified photosensitizer showed negligible cytotoxicity but this conjugate could decrease the viability of the αvβ3 integrin-overexpressing MDA-MB-231 cells. In another study, passively targeting tumor cells by loading tamoxifen into PNPs produced from PLGA, an FDA-approved, biocompatible polymer, tumor cells demonstrated an enhanced cleavage of their DNA. Tamoxifen-loaded PLGA nanocarriers applied to MDA-MB-231 cell lines exhibited higher cytotoxicity and greater bioavailability than tamoxifen administered in free form.[124] For the treatment of TNBC, the synthesis of layer-by-layer NCs loaded with a combination of siRNA and Dox, with a controlled release approach, was improved by Deng et al. It was revealed that the increase in the layers of poly-L-Arginine (PLA) PNPs synthesized using the layer-by-layer technique both increased their size to 140 nm and enabled them to achieve a high loading capacity. In addition, PNPs co-loaded with siRNA and Dox and targeting the multidrug-resistant protein 1 (MRP1) drug efflux pump exhibited very high drug efficacy in animal models of TNBC.[19] Alongside LNPs, polymer-based drug delivery systems emerge as a different approach for delivering combined drugs to the target. Although the synthetic polymers used in the production of PNPs could be modified using different methods to respond to needs, their size continues to be around several hundred nanometers, which is higher than LNPs, this physical character affecting their biodistribution.[125]

In addition, nanofibers, which are among the biomaterials produced from synthetic or natural polymers, are one of the PNC groups developed for many different application areas such as drug delivery systems

DOI: http://dx.doi.org/10.32571/ijct.1139627 E-ISSN: 2602-277X

or cosmetics. Biocompatible polymers such as chitosan, PVA, PLA, and PEG, which have been widely preferred in drug delivery systems have been used in the synthesis of nanofibers.[126] The mechanical properties (elasticity and tensile strength) of nanofibers with a very large surface area/volume ratio also have exhibited the desired quality. Techniques to produce nanofibers from synthetic polymers: template synthesis, drawing, phase separation, electrospinning, and self-assembly.[127] Jayakumar et al., for example, employed the electrospinning process to create chitin and chitosan nanofibers.[128] In another study by Marty et al.,[129] nanofibers were fabricated as a drug delivery system to evaluate cell motility in metastatic breast cancer patients. Although nanofibers are a new approach as drug carriers, they have significant disadvantages such as their low drug loading capacity and toxic effects.

5. CONCLUSION

Cancer is a deadly disease that affects the whole world, and the number of cancer research projects is increasing. Breast cancer is one of the deadliest tumors, and typical breast cancer treatments include surgery, chemotherapy, and radiotherapy. Conventional therapy's lack of selectivity and targeting resulted in drug resistance and adverse effects that limited practical uses. In this context, targeted nanoparticles emerge as promising cancer treatment candidates. In this review, targeted nanocarrier systems that have the potential to be used in breast cancer treatment are emphasized. In various in vitro and in vivo studies on breast cancer, researchers have modified nanocarrier drug delivery systems with ligands specific to the receptors overexpressed at the tumor site to target cancer cells. These nanoparticle systems improve targeted and efficient drug delivery, provide slow and controlled drug release, reduce side effects, and reverse multidrug resistance. With the development of target-specific nanocarrier systems, the introduction of new materials, and the increased focus on breast cancer research, the value of targeted nanocarrier systems in breast cancer treatment will increase.

Conflict of interest

Authors declare that there is no a conflict of interest with any person, institute, company, etc.

REFERENCES

1. DeSantis, C. E.; Fedewa, S. A.; Goding Sauer, A.; Kramer, J. L.; Smith, R. A.; Jemal, A. *CA: A Canc. J. for Clinic.* **2016**, *66*, 31–42.

2. Roberto, P.-B.; F., F. M.; Gemma, C.-V.; Denis, W.; Beatriz, P.-G.; Javier, L.; M., V. C.; Marcela, G.; José-Manuel, M.-M.; Francisco, A.-C.; Laura, B.-L.; Ignasi, T.; Trinidad, D.-S.; Nuria, A.; Nicolás, O.; Manolis, K.; Marina, P. *Environ. Health Persp.* **2016**, *124*, 1575–1582.

3. Wang, X.; Li, L.; Gao, J.; Liu, J.; Guo, M.; Liu, L.; Wang, W.; Wang, J.; Xing, Z.; Yu, Z.; Wang, X. *The Oncologist.* **2016**, *21*, 1362–1368.

4. Wielsøe, M.; Gudmundsdottir, S.; Bonefeld-Jørgensen, E. C. *Public Health.* **2016**, *137*, 50–58.

5. Namiranian, N.; Moradi-Lakeh, M.; Razavi-Ratki, S. K.; Doayie, M.; Nojomi, M. *Asian Pacific J. of Canc. Preven.* **2014**, *15,* 9535–9541.

6. Shield, K. D.; Soerjomataram, I.; Rehm, J. *Alcoholism: Clinic. and Exp. Research.* **2016**, *40*, 1166–1181.

7. Hanf, V.; Hanf, D. *Breast Care.* **2014**, *9*, 398–405.

8. Senapati, S.; Mahanta, A. K.; Kumar, S.; Maiti, P. *Signal Transduction and Targeted Therapy.* **2018**, *3*, 1–19.

9. Prihantono; Faruk, M. *Annals of Med. and Surgery* **2021**, *70*, 102793.

10. Tharkar, P.; Varanasi, R.; Wong, W. S. F.; Jin, C. T.; Chrzanowski, W. *Front. in Bio. and Biotech.* **2019**, *7*.

11. Mansoori, B.; Mohammadi, A.; Davudian, S.; Shirjang, S.; Baradaran, B. *Advan. Pharm. Bull.* **2017**, *7*, 339–348.

12. Fang, X.; Cao, J.; Shen, A. *J. of Drug Delivery Sci. and Techn.* **2020**, *57*.

13. Kaushik, N.; Borkar, S. B.; Nandanwar, S. K.; Panda, P. K.; Choi, E. H.; Kaushik, N. K. *J. of Nanobiotechn.* **2022**, *20*, 152.

14. Ruman, U.; Fakurazi, S.; Masarudin, M. J.; Hussein, M. Z. *Intern. J. of Nanomed.* **2020**, *15*, 1437–1456.

15. Ke, X.; Ng, V. W. L.; Ono, R. J.; Chan, J. M. W.; Krishnamurthy, S.; Wang, Y.; Hedrick, J. L.; Yang, Y. *J. of Contr. Rel.* **2014**, *193*, 9–26.

16. Montané, X.; Bajek, A.; Roszkowski, K.; Montornés, J. M.; Giamberini, M.; Roszkowski, S.; Kowalczyk, O.; Garcia-Valls, R.; Tylkowski, B. *Mol. (Basel, Switzerland).* **2020**, *25*.

17. Yao, Y.; Zhou, Y.; Liu, L.; Xu, Y.; Chen, Q.; Wang, Y.; Wu, S.; Deng, Y.; Zhang, J.; Shao, A. *Front. in Mol. Biosci.* **2020**, *7*, 193.

18. Karahaliloğlu, Z.; Kilicay, E.; Alpaslan, P.; Hazer, B.; Baki Denkbas, E. *J. of Bio. and Comp. Pol.* **2017**, *33*, 38–62.

DOI: http://dx.doi.org/10.32571/ijct.1139627 **E-ISSN: 2602-277X**

19. Deng, Z. J.; Morton, S. W.; Ben-Akiva, E.; Dreaden, E. C.; Shopsowitz, K. E.; Hammond, P. T. *ACS Nano* **2013**, *7*, 9571–9584.

20. Singh, S. K.; Singh, S.; Lillard, J. W. J.; Singh, R. *Inter. J. of Nanomed.* **2017**, *12*, 6205–6218.

21. You, Y.; Xu, Z.; Chen, Y. *Drug Delivery.* **2018**, *25*, 448–460.

22. Xu, R.; Sui, J.; Zhao, M.; Yang, Y.; Tong, L.; Liu, Y.; Sun, Y.; Fan, Y.; Liang, J.; Zhang, X. *Poly. Test.* **2022**, *113*, 107669.

23. Pourradi, N. M. A.; Babaei, H.; Hamishehkar, H.; Baradaran, B.; Shokouhi-Gogani, B.; Shanehbandi, D.; Ghorbani, M.; Azarmi, Y. *Tox. and App. Pharm.* **2022**, *446*, 116036.

24. Khan, N.; Ruchika; Dhritlahre, R. K.; Saneja, A. *Drug Discovery Today* **2022**, *27*, 2288–2299.

25. Colomer, R.; Aranda-López, I.; Albanell, J.; García-Caballero, T.; Ciruelos, E.; López-García, M. Á.; Cortés, J.; Rojo, F.; Martín, M.; Palacios-Calvo, J. *Clin. & Trans. Oncology: Off. Publ. of the Fed. of Span. Onc. Societies and of the Nat. Canc. Inst. of Mexico* **2018**, *20,* 815–826.

26. Jin, S.; Ye, K. *Recent patents on anti-cancer drug discovery.* **2013**, *8*, 143–153.

27. Mao, J. J.; Chung, A.; Benton, A.; Hill, S.; Ungar, L.; Leonard, C. E.; Hennessy, S.; Holmes, J. H. *Pharm. and Drug Safety.* **2013**, *22*, 256–262.

28. Tai, W.; Mahato, R.; Cheng, K. *J. of Cont. Rel.: Off. J. of the Cont. Rel. Society.* **2010**, *146*, 264–275.

29. Hurst, D. R.; Welch, D. R. *FEBS Lett.* **2011**, *585*, 3185–3190.

30. Rivera-Guevara, C.; Camacho, J. *Recent Patents on Anti-Canc. Drug Disc.* **2011**, *6*, 237–245.

31. Dreaden, E. C.; Mwakwari, S. C.; Sodji, Q. H.; Oyelere, A. K.; El-Sayed, M. A. *Biocon. Chem.* **2009**, *20*, 2247–2253.

32. Li, Y.; Humphries, B.; Yang, C.; Wang, Z. *Nanomat. (Basel, Switzerland)* **2018**, *8*.

33. Duffy, M. J.; Harbeck, N.; Nap, M.; Molina, R.; Nicolini, A.; Senkus, E.; Cardoso, F. *Euro. J. of Canc. (Oxford, England: 1990)* **2017**, *75*, 284–298.

34. Rugo, H. S.; Rumble, R. B.; Macrae, E.; Barton, D. L.; Connolly, H. K.; Dickler, M. N.; Fallowfield, L.; Fowble, B.; Ingle, J. N.; Jahanzeb, M.; Johnston, S. R. D.; Korde, L. A.; Khatcheressian, J. L.; Mehta, R. S.; Muss, H. B.; Burstein, H. J. *ACS of Clinic. Onc.* **2016**, *34*, 3069–3103.

35. Parvani, J. G.; Gujrati, M. D.; Mack, M. A.; Schiemann, W. P.; Lu, Z.-R. *Canc. Research.* **2015**, *75*, 2316–2325.

36. Wu, X.; Han, Z.; Schur, R. M.; Lu, Z.-R. *ACS Biomat. Sci. & Eng.* **2016**, *2*, 501–507.

37. Deng, X.; Cao, M.; Zhang, J.; Hu, K.; Yin, Z.; Zhou, Z.; Xiao, X.; Yang, Y.; Sheng, W.; Wu, Y.; Zeng, Y. *Biomat.* **2014**, *35*, 4333–4344.

38. Devulapally, R.; Sekar, N. M.; Sekar, T. V; Foygel, K.; Massoud, T. F.; Willmann, J. K.; Paulmurugan, R. *ACS Nano.* **2015**, *9*, 2290–2302.

39. Kostryukova, L. V; Tereshkina, Y. A.; Korotkevich, E. I.; Prozorovsky, V. N.; Torkhovskaya, T. I.; Morozevich, G. E.; Toropygin, I. Y.; Konstantinov, M. A.; Tikhonova, E. G. *Biomedit. Khimiia.* **2020**, *66* (6), 464–468.

40. Jafari, M.; Sriram, V.; Xu, Z.; Harris, G. M.; Lee, J.-Y. *Carb. Pol.* **2020**, *249*, 116837.

41. Chowdhury, N.; Chaudhry, S.; Hall, N.; Olverson, G.; Zhang, Q.-J.; Mandal, T.; Dash, S.; Kundu, A. *AAPS Pharm. Sci. Tech.* **2020**, *21*, 202.

42. Sui, J.; He, M.; Yang, Y.; Ma, M.; Guo, Z.; Zhao, M.; Liang, J.; Sun, Y.; Fan, Y.; Zhang, X. *ACS App. Mat. & Inter.* **2020**, *12*, 51198–51211.

43. Kim, B.; Shin, J.; Wu, J.; Omstead, D. T.; Kiziltepe, T.; Littlepage, L. E.; Bilgicer, B. *Cont. Rel. Soc.* **2020**, *322*, 530–541.

44. Shieh, M.-J.; Hsu, C.-Y.; Huang, L.-Y.; Chen, H.-Y.; Huang, F.-H.; Lai, P.-S. *J. of the Cont.Rel. Soc.* **2011**, *152*, 418–425.

45. Yalcin, S.; Unsoy, G.; Mutlu, P.; Khodadust, R.; Gunduz, U. *Amer. J. of Ther.* **2014**, *21*, 453–461.

46. Bazylińska, U.; Zieliński, W.; Kulbacka, J.; Samoć, M.; Wilk, K. A. *Colloids and Surfaces. B, Biointer.* **2016**, *137*, 121–132.

47. Mamnoon, B.; Loganathan, J.; Confeld, M. I.; De Fonseka, N.; Feng, L.; Froberg, J.; Choi, Y.; Tuvin, D. M.; Sathish, V.; Mallik, S. *ACS App. Biomat.* **2021**, *4*, 1450–1460.

48. Liao, W.-S.; Ho, Y.; Lin, Y.-W.; Naveen Raj, E.; Liu, K.-K.; Chen, C.; Zhou, X.-Z.; Lu, K.-P.; Chao, J.-I. *Acta biomat.* **2019**, *86*, 395–405.

DOI: http://dx.doi.org/10.32571/ijct.1139627 E-ISSN: 2602-277X

49. Cristofolini, T.; Dalmina, M.; Sierra, J. A.; Silva, A. H.; Pasa, A. A.; Pittella, F.; Creczynski-Pasa, T. B. *Mat.Sci. & Eng. C, Mat. for Bio. App.* **2020**, *109*, 110555.

50. Tade, R. S.; Patil, P. O. *ACS Biomat. Sci. & Eng.* **2020**, *6*, 5987–6008.

51. Tampaki, E. C.; Tampakis, A.; Alifieris, C. E.; Krikelis, D.; Pazaiti, A.; Kontos, M.; Trafalis, D. T. *Clinic. Drug Invest.* **2018**, *38*, 639–648.

52. Nakajima, M.; Sakoda, Y.; Adachi, K.; Nagano, H.; Tamada, K. *Canc. Sci.* **2019**, *110*, 3079–3088.

53. Zhang, N.; Zhang, J.; Wang, P.; Liu, X.; Huo, P.; Xu, Y.; Chen, W.; Xu, H.; Tian, Q. *Anti-cancer Drugs.* **2018**, *29*, 307–322.

54. Mohammadinejad, A.; Taghdisi, S. M.; Es'haghi, Z.; Abnous, K.; Mohajeri, S. A. *Journal of the Euro. Fed. for Pharm. Sci.* **2019**, *134*, 60–68.

55. Hanafi-Bojd, M. Y.; Jaafari, M. R.; Ramezanian, N.; Xue, M.; Amin, M.; Shahtahmassebi, N.; Malaekeh-Nikouei, B. *Euro. J. of Pharm. and Biopharm.* **2015**, *89*, 248–258.

56. Fang, J.; Nakamura, H.; Maeda, H. *Advan. Drug Delivery Rev.* **2011**, *63*, 136–151.

57. Cheng, R.; Meng, F.; Deng, C.; Klok, H.-A.; Zhong, Z. *Biomat.* **2013**, *34*, 3647–3657.

58. Torchilin, V. *Advan. Drug Delivery Rev.* **2011**, *63*, 131–135.

59. Godlewski, M. M.; Kaszewski, J.; Kielbik, P.; Olszewski, J.; Lipinski, W.; Slonska-Zielonka, A.; Rosowska, J.; Witkowski, B. S.; Gralak, M. A.; Gajewski, Z.; Godlewski, M. *Nanotechn. Rev.* **2020**, *9*, 274–302.

60. Vines, J. B.; Yoon, J.-H.; Ryu, N.-E.; Lim, D.-J.; Park, H. *Front. in Chem.* **2019**, *7*.

61. Moore, J. A.; Chow, J. C. L. *Nano Exp.* **2021**, *2*, 22001.

62. Siddique, S.; Chow, J. C. L. *App. Sci.* 2020.

63. Su, X.-Y.; Liu, P.-D.; Wu, H.; Gu, N. *Canc. Bio. & Med.* **2014**, *11*, 86–91.

64. Liu, P.; Huang, Z.; Chen, Z.; Xu, R.; Wu, H.; Zang, F.; Wang, C.; Gu, N. *Nanoscale.* **2013**, *5*, 11829–11836.

65. Wahab, R.; Siddiqui, M. A.; Saquib, Q.; Dwivedi, S.; Ahmad, J.; Musarrat, J.; Al-Khedhairy, A. A.; Shin, H.-S. *Colloids and surfaces. B, Bioprinter.* **2014**, *117*, 267–276.

66. Wang, Y.; Yang, F.; Zhang, H. X.; Zi, X. Y.; Pan, X. H.; Chen, F.; Luo, W. D.; Li, J. X.; Zhu, H. Y.; Hu, Y. P. *Cell Death & Dis.* **2013**, *4*, e783.

67. Pešić, M.; Podolski-Renić, A.; Stojković, S.; Matović, B.; Zmejkoski, D.; Kojić, V.; Bogdanović, G.; Pavićević, A.; Mojović, M.; Savić, A.; Milenković, I.; Kalauzi, A.; Radotić, K. *Chemico-biological Inter.* **2015**, *232*, 85–93.

68. Yeh, Y.-C.; Creran, B.; Rotello, V. M. *Nanoscale.* **2012**, *4*, 1871–1880.

69. Ghosh, P.; Han, G.; De, M.; Kim, C. K.; Rotello, V. M. Gold Nanoparticles in Delivery Applications. *Advan. Drug Delivery Rev.* **2008**, *60*, 1307–1315.

70. Zhao, Y.; Detering, L.; Sultan, D.; Cooper, M. L.; You, M.; Cho, S.; Meier, S. L.; Luehmann, H.; Sun, G.; Rettig, M.; Dehdashti, F.; Wooley, K. L.; DiPersio, J. F.; Liu, Y. *ACS Nano.* **2016**, *10*, 5959–5970.

71. Chen, B.; Wu, W.; Wang, X. *Curr. Canc. Drug Targets.* **2011**, *11*, 184–189.

72. Wang, Y.-X. J.; Xuan, S.; Port, M.; Idee, J.-M. *Curr. Pharm. Design.* **2013**, *19*, 6575–6593.

73. Gupta, A. K.; Gupta, M. *Biomat.* **2005**, *26*, 3995–4021.

74. Kumar, A. V. P.; Dubey, S. K.; Tiwari, S.; Puri, A.; Hejmady, S.; Gorain, B.; Kesharwani, P. *Inter. J. of Pharm.* **2021**, *606*, 120848.

75. Jeon, M.; Lin, G.; Stephen, Z. R.; Kato, F. L.; Zhang, M. *Advan. Thera.* **2019**, *2*, 1900081.

76. Attari, E.; Nosrati, H.; Danafar, H.; Kheiri Manjili, H. *J. of Biomed. Mat. Research Part A.* **2019**, *107*, 2492–2500.

77. Soleymani, M.; Khalighfard, S.; Khodayari, S.; Khodayari, H.; Kalhori, M. R.; Hadjighassem, M. R.; Shaterabadi, Z.; Alizadeh, A. M. *Sci. Rep.* **2020**, *10*, 1695.

78. Kairdolf, B. A.; Smith, A. M.; Stokes, T. H.; Wang, M. D.; Young, A. N.; Nie, S. *Annual Rev. of Anal. Chem. (Palo Alto, Calif.)* **2013**, *6*, 143–162.

79. Yaghini, E.; Pirker, K. F.; Kay, C. W. M.; Seifalian, A. M.; MacRobert, A. J. *Small (Weinheim an der Bergstrasse, Germany).* **2014**, *10*, 5106–5115.

DOI: http://dx.doi.org/10.32571/ijct.1139627 E-ISSN: 2602-277X

80. Yezhelyev, M. V.; Al-Hajj, A.; Morris, C.; Marcus, A. I.; Liu, T.; Lewis, M.; Cohen, C.; Zrazhevskiy, P.; Simons, J. W.; Rogatko, A.; Nie, S.; Gao, X.; O'Regan, R. M. *Advan.Mat.* **2007**, *19*, 3146–3151.

81. Samimi, S.; Ardestani, M. S.; Dorkoosh, F. A. *J. of Drug Delivery Sci. and Tech.* **2021**, *61*, 102287.

82. Chung, S.; Revia, R. A.; Zhang, M. *Advan. Mat.* **2021**, *33* (22), 1904362.

83. Gao, Y.; Gao, D.; Shen, J.; Wang, Q. *Front. in Chem.* **2020**, *8*.

84. Tsai, C.-P.; Chen, C.-Y.; Hung, Y.; Chang, F.-H.; Mou, C.-Y. *J. of Mat. Chem.* **2009**, *19*, 5737–5743.

85. Meng, H.; Mai, W. X.; Zhang, H.; Xue, M.; Xia, T.; Lin, S.; Wang, X.; Zhao, Y.; Ji, Z.; Zink, J. I.; Nel, A. E. *ACS Nano* **2013**, *7*, 994–1005.

86. Milgroom, A.; Intrator, M.; Madhavan, K.; Mazzaro, L.; Shandas, R.; Liu, B.; Park, D. *Coll. and surfaces. B, Bioint.* **2014**, *116*, 652–657.

87. Fortuni, B.; Inose, T.; Ricci, M.; Fujita, Y.; Van Zundert, I.; Masuhara, A.; Fron, E.; Mizuno, H.; Latterini, L.; Rocha, S.; Uji-I, H. *Sci. Rep.* **2019**, *9*, 2666

88. Moodley, T.; Singh, M. *Mol. (Basel, Switzerland)* **2020**, *25*.

89. Augustine, S.; Singh, J.; Srivastava, M.; Sharma, M.; Das, A.; Malhotra, B. D. *Biomat. Sci.* **2017**, *5*, 901–952.

90. Chadar, R.; Afzal, O.; Alqahtani, S. M.; Kesharwani, P. *Coll. and Surfaces. B, Bioprinter.* **2021**, *208*, 112044.

91. Xiao, Y.; Gao, X.; Tarantula, O.; Treado, S.; Urbas, A.; Holbrook, R. D.; Cavicchi, R. E.; Avedisian, C. T.; Mitra, S.; Savla, R.; Wagner, P. D.; Srivastava, S.; He, H. *BMC Canc.* **2009**, *9*, 351.

92. Hampel, S.; Kunze, D.; Haase, D.; Krämer, K.; Rauschenbach, M.; Ritschel, M.; Leonhardt, A.; Thomas, J.; Oswald, S.; Hoffmann, V.; Büchner, B. *Nanomed.* **2008**, *3*, 175–182.

93. Liu, Z.; Sun, X.; Nakayama-Ratchford, N.; Dai, H. *ACS Nano* **2007**, *1*, 50–56.

94. Liu, Z.; Chen, K.; Davis, C.; Sherlock, S.; Cao, Q.; Chen, X.; Dai, H. *Canc. Res.* **2008**, *68*, 6652–6660.

95. Shao, W.; Paul, A.; Zhao, B.; Lee, C.; Rodes, L.; Prakash, S. *Biomat.* **2013**, *34*, 10109–10119.

96. Casais-Molina, M. L.; Cab, C.; Canto, G.; Medina, J.; Tapia, A. *J. of Nanomat.* **2018**, 2058613.

97. Raza, K.; Thotakura, N.; Kumar, P.; Joshi, M.; Bhushan, S.; Bhatia, A.; Kumar, V.; Malik, R.; Sharma, G.; Guru, S. K.; Katare, O. P. *Inter. J. of Pharm.* **2015**, *495*, 551–559.

98. Mehra, N. K.; Jain, A. K.; Lodhi, N.; Raj, R.; Dubey, V.; Mishra, D.; Nahar, M.; Jain, N. K. *Cri. Rev. in Thera. Drug Carr. Syst.* **2008**, *25*, 169–206.

99. Kong, T.; Hao, L.; Wei, Y.; Cai, X.; Zhu, B. *Cell Pro.* **2018**, *51*, e12488.

100. Esfandiari, N.; Arzanani, M. K.; Soleimani, M.; Kohi-Habibi, M.; Svendsen, W. E. *Tumour Bio.: The J. of The Inter. Soc. for Oncodev. Bio. and Med.* **2016**, *37*, 1229–1236.

101. Le, D. H. T.; Lee, K. L.; Shukla, S.; Commandeur, U.; Steinmetz, N. F. *Nanoscale* **2017**, *9*, 2348–2357.

102. Steinmetz, N. F. *Nanomed.* **2010**, *6*, 634–641.

103. Fritze, A.; Hens, F.; Kimpfler, A.; Schubert, R.; Peschka-Süss, R. *Biochimica et Biophysica Acta (BBA) – Biomemb.* **2006**, *1758* (10), 1633–1640.

104. Boman, N. L.; Masin, D.; Mayer, L. D.; Cullis, P. R.; Bally, M. B. *Canc. Res.* **1994**, *54*, 2830–2833.

105. Marcial, S. P. S.; Carneiro, G.; Leite, E. A. *J. of Nano. Res.* **2017**, *19*, 1–11.

106. Yang, T.; Cui, F.-D.; Choi, M.-K.; Cho, J.-W.; Chung, S.-J.; Shim, C.-K.; Kim, D.-D. *Inter.J. of Pharm.* **2007**, *338*, 317–326.

107. Wong, M.-Y.; Chiu, G. N. C. *Nanomed.* **2011**, *7*, 834–840.

108. Dhankhar, R.; Vyas, S. P.; Jain, A. K.; Arora, S.; Rath, G.; Goyal, A. K. *Art. Cells, Blood Subs., and Biotech.* **2010**, *38*, 230–249.

109. Hayes, M. E.; Drummond, D. C.; Kirpotin, D. B.; Zheng, W. W.; Noble, C. O.; Park, J. W.; Marks, J. D.; Benz, C. C.; Hong, K. *Gene Ther.* **2006**, *13*, 646–651.

110. Hortobagyi, G. N.; Ueno, N. T.; Xia, W.; Zhang, S.; Wolf, J. K.; Putnam, J. B.; Weiden, P. L.; Willey, J. S.; Carey, M.; Branham, D. L.; Payne, J. Y.; Tucker, S. D.; Bartholomeusz, C.; Kilbourn, R. G.; De Jager, R. L.; Sneige, N.; Katz, R. L.; Anklesaria, P.; Ibrahim, N. K.; Murray, J. L.; Theriault, R. L.; Valero, V.; Gershenson, D. M.; Bevers, M. W.; Huang, L.; Lopez-Berestein, G.; Hung, M. C. *J. of Clin. Onco.: Off. J. of The Amer. Soc. of Clin. Onco.* **2001**, *19*, 3422–3433.

111. Cao, J.; Wang, R.; Gao, N.; Li, M.; Tian, X.; Yang, W.; Ruan, Y.; Zhou, C.; Wang, G.; Liu, X.; Tang, S.; Yu,

DOI: http://dx.doi.org/10.32571/ijct.1139627 **E-ISSN: 2602-277X**

Y.; Liu, Y.; Sun, G.; Peng, H.; Wang, Q. *Biomat. Sci.* **2015**, *3*, 1545–1554.

112. Şalva, E.; Turan, S. Ö.; Eren, F.; Akbuğa, J. *Inter. J. of Pharm.* **2015**, *478*, 147–154.

113. Nishimura, Y.; Mieda, H.; Ishii, J.; Ogino, C.; Fujiwara, T.; Kondo, A. *J. of Nanobiotech.* **2013**, *11*, 19.

114. Chen, Y.; Bathula, S. R.; Li, J.; Huang, L. *J. of Bio. Chem.* **2010**, *285*, 22639–22650.

115. Dhanjal, D. S.; Mehta, M.; Chopra, C.; Singh, R.; Sharma, P.; Chellappan, D. K.; Tambuwala, M. M.; Bakshi, H. A.; Aljabali, A. A. A.; Gupta, G.; Nammi, S.; Prasher, P.; Dua, K.; Satija, S. *Academic Press*, **2021,** 253–272.

116. Pandey, A.; Jain, R. *Springer Inter.Publishing: Cham*, **2020**, 1–19.

117. Pulingam, T.; Foroozandeh, P.; Chuah, J.-A.; Sudesh, K. *Nanomat. (Basel, Switzerland)* **2022**, *12*.

118. Wang, B.; Wang, S.; Zhang, Q.; Deng, Y.; Li, X.; Peng, L.; Zuo, X.; Piao, M.; Kuang, X.; Sheng, S.; Yu, Y. *Acta Biomaterialia.* **2019**, *96*, 55–67.

119. Jin, H.; Pi, J.; Zhao, Y.; Jiang, J.; Li, T.; Zeng, X.; Yang, P.; Evans, C. E.; Cai, J. *Nanoscale* **2017**, *9* (42), 16365–16374.

120. Masood, F. *Mat. Sci. and Eng.: C* **2016**, *60*, 569–578.

121. Shenoy, D. B.; Amiji, M. M. *Inter. J. of Pharm.* **2005**, *293* (1), 261–270.

122. Lee, J. H.; Nan, A. *J. of Drug Del.* **2012**, *2012*, 915375.

123. Jin, G.; He, R.; Liu, Q.; Dong, Y.; Lin, M.; Li, W.; Xu, F. *ACS App. Mat. & Inter.* **2018**, *10*,10634–10646.

124. Pandey, S. K.; Patel, D. K.; Maurya, A. K.; Thakur, R.; Mishra, D. P.; Vinayak, M.; Haldar, C.; Maiti, P. *Inter. J. of Bio.Macromol.* **2016**, *89*, 99–110.

125. Alexis, F.; Pridgen, E.; Molnar, L. K.; Farokhzad, O. C. *Mol. Pharm.* **2008**, *5*, 505–515.

126. Sedghi, R.; Shaabani, A.; Mohammadi, Z.; Samadi, F. Y.; Isaei, E. *Carbohydrate Poly.* **2017**, *159*, 1–10.

127. Zahmatkeshan, M.; Adel, M.; Bahrami, S.; Esmaeili, F.; Rezayat, S. M.; Saeedi, Y.; Mehravi, B.; Jameie, S. B.; Ashtari, K. *Springer Inter. Publishing: Cham*, **2018**, 1–47.

128. Jayakumar, R.; Prabaharan, M.; Nair, S. V; Tamura, H. *Biotech. Advan.* **2010**, *28*, 142–150.

129. Marty, M.; Cognetti, F.; Maraninchi, D.; Snyder, R.; Mauriac, L.; Tubiana-Hulin, M.; Chan, S.; Grimes, D.; Antón, A.; Lluch, A.; Kennedy, J.; O'Byrne, K.; Conte, P.; Green, M.; Ward, C.; Mayne, K.; Extra, J.-M. *J.of Clin. Onco.* **2005**, *23*, 4265–4274.

DOI: http://dx.doi.org/10.32571/ijct.1148438 **E-ISSN: 2602-277X**

International Journal of Chemistry and Technology

http://dergipark.org.tr/ijct

Research Article

Some pharmacological properties of *Alyssum stylare* (Boiss. & Balansa) Boiss.

Imran UYSAL

Osmaniye Korkut Ata University, Bahçe Vocational School of Higher Education, Department of Food Processing, Bahçe-Osmaniye, Türkiye

Received: 25 July 2022; Revised: 25 August 2022; Accepted: 31 August 2022

*Corresponding author e-mail: imranuysal@osmaniye.edu.tr

Citation: Uysal, I. *Int. J. Chem. Technol.* **2022**, 6 (2), 93-96.

ABSTRACT

From ancient times to the present, plants have been used in many different areas. One of the most striking of these areas is alternative medicine. Türkiye is a country rich for plants diversity both in terms of location and other favorable conditions. This diversity reveals the importance of alternative medicine. In this respect, it is extremely necessary to determine the pharmacological properties of plants. In our study, *Alyssum stylare* (Boiss. & Balansa) Boiss. total oxidant status (TOS), total antioxidant status (TAS), oxidative stress index (OSI) as well as its status against antimicrobial agents were examined. After the above-ground part of the plant sample was dried and powdered by taking the necessary precautions, extraction was carried out Rel Assay kits were preferred for ethanol extract and TOS, TAS, OSI data. Its antimicrobial status was determined using the agar diffusion method. Consequently, of the study, the TAS capacity of the plant extract was 7.911±0.217 mmol/L, the TOS capacity was 11.587±0.202 µmol/L, and the OSI capacity was 0.146±0.001. It was used that it was effective against standard bacteria strains at 25-100 µg/mL and 200 µg/mL concentrations against fungi strains. Consequently, it is thought that *A. stylare* can be used in studies conducted for antioxidant and antimicrobial.

Keywords: Antioxidant, oxidant, antimicrobial agent, medicinal plants.

Alyssum stylare (Boiss. & Balansa) Boiss'in bazı farmakolojik özellikleri

ÖZ

Antik çağlardan günümüze kadar bitkiler birçok farklı alanda kullanılmıştır. Bu kullanım alanlarının en dikkat çekenlerinden biri de alternatif tıptır. Türkiye hem konumu hem de diğer uygun koşullar bakımından bitkiler için zengin bir ülkedir. Bu zenginlik alternatif tıbbın önemini ortaya koymaktadır. Bu açıdan bitkilerin farmakolojik özelliklerinin belirlenmesi son derece gereklidir. Çalışmamızda *Alyssum stylare* (Boiss. & Balansa) Boiss'in toplam oksidan durumu (TOS), toplam antioksidan durumu (TAS), oksidatif stres indeksi (OSI) ve antimikrobiyal ajanlara karşı durumu incelenmiştir. Bitki örneğinin toprak üstü kısmı gerekli önlemler alınarak kurutulup toz haline getirildikten sonra ekstraksiyon yapılmıştır. Etanol ekstraktı ve TOS, TAS, OSI verileri için Rel Assay kitleri tercih edilmiştir. Antimikrobiyal durumu, agar difüzyon yöntemi kullanılarak belirlendi. Çalışmamız sonucunda bitki ekstraktının TAS değeri 7.911±0.217 mmol/L, TOS değeri 11.587±0.202 µmol/L ve OSI değeri 0.146±0.001 olarak bulunmuştur. Standart bakteri suşlarına karşı 25-100 µg/mL ve mantar suşlarına karşı 200 µg/mL konsantrasyonda etkili olduğu belirlendi. Sonuç olarak *A. stylare*'in antioksidan ve antimikrobiyal açıdan çalışmalarda kullanılabileceği düşünülmektedir.

Anahtar Kelimeler: Antioksidan, oksidan, antimikrobiyal ajan, tıbbi bitkiler.

1. INTRODUCTION

Conditions like environmental pollution, alcohol consumption, UV rays, and smoking cause free radical formation in humans.[1] If there is a deficiency in the reduction of oxygen, reactive oxygen species are formed. Consequently, these formations and deficiencies cause oxidative stress.[2] Consequently of oxidative stress, it can cause many diseases in humans like Parkinson's, alzheimer's, cardiological disorders and cancer. Antioxidants come first in combating these conditions. In this context, supplemental antioxidants are used.[3] Many studies have shown that plants can be natural antioxidant agents. From past times to the present, plants have always been in the field of interest of people. When we look at the archaeological studies, human being recognize the plants and they have been; used in many areas like food, relieving health problems, shelter, comforting, spice and sweetener by people.[4-5] Recently, it has been seen that the most preferred among these usage areas is herbal

DOI: http://dx.doi.org/10.32571/ijct.1148438 E-ISSN: 2602-277X

medicine.[6] The World Health Organization (WHO) has introduced the definition of "herbal medicine" to the use of drugs or herbal mixtures for treatment and solving diseases.[7-8] In this direction, it is very valuable to determine the pharmacological properties of plants. Many assessments of plants; It has shown that it has many biological activities such as antimicrobial, antiproliferative, antienflammatory, DNA damage protective, antiaging, antioxidant, anticancer.[9-17]. *Alyssum* L. is a genus of the Brassicaceae family. It consists of approximately 195 species. There are annual and perennial ones. *Alyssum* L. is generally distributed in rocky, stony and sandy areas in Europe, Asia and North Africa.[18-19] With this research, it was aimed to determine the attitude of *A. stylare* species against antioxidant, oxidant and antimicrobial agents.

2. MATERIALS AND METHODS

A. stylare sample used in the study was collected from Sivas (Turkey). *A. stylare* plant sample was identified by using the volume 1 page 374 section of the flora of Turkey book. The soil-containing parts of the *A. stylare* sample collected from the field were removed. The above-ground parts to be used were dried in a ventilated and shaded environment. After the drying process was completed, 30 g of the samples were weighed and then powdered with the help of some shredding apparatus. The powdered samples were extracted with 200 mL EtOH at 50 ^{0}C for approximately 6 hours. The solvent in the extract was removed with the help of Heidolph Laborota 4000 Rotary Evaporator.

2.1. Antimicrobial Activity

The effect of ethanol extract of *A. stylare* against bacteria and fungi strains was investigated by agar diffusion technique, which is one of the methods used in antimicrobial studies.

Bacterial strains: *Staphylococcus aureus* MRSA ATCC 43300, *Escherichia coli* ATCC 25922, *Pseudomonas aeruginosa* ATCC 27853, *Enterococcus faecalis* ATCC 29212, *S. aureus* ATCC 29213 and *Acinetobacter baumannii* ATCC 19606 were used. Fungal strains:, *Candida krusei* ATCC 34135, *C. albicans* ATCC 10231 and *C. glabrata* ATCC 90030 were used. With this method, the lowest concentration (MIC) that inhibits the growth of the strains was determined.[20-22]

2.2. Antioxidant Activity

Total antioxidant (TAS) and total oxidant (TOS) capacity of Ethanol extract of *A. stylare* were intended. Rel Assay kits were preferred for TAS and TOS capacity. Hydrogen peroxide was used in the calibration of the TOS kit. Trolox was used in the calibration of the TAS kit. Analyzes were performed according to the protocol determined by the manufacturer.[23-24] Oxidative stress index (OSI) was determined by the ratio of TOS capacity to TAS capacity according to the formula below.[25]

$$\text{OSI (AU)} = \frac{\text{TOS, } \mu\text{mol } H_2O_2 \text{ equiv./L}}{\text{TAS, mmol Trolox equiv./L X 10}}$$

3. RESULTS AND DISCUSSION

3.1. Antimicrobial Activity

Microorganisms are among the main causes of many diseases lately. The strong of many microorganisms to drugs, especially consequently of unconscious antibiotic use, has made it difficult to combat microbial diseases.[26] Many different researchers have focused on the discovery of new antimicrobial drugs. Plants have been one of the focal points of these researchers.[27] With this research you have done, the capacity of EtOH extract of *A. stylare* plant on Antimicrobial agents were examined. The obtained results are shown in Table 1.

Table 1. Antimicrobial Activity of *A. stylare* Extract

Sample	A	B	C	D	E	F	G	H	J
A. stylare	25	25	100	50	50	100	200	200	200

***(A)** *S. aureus*, **(B)** *S. aureus* MRSA, **(C)** *E. faecalis*, **(D)** *E. coli*, **(E)** *P. aeruginosa*, **(F)** *A. baumannii*, **(G)** *C. glabrata*, **(H)** *C. albicans*, **(J)** *C. krusei*
*25, 50, 100, 200 µg/mL extract concentrations

According to the study data, it was observed that *A. stylare* exhibited the highest efficacy against *S. aureus* and *S. aureus* MRSA at 25 µg/mL extract concentration. It was also effective against *E. coli* and *P. aeruginosa* at an extract concentration of 50 µg/mL, and against *E. faecalis* and *A. baumannii* at 100 µg/mL extract concentration. The plant extract was found to be effective against fungal strains (*C. glabrata, C. albicans* and *C. krusei*) at 200 µg/mL extract concentration. In this context, it was observed that the plant extract was more effective against bacterial strains than fungal strains. In previous antimicrobial activity studies on *Alyssum* species, antimicrobial activity of ethanol extracts of *A. caricum*, *A. discolor* and *A. sibiricum* was investigated using disk diffusion method. Consequently of the study, it was reported that the plant extracts were effective against S. *enteritidis*, *S. aureus*, *S. epidermidis*, *Listeria monocytogenes*, *L. innocua*, *B. subtilis*, *Enterobacter*

DOI: http://dx.doi.org/10.32571/ijct.1148438 E-ISSN: 2602-277X

aerogenes, *E. coli*, *Klebsiella pneumoniae*, *E. faecium*, *E. faecalis*, *E. durans*, *P. aeruginosa*, *P. fluorescens*, *Salmonella typhimurium*, *S. kentucky* and *S. infantis* at different concentrations.[28] In another study, it was reported that methanol extract of *A. fulvescens* subsp. *fulvescens* has antimicrobial activity against *E. coli*, *P. aeruginosa*, *S. aureus*, *B. subtilis* and *Micrococcus luteus*.[29] In this context, in our research, it was researched that the extract of *A. stylare* has significant antimicrobial activity against the standard antimicrobial agents used. Consequently, it has been determined that the plant can be used as a natural antimicrobial agent.

3.2. Antioxidant Activity

Reactive oxygen species (ROS) occurring at high levels turn into a harmful situation for living things.[30] Antioxidants of endogenous and exogenous origin fight ROS. In some cases, antioxidants are insufficient. In these insufficient cases, oxidative stress occurs. Complementary antioxidants are used as a solution.[31-32] In this study, TAS, TOS and OSI capacity of *A. stylare* ethanol extract were determined.

According to the findings, the TAS capacity of *A. stylare* was determined as 7.911±0.217 mmol, the TOS capacity was 11.587±0.202 µmol and the OSI capacity was 0.146±0.001. In our study, TAS, TOS and OSI capacity of *A. stylare* were determined for the first time. In studies on different plant species, TAS capacity of *Lepidium spinosum* ARD. was determined 4.550 mmol, the TOS capacity 12.610 µmol and the OSI capacity 0.277.[33] TAS capacity of *Mentha longifolia* (L.) HUDSON subsp. *longifolia* (L.) HUDSON was determined 3.628 mmol, the TOS capacity 4.046 µmol and the OSI capacity 0.112.[34] The TAS capacity of *Euphorbia eriophora* BOISS. was determined 5.390 mmol, the TOS capacity 20.971 µmol and the OSI capacity 0.390.[35] The TAS capacity of *Echium italicum* was determined 6.056 mmol, the TOS capacity 19.107 µmol and the OSI capacity 0.316.[36] The TAS capacity of *Satureja hortensis* was determined 5.403 mmol, the TOS capacity 3.537 µmol and the OSI capacity 0.065.[37] The TAS capacity of *Ferulago platycarpa* BOISS. ET BAL. was determined 5.688 mmol, the TOS capacity 15.552 µmol and the OSI capacity 0.273.[38]

The TAS capacity of *Marrubium globosum* MONTBRET ET AUCHER EX BENTHAM. was determined 7.677 mmol, the TOS capacity 12,387 µmol and the OSI capacity 0.162.[39] Compared to these studies, the TAS capacity of *A. stylare* was higher than *L. spinosum*, *M. longifolia* subsp. *longifolia*, *E. eriophora*, *E. italicum*, *S. hortensis* and *F. platycarpa*. The TAS capacity shows all of the antioxidant compounds found in living organisms.[40,41] In our study, it was determined that the antioxidant potential of the plant is high. The TOS capacity is an indicator of the totality of oxidant-containing compounds in living organisms.[15] The OSI capacity shows how much the oxidant compounds detected in living organisms suppress by antioxidant compounds.[42,43] It is recommended to avoid or limit the consumption of foods with high OSI capacity. The TOS and OSI capacity of *A. stylare* were higher than *M. longifolia* subsp. *longifolia* and *S. hortensis*, and lower than *L. spinosum*, *E. eriophora*, *E. italicum*, *F. platycarpa* and *M. globosum*. In this context, it was determined that the TOS capacity of *A. stylare* was at normal levels. Consequently, it is predicted that the plant can be evaluated in terms of antioxidants.

4. CONCLUSIONS

Consequently, antimicrobial antioxidant oxidant data of *A. stylare* species were determined. It was determined that *A. stylare* has a high capacity in terms of both antioxidant and oxidant when compared with the species in other studies in terms of antioxidant and oxidant. It was found that *A. stylare* EtOH extract reacted at a concentration of 25-100 µg/mL in bacterial strains and 200 µg/mL in fungal strains used in the antimicrobial study. it is predicted that *A. stylare* has an important antioxidant and antimicrobial capacity and can be used in this field.

REFERENCES

1. Davies, K.J.A. *International Union of Biochemistry and Molecular Biology Life*, **2000**, 50, 279-289.

2. Pellegrini, N.; Miglio, C.; Del Rio, D. *International Journal of Food Sciences and Nutrition*, **2009**, 60, 12–22.

3. Mohammed, F. S.; Sevindik, M.; Bal, C.; Akgül, H.; Selamoglu, Z. *Communications Faculty of Sciences University of Ankara Series C Biology*, **2019**,28, 128-142.

4. Michel, J.; Abd Rani, N. Z.; Husain, K. *Frontiers in pharmacology*, **2020**, 11, 852.

5. Akhter, S.; Batool, A. I.; Selamoglu, Z.; Sevindik, M.; Eman, R.; Mustaqeem, M.; Aslam, M. *Antibiotics*, **2021**, 10, 1011.

6. Mohammed, F. S.; Şabik, A. E.; Doğan, M.; Selamoğlu, Z.; Sevindik, M. *Bulletin of Biotechnology*, **2020**, 1, 43-45.

7. Fitzgerald, M.; Heinrich, M.; Booker, A. *Frontiers in pharmacology*, **2020**, 10, 1480.

8. Wang, W.; Xu, J.; Fang, H.; Li, Z.; Li, M. *Plant Science*, **2020**, 298, 110573.

DOI: http://dx.doi.org/10.32571/ijct.1148438 **E-ISSN: 2602-277X**

9. Krishnaiah, D.; Sarbatly, R.; Nithyanandam, R. *Food and bioproducts processing*, **2011**, 89, 217-233.

10. Miastkowska, M.; Sikora, E. Cosmetics, **2018**, 5, 55.

11. Pehlivan, M.; Mohammed, F. S.; Sevindik, M.; Akgul, H. *Eurasian Journal of Forest Science*, **2018**, 6, 22-25.

12. Kına, E.; Uysal, İ.; Mohammed, F. S.; Doğan, M.; Sevindik, M. *Turjaf*, **2021**,9, 1905-1907.

13. Liaudanskas, M.; Žvikas, V.; Petrikaitė, V. *Antioxidants*, **2021**, 10, 1115.

14. Mohammed, F. S.; Uysal, I.; Sevindik, M. *Kadirli Uygulamalı Bilimler Fakültesi Dergisi*, **2021**, 1, 109-115.

15. Mohammed, F. S.; Korkmaz, N.; Doğan, M., Şabik, A. E.; Sevindik, M. *Journal of Faculty of Pharmacy of Ankara University*, **2021**, 45, 524-534.

16. Shahbazi, R.; Sharifzad, F.; Bagheri, R.; Alsadi, N.; Yasavoli-Sharahi, H.; Matar, *C. Nutrients*, **2021**, 13, 1516.

17. Unal, O.; Eraslan, E. C.; Uysal, I.; Mohammed, F. S.; Sevindik, M.; Akgul, H. *Fresen Environ Bull*, **2022**, 31, 7341-7346.

18. Al-Shehbaz, I. A. J. *Arn. Arbor.*, **1987**, 68, 185–240.

19. Warwick, S.I.; Francis, A.; Al-Shehbaz, I.A. *Plant Syst. Evol.*, **2006**, 259, 249–258.

20. Bauer, A.W.; Kirby, W.M.; Sherris, J.C.; Turck, M. *Am J Clin Pathol.*, **1966**, 45, 493-96.

21. Hindler, J.; Hochstein, L.; Howell, A. *Preparation of routine media and reagents used in antimicrobial susceptibility testing. Part 1. McFarland standards, p. 5.19.1-5.19.6. In H. D. Isenberg (ed) Clinical microbiology procedures handbook*, vol. 1. American Society for Microbiology, Washington, D.C. USA, 1992.

22. Matuschek, E.; Brown, D.F.; Kahlmeter, G. *Clin Microbiol Infect.*, **2014**, 20, 255-266.

23. Erel, O. *Clinical biochemistry*, **2004**, 37, 277-285.

24. Erel, O. *Clinical biochemistry*, **2005**, 38, 1103-1111.

25. Sevindik, M. *Fresen Environ Bull*, **2019**, 28, 3713-3717.

26. González-Lamothe, R.; Mitchell, G.; Gattuso, M.; Diarra, M. S.; Malouin, F.; Bouarab, K. *International journal of molecular sciences*, **2009**, 10, 3400-3419.

27. Mohammed, F. S.; Akgul, H.; Sevindik, M.; Khaled, B. M. T. *Fresen Environ Bull*, **2018**, 27, 5694-5702.

28. Tozyılmaz, V.; Ceylan, Y.; Bülbül, A.S. *KSÜ Tarım ve Doğa Derg.*, **2021**, 24,715-724.

29. Ozay, C.; Mammadov, R. *Acta Biologica Hungarica*, **2017**, 8, 310–320.

30. Mohammed, F. S.; Pehlivan, M.; Sevindik, M. *International Journal of Secondary Metabolite*, **2019**, 6, 317-322.

31. Mohammed, F. S.; Karakaş, M.; Akgül, H.; Sevindik, M. *Fresen Environ Bull.*, **2019**,28, 7419-7426.

32. Mohammed, F. S.; Günal, S.; Şabik, A. E.; Akgül, H., Sevindik, M. *KSU J. Agric Nat*, **2020**, 23, 1114-1118.

33. Mohammed, F. S.; Kına, E.; Uysal, İ.; Mencik, K.; Dogan, M.; Pehlivan, M.; Sevindik, M. *Turjaf*, **2022**, 10, 1116-1119.

34. Sevindik, M.; Akgul, H.; Pehlivan, M.; Selamoglu, Z. *Fresen Environ Bull.*, **2017**, 26, 4757-4763.

35. Akgül, H.; Mohammed, F. S.; Kına, E.; Uysal, İ.; Sevindik, M.; Doğan, M. *Turjaf*, **2022**, 10, 272-275.

36. Uysal, İ.; Mohammed, F. S.; Şabik, A. E.; Kına, E.; Sevindik, M. *KSU J. Agric Nat*, **2021**, 9, 1902-1904.

37. Mohammed, F. S.; Daştan, T.; Sevindik, M.; Selamoğlu, Z. *Cumhuriyet Medical Journal*, **2019**, 41, 558-562.

38. Mohammed, F. S.; Günal, S.; Pehlivan, M.; Doğan, M.; Sevindik, M.; Akgül, H. *Gazi University Journal of Science*, **2020**, 33, 670-677.

39. Pehlivan, M.; Mohammed, F. S.; Şabik, A. E.; Kına, E.; Dogan, M.; Yumrutaş, Ö.; Sevindik, M. Some *KSU J. Agric Nat*, **2021**, 9, 1129-1132.

40. Mohammed, F. S.; Şabik, A. E.; Sevindik, E.; Pehlivan, M.; Sevindik, M. *KSU J. Agric Nat*, **2020**, 8,1171-1173.

41. Korkmaz, N.; Dayangaç, A.; Sevindik, M. *J. Fac. Pharm. Ankara*, **2021**, 45, 554-564

42. Mohammed, F. S.; Kına, E.; Sevindik, M.; Doğan, M.; Pehlivan, M. *Indian Journal of Natural Products and Resources Formerly Natural Product Radiance*, **2021**, 12, 459-462.

43. Akgül, H.; Korkmaz, N.; Dayangaç, A.; Sevindik, M. *Turjaf*, **2020**, 8, 2222-2224.

DOI: http://dx.doi.org/10.32571/ijct.1146979 **E-ISSN: 2602-277X**

International Journal of Chemistry and Technology

http://dergipark.org.tr/ijct

Research Article

Nutritive value, antimicrobial and antioxidant activities of *Tchihatchewia isatidea* Boiss

Sevda KIRBAĞ[1*] Mürşide Gizem BİRCAN[1] Burak BİRCAN[2]

[1]*Fırat University, Faculty of Arts & Sciences, Department of Biology, Elazığ, Türkiye*

[2]*Osmaniye Korkut Ata University, Vocational School of Health Services, Osmaniye, Türkiye*

Received: 22 July 2022; Revised: 18 October 2022; Accepted: 24 October 2022

*Corresponding author e-mail: skirbag@firat.edu.tr

Citation: Kırbağ, S.; Bircan, M. G.; Bircan, B. *Int. J. Chem. Technol.* 2022, 6 (2), 97-101.

ABSTRACT

Tchihatchewia isatidea Boiss (Brassicaceae) is popularly known as "Paint and Bridal Flower". Flower pieces and extracts can be used for painting, wound healing, and cough treatments. In this study, the nutritional and medicinal properties of *T. isidea* were determined. For this purpose, carbohydrate, crude oil, crude protein, crude cellulose, energy, crude ash, dry matter, moisture, element, vitamin, antioxidant capacity, DNA protective, and antimicrobial effects of *T. isatidea* were investigated. Crude ash, crude protein, crude fat, crude cellulose, carbohydrate, dry matter, energy, organic matter, K, Ca, Na, Fe, Cu, Zn, Pb, Mn, vitamin E and vitamin A paremeters of *T. Isatidea* were 14.37%, 20.60%, 1.82%, 29.02%, 63.21%, 91.57%, 351.62 kcal 72.20%, 42.5 mg/kg, 102.4 mg/kg, 260 mg/kg, 1.59 mg/kg, 0.121 mg/kg, 1.160 mg/kg, 2.16 mg/kg, 7.49 mg/kg, 22.95 mg/g and 2.82 mg/g, respectively. The DPPH (α, α-Diphenyl-1-picrylhydrazyl) radical scavenging activity of the plant extract was 82.34% at 100 µL, 68.20% at 50 µL, 30.80% at 25 µL and 11.68% at 10 µL. The total oxidant level was 69.96 µmol/L, the total antioxidant level of *T. isatidea* was 3.91 µmol/L and 133.56 nmol/g Malondialdehyde (MDA). In the existence of UV and H_2O_2, it was found that the *T. isatidea* plant extract protects scDNA. It has also been established that the flower extract of the plant hinders the growth of pathogenic microorganisms at varying rates. Because of its thorny structure, the plant which can not be used as a vegetable can be transformed into a dried powdered form of powder and can be consumed with water in the form of a decoction or infusion. The plant can be mixed with powdered petroleum jelly and used as an external wound healing agent.

Keywords: *T. isatidea*, paint flower, nutritional content, antimicrobial activity, antioxidant activity.

Tchihatchewia isatidea Boiss'in besin değeri, antimikrobiyal ve antioksidan aktiviteleri

ÖZ

Tchihatchewia isatidea Boiss (Brassicaceae) halk arasında "Boya ve Gelin Çiçeği" olarak bilinir. Çiçek parçaları ve özleri boyama, yara iyileştirme ve öksürük tedavilerinde kullanılabilmektedir. Bu çalışmada *T. isatidea*'nın besleyici ve tıbbi özellikleri belirlenmiştir. Bu amaçla *T. isatidea*'nın karbonhidrat, ham yağ, ham protein, ham selüloz, enerji, ham kül, kuru madde, nem, element, vitamin, antioksidan kapasite, DNA koruyucu ve antimikrobiyal etkileri araştırıldı. *T. isatidea*'nın ham kül, ham protein, ham yağ, ham selüloz, karbonhidrat, kuru madde, enerji, organik madde, K, Ca, Na, Fe, Cu, Zn, Pb, Mn, E vitamini ve A vitamini parametreleri sırasıyla 14.37%, %20.60, %1.82, %29.02, %63.21, %91.57, 351.62 kcal %72.20, 42.5 mg/kg, 102.4 mg/kg, 260 mg/kg, 1.59 mg/kg, 0.121 mg/kg, 1.160 mg/ kg, 2.16 mg/kg, 7.49 mg/kg, 22.95 mg/g ve 2.82 mg/g olarak bulundu. Bitki ekstraktının DPPH (a, a-Difenil-1-pikrilhidrazil) radikal süpürme aktivitesi 100 µL'de %82.34, 50 µL'de %68.20, 25 µL'de %30.80 ve 10 µL'de %11.68 olarak belirlendi. *T. isatidea*'nın toplam oksidan seviyesi (TOS) 69.96 µmol/L, toplam antioksidan seviyesi (TAS) 3.91 µmol/L ve Malondialdehit (MDA) seviyesi 133.56 nmol/g olarak belirlendi. *T. isatidea* bitki ekstraktının UV ve H_2O_2 varlığında scDNA'yı koruduğu tespit edilmiştir. Bitkinin çiçek özütünün patojenik mikroorganizmaların büyümesini değişen oranlarda engellediği belirlenmiştir. Dikenli yapısından dolayı sebze olarak kullanılamayan bitki, kuru toz haline getirilerek su ile kaynatma veya demleme yöntemiyle tüketilebilir. Bitki, toz vazelin ile karıştırılabilir ve harici bir yara iyileştirici ajan olarak kullanılabilir.

Anahtar Kelimeler: *T. isatidea*, boya çiçeği, besin değeri, antimikrobiyal aktivite, antioksidan aktivite.

1. INTRODUCTION

It is approximated that the number of plant kinds is between 250,000 and 500,000.[1] According to WHO data; 80% of the world population and 95% of the African population benefit from treatment methods based on medicinal plants. It is estimated that about 70,000 medical plant species are utilized for this purpose.

DOI: http://dx.doi.org/10.32571/ijct.1146979 E-ISSN: 2602-277X

Approximately, 21,000 of these plant species are being used in the pharmaceutical industry.[2] *T. isatidea*, is one of the plants used for medical targets and the textile industry in Turkey, which belongs to the Brassicaceae family and is publicly named Paint Flower, Reddish Bride, and Bridal Flower.[3-5] *T. isatidea*, is a paleoendemic species in Turkey, which is generally found in Giresun, Sivas, Gümüşhane, Tunceli, Erzurum, Elazığ, Kars and Erzincan regions of the country. It is known that *T. isatidae* naturally grows in the surroundings of Sivas and Divriği, and its flowers are used as a natural paint material.[3] The extract, which is made by mixing *T isatidea* and *Hesperis schischkinii* Tzvelev (Mus evening star) root parts, and *Pistacia atlantica* Desf. (chewing gum) resin, has been reported to be used in wound healing in Ovacik-Tunceli region.[6] In Eastern Anatolia, it was found that the roots of *T. isatidea* were pounded and used as wound medicine.[7] Around Maden-Elazığ, flowers and root parts of *T. isatidea* have been used as cough suppressants.[4] This study purposed to determine the nutrient content of *T.isatidea* (crude ash, dry matter, crude oil, carbohydrate, crude protein, organic substance, element and vitamin), as well as free radical scavenging activity (DPPH), total antioxidant and oxidant levels, DNA damage reducing effect, and antimicrobial activity.

2. MATERIALS AND METHODS

2.1. Sample collection

T. isatidea was gathered from the surroundings of Karakaş, Baskil-Elazığ, Turkey (’38°37’01.6"N 38°41’46.4"E, 38°34’26.4"N 38°46’37.6"E ve 38°34’34.1"N 38°45’24.6"E’). The plant was collected during the spring season (from April to May). Samples were cleaned, dried, and stored at room temperature.

2.2. Proximate analysis

The approximate compositions of *T. isatidea* containing crude protein, moisture, crude ash, dry matter, organic matter and crude fat were determined accordingly AOAC [7]methods. The determination of total nitrogen (N) were determined by Kjeldahl method. Crude protein was calculated as N×6,25. Crude fat was determined at 550°C using both the total ash combustion and the soxhlet extraction method with a solvent carried out as described by AOAC.

2.3. Element analysis

Previously air-dried samples (at room temperature) were re-dried at 105°C overnight and crushed with pestle and a mortar. Samples were then dissolved in a mixture of HNO_3: H_2SO_4: H_2O_2 (10:1:1, 12 mL for 1 g sample) and heated at 100°C for about 10-15 min. After cooling, 50 mL of deionized water was added to reach 50 mL and then the mixture was filtered. All the glassware was cleaned with deionized water in order to avoid contamination. While amounts of Fe, Zn, Mn, Cu, Cd, Co, Cr, Pb and Ni were determined by atomical absorption spectrometer, amounts of Ca, Na, and K was determined by atomic emission spectrometer.[8]

2.4. Analysis of A, E Vitamins

Plant extract was prepared accordingly literature to determine number of vitamins. Content vitamins were analyzed by HPLC (296 and 326 nm for vitamin E and A, respectively). [9-11]

2.5. Antioxidant assay by DPPH free radical scavenging activity

The DPPH radical scavenging property of plant extract was measured by method of Brand-Williams et al.[12] A solution of 25 mg/L DPPH in methanol was prepared and 4.0 mL of this solution was mixed with 500, 250, 100, and 50 µg/mL of extract. The absorbance of mixture was measured at 517 nm. The reduced absorbance, amount of DPPH remaining, was determined as free radical scavenging activity. Radical scavenging activity (%) = (Abs control – Abs sample) / (Abs control) × 100 where Abs control is absorbance of DPPH radical + methanol; Abs sample is absorbance of DPPH radical + sample extract/standard.

2.6. Determination of MDA, Total Antioxidant activity and Total Oxidant activity

MDA analysis were made according to method described by literatures[10,11,13]. MDA levels were determined by HPLC .TAS and TOS values were measured with Rel Assay brand commercial kits (Rel Assay Kit Diagnostics, Turkey). Trolox was used as a calibrator for TAS tests and results were expressed in mmol Trolox equiv./L.[15] Hydrogen peroxide was used as a calibrator for TOS tests and results were expressed in mmol H_2O_2 equiv./L.[16]

2.7. The Determination of DNA Protective Activity

pBR322 plasmid DNA (vivantis) was used to detect ability of the samples to protect DNA from UV and oxidative damage. Plasmid DNA was damaged with H_2O_2 and UV in the presence of extracts. Taking into consideration that working samples are studied by modifying the method determined by Russo et al.[16], a gel-closure technique was used to prevent them from dispersing into the TBE when mixed with TBE. After sample and control loads were applied on a 1% agarose gel, a 1.5% agarose gel coating was applied to close the wells once more. Then screening was performed.

2.8. Preparation of microorganism cultures

Bacterial strains (*Salmonella enterica typhimirium, Staphylococcus aureus* COWAN 1, *Enterococcus*

DOI: http://dx.doi.org/10.32571/ijct.1146979 E-ISSN: 2602-277X

faecium, Proteus mirabilis, Listeria monocytegenes, B. subtilis, Bacillus megaterium DSM32, *Klebsiella pneumoniae* FMC 5, *Staphylococcus cohnii, Enterobacter aeregenes* CCM 2531, *Escherichia coli* ATCC 25922, *Pseudomonas aeruginosa* DMS50071, *Proteus vulgaris* FMC1) and yeast (*C. tropicalis* ATCC1380, *Candida albicans* FMC17, *C. glabrata* ATCC 66032, *Epidermophyton* sp. and *Trichophyton* sp.) malt extracts in nutrient buyyon were inoculated, respectively (48 h at 25±1°C for yeast, 24 h at 35±1°C for bacteria). Disc Diffusion Method was used in this study. Petri dishes prepared in this manner were incubated at 4°C for 1.5-2 h, then incubated for 24 h at 37±1°C with bacteria-inoculated plates and plates at yeast and dermophyte-grafted plates at 25±1°C for 3 days.[17] The inhibition zones (mm) formed on the feeder at the end of the period were evaluated. Standard antibiotic discs were used for the control group.

3. RESULTS AND DISCUSSION

3.1. Nutritional Content of *T. isatidea*

Crude ash, crude protein, crude fat, crude cellulose, carbohydrate, dry matter and energy paremeters of *T. isatidea* were 14.37%, 20.60%, 1.82%, 29.02%, 63.21%, 91.57%, 351.62 kcal, 72.20% and 351.62 kcal respectively (Table 1).

Table 1. Nutritional Content of *T. isatidea*.

Dry Matter (%)	Crude Ash (%)	Crude Cellulose (%)	Crude Fat (%)
%91.57	**%14.37**	**%29.02**	**%1.82**
Organic Matter (%)	Carbohydrate (%)	Crude Protein (%)	Energy (Kcal)
%77.20	**%63.21**	**%20.60**	**351.62**

3.2. Element Content of *T. isatidea*

Mn, Fe, Zn, Cu and Pb element contents of *T. isatidea* were 7.49 mg / kg, 1.59 mg / kg, 11.60 mg / kg, 0.12 mg / kg and 2.16 mg / kg. Cr, Co and Cd were not detected (Table 2).

3.3. Vitamin content of *T. isatidea*

The vitamin A and vitamin E content of *T. isatidea* were 2.82 µg/g and 22.95 µg/g respectively (Table 3).

Table 2. Element content of T. isatidea

Micro elements	mg kg^{-1}±SD
Mn	7.49±0.12
Fe	1.59±0.03
Zn	11.60±0.11
Cu	0.12±0.01
Pb	2.16±0.07
Cr	0
Co	0
Cd	0

(Study conducted as three replicates and means ± calculated as standard deviation)

Table 3. Vitamin A and vitamin E content of *T. isatidea*.

	Vitamin A	Vitamin E
T. isatidea	2.82 µg/g	22.95 µg/g

3.4. Free radical scavenging activity (DPPH) of *T. isatidea*

According to DPPH (α, α-Diphenyl-1-picrylhydrazyl) free radical clearing results; *T. isatidea* was detected to be effective from 10 µL, and continuing linearly up to 100 µL in a concentration dependent manner (Table 5).

Table 5. Free radical scavenging activity (DPPH) of *T. isatidea*.

DPPH	10 µL	25 µL	50 µL	100 µL
T. isatidea	11.68±0.27	30.80±0.35	68.20±0.56	82.34±1.06

(Study conducted as three replicates and means ± calculated as standard deviation)

MDA was 133.56 nmol / g, TAS was 3.91 mmol Trolox Eq/L and TOS was 6.96 µmol H_2O_2 Eq/L

Table 6. MDA, TAS and TOS values of *T. isatidea*.

MDA	TAS	TOS
133.56 nmol/g	3.91 mmol Trolox Eq/L	6.96 µmol H_2O_2 Eq/L

3.5. DNA protective activity of *T. isatidea*

First 4 lines were used as controls. It was observed three bands (scDNA, linDNA and ocDNA) in 1st and 2nd lines of this study. In the third line, in the presence of H_2O_2, the interaction between UV and DNA resulted in OH radical to damage the DNA. We detected three bands in the 4th line as well (Figure 1). Under the presence of strong UV light and H_2O_2, protection potential of pBR322 plasmid DNA of the *T. isatidea* extracts were observed.

3.6. Antimicrobial activity of *T. isatidea*

Antimicrobial effect of plant is shown on Table 7.

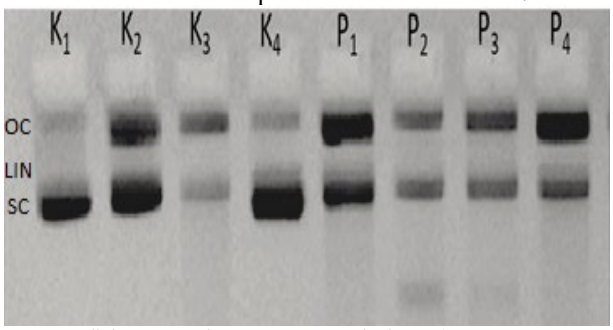

(SC: Supercoiled DNA, LIN: Linear DNA, OC: Open-circular DNA)
C1: Plasmid DNA (3 µL) + distillate water (6 µL)
C2: Plasmid DNA (3 µL) + distillate water (6 µL) + ultraviolet
C3: Plasmid DNA (3 µL) + distillate water (6 µL) + ultraviolet+ hydrogen peroxide (1 µL)
C4: Plasmid DNA (3 µL) + distillate water (6 µL) + hydrogen peroxide (1 µL)
P1: Plasmid DNA (3 µL) + hydrogen peroxide (1 µL) + ultraviolet+ 1/10 Sample (5 µL)
P2: Plasmid DNA (3 µL) + hydrogen peroxide (1 µL) + ultraviolet+ 1/5 Sample (5 µL)
P3: Plasmid DNA (3 µL) + hydrogen peroxide(1 µL) + ultraviolet+ 1/2.5 Sample (5 µL)
P4: Plasmid DNA (3 µL) + hydrogen peroxide (1 µL) + ultraviolet+ 1/1.25 Sample (5 µL)

Figure 1. Gel image showing DNA protection pctivity of *T. isatidea*

DOI: http://dx.doi.org/10.32571/ijct.1146979 E-ISSN: 2602-277X

The development of microorganisms were inhibited best by the extract prepared with methanol, ethanol and water, in order. With the extract prepared by using methanol, the inhibition zone changed between 10-13 mm, and the largest zone was found on *B. subtilis* culture. Ethanol were investigated, inhibition zones between 9-11 mm were observed, and again the extract was most effective on *B. subtilis* culture. The plant extract prepared by using water was not effective on some microorganisms.

3.7. Discussion

Crude ash, crude protein, crude fat, crude cellulose, carbohydrate, dry matter, energy, organic matter, K, Ca, Na, Fe, Cu, Zn, Pb, Mn, vitamin E and vitamin A paremeters of *T. isatidea* were 14.37%, 20.60%, 1.82%, 29.02%, 63.21%, 91.57%, 351.62 kcal 72.20%, 42.5 mg/kg, 102.4 mg/kg, 260 mg/kg, 1.59 mg/kg, 0.121 mg/kg, 1.160 mg/kg, 2.16 mg/kg, 7.49 mg/kg, 22.95 mg/g and 2.82 mg/g, respectively (Table 1). It has been reported that crude ash, crude fat, protein and carbohydrate 0.28%, 0.40%, 2.88%, 8.28% in *E. sativa*[18], cooked broccoli protein 3.80 g/100 g and raw broccoli 4.40 g were determined.[19] In the other study reported Mn 7.49 mg/g, Fe 1.59 mg/g, K 42.05 mg/g, Na 2.60 mg/g, Zn 11.60 Cu 0.12 mg/g, Pb.16 mg/g of *T. isatidea*, Cr and Cd wasn't founded. In *E. sativa*, Mn 30.50 mg/g and Fe 30.89 mg/g, K 2.265 mg/g, Pb 0.22 mg/g, Cr 0.68 and Cd 0.84 mg/g were found.[18] In cabbage and cauliflower, Fe was 0.3 and 0.1 mg/g, respectively.[20] The amounts of Fe in raw broccoli, red cabbage, and white cabbage were determined to be 1.2, 0.6 and 0.4 mg/g, respectively.[21] The contents of element K in cabbage and cauliflower were determined to be 161 and 39 mg/g, respectively.[20] It was determined that the highest amount of Fe element belongs to *E. sativa* when all the data obtained are compared. The elemental amounts of the plant were found to be similar or different from other species. The differences are due to the different occurrence of species, the different habitats, and sometimes even the active substances in different organs of a plant. The amount of vitamin A and E in *T. isatidea* was determined to be 2.82 µg/g, be 22.95 µg/g. Vitamin A of the same plant was determined to be 1.75 µg/g vitamin E 3.96 µg/g.[21] The differences in vitamin amounts in the studies and the high vitamin content may be related to the time and location of the sample collection.

Table 7. Antimicrobial Activity of *T. isatidea.*

	E.coli	*P.vulgaris*	*P.aeruginosa*	*K.pneumoniae*	*C.albicans*
T. and Water	9	-	8	-	-
T. and Ethanol	10	9	10	9	9
T. and Methanol	12	10	11	10	10
Standard	13**	11**	11**	19**	9**
	B.subtilis	*B.megaterium*	*S.aureus*	*L.monocytogenes*	
T. Water	10	-	8	8	
T. Ethanol	11	9	9	10	
T. Methanol	13	10	11	11	
Standard	19**	9**	13**	18*	

It has been determined that the DPPH effect of *T. isatidea* is effective from 10 µL and this effect is linearly increased to 100 µL depending on the concentration. *D. virgate* was detected in DPPH 26.03 IC50 (µg/mL), *D. erucoides* 27.02 IC50 (µg/mL).[22] In the study, it was determined that the DNA protective activity of the plant was variable depending on the concentration of the plant. It has been determined that leaves of *Lepidium latifolium* (Brasicaeae) have DNA protective activity. It is thought that glucosinates detected in plants belonging to Brassicae can protect the cells from DNA damage and can inactivate carcinogens.[23-25] Studies have shown that *T. isatidea* methanol extract inhibits microorganism growth best. *Bacillus subtilis* 14 mm inhibition zone, *Staphylococcus aureus* 16 mm, *Pseudomonas aeruginosa* 17 mm, *Klebsiella pneumoniae* 31 mm, *Escherichia coli* 7 mm, *Enterobacter* sp., The methanolic extract of *Farsetia aegyptia* (Brassicaceae) 4 mm, *Salmonella typhimurium* 10 mm, inhibited their development at different rates, and did not prevent the development of *Candida albicans.*[26] *Diplotaxis virgata* (Cav.); *L. monocytogenes* 20 mm, *S. aureus* 19 mm, P. *aeruginosa* 15 mm, *E. coli* 22 mm, and *K. pneumoniae* 16 mm. An antimicrobial study of the *D. erucoides* (L.) extract was made; *L. monocytogenes* 16 mm, *S. aureus* 20 mm, *P. aeruginosa* 20 mm, *E. coli* 16 mm, and *K. pneumoniae* 17 mm.[22] In this study, it can be said that antimicrobial results are caused by plant species which are different from other studies.

Conclusion

In this study, it was determined that *T. isatidea* nutrient contains, antioxidant and antimicrobial properties as well

DOI: http://dx.doi.org/10.32571/ijct.1146979 E-ISSN: 2602-277X

as many other plants belonging to Brassicaceae. It is especially important to investigate the glucosinates of the plant. Because of its thorny structure, the plant which can not be used as a vegetable can be transformed into a dried powdered form of powder and can be consumed with water in the form of a decoction or infusion. The plant can be mixed with powdered petroleum jelly and used as an external wound healing agent.

ACKNOWLEDGMENT

We thank FUBAP for providing financial resources F. F.16.44.

Conflict of interests

I declares that there is no a conflict of interest with any institute, person, company, etc.

REFERENCES

1. Cowan, M. M.; *Clin Microbiol Rev*. **1999**, 12(4), 564-582.

2. Başaran, A. A.; *MİSED*. **2012**, (27-28), 22-26.

3. Baytop, T.; *İstanbul Üniversitesi Yayınları*, **1984**, (3255).

4. Çakılcıoğlu, U.; Khatun, S.; Turkoglu, I.; Hayta, S.; *J. Ethnopharmacol.* **2011,** 1;137(1):469-86.

5. Gülbağ, F.; *Türkiye Tohumcular Birliği Dergisi*. **2014**, 12-15.137(1), 469-486.

6. Tuzlacı, E.; Doğan, A.; *J.Res.Pharm*. **2010**, 14(1), 136-143.

7. Altundag. E.; Ozturk, M.; *Procd Soc Behv*. **2011**, 19756-777.

8. *AOAC*.; **1990**, ISBN: 0-995584-42-0, ISSN: 0066-961X.

9. Miller, K. W.; Lorr, N. A.; Yang, C. S.; *Analytical Biochemistry*. **1984,** 138(2), 340-345.

10. Cerhata, D.; Bauerova, A.; Ginter, E.; *Ceska Slov Farm*. **1994**, 43(4), 166-168.

11. Karatepe, M.; *LC GC N Am*. **2004**, 22(4), 362-365.

12. Brand-Williams, W.; Cuvelier, M.; Berset, C.; *LWT-Food SCI Technol*. **1995,** 28(1), 25-30.

13. Tavazzi, B.; Lazzarino, G.; Di-Pierro, D.; Giardina, B.; *Free Radical Bio Med.* **1992**, 13(1):75-78.

14. Halliwell, B.; Gutteridge, J. M. C.; *Free Radical Bio Med.* **2000**, p. 617–24).

15. Tarpey, M. M.; Wink, D. A.; Grisham, MB.; *Am J Physiol*. **2004**, 286(3): R431–44.

16. Russo, A.; Acquaviva, R.; Campisi, A.; Sorrenti, V.; DiGiacomo, C.; Virgata, G.; Barcellona, ML.; Vanella, A.; *Cell. Biol. Toxicol*. **2000,** 16: sayfa 91-98.

17. Collins, C. H.; Patricia, M.; Lyne, J. M.; Grange, J. O.; *Falkinham Collins and Lyne's Microbiological Methods*. **2004**, 140-440.

18. Khan, H.; Jan, S. A.; Javed, M.; Shaheen, R.; Khan, Z.; Ahmad, A.; Safi, S. Z.; Imran, M.; *J Food Biochem.* **2016**, 40(1), 61-70.

19. Campbell, B.; Han, D.; Triggs, C. M.; Fraser, A. G.; Ferguson, L. R.; *FFHD.* **2012**, 2(11), 460-486.

20. Gebhardt, S.; Thomas, R.; *Agricultural Research Service, Home and Garden Bulletin*, **2002**, (72).

21. Birişik, A.; Karataş, F.; Yılmaz, S.; Özdemir, F. A.; *Fırat Unv. Journal of Science*. **2013**, 25(1), 1-5.

22. Salah, N. B.; Casabianca, H.; Jannet, H. B.; Chenavas, S.; Sanglar, C.; Fildier, A.; *D. virgata & D. erucoides*, *Molecules*. **2015**, 20(10), 18128-18143.

23. Akan, S.; Veziroğlu, S.; Özgün, Ö.; Ellialtıoğlu, Ş.; *Yüzüncü Yıl Üniversitesi Tarım Bilimleri Dergisi*, **2013**, 23(3), 289-295.

24. Al-Gendy, A. A.; Nematallah, K. A.; Zaghloul, S. S.; Ayoub, N. A.; *Pharm Biol*. **2016**, 54(12), 3257-3263.

25. Blažević, I.; Radonić, A.; Mastelić, J.; Zekić, M.; Skočibušić, M.; Maravić, A.; *Food Chem*. **2010**, 121(4), 1020-1028.

26. Atta, E.; Hashem, A.; Eman, R. S.; *Chem Nat Compd*. **2013**, 49(3), 432-436.

DOI: http://dx.doi.org/10.32571/ijct.1187158 **E-ISSN: 2602-277X**

International Journal of Chemistry and Technology

http://dergipark.org.tr/ijct

Research Article

Effect of phosphogypsum use as a waste recycling on GHG emissions by mineral carbonisation method

Ahmet Ozan GEZERMAN

Toros Agri - Industry, Research & Development Center, Karaduvar, Mersin, Türkiye

Received: 10 October 2022; Revised: 23 December 2022; Accepted: 23 December 2022

*Corresponding author e-mail: ozan.gezerman@toros.com.tr

Citation: Gezerman, A. O. *Int. J. Chem. Technol.* **2022**, 6 (2), 102-107

ABSTRACT

The release of greenhouse gas emissions into the atmosphere as a result of anthropogenic sources and industrial applications has triggered the increase in global temperatures called global warming and related climate change. Phosphogypsum (PG) is a by-product of the wet process phosphoric acid (H_3PO_4) production process, which chemically consists of calcium sulfate dihydrate ($CaSO_4{\cdot}2H_2O$) with some impurities. Annual PG accumulation has reached 300 Mtons and a strategy is needed to ensure efficient, continuous and bulk consumption. Due to the high amount of calcium it contains, PG is a material suitable for use in CO_2 capture and storage processes to form stable solid carbonate compounds. This process, called mineral carbonisation of PG, contributes to sustainable development goals by providing the multiple benefits of both the utilisation of an industrial by-product and the realisation of CO_2 capture and storage technology.

Keywords: Phosphogypsum, carbon capture, accumulation, waste management.

Mineral karbonizasyon yöntemiyle atık geri dönüşümü olarak fosfojips kullanımının sera salımları üzerindeki etkisi

ÖZ

Antropojenik kaynaklar ve endüstriyel uygulamalar sonucu atmosfere sera gazı emisyonlarının salınması, küresel ısınma olarak adlandırılan küresel sıcaklıklardaki artışı ve buna bağlı olarak iklim değişikliğini tetiklemiştir. Fosfojips (PG), kimyasal olarak bazı safsızlıklar içeren kalsiyum sülfat dihidrattan ($CaSO_4.2H_2O$) oluşan, ıslak proses fosforik asit (H_3PO_4) üretim prosesinin bir yan ürünüdür. Yıllık PG birikimi 300 Mton'a ulaşmış olup verimli, sürekli ve toplu tüketimi sağlamak amacıyla bir stratejiye ihtiyaç vardır. PG, içerdiği yüksek kalsiyum miktarı nedeniyle kararlı katı karbonat bileşikleri oluşturmak için CO_2 tutma ve depolama işlemlerinde kullanıma uygun bir malzemedir. PG'nin mineral karbonizasyonu olarak adlandırılan bu süreç, hem endüstriyel bir yan ürünün kullanımının hem de CO_2 yakalama ve depolama teknolojisinin gerçekleştirilmesinin birçok faydasını sağlayarak sürdürülebilir kalkınma hedeflerine katkıda bulunur.

Anahtar Kelimeler: Fosfojips, karbon yakalama, biriktirme, atık yönetimi.

1. INTRODUCTION

1.1. Greenhouse gas emissions and their effects on climate change

Global warming is caused by carbon dioxide emissions released as a result of industrial processes. Along with the carbon dioxide emission resulting from industrial processes, the increase in temperatures in sea water and other living spaces with the effect of sunlight draws attention. This temperature increase has negative consequences such as inefficiency for agricultural work, especially in agricultural areas.[1,2]

Carbon dioxide emissions generally occur from thermal power plants, industrial plants that apply the heating process, and processes that produce petrochemicals. Compared to other greenhouse gases, it is accepted that the main component of increasing greenhouse gas emissions is carbon dioxide (CO_2), which has a share of

DOI: http://dx.doi.org/10.32571/ijct.1187158 E-ISSN: 2602-277X

approximately 64%.[3] If current activities that cause CO_2 emissions continue, stabilisation of greenhouse gas concentrations will not be possible. Fossil fuels are the dominant form in meeting the energy needs on a global scale, and fossil fuel consumption accounts for approximately 75% of anthropogenic CO_2 emissions. It was stated that the annual average increase in CO_2 emissions between 1970 and 2000 had a share of 1.72%, and this rate increased to 2.75% between 2010 and 2014. CO_2 emissions from the energy sector are around 30 billion tons per year and are expected to nearly double by 2050.[4,5] For this reason, stabilizing the CO_2 concentration in the atmosphere is important and it is estimated that CO_2 levels can be reduced by about 85% in the next century, with a decrease of approximately 20 billion tons of CO_2 formation per year.[6,7] This approach requires the adoption of a common goal of controlling global warming by reducing global CO_2 emissions.[8,9] In this context, research on greenhouse gas and carbon neutrality has become widespread and important at the global level. There have been several initiatives in recent history to reduce carbon dioxide emissions. With these initiatives, efforts are made to prevent the worldwide temperature increase caused by carbon dioxide gas.[10,11]

Reducing industrial carbon dioxide emissions, which cause worldwide temperature rise, has been the main goal. Therefore, various processes such as carbon capture and capture come to the fore as an industrial carbon removal method. However, the use of raw materials with low carbon content is also considered as another method to reduce carbon gas emissions. [12,13] The carbon capture and storage method is a critical method accepted by the authorities within the scope of global greenhouse gas emission reduction studies and included in the scenarios.[14] The basic steps of carbon capture and storage methods consist of post-combustion and pre-combustion CO_2 capture, separation from other gases, transport and isolating CO_2 from the atmosphere by storage.[15-17]

1.2. Mineral carbonisation method

Mineral carbonisation is expressed as a decarbonisation process for industrial plants that emit carbon dioxide, using the carbon gas release to create raw materials using the mineralisation method.[18,19] However, there are also challenges such as slowing the kinetics of mineral-fluid reactions and accelerating the carbonation process throughout the process.[20,21]

Alkaline earth metals such as Ca and Mg are the most suitable metals for the mineral carbonisation method. However, due to their highly reactive nature, these metals are rare and generally found in silicate forms.[22] The most common natural silicate minerals are olivine (Mg_2SiO_4), wollastonite ($CaSiO_3$) and serpentine ($Mg_3Si_2O_5(OH)_4$). In addition to natural minerals, industrial solid wastes such as waste ash, waste cement, steel production slag and mine waste are also potential materials that can be used as raw materials in the carbonisation process.[23-25]

1.3. Phosphogypsum as an industrial waste and its recycling mechanism

Phosphogypsum (PG) is a by-product of the "wet process" based on the production of phosphoric acid (H_3PO_4) by the decomposition of natural phosphate rock in sulfuric acid (H_2SO_4) at 70-80 °C. Phosphogypsum is formulated as calcium sulfate containing two moles of water and must be cleaned of toxic elements before it can be used as raw material.[26-30] The PG formed as a result of the process is in the form of sludge in the first stage and is sent to the storage area after the filtering stage. During the long storage period, the sludge loses its water content and sediment formation is observed over time.

Various research studies have been reported in the literature regarding the use of phosphogypsum in agricultural areas.[31-34] PG is used as a setting retarding additive or mineralizing agent in the clinker production process in the cement industry.[35-37] Although there are applications in the building material sector for its use as a filler in gypsum boards, brick manufacturing or road construction, these studies are still under development and cannot yet provide regular and bulk consumption of PG.[38]

Phosphogypsum is formed during the production of phosphoric acid and its amount may increase depending on the production capacity of phosphoric acid.[39,40] Due to the internal contamination of phosphogypsum, its use as a raw material is not common and requires pretreatment for cleaning before use.[41-45]

Since the use of phosphogypsum, which is produced as a waste in phosphoric acid processes, as a raw material is very limited, it is necessary to work on various methods to improve the raw material properties.[46,47] In recent studies carried out within the scope of reuse studies of PG, it has been stated that natural ores or industrial wastes show good efficiency in the production of sulfate compounds, and there are various studies for the conversion of gypsum to alkaline sulfates such as $(NH_4)_2SO_4$, K_2SO_4, Na_2SO_4. Studying the mineral carbonation process by reacting phosphogypsum with magnesium, calcium and silicon salts can be considered as important steps towards carbon dioxide removal. It has been stated that the use of PG or FGD is more advantageous than other industrial wastes.

1.4. Mineral carbonisation of phosphogypsum

Although the impurities it contains limit the usage area, there are also environmentally friendly applications for the recovery of PG. One of these approaches includes the use of PG as a calcium source in the CO_2 capture capture

DOI: http://dx.doi.org/10.32571/ijct.1187158 E-ISSN: 2602-277X

process to reduce greenhouse gas emissions.[48-50] Phosphogypsum contains a significant amount of calcium and does not require a different granulation process due to its low particle size, therefore, it does not cause any energy cost in terms of pre-treatment of phosphogypsum.[51-54]

The carbonisation process of PG can be done with various alkaline sources. In the mineral carbonisation of PG, PG acts as a carbon scavenger in the form of $Ca(OH)_2$ in the first stage. Sulphate is obtained by alkali dissolution using soda, and then mineral carbonate is formed by the instantaneous reaction with CO_2.[55] In another mineral carbonisation approach, ammonium hydroxide (NH_4OH) is used as an alkali source. In this case, in the first stage, ammonium carbonate ($(NH_4)_2CO_3$) is formed by the reaction of $(NH_4)OH$ with CO_2, in the next stage ammonium sulfate ($(NH_4)_2SO_4$) and limestone ($CaCO_3$) are formed by the reaction of $(NH_4)_2CO_3$ and PG.[56-58]

Carbonate and sulfate salts formed as a result of mineral carbonisation of PG are used as filling materials for various applications in the fertilizer and building materials industry. As a result of the mineral carbonisation process, both economically valuable products are obtained and large amounts of CO_2 are converted into stable solids in the form of carbonate in accordance with carbon emission control strategies. Mineral carbonisation can be carried out by processes such as membrane electrolysis or thermal degradation.[59]

2. RESULTS AND DISCUSSION

2.1. Environmental evaluation of mineral carbonisation of phosphogypsum

Phosphogypsum may contain various elemental contamination such as Fe and Al during storage due to process conditions and raw material properties. Environmental problems may occur in the long term due to the disposal and regular storage of PG, its limited recycling due to its chemical structure, and the limitation of its use in different industrial areas, especially its radionuclide content. While there are various studies on the use of phosphogypsum as a raw material, the use of phosphogypsum as a raw material in these processes is well below the production amount of phosphogypsum, and its use in the decarbonsation process by using it together with carbon dioxide will provide significant benefits to the greenhouse gas emission process.[60,61]

The high amounts of calcium and sulfur in phosphogypsum make it a valuable by-product. In this context, the methods to be developed for the evaluation of PG can be evaluated as a positive solution both in terms of using the stored material as raw material in the production of products with added value, and as an environmentally positive solution within the framework of waste minimisation.[62] Previous studies on environmental applications of PG indicate that PG is a suitable raw material as a mineral carbonisation process to reduce CO_2 emissions, especially within the framework of the CO_2 capture capture method.[63-65] Again, according to literature studies, 100-280 Mtons of PG can bind 26-72 Mtons of CO_2. In this context, approximately 1:5 mass (PG:CO_2) consumption can be achieved as a result of mineral carbonisation of PG.

3. CONCLUSIONS

The amount of CO_2 released into the atmosphere as a result of industrial applications has reached 30 Gtons per year. Such a large and continuous release of CO_2 causes some climatic consequences, especially global warming and climate change problems. Within the scope of combating global warming, which aims to reduce CO_2 emissions, carbon capture and storage technologies are at the forefront. Mineral carbonisation processes ensure that CO_2 is stored as stable solid carbonates, preventing further CO_2 release.

Phosphogypsum, which is released as a reaction product in the production of phosphoric acid, can be used as an industrial raw material in processes such as the ceramic industry. However, the amount of use in these processes is far below the production rate. Storage due to the toxic contamination it contains brings environmental risks. Therefore, the use of phosphogypsum as a raw material in larger scale industries is becoming important.

The increase in carbon dioxide emissions as a result of industrial processes causes an increase in temperature in the atmosphere and climate irregularities. Various decarbonsation methods are being studied to reduce carbon dioxide emissions. Mineral carbonsation is one of the important processes that stand out among these processes. Increasing the raw material properties with the phosphogypsum mineral carbonsation process will be a very important step in reducing industrial carbon emissions.

Conflict of interests

I declares that there is no a conflict of interest with any person, institute, company, etc.

REFERENCES

1. Ajam, L.; Ouezdou, M B.; Felfoul, H. S.; El Mensi, R. Characterisation of the Tunisian phosphogypsum and its valorisation in clay bricks, *Constr Build Mater*, **2009**;23:3240-3247.

2. Altiner, M. Effect of alkaline types on the production of calcium carbonate particles from gypsum waste for fixation of CO_2 by mineral carbonation, *Int. J. Coal Prep. Util,* **2019**;39: 113-131.

DOI: http://dx.doi.org/10.32571/ijct.1187158 E-ISSN: 2602-277X

3. Azdarpour, A.; Asadullah, M.; Junin, R.; Manan, M.; Hamidi, H.İ; Mohammadian, E.; Direct carbonation of red gypsum to produce solid carbonates, *Fuel Process. Technol.*;**2014**; 126: 429- 434.

4. Bao, W.; Zhao, H. Li; H.; Li, S.; Lin, W. Process simulation of mineral carbonation of phosphogypsum with ammonia under increased CO_2 pressure, *J. CO_2 Util.*; **2017**;17: 125-136.

5. Berghout, N.; van den Broek, M.; Faaij, A. Techno-economic performance and challenges of applying CO_2 capture in the industry: A case study of five industrial plants, *Int. J. Greenh. Gas Control.;* **2013**;17: 259-279.

6. Binnemans, K.; Jones, P. T.; Blanpain, B.; van Gerven, T.; Pontikes, Y. Towards zero-waste valorisation of rare-earth-containing industrial process residues: a critical review, *J. Clean. Prod.*; **2015**; 99: 17-38.

7. Canovas, C. R.; Chapron, S.; Arrachart, G.; Pellet-Rostaing, S. Leaching of rare earth elements (REEs) and impurities from phosphogypsum: A preliminary insight for further recovery of critical raw materials, *J. Clean. Prod.*; **2019**;219: 225-235.

8. Canovas, C. R.; Perez-Lopez, R.; Macias, F.; Chapron, S.; Nieto, J. M.; Pellet-Rostaing, S. Exploration of fertilizer industry wastes as potential source of critical raw materials, *J. Clean. Prod.*; **2017**;143: 497-505.

9. Cardenas-Escudero, C.; Morales- Florez, V.; Perez-Lopez, R.; Santos, A.; Esquivias, L. Procedure to use phosphogypsum industrial waste for mineral CO_2 sequestration, *J. Hazard. Mater.*; **2011**;196: 431-435.

10. Chen, J.; Wang, Y.; Shi, Q.;Peng, X.; Zheng, J. An international comparison analysis of CO_2 emissions in the construction industry, *Sustain. Dev.*; **2021**;29: 754-767.

11. Chernysh, Y.; Yakhnenko, O.; Chubur, V.; Roubik, H. Phosphogypsum recycling: A review of environmental issues, current trends, and prospects, *Appl. Sci.;* **2021**;11: 1575-1585.

12. Choura, M.; Maalouf, F.; Keskes, M.; Cherif, F. Sulphur matrix from phosphogypsum: a sustainable route to waste valorisation, Beneficiation of Phosphates: *New Thought, New Technology, New Development*, **2012**; 1:297-302.

13. Chen, Q.; Ding, W.; Sun, H.; Peng, T.; Ma, G. Indirect mineral carbonation of phosphogypsum for CO_2 sequestration, *Energy*, **2020**;206: 118148.

14. Danielik, V.; Fellner, P.; Jurisova, J.; Kralik, M. Determination of the reactivity of $CaSO_4.2H_2O$, *Acta Chim. Slov.*;**2016**; 9 : 1-5.

15. Davis, S. J.; Caldeira, K.; Matthews, D. H. Future CO_2 emissions and climate change from existing energy infrastructure, *Science*, **2010**;329: 1330-1333.

16. Dri, M.; Sanna, A.; Maroto-Valer, M. M. Dissolution of steel slag and recycled concrete aggregate in ammonium bisulphate for CO_2 mineral carbonation, *Fuel Process. Technol.*; **2013**;113: 114-122.

17. Dri, M.; Sanna, A.; Maroto-Valer, M. M. Mineral carbonation from metal wastes: Effect of solid to liquid ratio on the efficiency and characterisation of carbonated products, *Appl. Energy*, **2014**,113: 515- 523.

18. Ennaciri, Y.; Bettach, M.; Cherrat, A.; Zegzouti, A. Conversion of phosphogypsum to sodium sulfate and calcium carbonate in aqueous solution, *J. Mater. Environ. Sci.*; **2016**;7: 1925-1933.

19. Esquivias, L.; Morales-Florez, V.; Santos, A. 9-Carbon dioxide sequestration by phosphogypsum based procedure, Carbon Dioxide Sequestration in Cementitious Construction Materials, *Woodhead Publishing Series in Civil and Structural Engineering*.**2018**.

20. Gadikota, G.; Matter, J.; Kelemen, P.; Park, A. A. Chemical and morphological changes during olivine carbonation for CO_2 storage in the presence of NaCl and $NaHCO_3$, *Phys. Chem. Chem. Phys*, **2014**;16: 4679-4693.

21. Gibbins, J.; Chalmers, H. Carbon capture and storage, *Energy Policy*, 2008;36: 4317-4322.

22. Goodwin, P.; Katavouta, A.; Roussenov, V. M.; Foster, G. L.; Rohling, E. J.; Williams, R. G. Pathways to 1.5 °C and 2°C warming based on observational and geological constraints, *Nat. Geosci.*; **2018**;11: 102-107.

23. Hammas- Nasri, I.; Elgharbi, S.; Ferhi, M.; Horchani-Naifer, K.; Ferid, M. Investigation of phosphogypsum valorisation by the integration of the Merseburg method, *New J. Chem.*; **2020**;44: 8010-8017.

24. Hammi, K. M.; Hammi, H.; Hamzaoui, A. H. Use of mixture design approach for the optimisation and performance of cost- effective cementitious quaternary system: Portland cement- fly ash- silica fume-phosphogypsum, *Chemistry Africa*, **2021**;4: 835-848.

25. Hanein, T.; Simoni, M.; Woo, C. L.; Provis, J. L.; Kinoshita, H. Decarbonisation of calcium carbonate at atmospheric temperatures and pressures, with simultaneous CO_2 capture, through production of sodium carbonate, *Energy Environ. Sci.*; **2021**;14: 6595-6604.

26. Huang, Y.; Qian, J.; Lu, L.; Zhang, W.; Wang, S.; Wang, W.; Cheng, X. Phosphogypsum as a component of calcium sulfoaluminate cement: Hazardous elements

DOI: http://dx.doi.org/10.32571/ijct.1187158 E-ISSN: 2602-277X

immobilisation, radioactivity and performances, *J. Clean. Prod.*; **2020**;248: 119287-119296.

27. Hudson-Edwards, K. A.; Jamieson, H. E.; Lottermoser, B. G.; Mine wastes: Past, present, future, *Elements*, **2011**;7: 375-380.

28. Huijgen, W. J. J.; Witkamp, G. J.; Comans, R. N. J. Mineral CO_2 sequestration by steel slag carbonation, *Environ. Sci. Technol.;* **2005**;39: 9676-9682.

29. Idboufrade, A.; Bouargane, B.; Ennasraoui, B.; Biyoune, M. G.; Bachar, A.; Bakiz, B.; Atbir, A.; Billah, S. M. Phosphogypsum two-step-ammonia-carbonation resulting in ammonium sulfate and calcium carbonate synthesis: Effect of the molar ratio OH^-/Ca^{2+} on the conversion process, *Waste Biomass Valor.*; **2021**;93.

30. IFA, Phosphogypsum: Leadership, innovation, partnership, https://www.fertilizer.org/member/Download.aspx?PUBKEY=CF5FFAD6-0DBA-4473-BEE2-6D3B15280CBA (10.12.2021).

31. Jia, R.; Wang, Q.; Luo, T.; Reuse of phosphogypsum as hemihydrate gypsum: The negative effect and content control of H3PO4, *Resour Conserv Recycl*, **2021**; 174: 105830-105840.

32. Kandil, A. T.; Cheira, M. F.; Gado, H. S.; Soliman, M. H.; Akl, H. M. Ammonium sulfate preparation from phosphogypsum waste, *J. Radiat. Res. Appl. Sci.*; **2017**;10: 24-33.

33. King, A. D.; Sniderman, J. M. K.; Dittus, A: J.; Brown, J. R.; Hawkins, E.; Ziehn, T. Studying climate stabilisation at Paris Agreement levels, *Nat. Clim. Change.*; **2021**;11: 1010-1013.

34. Kuramochi, T.; Ramirez, A.; Turkenburg, W.; Faaij, A. Comparative assessment of CO_2 capture technologies for carbon- intensive industrial processes, *Prog. Energy Combust. Sci.*; **2012**;38: 87-112.

35. Lachehab, A.; MErtah, O.; Kherbeche, A.; Hassoune, H. Utilisation of phopshogypsum in CO_2 mineral sequestration by producing potassium sulphate and calcium carbonate, *Minerals Science for Energy Technologies*, **2020**;3: 611-625.

36. Lambert, A.; Tam, J.; Azimi, G. Microwave treatment for extraction of rare earth elements from phopshogypsum, *Rare Met.*; **2017**; 1:47-53.

37. Li, Z.; Xie, Z.; Deng, J. He, D.; Zhao, H.; Liang, H. Leaching kinetics of rare earth elements in phosphoric acid from phosphate rock, *Metals*, **2021**;11: 239-245.

38. Mattila, H. P.; Zevenhoven, R. Mineral carbonation of phosphogypsum waste for production of useful carbonate and sulfate salts, *Front. Energy Res.*; **2015**;3: 48-55.

39. Metzger, R. A.; Benfors, G.; Hoffert, M. I. To bury or to burn: Optimum use of crop residues to reduce atmospheric CO_2, *Clim. Change*, **2002**;54: 369-374.

40. Min, C.; Shi, Y.; Liu, Z. Properties of cemented phosphogypsum (PG) backfill in case of partially substitution of composite Portland cement by ground granulated blast furnace slag, *Constr Build Mater*, **2021**;305: 124786.

41. Mosher, K.; He, J.; Liu, Y.; Rupp, E.; Wilcox, J. Molecular simulation of methane adsorption in micro- and mesoporous carbons with applications to coal and gas shale systems, *Int. J. Coal Geol.;* **2013**;109-110: 36-44.

42. Oelkers E. H.; Gislason, S. R.; Matter, J. Mineral carbonation of CO_2, *Elements*, **2008**;4: 333-337.

43. Olajire, A. A. CO_2 capture and separation technologies for end-of-pipe applications- A review, *Energy*,**2010**; 35: 2610-2628.

44. Olajire, A. A. A review of mineral carbonation technology in sequestration of CO_2, *J. Pet. Sci. Eng.*; **2013**;109: 364-392.

45. Ren.; K.; Cui, N.; Zhao, S.; Zheng, K.; Ji, X.; Feng, L.; Cheng, X.; Xie, N. Low-carbon sustainable composites from waste phosphogypsum and their environmental impacts, *Cryst.;* **2021**;11: 719-725.

46. Rendel, P. M. The kinetics and thermodynamics of gypsum precipitation under conditions relevant to CO_2 geological storage, PhD Thesis, Ben-Gurion University, Israel.2018

47. Romero-Hermida, I.; Santos, A.; Perez-Lopez, R.; Garcia- Tenorio, R.; Esquivias, L.; Morales-Florez, V. New method for carbon dioxide mineralisation based on phosphogypsum and aluminium-rich industrial wastes resulting in valuable carbonated by-products, *J. CO_2 Util.;* **2017**;18: 15-22.

48. Romero-Hermida, M. I.; Flores-Ales, V.; Hurtado-Bermudez, S.J.; Santos, A.; Esquivias, L. Environmental impact of phosphogypsum-derived building materials, *Int. J. Environ. Res.* Public Health.; **2020**;17: 4248-4255.

49. Rychkov, V. N.; Kirillov, E. V.; Kirilov, S. V.; Semenishchev, V. S.; Bunkov, G. M.; Botalov, M. S.; Smyshlyaev, D. V.; Malyshev, A. S. Recovery of rare earth elements from phosphogypsum, *J. Clean. Prod.;* **2018**;196: 674-681.

DOI: http://dx.doi.org/10.32571/ijct.1187158 E-ISSN: 2602-277X

50. Shang, D.; Geissler, B.; Mew, M.; Satalkina, L.; Zenk, L.; Tulsidas, H.; Barker, L.; El-Yahyaoui, A.; Hussein, A.; Taha, M.; Zheng, Y.; Wang, M.; Yao, Y.; Liu, X.; Deng, H.; Zhong, J.; Li, Z.; Steiner, G.; Haneklaus, N.; Unconventional uranium in China's phosphate rock: Review and outlook, *Renew. Sust. Energ. Rev.*; **2021**;140: 110740-110745.

51. Sanna, A.; Uibu, M.; Caramanna, G.; Kuusik, R.; Maroto-Valer, M. M. A review of mineral carbonation technologies to sequester CO_2, *Chem. Soc. Rev.;* **2014**;43: 8049-8080.

52. Snaebjörnsdottir, S. O.; Sigfusson, B.; MArieni, C.; Goldberg, D.; Gislason, S. R.; Oelkers, E. H. Carbon dioxide storage through mineral carbonation, *Nat. Rev. Earth Environ*.**;** **2020**;1: 90-102.

53. Svensson, R.; Odenberger, M.; Johnsson, F.; Strömberg, L. Transportation systems for CO_2 application to carbon capture and storage, *Energy Convers. Manag*.; **2004**; 45: 2343-2353.

54. Tan, Y.; Process simulation of the influence of phosphate rock impurities on the production index of superphosphate, *IOP Conf. Ser.: Earth Environ. Sci*.; **2021**;772: 012047-012055.

55. Xiao, W.; Yao, X.; Zhang, F. Recycling of oily sludge as a roadbed material utilizing phosphogypsum-based cementitious materials, *Adv. Civ. Eng*, **2019**;1: 6280715-628725.

56. Xie, H.; Wang, J.; Hou, Z.; Wang, Y.; Liu, T.; Tang, L.; Jiang, W. CO_2 sequestration through mineral carbonation of waste phosphogypsum using the technique of membrane electrolysis, *Environ. Earth Sci*.; **2016**;75: 1216-1222.

57. Van Soest, H.; Elzen, M. G. J.; Vuuren, D. P. Net-zero emission targets for major emitting countries consistent with the Paris Agreement, *Nat. Commun*.; **2021**;12: 2140-2155.

58. Wei, Z.; Deng, Z. Research hotspots and trends of comprehensive utilisation of phosphogypsum: Bibliometric analysis, *J. Environ. Radioact*.; **2022**;1:106778-106785.

59. Yadav, V. K.; Yadav, K. K.; Cabral- Pinto, M. M. S.; Choudhary, N.; Gnanamoorthy, G.; Tirth, V.; Prasad, S.; Khan, A. H.; Islam, S.; Khan, N. A. The processing of calcium rich agricultural and industrial waste for recovery of calcium carbonate and calcium oxide and their application for environmental cleanup: A review, *Appl. Sci*.**;** **2021**;11: 4212-4217.

60. Yang, L.; Zhang, Y.; Yan, Y. (2016), Utilisation of original phosphogypsum as raw material for the preparation of self-leveling mortar, J. Clean. Prod.; **2016**;127: 204-213.

61. Zandalinas, S. I.; Fritschi, F. B.; Mittler, R. Global warming, climate change, and environmental pollution: Recipe for a multifactorial stress combination disaster, *Trends Plant Sci*, **2021**;26: 588-599.

62. Zhang, W.; Zhang, F.; Ma, L.; Yang, J.; Wei, Y.; Kong, D. CO_2 capture and process reinforcement by hydrolysate of phosphogypsum decomposition products, *J. CO_2 Util*, **2020**;36: 253-262.

63. Zhao, H.; Li, H.; Bao, W.; Wang, C.; Li, S.; Lin, W. Experimental study of enhanced phosphogypsum carbonation with ammonia under increased CO_2 pressure, *J. CO_2 Util*, **2015**;11: 10-19.

64. Zhao, Q.; Liu, C.; Jiang, M.; Saxen, H.; Zevenhoven, R. Preparation of magnesium hydroxide from serpentinite by sulfuric acid leaching for CO_2 mineral carbonation, *Miner. Eng*.**;** **2015**;79: 116-124.

65. Zhao, S.; Ma, L.; Yang, J.; Zheng, D.; Liu, H.; Yang, J. Mechanism of CO_2 capture technology based on the phosphogypsum reduction thermal decomposition process, *Energy Fuels*, **2017**;31: 9824-9832.

DOI: http://dx.doi.org/10.32571/ijct.1171249 **E-ISSN: 2602-277X**

International Journal of Chemistry and Technology

http://dergipark.org.tr/ijct

Research Article

Effect of different salt concentrations on some forage pea cultivars during germination and early seedling stage

Nilay KAYIN[1*], Ferzat TURAN[2], Emine Serap AYDEMİR[3]

[1]*Department of Biotechnology, Faculty of Agriculture and Natural Sciences, Bilecik Şeyh Edebali University, Bilecik 11050, Türkiye*

[2] *Department of Field Crop, Faculty of Agriculture, Sakarya university of applied sciences, Sakarya 54580, Türkiye*

[3]*Field Crops, Faculty of Agriculture and Natural Sciences, Bilecik Şeyh Edebali University, Bilecik 11050, Türkiye*

Received: 6 September 2022; Revised: 9 November 2022; Accepted: 14 November 2022

*Corresponding author e-mail: nilaykayin@gmail.com

Citation: Kayın, N.; Turan, F.; Aydemir, E.S. *Int. J. Chem. Technol.* **2022**, 6 (2), 108-113.

ABSTRACT

In the present study, in order to reveal the differences in the germination of forage pea varieties at different salt concentrations and the differences in the physical properties of the roots and seedlings, the effect of different salt concentrations on nine different varieties of forage peas was carried out in Bilecik Şeyh Edebali University, Faculty of Agriculture and Natural Sciences, Agricultural Research and Biotechnology Center Laboratories in 2022. The effects of different salt concentrations (0, 25, 50, 75, 100, 125, 150, 175 and 200 mM) on nine forage pea cultivars (cv. Ürünlü, cv. Töre, cv. Ateş, cv. Guifredo, cv. Taşkent, cv. Özkaynak, cv. Kurtbey, cv. Uysal and cv. Nany) during the germination and early seedling stage were examined. The experiment was carried out according to Completely Randomized Factorial Designs with 3 replications. In the research; germination speed and power, root dry and fresh weight, root dry and fresh length, seedling dry and fresh weight, seedling dry and fresh length were investigated. According to the results obtained, a significant decrease was observed in germination speed and power, root dry and fresh weight, root dry and fresh length, seedling dry and fresh weight, seedling dry and fresh length of forage pea cultivars due to increasing salt concentration. It was determined that cv. Töre field pea has the highest germination rate and power. In addition, cv. Töre is followed by cv. Ateş in all parameters. The cultivars with the lowest germination rate and vigour were cv. Guifredo and cv. Uysal. As a result, the growth of forage pea varieties slowed down due to increasing salt concentration.

Keywords: Field Pea (*Pisum arvense L.*), salt stress, germination, seedling growth

Bazı yem bezelye çeşitlerinde farklı tuz konsantrasyonlarının çimlenme ve erken fide aşamasında etkisi

ÖZ

Bu çalışmada, farklı tuz konsantrasyonların da yem bezelyesi çeşitlerinin çimlenme ve oluşan kök ve fidelerin fiziksel özelliklerindeki farklılıklarını ortaya koymak amacıyla, farklı tuz konsantrasyonun yem bezelyesinin dokuz farklı çeşidi üzerine etkisi incelenmek üzere Bilecik Şeyh Edebali Üniversitesi Ziraat ve Doğa Bilimleri Fakültesi Tarımsal Araştırma ve Biyoteknoloji Merkezi Laboratuvarlarında 2022 yılında gerçekleştirilmiştir. Biri kontrol ve sekiz farklı tuz konsantrasyonunun (25, 50, 75, 100, 125, 150, 175 ve 200 mM) dokuz farklı yem bezelye çeşidinin (Ürünlü, Töre, Ateş, Guifredo, Taşkent, Özkaynak, Kurtbey, Uysal ve Nany) çimlenme ve fide gelişimi üzerine etkileri incelenmiştir. Deneme 3 tekerrürlü olarak tesadüfi parselleri faktöriyel deneme desenine göre yürütülmüştür. Araştırmada, çimlenme hızı ve gücü, kök kuru ve yaş ağırlığı, kök kuru ve yaş uzunluğu, fide kuru ve yaş ağırlığı, fide kuru ve yaş uzunluğu incelenmiştir. Elde edilen sonuçlara göre yem bezelyesi çeşitlerinde artan tuz konsantrasyonuna bağlı olarak, çimlenme hızı ve gücü, kök kuru ve yaş ağırlığı, kök kuru ve yaş uzunluğu, fide kuru ve yaş ağırlığı, fide kuru ve yaş uzunluğunda belirgin bir azalış gözlenmiştir. En yüksek çimlenme hızı ve gücüne sahip olan Töre yem bezelyesi çeşidi olarak tespit edilmiştir. Ayrıca Ateş çeşidi tüm parametrelerde Töre çeşidini takip etmiştir. En düşük çimlendirme hızı ve gücüne sahip çeşitler ise Guifredo ve Uysal tespit edilmiştir. Sonuç olarak artan tuz konsantrasyonuna bağlı olarak yem bezelyesi çeşitlerinin gelişimi yavaşlamıştır.

Anahtar Kelimeler: Yem bezelyesi (*Pisum arvense L.*), tuz stresi, çimlenme, fide gelişimi.

DOI: http://dx.doi.org/10.32571/ijct.1171249 E-ISSN: 2602-277X

1. INTRODUCTION

As a result of the rapid increase in the world population day by day, balanced and adequate nutrition problem has emerged and this situation has increased the importance of agricultural areas and animal production. Parallel to the population increase, the number of animals could not be increased to the desired level and this situation was also reflected in the red meat prices. In addition, adequate attention has not been given to the correct management of pastures and improvement studies and to increase the cultivation areas of forage crops for ensuring the adequate and balanced feeding of our current animals. However, animal husbandry is extremely important in terms of the development of countries, increasing export potential, supplying raw materials to industry, preventing unemployment in rural areas, and providing new employment.[1-3]

In countries with developed animal husbandry, the cultivation rate of forage crops constitutes 25% of the total agricultural land in England, 30% in Italy, 31% in the Netherlands and 36% in Germany.[4] It constitutes 13.65% in Türkiye and this ratio needs to be increased in order to close the roughage deficit in the country.[4,5] For this reason, field pea (*Pisum arvense L.*), which has a high nutritional value and is preferred by animals, is an important forage plant at the point of closing this deficit. In addition, field peas, whose grains, green and dry grass are used as a forage plant, are preferred both as a pasture plant and as a green manure crop.[5-7] In addition, field peas which are grown for animal feeding as silage are delicious as well as their high nutritional value.[8] However, salinity is an important problem for forage crops, especially for field peas.[9]

While plants continue their lives, diseases, damages or physiological changes occur that prevent their development. The negative changes that occur in the plant in these situations, are called stress. This stress is the condition that prevents growth, development and metabolism in the plant. Stress first negatively affects the metabolic and physiological mechanisms, and then causes damage to the plant and a decrease in product quality. Stress factors are divided into two as abiotic and biotic agents according to their source. Stress factors show their effects on the plant simultaneously and in combination. Abiotic stress agents are environmental factors such as temperature, frost, drought, salinity, excess water, radiation, oxidative stress, wind, various chemicals and nutrient deficiency in the soil, while biotic stress agents are pathogens, insects and herbivores including viruses, bacteria and fungi.[5,10]

Biotic and abiotic stress factors significantly limit plant growth and cause large yield losses in agriculture.[11,12] Especially abiotic stress factors prevent the survival of plants. The importance of these stress factors will increase in the future due to global climate change. According to 2003 report of the Intergovernmental Panel on Climate Change, crop production in Europe has decreased by about 30% due to the stress factors[9,13] salinity which is one of the abiotic stress factors, is the primary factor that will directly affect crop yield today and in the future.[13-16] According to the data of Food and Agriculture Organization of the United Nations (FAO, 2018), the area of salty soils in the world continues to increase regularly, data claims that 50% of them will face salinity problem by 2050.[5,14,17] Currently, over 6% of the world's land area and 20% of the world's irrigated land is affected by salinity salinity causes water deficit by reducing the osmotic potential of the solutes in the soil, even in well-irrigated soils, thus making it difficult for the roots to draw water from the surrounding environment (soil solution).[18,19]

Salinity is the accumulation of salt near the soil surface when the salts mixed with the groundwater due to washing in arid and semi-arid regions reach the soil surface by capillary way and the water evaporates and leaves the soil. This situation changes the soil structure and causes significant losses in plant yield and quality. In addition, salinity is not a concept limited to arid and semi-arid regions. The reason is that all soils and water resources on the earth contain a certain amount of salt, regardless of their quality.[5,20]

It is critical to study different genotypes of abiotic stress factor such as salt stress in order to grow field peas efficiently. Due to this critical situation, Avcı et al.[21] and Demirkol et al.[5] studied the effects of salt stress on the germination and early seedling growth of field pea in Türkiye. In another study, Okçu et al.[22], Petrovic et al.[23], and Pereira et al.[24] studied the responses of different pea genotypes to salt stress. In addition, they revealed that salinity reduces root and seedling formation and explained that this effect is dependent on salt concentration differences. The aim of this research is to evaluate the relationship between germination rate and germination rate and root and seedling growth of four types of field pea genotypes in sterile conditions and at different salt concentrations. The purpose of the study was to determine the germination rates and strengths, fresh and dry weights of some proprietary feed peas at different salt concentrations, and to improve this characteristic of feed pea varieties with low salinity tolerance by gene transfer in the continuation of the study.

2.MATERIALS AND METHODS

This study was carried out in 2022 at Bilecik Şeyh Edebali University Faculty of Agriculture and Natural Sciences Agricultural Research and Biotechnology Center Laboratories to examine the effects of different salt concentrations on germination and seedling

DOI: http://dx.doi.org/10.32571/ijct.1171249 E-ISSN: 2602-277X

development in nine different cultivars of field peas. Registered varieties such as cv. Ürünlü, cv. Töre, cv. Ateş, cv. Guifredo, cv. Taşkent, cv. Özkaynak, cv. Kurtbey, cv. Uysal and cv. Nany was used in the study. Nine different concentrations of NaCl (0, 25, 50, 75, 100, 125, 150, 175 and 200 mM) solutions were used in the study. Six ml of NaCl solution for each doses were added to each petri dishes containing five forage pea seeds. The seeds were firstly subjected to surface sterilization by mixing them with a 20% bleach solution for 7 minutes. Germination papers were first placed in sterile petri dishes, then 6 ml of NaCl solutions were added, and the seeds with surface sterilization were placed in each petri dishes with forceps as to be 5 seeds each. Afterwards, it was left to germinate for 8 days at 20±2°C in the climate chamber. The seeds were checked daily and the seeds with a rootlet length of 2 mm were considered as germinated. Seed germination speed at the end of the 5th day and the seed germination power at the end of the 8th day were calculated as described by Demirkol et al.[5] and Okçu et al.[22]. Mean germination speed/ power was calculated with the formula of Ellis and Roberts[25]:

Germination Seed/ Power (%) = (Number of germinated seeds/total number of seeds) ×100

2.1.Determining the root and seedling lengths

At the end of the 8th day, the roots and seedlings of the germinated seeds were cut with the help of a scalpel. The lengths of these roots and seedlings were measured with the help of a ruler.

2.2.Measuring the fresh and dry weights of the roots and seedlings

At the end of the 8th day, the roots and seedlings of the germinated seeds were cut with the help of a scalpel. Each of these roots and seedlings was weighed on sensitive scales and their wet weights were determined. Then, each root and seedling were dried in an oven at 65°C for 48 hours and dry weights were measured on a precision scale.

2.3.Statistical analysis

Data were subjected to Completely Randomized Factorial Designs analysis of variance, and the post hoc tests were performed using Duncan's Multiple. [26]

3.RESULTS AND DISCUSSION

In the study, it was revealed that different salt concentrations have significant effects on the germination and seedling growth of field pea varieties. It was revealed that cv. Töre, cv. Ateş, cv. Özkaynak and cv. Taşkent field pea cultivars had high germination rates.

Among these varieties, cv. Töre showed salt tolerance up to 175 mM salt concentration. It was determined that the germination rate of cv. Töre and cv. Taşkent at 200 mM salt level decreased by compared to the control condition. In cv. Guifredo and cv. Uysal, the germination rate at 25 mM salt concentration decreased according to the control condition. At 200 mM salt concentration, in addition to cv. Uysal, the germination rate decreased in cv. Urunlu, cv. Ozkaynak, cv. Kurtbey and cv. Nany according to the control condition. In general, it was determined that the increase in salt concentration adversely affected the germination rate at 150 mM and higher concentrations. (Figure 1).

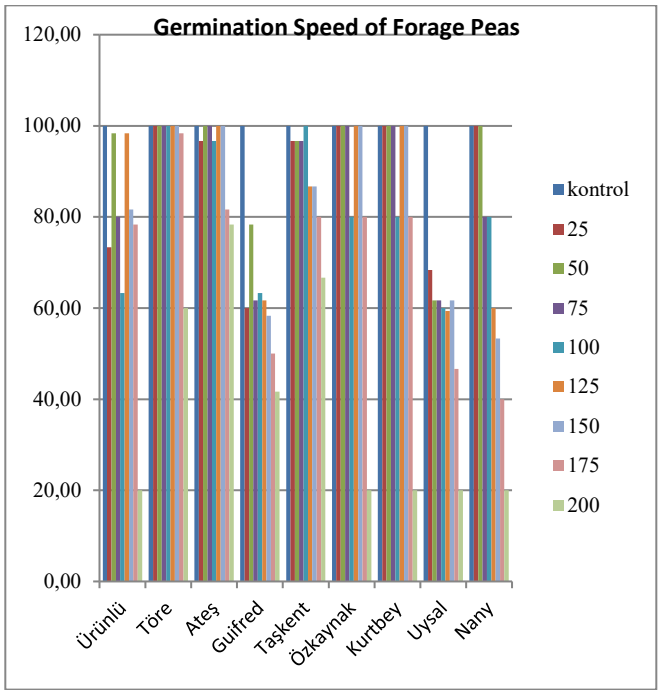

Figure 1. Germination speed of field peas at different salt concentrations (%)

Similarly, it was revealed that the germination power was parallel to the germination rate. At a salt concentration of 175 mM, the cv. Töre field pea has the highest germination power (Figure 2). Similar to these findings, Küçüközcü and Avcı[27] stated that the increase in salinity began to negatively affect germination at 10 ds/m and higher levels. Demirkol et al.[5] observed a significant decrease in germination rate in parallel with increasing salinity after 90 mM. Contrary to these findings, Okçu et al.[22] and Avcı et al.[21] reported that the germination percentage did not change according to the salinity level.In general, a decrease in root length was observed depending on the increase in salt concentration. In the mean salt concentration, decrease in root length was detected according to the control condition. It was revealed that the least decrease in root length at 200 mM salt concentration compared to the control condition was Töre and Ateş field pea varieties.

DOI: http://dx.doi.org/10.32571/ijct.1171249 E-ISSN: 2602-277X

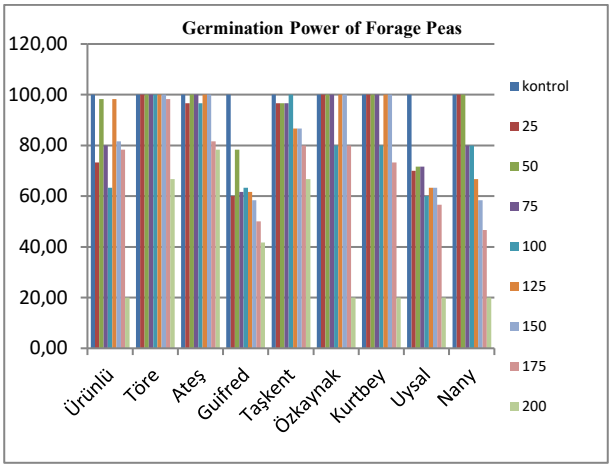

Figure 2. Germination power of field peas at different salt concentrations (%)

According to the control condition, the highest decrease was observed in the product with 25 mM salt concentration and in Taşkent field pea varieties. Töre has the longest root length at 150 mM, which is the critical salt concentration for germination speed and power. The highest root length was determined in Töre and Ateş varieties at 200 mM salt concentration (Figure 3).

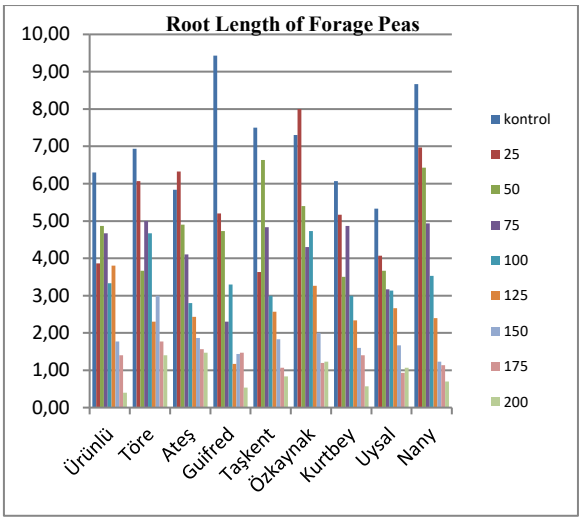

Figure 3. Root length of field peas at different salt concentrations (cm)

A decrease was observed in seedling length depending on the increase in salt concentration. The maximum decrease in seedling length was observed in Guifredo, Kurtbey and Özkaynak field pea varieties. On the other hand, the decrease in seedling length was observed in Urünlü, Töre, Ateş and Uysal field pea varieties. The longest seedling length was determined in Töre, Ateş, Özkaynak and Nany field pea varieties at 150 mM, which was determined as the critical salt concentration. All of the field pea varieties were significantly affected by the 200 mM salt concentration. In the study, root length was affected by lower salt concentrations than seedling length. Root length began to be affected at 25 mM salt concentration. Seedling length showed a significant decrease around 100 mM salt concentration (Figure 3 and Figure 4). Similar to these findings, Küçüközcü and Avcı[27] revealed that the salt rate of 20 ds/m negatively affects almost all varieties. Demirkol et al.[5] also found that salinity affected seedling growth negatively and the effect of pea genotypes on roots started at lower doses than shoots.

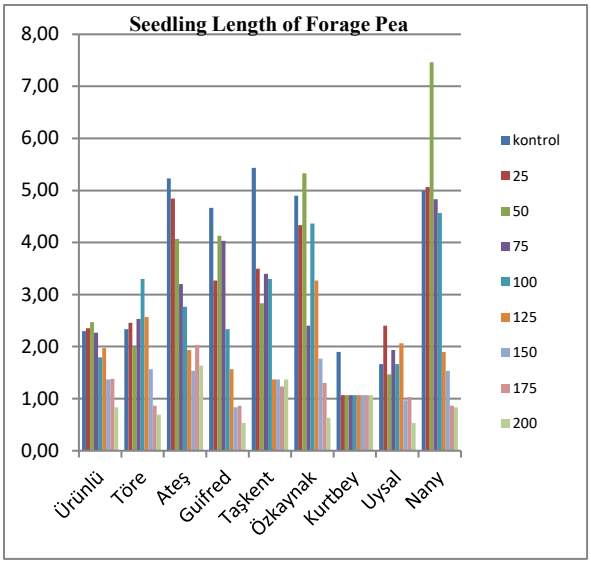

Figure 4. Seedling length of field pea varieties at different salt concentrations (cm)

In general, root fresh weight decreased with the increase of salt concentration The highest wet weights among all roots were obtained in the control condition. Excluding Ateş and Kurtbey field pea varieties, the root fresh weight was close to the control condition (Figure 5).

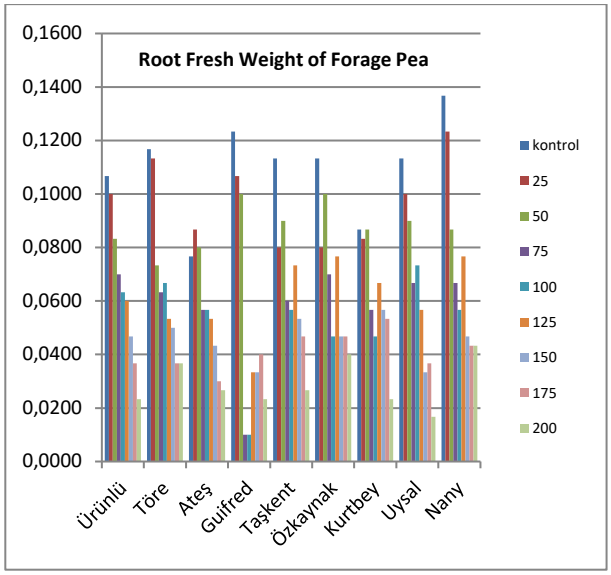

Figure 5. Root fresh weight of field pea varieties at different salt concentrations (g root^{-1})

Depending on the increase in salt concentrations, a decrease in root dry weight was also observed. In

DOI: http://dx.doi.org/10.32571/ijct.1171249 E-ISSN: 2602-277X

addition, no change was observed in root dry weight of Urunlu and Nany field pea varieties up to 175 mM salt concentration. In other field pea varieties, various fluctuations in root dry weight values were determined depending on the salt concentration (Figure 6).

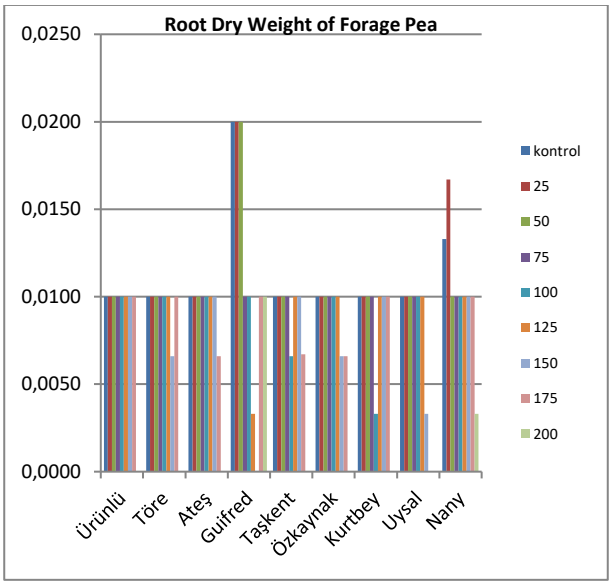

Figure 6. Root dry weight of field pea varieties in different salt concentrations (g root^{-1})

Depending on the increase in salt concentrations, a decrease in seedling fresh weight was also observed. Guifredo field pea variety with the highest seedling fresh weight among all varieties. However, the highest decrease was observed in Guifredo variety at 50 mM salt concentration with according to the control condition. When evaluated by root and seedling weight, root fresh weight was found to be higher in the control condition, while root and seedling fresh weights were found to be close at 200 mM salt concentration. While there were fluctuations in the dry weight of the seedlings at different salt concentrations, no significant change was observed when the 200 mM salt concentration was compared with the control conditions (Figure 7 and Figure 8).

In the studies, among all seedlings, the highest fresh and dry weights were obtained in Gölyazı variety under control condition, while the lowest value was obtained in 20 dS/m treatment in Taşkent variety. As the salinity increased, fresh and dry weights decreased in all varieties except Özkaynak, whose fresh and dry weights were positively affected by 5 dS/m salinity.

The lowest rate of decrease in fresh weight at 15 dS/m salinity was also recorded in this variety. Although all decrease rates in fresh weight of seedlings at 20 dS/m were similar, Taşkent variety was the most affected. Avcı et al.21, Tsegay and Andargie28, Demirkol et al.5 who supported these findings reported that fresh and dry weights of seedlings decreased in pea genotypes due to increased salinity.

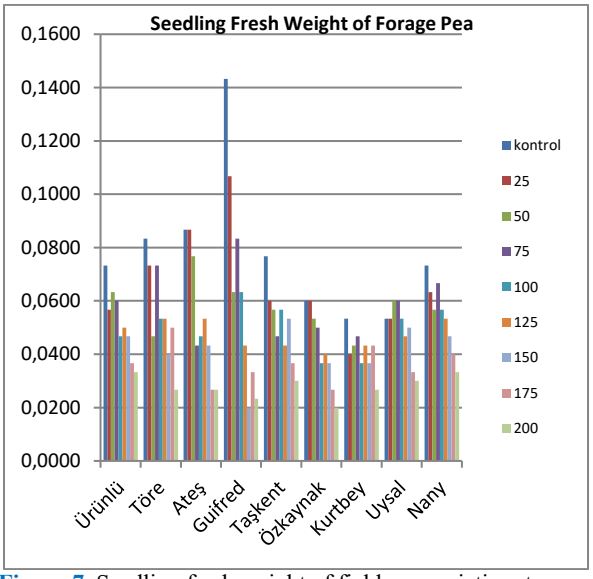

Figure 7. Seedling fresh weight of field pea varieties at different salt concentrations (g seedling^{-1})

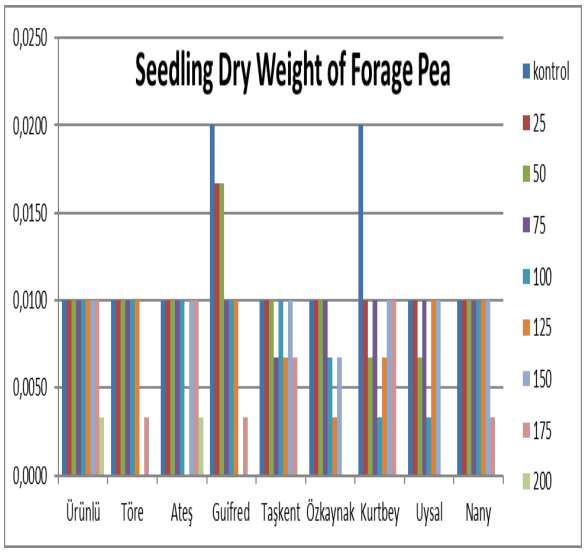

Figure 8. Seedling dry weight of field pea varieties at different salt concentrations (g seedling^{-1})

4.CONCLUSION

As a result, a significant decrease was observed in germination speed, germination power, root-seedling length and fresh-dry weights depending on the increasing salt concentration. It has been determined that Töre field pea variety has the highest germination rate and power. In addition, Ateş field pea followed Tore variety in all parameters. The varieties with the lowest germination speed and power are Guifredo and Uysal forage peas. The critical salt concentration was determined as 150 mM in the research. The first change for salt-tolerant varieties was observed at this concentration. As a result of the present study, salinity-sensitive and tolerant varieties were determined and the effects of different salt concentrations was investigated. Ateş and Töre varieties resistant to salt stress, Guifredo,

DOI: http://dx.doi.org/10.32571/ijct.1171249 E-ISSN: 2602-277X

and Uysal varieties that are sensitive will be used to improve salt tolerance by gene transfer as the continuation of this study. In this way, the effects of the Osmyb4 gene, which will be transferred to Ateş, Töre Guifredo, and Uysal varieties, on salinity will be evaluated. Also, more comprehensive field studies will be conducted to determine salinity stress.

Conflict of interests

I declares that there is no a conflict of interest with any institute, person, company, etc.

REFERENCES

1. Saygı, Y. D.; Alarslan, Ö. F. *Vet Hekim Der Derg,* **2012**, 83, 2, 25-35.

2. Ateş, E.; Tekeli, A. S. *KSU J. Agric Nat,* **2017**, 20, 13-16.

3. Öztürk, O.; Şen, C.; Aydın, B. *J. Central Research Inst. Field Crops,* **2019**, 28, 1, 29-38.

4. Özkan, U. *Turk. J Agr Eng Res,* **2020**, 1, 1, 29-43.

5. Demirkol, G.; Yılmaz, N.; Önal Aşcı, Ö. *KSU J. Agric Nat,* **2019**, 22, 3, 354-359.

6. Açıkgöz, E. *Yem bitkileri*, 3th ed.; Uludağ Üniversitesi Vakfı Yayınevi, Bursa, Türkiye, 2001.

7. Tekeli, A. S.; Ateş, E. *J. Cent. Eur. Agric,* **2003**, 4, 4, 313-317.

8. Yavuz, T. *J. Field Crop Cent Research Inst,* **2017**, 26, 1, 67-74.

9. Arslan, M.; Çetin, S.; Erdurmuş, C. *Ziraat Mühendisliği,* **2013**, 360, 32-39.

10. Yılmaz, E.; Tuna, A. L.; Bürün, B. *C.B.Ü. Fen Bil. Derg,* **2011**, 7, 1, 47- 66.

11. Aydın, G. *Anadolu J Agr Sci,* **2020**, 35, 115-123.

12. Hirayama,T.; Shinozaki,K. *Plant J,* **2010**, 61, 1041-1052.

13. Mohamed, A. A.; Aly, A. A. *Am-Euras. J. Sci. Res,* **2008**, 3, 2, 139-146.

14. Kang, J.; Xie, W.; Sun, Y.; Yang, Q.; Wu, M. *Afr. J. Biotechnol,* **2010**, 9, 45, 7589-7594.

15. Bu, Y.; Kou, J.; Sun, B.; Takano, T.; Liu, S. *FEBS Lett,* **2015**, 589, 1308-1313.

16. Korkmaz, H.; Durmaz, A. *GÜ Fen Bil Derg.* **2017**, 7, 2, 192-207.

17. Tiryi, İ. *KSU J. Agric Nat,* **2018**, 21, 5, 800-808.

18. Rhods, D.; Rich, P. J. *Plant Physiol*, **1988**, 88, 102-108.

19. Izad M. H.; Rabbani, J.; Emam, Y.; Tahmasebi, A.; Pessarakl M. *J. Plant Nutr*, **2014**, 37, 520-531.

20. Doğr,A.; Canavar, S. *APJES,* **2020**, 8, 1, 155-174.

21. Avcı, S.; Şahan, S.; Kaya, M.D. *Determination of Salt-Stress Response in Forage Pea Cultivars During Germination and Early Seedling Growth*, In: 2nd İnternational Conference on Agriculture, Çeşme/İzmir, Türkiye, Apr 02-05, **2018.**

22. Okçu, G.; Kaya, M. D; Atak, M. *Turk J Agric For*, **2005**, 29, 4, 237-242.

23. Petrović, G.; Jovicic, D.; Nikolic, Z.; Tamindzic, G.; Ignjatov, M.; Milosevic, D.; Milosevic, B. *GENETIKA,* **2016**, 48, 1, 373- 381.

24. Pereira Isabella, C.; Catão Hugo, C. R. M; Caixeta, F. *Rev. Bras. Eng. Agríc. Ambient,* **2020**, 24, 2, 95-100.

25. Ellis, R.H.; Roberts, E.H. **1980**, In: Hebblethwaite PD (Ed), Seed Production, London: Butterworths, England, 605-635.

26. Sokal, R.R. and Rohlf, F.J. **1981**, Biometry. W. H. Freeman and Company, San Francisco, California.

27. Küçüközcü, G.; Avcı, S. *Int J Agric Environ Food Sci*, **2020**, 34, 3, 368-375.

28. Tsegay, B. A.; Andargie, M. *J. Crop Sci. Biotech*, **2018**, 21, 3, 261-267.

DOI: http://dx.doi.org/10.32571/ijct.1135548 **E-ISSN: 2602-277X**

International Journal of Chemistry and Technology

http://dergipark.org.tr/ijct

Research Article

Polymer – flufenamic acid delivery systems for injured skin

Minodora Maria MARIN[1], Mihaela Violeta GHICA[2], Durmuş Alpaslan KAYA[3], Denisa Ioana UDEANU[4], Mădălina Georgiana ALBU KAYA[1*], Cristina-Elena DINU-PÎRVU[2], Lăcrămioara POPA[2], Valentina ANUȚA[2], Razvan Mihai PRISADA[2]

[1] *The National Research & Development Institute for Textiles and Leather, Division of Leather and Footwear Research Institute, Department of Collagen Research, Bucharest, Romania*

[2] *"Carol Davila" University of Medicine and Pharmacy, Faculty of Pharmacy, Department of Physical and Colloidal Chemistry, Bucharest, Romania*

[3] *Hatay Mustafa Kemal University, Faculty of Agriculture, Department of Field Crops, 31060, Antakya-Hatay, Turkey*

[4] *"Carol Davila" University of Medicine and Pharmacy, Faculty of Pharmacy, Department of Clinical Laboratory and Food Safety, Bucharest, Romania*

Received: 24 June 2022; Revised: 22 September 2022; Accepted: 26 September 2022

*Corresponding author e-mail: albu_mada@yahoo.com

Citation: Marin, M. M.; Ghica, V. M.; Kaya, D. A.; Udeanu, D.I.; Albu Kaya, M. G.; Dinu-Pirvu, C. E.; Popa, L.; Anuta, V.; Prisada, R. M. *Int. J. Chem. Technol.* **2022**, 6 (2), 114-121.

ABSTRACT

Collagen, the main protein of the body, is extracted in different forms and used as reservoir for drug delivery. The aim of this work was to obtain a drug delivery system based on collagen-dextran matrices cross-linked with glutaraldehyde as support and flufenamic acid and/or microcapsules with flufenamic acid as drug. The flufenamic acid was encapsulated in polymeric microcapsules consisting in gelatin, alginate, and sodium carboxymethyl cellulose. The morphology of matrices was determined by water absorption and contact angle. The biodegradation was performed in collagenase solution. In vitroflufenamic acid release profiles were built and the kinetic mechanism was set according to different mathematical models. The pharmacological studies followed the effect of collagen formulations treatment on the healing process of Wistar rats which were induced experimental wounds. The studied matrices proved that flufenamic acid delivery can be controlled, and the healing can be completed using the designed spongious matrices.

Keywords: Collagen sponges, microcapsules, flufenamic acid, kinetic release, wound healing.

Doku yaralanmaları için polimer-flufenamik asit salınım sistemleri

ÖZ

Vücudun ana proteini olan kolajen, farklı formlarda ekstrakte edilmekte ve ilaç salınımı için rezervuar olarak kullanılmaktadır. Bu çalışmanın amacı, destek olarak glutaraldehit ile çapraz bağlanmış kolajen-dekstran matrislerine ve ilaç olarak flufenamik asit ve/veya flufenamik asitli mikrokapsül içeren ilaç dağıtım sistemleri elde etmektir. Flufenamik asit, jelatin, aljinat ve karboksimetil selülozdan oluşan bir polimerik mikrokapsül içinde kapsüllenmiştir. Matris morfolojisi, su emme ve temas açısı ölçümleriyle belirlenmiştir. Biyolojik bozunma kolajenaz solüsyonunda gerçekleştirilmiştir. İn vitro flufenamik asit salımı, USP aparatına uyarlanmış bir sandviç cihaz kullanılarak belirlenmiş, kinetik mekanizma ise ilaç salımı için mevcut matematiksel modellere göre belirlenmiştir. Hayvan çalışmalarında wistar sıçanlarında deneysel olarak indüklenen yaralarda kolajen formülasyonlarının iyileşme süreci üzerindeki etkileri izlenmiştir. Çalışmada elde edilen matrisler incelendiğinde, flufenamik asit iletiminin kontrol edilebileceğini ve iyileşmenin tamamen bu süngerimsi matrisler kullanılarak yapılabileceğini kanıtlamıştır.

Anahtar Kelimeler: İlaç salımı, kolajen, sünger, flufenamik asit.

DOI: http://dx.doi.org/10.32571/ijct.1135548 E-ISSN: 2602-277X

1. INTRODUCTION

Worldwide, the most common type of injury are skin lessions, such as burns.[1] In the past, the treatment of burns was rudimentary, and a lot of patients died because of hypervolemic shock immediately after they suffered burns.[2]

So far the progress of burn therapy, regenerative medicine and pharmacotherapy is high. However, treating burn injuries continue to be a challenge for researchers, despite the numerous materials available for the patients.[3] In the last years many biomaterials for skin regeneration based on natural and synthetic polymers and loaded with drugs have been developed. In order to design the most suitable biomaterial for the treatment of burn wounds, several natural polymers were selected for this research.

Collagen represents the major fibrous protein component in connective tissues like skin, tendons, ligaments, cartilage, cornea etc. Having exceptional characteristics, collagen is used in varied scaffolds as wound dressings, antithrombogenic surfaces, ophthalmologic shields, artificial blood vessels, bone substitutes and valves, and drug delivery systems.[4-6] Gelatin is obtained by collagen denaturation and, in the medical field, is used for the manufacture of hydrogels, nano and microsphere particles, nanofibers, pharmaceutical additives and drug delivery carries for bioactive substances.[7-9]

Alginate is a natural polymer from polysaccharides class, extracted from a diversity of brown algae such as *Macrocystis pyrifera*, *Laminaria hyperborea*, and *Ascophyllum nodosum*.[10-12] This natural polymer, due to its good properties like adequate bioadhesion and mucoadhesion, and biocompatibility is used in medical applications mostly for drug delivery systems and microencapsulation of cells.[13,14]

Dextran is a polysaccharide produced by lactic acid bacteria or their enzymes in the presence of sucrose.[15,16] The main properties of dextran such as anticoagulant, antithrombotic, osmotic agent, and intravenous plasma lubricant, also cryopreservative for vaccines and organs[17] allow it to be a good candidate in medical field. Sodium carboxymethyl cellulose is furthermost a promising cellulose byproduct. Due to its representative characteristics like mechanical strength, tunable hydrophilicity, viscous properties,low price it can be used in food industry, functionalisation of textiles, pharmaceutical industries and biomedical area.[18]

An ideal biomaterial for burn injuries must present proper biocompatibility, absorbability, antimicrobial properties, ease of use and personalised tailored size.[19] A scaffold based only on natural polymers can not reach such requirements so an ideal wound dressing needs to be combined with some anti-inflammatory drugs. For this reason, flufenamic acid was selected. Flufenamic acid is a non-steroidal anti-inflammatory drug (NSAID) from the anthranilic group with analgesic, anti-inflammatory and antipyretic characteristics.[20]

In our previous work we studied similar spongious matrices but with different concentrations of polymers and cross-linking agent.[21] The aim of this study was the development of a multiparticulate drug delivery system based on a polymeric matrix, with controlled delivery of an anti-inflammatory drug loaded with polymeric microparticles and also with anti-inflammatory drug incapsulated, and the investigation of their biocompatibility, release kinetics and efficiency using preclinical studies involving animal models.

2. MATERIALS AND METHODS

2.1. Materials

Type I fibrillar collagen gel (Coll) of 1.92% (*w*/*v*) and gelatin (Gel) with 2.5% were obtained from calf hide using technology developed in Collagen Department of INCDPT Division ICPI.[22] Collagen matrices consisted in collagen gel, dextran sulfate sodium salt (Dex) and flufenamic acid (FA). The microcapsules consisted in gelatin, sodium carboxymethyl cellulose (CMCNa) and sodium alginate salt. The crosslinking was performed with glutaraldehyde (GA) for matrices and calcium chloride ($CaCl_2$) for microcapsules. Sodiumhydroxide was of analytical grade and the water was distilled.

2.2. Preparation of microcapsules and matrices

The microcapsules and matrices were prepared according with the method previously described[21] and have the compositions presented in the Table 1 and Table 2.

Table 1. Composition of microcapsules (MC).

Gelatin (g%)	CMCNa (g%)	Flufenamicacid (g%)	Sodium alginate (g%)
7.50	0.75	2.00	1.00

Two types of hydrogels were prepared with the following compositions: hydrogel H1 which consists in collagen (1.2%), dextran (0.6%) and glutaraldehyde (0.012%) and hydrogel H2 which consists in same composition as H1 with 0.5% flufenamic acid. The matrices were prepared by lyophilisation of hydrogels and their compositions are the following:

The obtained matrices named M1-M4 were than characterize by physical-chemical, biopharmaceutical and pharmacological analysis.

DOI: http://dx.doi.org/10.32571/ijct.1135548 E-ISSN: 2602-277X

Table 2. Composition of matrices.

Matrices	M1	M2	M3	M4
Ratio between hydrogels and microcpsules	H1 : MC 70 : 30	H1 : MC 85 : 15	H2 : MC 70 : 30	H2 : MC 85 : 15

2.3. Determination of water uptake capacity

The water up-take was determined in triplicate on matrices using the methods previously described[24] at different intervals of time. The following equation (*Equation 1*) was used to measure the water uptake capacity of matrices:

$$Water\ Uptake = \frac{Ww-Wd}{Wd}\ g/g \qquad (Equation1)$$

Where W_w represents the weight of wet matrices at immersion time, and W_d– the weight of dry scaffolds.

2.4. Enzymatic degradation

Enzymatic degradation of matrices was measured in triplicate using collagenase solution as previously described[24]. The following equation (*Equation 2)* was used to measure the amount of degraded matrices:

$$\%weight\ loss = \frac{Wi-Wt}{Wi}\ x\ 100 \qquad (Equation\ 2)$$

where Wi represents the initial weight, and *Wt*– the last weight.

2.5. Goniometric analysis

The monitoring of the sponges porous surface properties, quantified by contact angle (CA°) values, was carried out with CAM 101 (KSV Instruments), using the pendant drop dynamic method, as reported in our previous paper.[23] Using the Young equation (*Equation3*) the drop shape was fitted and the contact angle was evaluated.[24]

$$\gamma_{SG} = \gamma_{SL} + \gamma_{LG} \cdot cos\theta \qquad (Equation\ 3)$$

Where γ_{SG} is the interfacial tension S/G, γ_{SL} – the interfacial tension S/L, γ_{LG}– the superficial tension L/G, and θ– the contact angle.

2.6. Flufenamic acid in vitro release

The flufenamic acid *in vitro*delivery from the spongious collagen-basedmultiparticulate systemswas conducted with a paddle dissolution apparatus equipped with a sandwich device, as mentioned in our previous Works.[21] The amount of drug released at different periods of time was spectrophotometrically assessed using the calibration curve ($A_{1\%}^{1cm} = 534$, λ = 288 nm), and the drug cumulative release (%) was determined.

The experimental kinetic results were quantified using the general model – Power law(*Equation4*), also applying two particular cases for n=0.5 (Higuchi model) and n=1 (Zero-Order), and the flufenamic acid transport mechanism was established.

$$\frac{m_t}{m_\infty} = k \times t^n \qquad (Equation\ 4)$$

where m_t/m_∞ represents thefraction of the drugdelivered at different time *t, k* – the kinetic constant, *n* – the release exponent correlated with the drug transport mechanism.

2.7. The animal model for the induced burns

The pharmacological experiments were performed as we previously described.[21,25] Briefly, experiments were conducted using Wistar rats (200±10g weight), obtained from The Animal Biobase of "Carol Davila" University of Medicine and Pharmacy, Bucharest. The rats were kept in laboratory standard conditions. The pharmacological experiments were conducted according to the Directive 2010/63/EU of the European Parliament, respecting the national legislation. Five groups of five animals each were used. Thermic lesions were induced under anaesthesia with a special device of 10mm diameter on dorsal area. The animals were than treated with multiparticulate collagen-basedsystemsin the form of spongeas follows: M1-M4 sponges were used for the Group 1 – Group 4, and the control group (no dressing on the wounded area) was Group 5. A digital camera was used to evaluate the evolution of wound surface morphology, and the wound diameter was measured every two days during 17 days. In the following equation (*Equation5*) the healing processesis described according to the size profile of wound:

$$Healing\ process\ \% = \frac{(Wound\ diameter\ at\ t=0) - (Wound\ diameter\ at\ t)}{Wound\ diameter\ at\ t=0} x100$$

(Equation 5)

where the wound size is evaluated as an average measurement of the longest and shortest dimensions of the affected area. When of the crust of the lesion fell of, the wound was considered healed.

For all animals, two aspects were monitored: lesion inflammation or infection, and modification on the animal health status.

For statistical interpretation of data, GraphPad Prism 6

DOI: http://dx.doi.org/10.32571/ijct.1135548 E-ISSN: 2602-277X

was used. All the results were presented as mean with standard deviation. The Kolmogorov–Smirnov test was applied for normal distribution calculation and the statistical significance was calculated using ANOVA, *t*-student and Bonferroni tests. For the $p<0.01$ the results were highly significant, for the $p<0.05$ – significant, and for the $p>0.05$ – not significant, respectively.

3. RESULTS AND DISCUSSION

A primary indicator for the surface wettability of spongious matrices was considered the drop shape, recorded with a digital camera, corresponding to the contact angle value, as presented in Figure1.

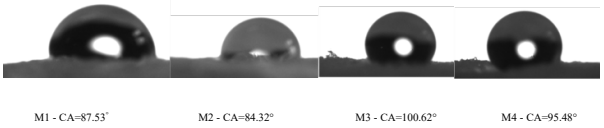

Figure 1. Images of the drops shape for the spongious matrices and the associated contact angle values.

The contact angle values are in the range 84.32 to100.62°, being strongly influenced by the way of drug incorporation. The highest values of CA were reported for M3 and M4collagen sponges with the drugincorporated in both forms (free and encapsulated), while for M1 and M2 sampleswith drug incorporated only in encapsulated form the CA was smaller, the decrease being about 1.09-1.19 times. It seems that the presence of the FA in free form in the designed multiparticulate systems led to a decrease of the sponge surface hydrophilicity. On the other hand, a smaller amount of microcapsules (M2 and M4) determined a decrease of CA values, corresponding to a higher spongious matrices surface wettability. The ability of water up-take of collagen matrices with free and encapsulated FA was determined. The swelling degree after 2 and 72 hours is presented in Figure 2. The matrices M1 and M2 presented higher up-take ability after 2 and 72 hours. The matrices with higher content of flufenamic acid (M3 and M4) (both free and encapsulated) are more hydrophobic than the others (M1 and M2). The results of water up-take are in correlation with contact angles values and show that both drug and amount of microcapsules influence the wettability properties of spongious matrices.

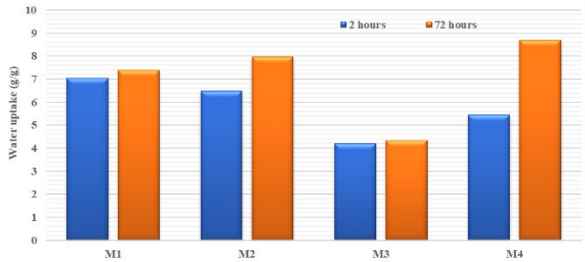

Figure 2. Water up-take for spongious matrices.

Enzymatic degradation of matrices was tested at different time intervals. All matrices presented good biodegradability, losing less than 20% mass in 24 hours (Figure 3).

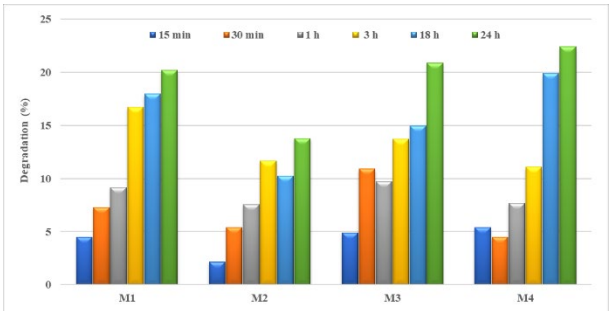

Figure 3. Enzymatic degradation of spongious matrices.

The most degradable matrix was M1 with lowest amout of flufenamic acid and without microcapsules. After 72 hours the matrices with flufenamic acid in free form were totally degraded and the ones with microcapsule content were degraded about 70% during same time.

The *in vitro* flufenamic acid kinetic profiles from collagen spongious matrices were built as drug cumulative released (%) as a function of time (Figure 4).

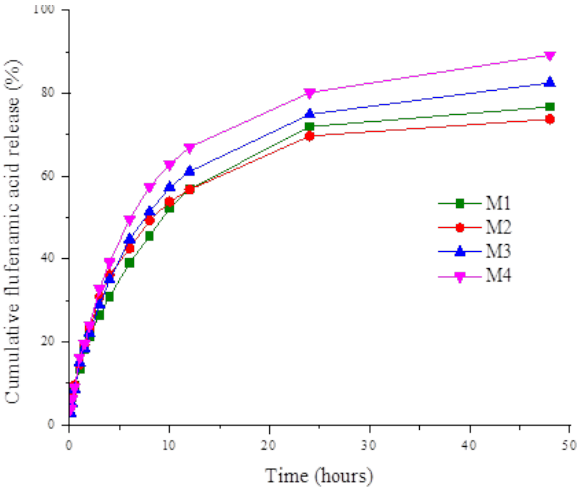

Figure 4. Time-dependent cumulative release patterns of flufenamic acid from spongious matrices collagen-based.

As seen in Figure 4, comparable kinetic profiles for all delivery systems with FA incorporated in various forms were obtained, and described by two stages: in the first hour, the initial drug released was between 13.52% (M1) and 16.37% (M4), followed by a gradual and slower release for a prolonged period up to 48hours.The cumulative flufenamic acid released percentage after 48 hours has varied between 76.77% (M1) and 89.22% (M4) (Table 3). It can be noticed that the samples with FA incorporated in free and encapsulated forms presented a higher burst release due to the presence of drug available in free form, near to the surface and delivered through desorption. After 48 hours, the released drug percentage

DOI: http://dx.doi.org/10.32571/ijct.1135548 E-ISSN: 2602-277X

for the sponges with drug incorporated in both forms is higher compared to sponges with the drug presented only in encapsulated form, the increase being about 1.07-1.20 times.The kinetic data are in line with sponges surface wettability (contact angles values around 90º or higher than 90º) and absorption capacity, respectively. As we underlined in our previous works,[21,26] this kinetic behaviour is desired for the local inflammation control as well as for monitoring the pain associated to a cutaneous wound lesion taking into account that the first 12-48 hours are important inhealing process of a wound. The experimental data were fitted with different kinetic models, obtaining the highest correlation coefficient (R) for the the Power law model. The respect of this model indicates a non-Fickiandrug transport mechanism, the release exponent being between 0.37 and 0.40.The parameters specific to this model (the kinetic constant and the release exponent) are listed in Table 3.

Table 3. Correlation coefficients for drug delivery from spongious matrices collagen-based obtained by application of various kinetic models; kinetic parameters specific to Power law model; drug released (%).

Collagen spongious matrices	Higuchi model	Zero-order model	Power law model	Release exponent	Kinetic constant ($1/min^n$)	Drug released (%)
M1	0.9684	0.8420	0.9805	0.40	0.036	76.77
M2	0.9523	0.8051	0.9750	0.37	0.045	73.79
M3	0.9630	0.8289	0.9767	0.39	0.039	82.55
M4	0.9590	0.8211	0.9747	0.39	0.044	89.22

3.1. The effect of collagen formulations treatment on the healing of induced wounds, using the animal model

In the case of treatment with collagen sponges (Figure 5, Figure 6, Figure 7 and Table 4), we observed that when applying spongious matrices M3 and M4 (drugincorporated in both forms), the lesiondiameter was maintained constant during the first 3 days of treatment. Starting from day 5, a significant decrease ($p<0.01$) of approximately 30% in lesion diameter was recorded in the case of the M4 multiparticulated system, followed by formulation M2 (flufenamic acid incorporated only in encapsulated form) with a 10% decrease of diameter compared to first day of treatment. From the applied treatments, the M4 formulation (flufenamic acid incorporated in the collagen spongious matrices both in free and encapsulated form) presentedthe most favorable dynamics of the healing process in the induced lesions throughout the 17 days of monitoring. The results, in this case, were statistically significant in the first 10 days compared to control group, not treated ($p<0.05$).

The physical-chemical, biopharmaceutical and preclinical studies involving animal models obtained in the present work are in line with the ones presented in our previous studies for similar spongious matrices but with different concentrations of polymers and cross-linking agent, conducting to flufenamic acid controlled delivery systems which proved that the healing processes can be completed using the designed multiparticulate formulations.[21,26]

Table 4. The evolution of lesion (mm) diameter in experimentally induced woundsafter the treatment with collagen formulations.

Collagen Sponges	Day 1 Mean±DS	Day 3 Mean±DS	Day 5 Mean±DS	Day 7 Mean±DS	Day 10 Mean±DS	Day 12 Mean±DS	Day 14 Mean±DS	Day 17 Mean±DS
M1	10.00±0.00	10.75±0.50	10.5±0.60	8.50±0.60	6.75±1.00	4.00±2.80	0.50±0.60	0.00±0.00
M2	10.00±0.00	10.83±0.25	9.00±0.25	7.75±1.00	5.75±1.00	4.00±0.80	0.75±1.50	0.00±0.00
M3	10.00±0.00	10.00±0.80	10.25±1.30	7.25±1.30	5.50±0.60	4.00±0.80	0.25±0.50	0.00±0.00
M4	10.00±0.00	9.86±0.40	7.00±2.20	5.33±1.00	3.14±1.90	1.71±1.70	0.29±0.50	0.00±0.00
Control	10.00±0.00	11.75±0.40	10.75±0.40	8.67±1.20	7.83±1.10	5.50±0.50	2.00±2.00	1.00±1.40
ANOVA (p)	NS	p<0.01	p<0.01	p<0.01	p<0.01	p<0.05	NS	NS

DOI: http://dx.doi.org/10.32571/ijct.1135548 E-ISSN: 2602-277X

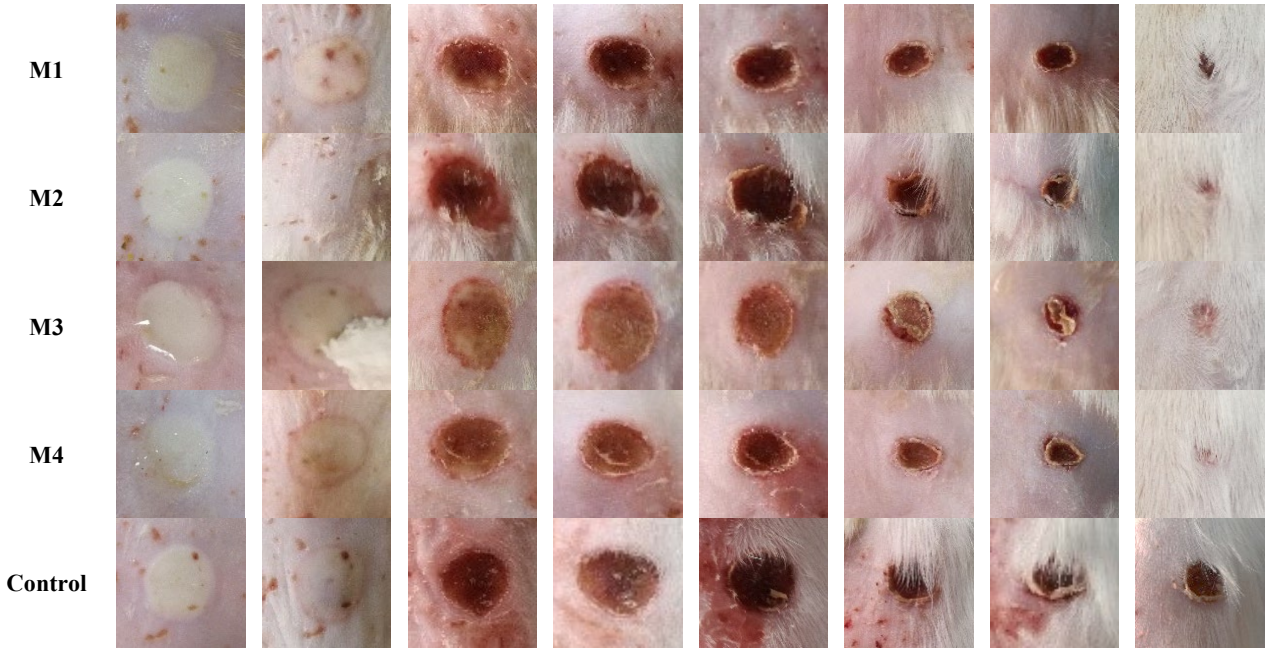

Figure 5. The healing process evolution for the induced wounds treated with collagenic sponges based on flufenamic acid in comparison with control group (not treated).

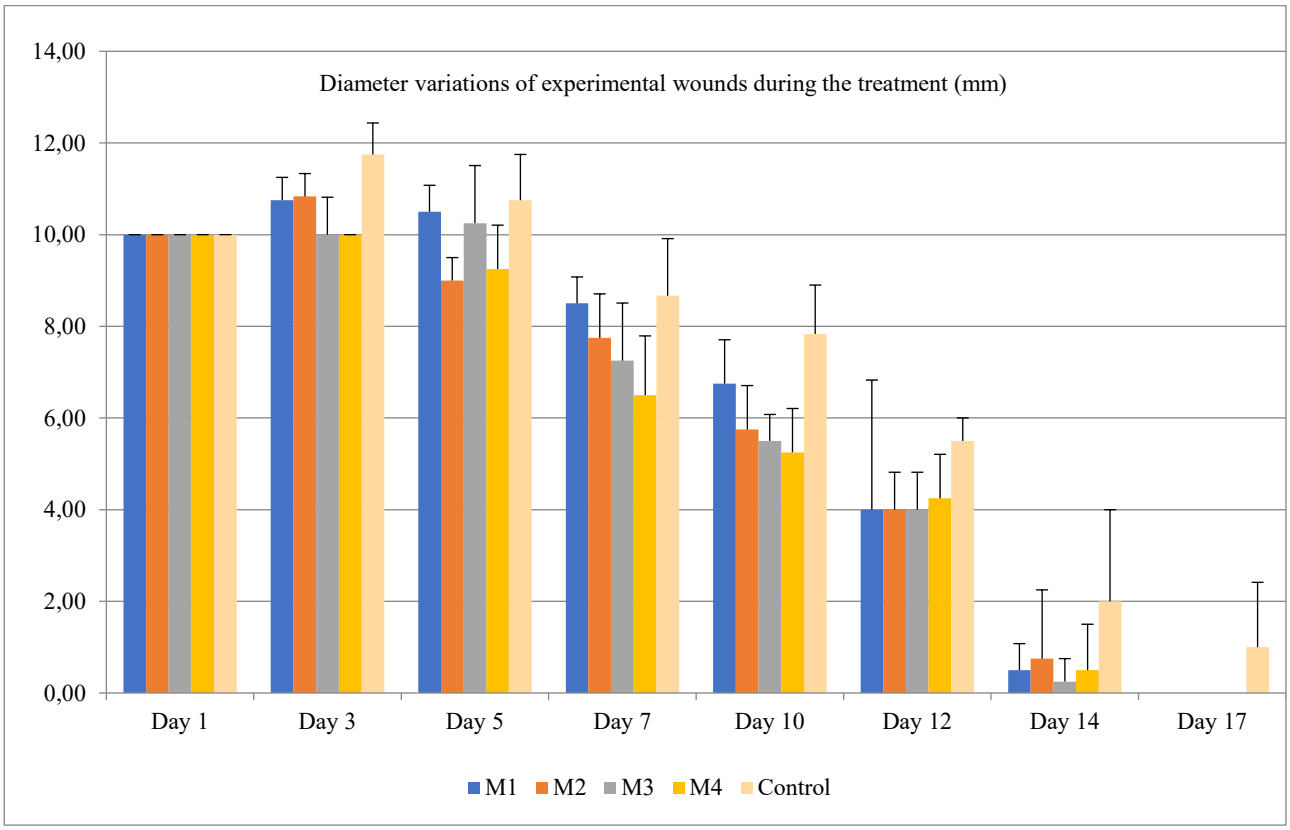

Figure 6. The diameter evolution of experimentally induced wound on animals after the treatment with collagenic formulations based on flufenamic acid (M1-M4) and control group.

DOI: http://dx.doi.org/10.32571/ijct.1135548 E-ISSN: 2602-277X

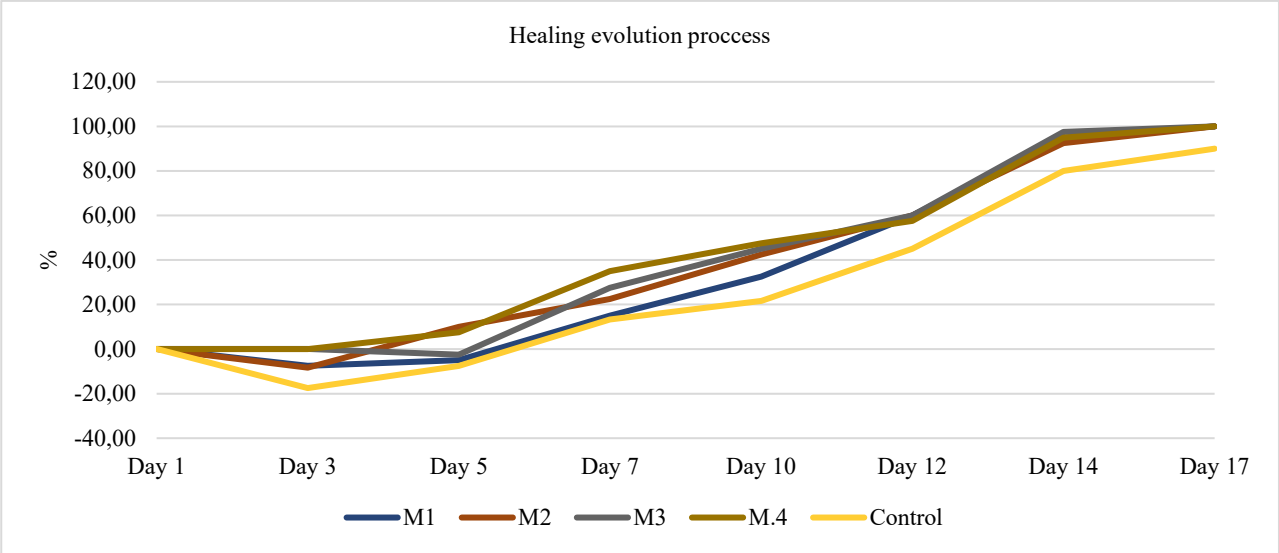

Figure 7. The healing process dynamics after the treatment with collagen formulations (M1-M4) and control group (not treated) in wounds induced on animals.

4. CONCLUSIONS

Drug delivery systems based on polymeric supports consisting in collagen and dextran, and flufenamic acid as drug were developed to be used in different skin lesions. To perform a controlled drug release, the flufenamic acid was presented both free in polymeric support and encapsulated. The microcapsules with flufenamic acid were embedded in spongious matrices in order to be slowly released for a longer period of time. Both water uptake and contact angle studies showed that the drug incorporated in both forms (free and encapsulated) influences the properties of spongious matrices, making them more hydrophobic. The stability to collagenase showed a slow biodegradation, of less than 20% mass loss in 24 hours. The release profiles indicated a non-Fickiandrug transport mechanism. The kinetic patterns obtained are suitable for the local inflammationand pain control specific to a cutaneous wound.The presence of flufenamic acid both in free and encapsulated form, respectively only in encapsulated form in the polymer matrix demonstrated a positive effect on the evolution of the healing process from the first days without topical and systemic side effects. The use in burnstreatment justified by the *in vivo* results of multiparticulate systems with anti-inflammatory drug showed significant pharmacological effects and no side effects with the acceleration of the healing process in case of medium severity burns.

ACKNOWLEDGEMENT

This work was peformed in the frame of PN-III-Experimental Demonstration Project, project number PED 160/03.01.2017, code PN-III-P2-2.1-PED-2016-0813 and contract no. 4 PFE/2021 by the Ministry of Research, Innovation and Digitization within Program 1 - Development of the national R&D system, Subprogram 1.2 - Institutional Performance - RDI excellence funding projects.

Conflict of interests

I declares that there is no a conflict of interest with any institute, person, company, etc.

REFERENCES

1. Greenhalgh, D.G. Management of Burns. *N. Engl. J. Med.*, **2019**, *380*, 2349–2359.

2. Nessler, M.; Chrapusta, A. *Leczenie Ran*. **2013**, *10*, 47–52.

3. Markiewicz-Gospodarek, A.; Kozioł, M.; Tobiasz, M.; Baj, J.; Radzikowska-Büchner, E.; Przekora, A. *Int. J. Environ. Res. Public Health*, **2022**, *19*, 1338.

4. Albu, M.G.; Titorencu, I.; Ghica, M.V. Collagen-Based Drug Delivery Systems for Tissue Engineering. In Biomaterials Applications for Nanomedicine; InTech, **2011**.

5. Harley, B.A.; Lynn, A.K.; Wissner-Gross, Z.; Bonfield, W.; Yannas, I. V.; Gibson, L.J. *J. Biomed. Mater. Res. Part A*, **2009**, *9999*A.

6. Healy, K.E.; Rezania, A.; Stile, R.A. *Ann. N. Y. Acad. Sci.,* **1999**, *875*, 24–35.

7. Alipal, J.; Mohd Pu'ad, N.A.S.; Lee, T.C.; Nayan, N.H..; Sahari, N.; Basri, H.; Idris, M.I.; Abdullah, H.Z. Mater. *Today Proc.,* **2021**, *42*, 240–250.

DOI: http://dx.doi.org/10.32571/ijct.1135548 **E-ISSN: 2602-277X**

8. Kumosa, L.S.; Zetterberg, V.; Schouenborg, *J. Acta Biomater.*,**2018**, *65*, 137–149.

9. Ma, K.; Cai, X.; Zhou, Y.; Wang, Y.; Jiang, T. *Macromol. Biosci.,* **2017**, *17*, 1600130.

10. Sosnik, A. *ISRN Pharm.,* **2014**, *2014*, 1–17.

11. Rinaudo, M. *Polym. Int.,* **2008**, *57*, 397–430.

12. Smidsrod, O.; Skjakbrk, G.*Trends Biotechnol.*, **1990**, *8*, 71–78.

13. Gasperini, L.; Mano, J.F.; Reis, R.L. *J. R. Soc. Interface,* **2014**, *11*, 20140817.

14. Choi, H.-G.; Kim, C.-K. *J. Control. Release,* **2000**, *68*, 397–404.

15. Díaz-Montes, E. *Polysaccharides,* **2021**, *2*, 554–565.

16. Heinze, T.; Liebert, T.; Heublein, B.; Hornig, S. Functional Polymers Based on Dextran. In *Polysaccharides II*; Springer Berlin Heidelberg; pp. 199–291, **2006**.

17. Naessens, M.; Cerdobbel, A.; Soetaert, W.; Vandamme, E.J. *J. Chem. Technol. Biotechnol.,* **2005**, *80*, 845–860.

18. Rahman, M.S.; Hasan, M.S.; Nitai, A.S.; Nam, S.; Karmakar, A.K.; Ahsan, M.S.; Shiddiky, M.J.A.; Ahmed, M.B. *Polymers (Basel).,* **2021**, *13*, 1345.

19. Shu, W.; Wang, Y.; Zhang, X.; Li, C.; Le, H.; Chang, F. *Front. Bioeng. Biotechnol.,* **2021**, *9*.788461.

20. Malinovskaja-Gomez, K.; Labouta, H.I.; Schneider, M.; Hirvonen, J.; Laaksonen, T. *Eur. J. Pharm. Sci.,* **2016**, *89*, 154–162.

21. Dinescu, S.; Ignat, S.; Lazar, A.; Marin, S.; Danilă, E.; Marin, M.M.; Udeanu, D.I.; Ghica, M.V.; Albu Kaya, M.G.; Costache, M. *J. Immun. Res.*, **2019**, 4513108.

22. Albu, M. G.*Collagen Gels and Matrices for Biomedical Applications*, Lambert Academic Publishing, Saarbrücken, 2011.

23. Ghica, M.V.; Albu, M.G.; Popa, L.; Moisescu, Ș., *Pharmazie*, **2013**, *68(5)*, 340-348.

24. Marin, M.M.;Albu Kaya, M.G.;Ghica, M.V.;Dănilă, E.;Coară, G.;Popa, L.; Chelaru, C.;Kaya, D.A.;Anuța, V.; Dinu-Pîrvu, C.E.;Cristescu, I. *Design and evaluation of doxycycline/collagen/chondroitin sulfate delivery systems used for cartilage regeneration*, Proceedings of the 8thInternationalConferenceonAdvancedMaterialsandSystems (ICAMS),Bucharest, 1-3 October 2020, p. 201-206, **2020**.

25. Udeanu, D.I.; Albu Kaya, M.G.; Ghica, M.V.; Marin, S.; Marin, M.M.; Kaya, D.A.; Popa, L., Dinu-Pîrvu, C.E. *Farmacia,***2018**, *66(5)*, 783-790.

26. Ghica, M.V.; Albu Kaya, M.G.; Udeanu, D.I.; Marin, M.M.; Marin, S.; Kaya, D.A.;Dinu-Pirvu, C.; Popa, L.; Danila, E. RO Patent 132850, October 29, **2021**.

DOI: http://dx.doi.org/10.32571/ijct.1199748 E-ISSN: 2602-277X

International Journal of Chemistry and Technology

http://dergipark.org.tr/ijct

Research Article

An overlook on the relationship between green finance and the environment

Yunus Emre KAHRAMAN

Osmaniye Korkut Ata University, Vocational School of Health Services, Osmaniye, Türkiye

Received: 5 November 2022; Revised: 16 December 2022; Accepted: 20 December 2022

*Corresponding author e-mail: yunusemrekahraman@osmaniye.edu.tr

Citation: Kahraman, Y. E. *Int. J. Chem. Technol.* **2022**, 6 (2), 122-128.

ABSTRACT

This study aims to explain the relationship between green economy, green finance and the environment. Environmental sensitivities have become related to production with the increase in global warming, greenhouse gas emissions and carbon emission rates. As the relationship between production and the economy has increased, some financial instruments have emerged in order to be environmentally sensitive. The purpose of these products is primarily to protect the environment and to include environmentally conscious people in this financial system. In the personal or individual green finance dimension, green mortgages, green home loans, green commercial building loans, green car loans and green credit cards are the most prominent green financing. When environmental green financing products related to firms are analyzed, we come across some products such as green project finance, green securities, green technology leasing, carbon finance. Eco fund and carbon fund in the asset management section, car insurance, carbon insurance and green insurance in the insurance section. Considering that our environment is essential for all humanity, supporting and increasing green financing products that are environmentally sensitive will make more positive contributions both our country and the world.

Keywords: Environment, green projects, finance, financing, green financing.

Yeşil finansman ve çevre ilişkisine bir bakiş

ÖZ

Bu çalışmada; Yeşil ekonomi, yeşil finansman ve çevre ilişkisi anlatılmaya çalışılmıştır. Çevre ile ilgili hassasiyetler küresel ısınma, sera gazı salınımı ve karbon emisyon oranlarının artışı ile birlikte, üretim ile ilişkili hale gelmiştir. Üretim ve ekonomiyle ilgili hale gelmesinden sonra çevreye duyarlı olabilmek açısından bazı finansal enstrümanların ortaya çıkmıştır. Bu enstrümanların amacı ilk olarak çevreyi korumak ve çevre bilincine duyarlı kişileri bu finansal sistemin içerisine dahil etmektir. Kişisel veya kişilere yönelik yeşil finans boyutunda yeşil ipotek, yeşil ev kredisi, yeşil ticari bina kredisi, yeşil araba kredisi ve yeşil kredi kartları en öne çıkan yeşil finansman. Firmalar ile ilgili çevreci yeşil finansman ürünler incelendiğinde karşımıza yeşil proje finansmanı, yeşil menkul kıymetler, yeşil teknoloji kiralama, karbon finansı gibi bazı ürünler çıkmaktadır. Varlık yönetimi bölümünde ise Eco fonu ve karbon fonu, sigorta alanında bölümünde araba sigortası, karbon sigortası ve yeşil sigorta karşımıza çıkmaktadır. Çevremizin bütün insanlık açısından gerekli olduğu düşünüldüğünde, çevre hassasiyeti olun yeşil finansman ürünlerinin desteklenmesi ve arttırılması hem ülkemiz hem de dünya için daha olumlu katkılar sunacağı görülmektedir.

Anahtar Kelimeler: Çevre, çevreci projeler, finans, finansman, yeşil finansman.

1. INTRODUCTION

The term green economy was first used in 1989 in the book 'Blueprint for a Green Economy' by Pearce et al. Green economy was emphasized within the framework of sustainable development. Especially after the 2007-2008 crisis, the green economy started to gain an important place and agenda. The price increases and increased resource utilization, food shortages and climate changes that occurred with the crisis brought the green economy to the forefront.[1]

With the development and spread of the green economy, it has begun to be seen as a potential solution to global crises. The United Nations Environment Program (UNEP) put forward the idea of a 'green stimulus package' involving large-scale public investment in green technologies. In 2008, UNEP published an agreement for the development of the green economy called the 'Green Economy Initiative'.[2] This agreement demonstrated the potential of the green economy to support economic recovery by addressing the challenges of global crises, such as reducing carbon dependence, protecting water

DOI: http://dx.doi.org/10.32571/ijct.1199748 E-ISSN: 2602-277X

resources and ecosystems, and reducing poverty. It has been defined as the only fundamental way for the sustainability of the global economy.[3]

Nevertheless, many researchers see it as an opportunity for a fundamental change in the global economy.[4,5] In addition, many authors have argued that there are numerous job opportunities that will arise with the green economy.[6-10] In recent years, the green economy has been growing rapidly with products and services that improve the environment, including renewable energy, more efficient and cleaner technology, construction of environmentally friendly buildings, ecosystem-based products and services.[11]

A green economy is an economic system driven by public and private investment that aims to reduce carbon emissions and pollution, increase energy and resource efficiency, and prevent losses in ecosystems and biodiversity.[12] Green economy is also defined as an economic model that contributes to ecological order and improves people's welfare and social equity while eliminating environmental risks.

1.1. Neoclassical economics

Economics is a social science that seeks to explain the basis on which societies decide what, how and for whom to produce.[13] For this reason, the choices that individuals, societies, businesses and governments make in dealing with resource management and the effects of these choices constitute economics.[14]

In this case, economics is divided into two classes: micro and macro. Microeconomics can be defined as the study of the effects of choices made by individuals and businesses on government and the market, while macroeconomics can be defined as the study of global and national economies.[15]

1.2. Ecological economy

Ecological economics is a branch that examines the interaction of ecological and economic systems.[16] It is an economic system developed in response to the fact that neoclassical economics largely ignores the environment and nature. Environmental economics and natural resource economics, which are sub-disciplines of neoclassical economics, mostly consider the relationship between the economy and the environment. It considers nature and environmental economics as a subsystem of economics. In ecological economics, the economy is considered as a subsystem of nature.[16,17]

Some defining features of ecological economics aim to preserve natural capital, the stocks of natural ecosystems that provide goods and capital, since natural capital cannot be substituted by man-made capital. Because natural resources are finite, economic growth cannot be achieved indefinitely, and ecological economists envision that zero growth will ensure a stable economy. Consideration of ecosystem-dependent economies is defined as the involvement of social values in decision-making during the fair distribution of goods and services and focusing on sustainable economic development economics to improve human welfare.[15]

1.3. Green economy

Green economy has emerged not as an academic branch like other economic systems but in a grassroots-oriented way and is defined as different and more diverse than other economic approaches. Green economy was born out of the work of environmental and green politicians and is based on the process of building a sustainable economy in practice. Issues such as social justice and equality are prioritized over economic efficiency. It aims to meet the needs of the planet within an economic structure that includes women and the poor. It aims for a static, stable economy rather than economic growth. It focuses on human interaction rather than the market economy.[18]

1.4. Environment and economy

Changes in the environment and economy and their possible effects also have an impact on each other. Specifically, there are four main services that the environment provides to the economy,[16]

- Resource Supply: Natural resources are transferred from the environment to the economy and used in production. Examples are non-renewable resources such as minerals and fossils, and renewable resources that are grown and harvested.
- Waste Pool: Waste materials are generated as a result of production and consumption. As a result, it is provided from natural resources.
- Convenience: The environment provides people with sources of recreation and pleasure, such as walking, swimming and similar activities.
- Life Support: The maintenance of activities necessary for human life is a prerequisite for economic functioning.

1.5. Green growth

It is a strategy that supports economic growth by minimizing the impacts on the environment in line with ecological principles and sustaining the progress of economic processes by creating employment and additional opportunities.

1.6. Green finance

It is an approach to direct the financial sector towards low-carbon and efficient resource use and to pursue a policy compatible with climate change.

DOI: http://dx.doi.org/10.32571/ijct.1199748 E-ISSN: 2602-277X

1.7. Benefits of green finance

On the financial industry; Mr. Noh (2018) explained the benefits of green finance in the industrial field as the development of new financial products and risk management, the mobilization and efficient operation of emission trading markets, and the development of risk management techniques, Effects on economic growth; With the development of new technologies, the design of efficient trade schemes and the promotion of environmentally friendly industries, On Environmental Remediation; Actively trading in the carbon market, regulating legislation for a better environment and utilizing green technologies and industries for a better environment.[19]

2. GREEN FINANCIAL PRODUCTS

Green finance products that need to be researched and developed within the green economy are analyzed under four main headings. These are Retail finance, asset management, corporate finance and Insurance.

Generally, governments advance green finance strategies by providing and strengthening financing for green industries and green growth, developing new financial products, providing private investments in green infrastructure and sustainability, strengthening and financing green management corporate practices, and creating new markets for environmental goods and services. In addition, when green bonds are analyzed in terms of issuer types, green bond issuance financial and non-financial institutions are the leading ones.[20]

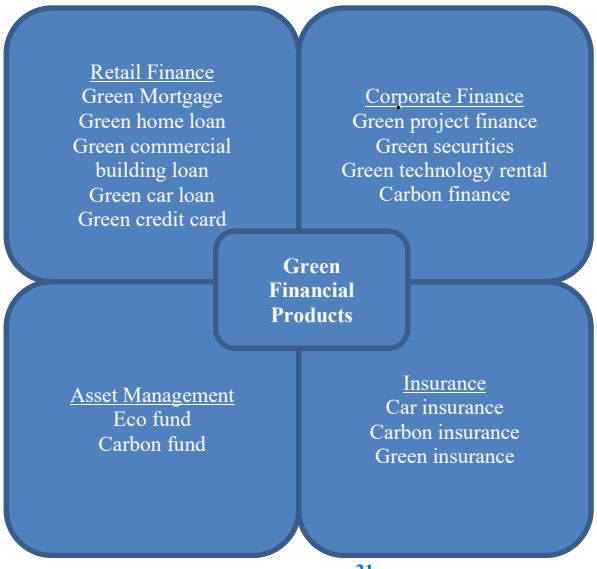

Figure 1: Green financial products. [21]

2.1. Retail finance

Retail finance is a financing system that includes commercial and personal products for SMEs and individuals. Services such as loans, credit cards, mortgages, cash management, insurance and bank transfers constitute retail services.[22] Loans provided for special purposes for projects carried out to prevent environmental problems are called 'Green Loans'. The most important feature of green loans is the provision of resource transfer for projects that meet the specified standards.

2.1.1. Green mortgage

The reconstruction or renovation of buildings by preserving and basing on environmental values includes the green mortgage application. It is referred to as "mortgage" in the US and "mortgage" in Turkey.[23] The Energy Efficiency Mortgage (EEM) is a government mortgage that provides financing at below-normal interest rates to develop and maintain green construction and save energy in all types of individual or institutional construction. Buildings in North America that have received low-interest financing to regulate green buildings have lower energy consumption and less pollution and waste than conventional buildings. Green mortgages are granted in return for at least 20% energy savings in new buildings and at least 30% energy savings in renovated buildings.[24]

Advantages of a green mortgage
-Lower interest rate
-Saving money
-Valuation of properties in case of certification
-Reimbursement of report costs

2.1.2. Green car loans

Green auto loans are incentive loans that encourage individuals to consume alternative fuels or to consume less fuel. Green auto loans cover all vehicles that emit less waste into the environment.

With the SmartWay "Smart Road" application organized by the United States Environmental Protection Agency (EPA), SmartWay has carried out studies to increase the transportation efficiency of vehicles by comparing them and aims to improve them by making measurements based on these values. With the SmartWay app;
- US trucking companies saved $33.4 billion in 2017.
- The SmartWay partnership contributed 248.8 million oil to save energy and reduced reliance on external fuels.
- 119 million tons of Nox, Co2 and Pm gases that cause air pollution were prevented from being emitted and clean areas were protected.[24]

2.1.3. Green credit cards

It is a product launched to make credit cards, which are widely used today, environmentally friendly. Green credit cards encourage the market for low-carbon services and products. A rewarding system is also applied for the purpose of incentivizing.

DOI: http://dx.doi.org/10.32571/ijct.1199748 E-ISSN: 2602-277X

Green credit card purchases of environmentally friendly products, paperless transactions, use of public transportation and reduced electricity and gas expenditures earn points that can be cashed in or traded. Discounts are offered for recycled vehicles and electric charging. The use of green credit cards, which enable them to reduce their carbon footprint, prevents the use of substances that harm the environment in many areas. Using e-mail instead of receipts in invoice collections, sending credit card statements via e-mail, and using credit cards more instead of paper money reduce paper production and protect trees.[26]

2.2. Corporate finance

Investments that provide financing support to projects that support and care about the protection of natural resources, taking into account environmental and social impacts, have supported the development of green banking services and products.[26]

Corporate Finance is a concept that provides high levels of resources to governments, corporations and public institutions. These activities are seen as financial instruments that trade in equities, foreign exchange and commodities.

2.2.1. Green project finance

The financing of a project is managed by the project sponsor and the company owned by the sponsor, together with project customers, suppliers and the company owning the project, signing many different and complex contracts. Usually, the borrowing banks undertake most of the debt financing.[27]

Project finance is a mix of debt and equity, as well as non-financeable finance. Loans for projects in areas such as petrochemicals, telecommunications and natural resources are referred to as project finance.

2.2.2. Green securities

Securities are the securitization of illiquid assets such as credit card receivables, mortgages, car loans and lease payments, and their transformation into a structure that can be bought and sold in the market.[29]

Green securities, on the other hand, provide the opportunity to transfer these securitized assets to banks by reducing the risks of environmental projects and how the risks of the projects will be regulated, maintaining the relationship between the financiers providing guarantees for the products and the institutions and banks.[30] In addition, when bonds, which are securities, are used for certain projects, they are called green bonds and are used only for these projects.[31] Green bonds, which were first introduced by the World Bank and the European Investment Bank in 2007, were created to be used in projects that will provide positive support for environmental and climatic events.[32]

2.2.3. Green technology

Green technology leasing is defined as equity and similar investment instruments provided by venture capitalists to projects in return for a certain share for new and renewable ideas and technological products.[33] The investment, which is realized with the motto of high risk, high return, continues with the transfer of experience and knowledge, feasibility and managerial support in addition to the capital provided.

2.2.4. Carbon finance

Carbon finance, which started with the initiative of the World Bank, is based on the calculation of the economic value of the damage caused by carbon emissions to the atmosphere. Carbon trading, which emerged with the emission limitations of the Kyoto Protocol, is a barter system in the market area. In this trade, there is an emission amount determined for each country, and countries that exceed this amount either go to restrictions or pay for their rights to countries below the amount.[32]

Carbon finance is a specialized form of environmental finance that calculates the cost of living by examining climate changes where carbon emissions are high. Since carbon dioxide makes up the majority of the gases released in these emissions, the market is called the carbon market. This market, which represents gases such as carbon dioxide, greenhouse gases and methane, operates by trading carbon stocks of high-emitting gases. Payments in the carbon market can be made through payments such as stocks, cash, borrowing, as well as emission reductions. It is also accepted as a payment method in technological investments that will realize emission reduction.[34]

Mandatory carbon markets are not yet at the desired levels and are limited in number. Developing them for each country will be a factor for enforcement and sanctions and will strengthen carbon emission limitations.

2.3. Asset management

Wealth management refers to the business unit of core banks that have realized rapid growth in the financial sector. It provides financial advice to clients in the areas of mutual funds, price discounting, planning, tax, managed asset programs and global banking.[35]

Asset management companies were established with the aim of restructuring, collecting and selling the receivables and asset purchases of insurance funds, financial institutions and banks in the financial sector.[36] In addition, it includes products such as green public

DOI: http://dx.doi.org/10.32571/ijct.1199748 E-ISSN: 2602-277X

funds, green investment and carbon funds provided by projects that support environmental and climatic development and protection.[37]

2.3.1. Green public fund

Green public funds provide loans with lower interest rates to green projects to be invested in by deducting interest and dividend income determined by banks from taxes. Savings from green public funds can only be used for green projects.[37] Launched in 1995 in Dutch banks with government support, the green fund initiative is a first in this field. Individuals who purchase green fund shares or invest in a green bank are exempt from capital allowances or income tax or can benefit from discounts. This paves the way for loans with lower interest rates.[22]

2.3.2. Green investment funds

Green investment funds are a type of investment that enables businesses to fund investments that will benefit green areas such as renewable energy, waste management and organic agriculture. Green investment funds avoid the complexity that can arise in the investment planning process. The first priority of funding is based on social and environmental criteria, followed by environmental and social policies. Finally, the funds are used for potential investments.[22] Funds used in previous projects are transferred to other stages with knowledge, experience and experience, and in this process, savings are achieved by being effective in reducing transaction costs and environmental impacts.[37]

2.3.3. Carbon fund

Carbon funds have been established in cooperation with development banks and private organizations to support projects developed to reduce gas emissions. While carbon funds established with government incentives aim to maintain Kyoto criteria, companies reduce costs and achieve savings in funds realized with private financing support. Carbon funds offer investors corporate social responsibility, cash return and marketing opportunities.[22] The World Bank established the first global carbon fund in 2000, and by 2014, a total of 187 million tons of carbon dioxide emissions were achieved. The Protoip Carbon Fund (PCF) was created by the World Bank for emission reduction purposes and the fund has a value of 180 million dollars.[38]

2.4. Insurance

Insurance consists of two main categories. General and Life Insurance. Green insurance is included in the general insurance category. Green insurance is divided into two categories. Insurance for products that vary according to their environmental characteristics and insurance products used for green technologies and carbon emission reduction activities.

Sustainable insurance is seen as a system that engages stakeholder interactions by identifying, managing and assessing social, governance and environmental issues and risks. It also aims to achieve environmental, economic and social sustainability through risk management and mitigation, innovative solutions and improved business performance.[39]

The Sustainable Insurance Fund (SIF) was launched in 2016 as an organization that keeps climate change on its agenda and collaborates with insurance regulators while promoting sustainability (SIF, 2018). Taking into account environmental and social activities, insurance companies work on identifying environmental factors and directing capital to green assets.[39]

2.4.1. Green car insurance

Green vehicle insurance is a type of insurance that supports the use of fuel-saving, hybrid and electric vehicles for environmental benefits.[37] Usage-based vehicle insurance (UBI) is an insurance concept referred to as pay-per-mile, pay-as-you-go. This type of insurance is usage-based and insurance costs vary depending on how and how much the vehicles are used. [40] This type of usage-based insurance protects the consumer and becomes more socially attractive, which depends on premium payments and driver behavior.[41]

2.4.2. Green building insurance

Traditional insurance products are insufficient to cover specialized systems and materials, complex structures and resources required for green building projects. Providing quality products that help prevent and improve climate and environmental losses are green building insurance products. Prevention of energy loss, use of environmentally friendly materials in building construction and repair, coverage of losses and various discount opportunities are green insurance products.[37]

Increasing costs for energy and carbon emissions have led to a growing emphasis on buildings from an environmental point of view. Comparing green building investments with conventional buildings raises a number of insurance issues. Products that address green building features are provided through green insurance in a scheme that aims to protect the environment.[42]

2.4.3. Carbon insurance

Climate and environmental changes are highly affected by human use of fuels for heating. Gas emissions resulting from human activities have become an important issue that cannot be ignored. In the face of this situation, measures are taken with carbon insurance. Carbon insurance is a form of insurance that supports activities such as reducing the emission of greenhouse

DOI: http://dx.doi.org/10.32571/ijct.1199748 E-ISSN: 2602-277X

gases and keeping emissions under control, including carbon sequestration strategies.[42]

Carbon insurance is a type of insurance that emerged to protect low-carbon projects and projects aimed at reducing gas emissions. It is a type of insurance that offers investors flexible and appropriate regulations such as emission reductions and carbon credits.

3. RESULT AND DISCUSSION

With the emergence of the green finance economy, environmentally sensitive green finance products have also emerged. The purpose of these products is primarily to protect the environment and to include environmentally conscious people in this financial system. Green mortgages, green home loans, green commercial building loans, green car loans and green credit cards are the most prominent green financing instruments in the retail market. In addition to these, on the corporate finance side, instruments such as green project finance, green securities, green technology leasing and carbon finance provide institutional support. Eco fund and carbon fund in the asset management segment, and car insurance, carbon insurance and green insurance in the insurance segment. As can be seen, when we consider the increasing global warming, environmentally conscious development and our debts to the environment, the financial system's efforts to find a place in this field by finding solutions to global warming are increasing day by day, and these demands are being met in the international arena. While the spread of green financing instruments not only to environmentalist individuals and companies but also to all segments of the public is a debt we owe to the environment, the fact that we will make the world we live in together a more liveable and healthier place is foreseen.

Conflict of interests

I declares that there is no a conflict of interest with any person, institute, company, etc.

REFERENCES

1. UNEP 2009. A G lobal Green New Deal: Policy Brief, United Nations Environment Programme, Economics and Trade Branch, Geneva

2. Barbier, E. B. *A Global Green New Deal: Rethinking the Economic Recovery*, Cambridge University Press, Cambridge, USA, 2010

3. Barbier, E. B.. *Rethinking the Economic Recovery: A Global Green New Deal*, UNEP, USA, 2009

4. Homer-Dixon, T . *The Upside of Down: Catastrophe*, Thomas Homer-Dixon Publisher: Vintage Canada, 2007

5. Jones, V. *The Green Collar Economy: How One Solution Can Fix Our Two Biggest Problems*, Harper Collins, New York, 2009

6. Esty, D. C. and Winston, A. S. *Green to Gold: How Smart Companies Use Environmental Strategy to Innovate* Hoboken, USA, 2006

7. Croston, G. 75 *Green Businesses: You Can Start to Make Money and Make a Difference*, Entrepreneur Press, Irvine, CA, 2008

8. Makower, J. *Strategies for the Green Economy: Opportunities and Challenges in the New World of Business*, McGraw-Hill, New York, USA, 2009

9. Kane, G. *The Three Secrets of Green Business: Unlocking Competitive Advantage in a Low Carbon Economy*, Earthscan, London, UK, 2010

10. Weybrecht, G.. *The Sustainable MBA: The Manager's Guide to Green Business, John Wiley & Sons*, Chichester, UK, 2010

11. UNEP. *Tow ards a Green Economy: Pathways to Sustainable Development and Poverty Eradication*, UNEP, Geneva, Switzerland, 2011

12. Soundarrajan, P., ; Vivek, N.; Muchall, H.M.; Agricultural Economics. 2016, 62(1), 35-44.

13. Begg, D., Vernasca, G., Fischer, S. and Dornbusch, R.. *Economics*, 10th ed; McGraw-Hill, Maidenhead, UK, 2011

14. Parkin, M., Po well, M. and Matthews, K.. *Economics*, 8th ed, Pearson Education, Harlow, UK, 2012

15. Newton, A.C. and Cantarello, E. *An Introductıon To The Green Economy, Science, systems and sustainability*, NY, USA, 2014

16. Common, M. and Stagl, S. *Ecological Economics: An Introduction*, Cambridge University Press, Cambridge, UK, 2005

17. Faber, M. Ecological Economics, 2008, 66, 1–7.

18. Cato, M. S. *Environment and Economy*, Routledge, London, UK, 2011

19. Noh H.J. *Financial Strategy to Accelerate Innovation for Green Growth*. Asian Development Bank Institute, Tokyo, Japan, 2018

20. Poyraz E. *Finansta Güncel Konular*; Tepeli Y. and Mingen C.,.; Nobel: Ankara, 2007; pp 87-117.

DOI: http://dx.doi.org/10.32571/ijct.1199748 **E-ISSN: 2602-277X**

21. Carroll A.B. *The Academy of Management Review*, 1979, 4, 497-505

22. UNEP. *Green Financial Products and Services Report*. Canada, 2007

23. Coşkun, Y. *Bankalarda Öz Disiplin Süreçlerinin Etkinliğinin Değerlendirilmesi*. SPK Yayınları. Ankara, Türkiye, 2008

24. Wentworth, A. European Banks Launch Green Mortgage Pilot Scheme (Online), http://www.climateaction.org/news/european-banks-launch-green-mortgage-pilotscheme/ (accessed September 14, 2022).

25. https://www.epa.gov/smartway/learn-about-smartway (accessed September 14, 2022)

26. Konsko, L. (2014). How Your Credit Card Can Help You Go Green? NerdWallet. (Online), https://www.businessinsider.com/make-everyday-purchases-greener-2014-4, (accessed September 10, 2022)

27. Güler, O. ve Tufan, E. Anatolia: Turizm Araştırmaları Dergisi, 2015, 26(1): 80-96.

28. Richard A., Brealey,Ian A., Cooper,Michel A. H., *Using Project Finance To Fund Infrastructure Invesments*. Journal of Applied Corporate Finance, Columbia, USA, 1996

29. Erdönmez, P. Bankacılık Dergisi. 2006, 57, 75-85.

30. Kuloğlu, E., Öncel, M. Gazi Üniversitesi Sosyal Bilimler Dergisi. 2015, 2(2), 2-19.

31. Kandır, S. Y., Yakar, S. Sosyal Bilimler Enstitüsü Dergisi. 2017, 26(2): 159-175.

32. Escarus, Önlenemeyen Gerçek: İklim Değişikliği, İklim Finansmanı 2016 Raporu. 2016

33. Rodoplu, G. *Para ve Sermaye Piyasaları*. 2002, Isparta, Türkiye.

34. Demireli, E. ve Hepkorucu, A., Ekonomi Bilimleri Dergisi. 2010, 2(2), 37-48

35. UNEP. *Pacific Island Mangroves in a Changing Climate and Rising Sea*, Nairobi, Kenya, 2006

36. Lök, H. Mukaddime, 2018, 9(2), 195-21

37. Sevim, U., Serçemeli, M. *Yeşil Finans ve Muhasebe Teori ve Uygulama*. Gazi Kitabevi, Ankara, Türkiye, 2018

38. Lecocq, F. American Journal and Agricultural Economics. 2003, 85(3): 703–707.

39. UNEP, Annual Report, Nairobi, Kenya, 2012

40. Grzadkowska, A. What İs Usage-Based İnsurance? (Online) 2018 https://www.insurancebusinessmag.com/asia/guides/what-is-usagebased-insurance116606.aspx (accessed September 5, 2022).

41. Ochenkowski, J., and Schinter, J. Insurance for Green Buildings., (Online) 2008, http://www.buildings.com/tabid/3334/ArticleID/6354/Default.aspx (accessed September 10, 2022).

42. Adler, J.H. Greenhouse policy without regrets. A free market approach to the uncertain risks of climate change. Competitive Enterprise Institute CEI, Washington, USA, 2000.

DOI: http://dx.doi.org/10.32571/ijct.1190931 E-ISSN: 2602-277X

International Journal of Chemistry and Technology

http://dergipark.org.tr/ijct

Research Article

Structural transition of $LiBeH_3$ under high pressure

Çağatay YAMÇICIER[1], Selgin AL[2*]

[1] *Department of Electric and Energy, Osmaniye Korkut Ata University, Osmaniye, Türkiye.*

[2] *Department of Environmental Protection Technologies, Izmir Democracy University, Izmir, Türkiye.*

Received: 18 October 2022; Revised: 8 November 2022; Accepted: 18 November 2022

*Corresponding author e-mail: selgin.al@idu.edu.tr

Citation: Yamçıçer, Ç.; Al, S. *Int. J. Chem. Technol.* **2022**, 6 (2), 129-134.

ABSTRACT

$LiBeH_3$ has been considered as a solid-state hydrogen storage material. This study investigated Pnma orthorhombic phase of $LiBeH_3$ under pressure. Ab initio constant pressure molecular dynamic simulation under pressure was adopted. The results depicted a phase transition from Pnma orthorhombic phase to $P2_1/m$ monoclinic phase at 270 GPa simulation pressure. The stability of each phase was examined using elastic constants. Based on the well-known Born stability criteria, both phases showed mechanical stability. Several moduli have been computed via elastic constants. The B/G ratios, Cauchy pressures and Poisson's ratios investigation revealed that $LiBeH_3$ is brittle at Pnma phase whereas it is ductile at $P2_1/m$ phase. The electronic band structures and partial and total density of states of phases were also obtained. A 2.058 eV band gap was seen for Pnma phase, and 3 eV band gap was seen for $P2_1/m$ phase.

Keywords: Phase transition, ab initio, elastic properties, stability.

Yüksek basınç altında $LiBeH_3$'ün yapısal faz geçişinin incelenmesi

ÖZ

$LiBeH_3$, katı hal hidrojen depolama malzemesi olarak literatürde çalışılmaktadır. Bu çalışma, basınç altında $LiBeH_3$'ün Pnma ortorombik fazını araştırmaktadır. Ab initio sabit basınç moleküler dinamik simülasyonu kullanılmıştır. Sonuçlar, 270 GPa simülasyon basıncında Pnma ortorombik fazdan $P2_1/m$ monoklinik faza bir faz geçişini göstermektedir. Her fazın kararlılığı, elastik sabitler kullanılarak incelenmiştir. Born stabilite kriterlerine göre, her iki faz da mekanik kararlılık göstermektedir. Elastik sabitler aracılığıyla diğer modüller de hesaplanmıştır. B/G oranları, Cauchy basınçları ve Poisson oranları, $LiBeH_3$'ün Pnma fazında kırılgan yapıya sahip olduğunu, $P2_1/m$ fazında ise sünek yapıya sahip olduğunu göstermektedir. Elektronik bant yapıları incelendiğinde, Pnma fazı için 2.058 eV bant aralığı, $P2_1/m$ fazı için 3 eV bant aralığı görülmektedir.

Anahtar Kelimeler: Faz geçişi, ab initio, elastik özellikler, kararlılık.

1. INTRODUCTION

The continues increase in world population and fast urbanization has caused a dramatic rise in energy consumption and demand. Most of this demand is still met by using hydrocarbon fuels and classic ways of producing electricity which has resulted in an increase in CO_2 emissions and other greenhouse gases. This created climate change crises and global warming. One of the popular options to mitigate climate change is that adopting renewable energy which provides a shift from hydrocarbon-based energy production to clean and sustainable energy production. One challenge with that approach is to store energy to avoid fluctuations and setbacks. Recently, hydrogen has been suggested as a reliable energy carrier to ease the problem of storing and transporting renewable energy safely.[1,2] Hence, there is growing research in literature to shift carbon-free energy generation using hydrogen as a carrier. Hydrogen energy requires four main stages: production, storage, transport, and end use. There are several materials under investigation for each stage. Hydrogen can be stored in different ways, compressed hydrogen storage, liquid hydrogen, metal hydrides and chemical hydrides.[3] The elemental metal hydrides such as magnesium hydride

DOI: http://dx.doi.org/10.32571/ijct.1190931 E-ISSN: 2602-277X

(MgH_2) and aluminum hydride (AlH_3) has been studied extensively.[4-6] Due to slow kinetics of hydrogenation and dehydrogenation and strong bond between magnesium and hydrogen MgH_2 is still under investigation. Light metal hydrides are under intense investigation due to their high hydrogen gravimetric density. $LiBeH_3$ is one of the studied materials which exists in different symmetries. The experimental studies are very little since Be is very toxic and requires precautions. Thus, most properties of $LiBeH_3$ were investigated computationally. The elastic properties of cubic and orthorhombic $LiBeH_3$ was studied by Rehmat et al.[7] It was reported that $LiBeH_3$ can be used as active photocatalyst for green hydrogen production.[8] The electronic and mechanical properties of cubic and orthorhombic $LiBeH_3$ have been studied theoretically.[9-11] In this study, elastic and electronic properties of orthorhombic $LiBeH_3$ will be studied by adopting first principles calculations. Also, phase transitions of $LiBeH_3$ will be examined under high pressure. The obtained phases then will be evaluated for phase stability.

2. METHOD OF COMPUTATION

The ab initio computations were adopted within the density functional theory as implemented in SIESTA method in order to calculate structural, elastic, and electronic properties of $LiBeH_3$.[12] Perdew-Burke-Ernzerhof, generalised gradient approximation (PBE-GGA) was used for the exchange correlation potential.[13] A 8x8x8 k-points mash was taken to sample the Brillouin zone. The electronic wave functions were expanded in plane-wave basis to set up a kinetic energy cut off to 30 Ry, while the cut off energy for the electronic charge density was set to 300 Ry. $LiBeH_3$ was modelled using 2x2x2 cells with periodic boundary conditions for 160 atoms supercells. The Brillouin zones (BZ) were sampled with the 8x6x8 and 8x8x8 Monkhorst-Pack k-point mesh for Pnma and $P2_1/m$ structures, respectively.

3. RESULTS AND DISCUSSION

3.1 Structural evolution

Firstly, the formation energy of $LiBeH_3$ has been computed as -0.221 eV. The negative formation energy indicates synthesizability and dynamic stability. Then pressure was applied to the structure. The volume change under pressure using the simulation cell (160 atoms with a 2x2x2 cells) is shown in **Figure 1**. V/V_o represents a reduction in volume compared to zero pressure volume. The cell parameters at 0 GPa (Pnma phase) are a= 4.6167 Å, b= 6.4320 Å and c = 4.5438 Å. The volume of simulation cell drops at 270 GPa about 3.90 %, and a phase transition from Pnma to $P2_1/m$ is observed. The cell parameters are 4.5217 Å, b= 4.5762 Å and c = 4.7251 Å. The atomic structures at both phases are illustrated in Figure 2.

It is possible to estimate the transition pressure higher than the actual phase transition due to adopting perfect structures and boundary conditions during the simulation[14-18] Hence, the thermodynamic theorem to calculate the transition pressure was also used. The energy-volume calculations have been carried out and presented in Figure 2 and Figure 4. The details of calculation was given in ref.[19] It can be seen from Figure 4 that both phases cross each other at 34 GPa, suggesting that the transition from Pnma phase to $P2_1/m$ phase occurs at 34 GPa.

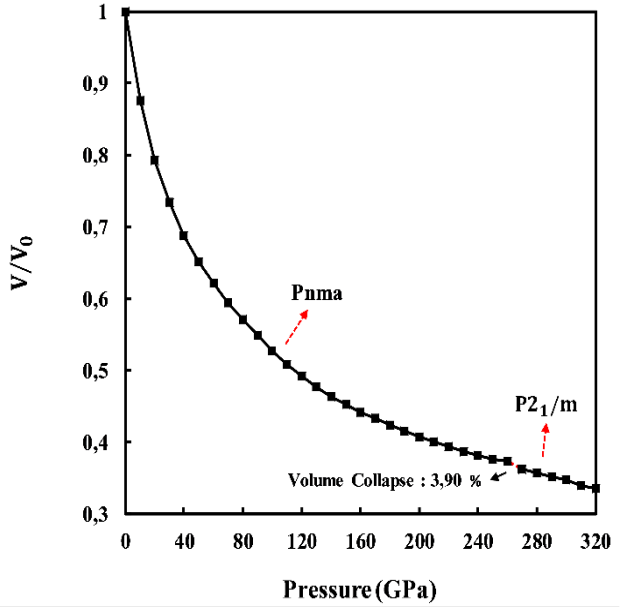

Figure 1. The change in volume of $LiBeH_3$ under hydrostatic pressure.

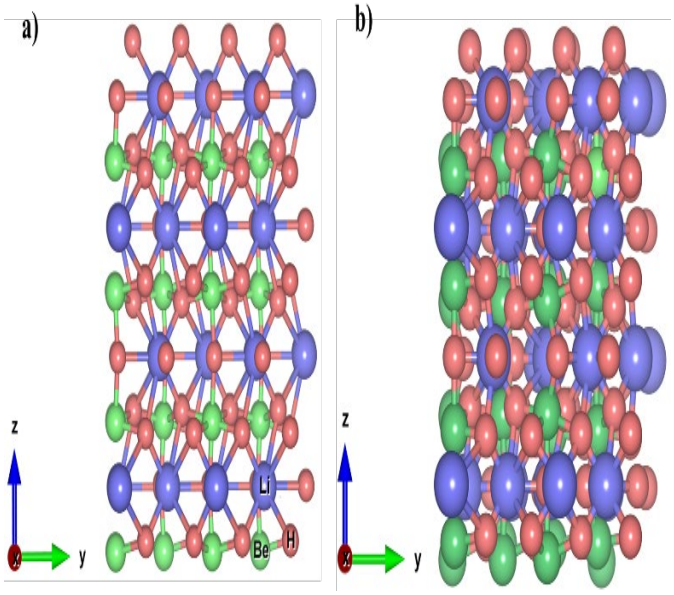

Figure 2. The structure of $LiBeH_3$ at a) 0 GPa (Pnma) b) 270 GPa ($P2_1/m$).

DOI: http://dx.doi.org/10.32571/ijct.1190931 E-ISSN: 2602-277X

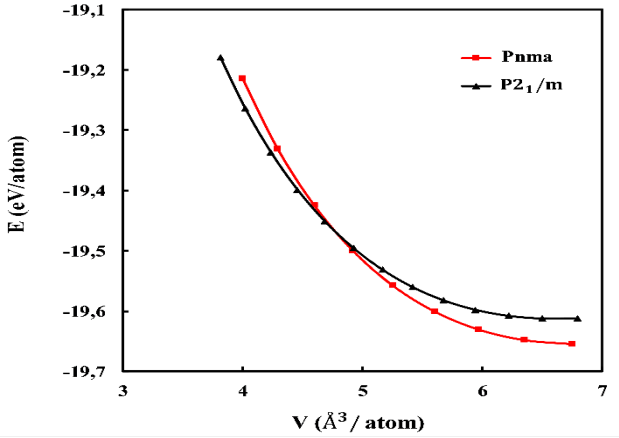

Figure 3. Energy volume of $LiBeH_3$ phases.

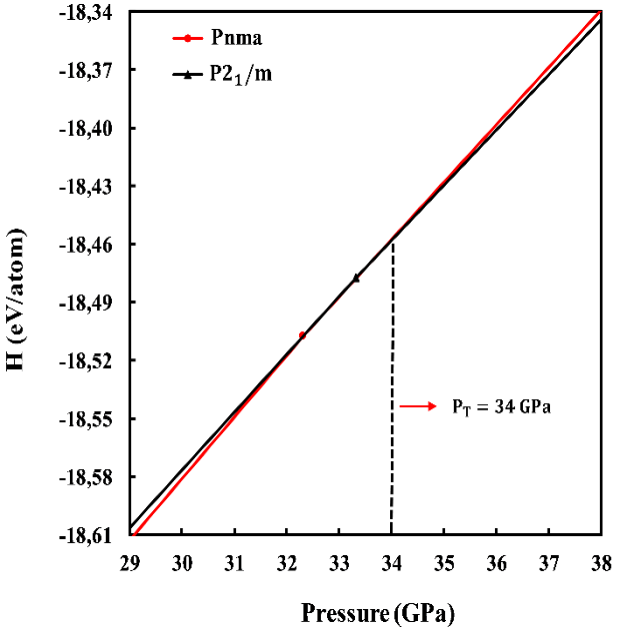

Figure 4. Enthalpy changes of phases under pressure.

3.2 Elastic properties

Elastic constants of materials provide information about materials' response when an external pressure is applied along with mechanical properties.[20,21] For an orthorhombic structure, there are nine elastic constants defined as C_{11}, C_{22}, C_{33}, C_{44}, C_{55}, C_{66}, C_{12}, C_{13}, C_{23}.[22,23] The well-known Born criteria for an orthorhombic structure is given as;[24,25]

$C_{11} + C_{33} - 2C_{13} > 0$, $C_{22} + C_{33} - 2C_{23} > 0$, $C_{11} + C_{22} - 2C_{12} > 0$,
$C_{11} > 0$, $C_{22} > 0$, $C_{33} > 0$, $C_{44} > 0$, $C_{55} > 0$, $C_{66} > 0$,
$C_{11} + C_{22} + C_{33} + 2(C_{12} + C_{13} + C_{23}) > 0$,
$1/3\ (C_{12} + C_{13} + C_{23}) < B < (C_{11} + C_{22} + C_{33})$ (1)

There are thirteen independent elastic constants are defined for a low symmetry monoclinic structure as C_{ij}.[26,27] Born stability criteria is defined as;[28,29]

$C_{33}C_{55} - C^2_{35} > 0$, $C_{44}C_{66} - C^2_{46} > 0$,
$C_{22} + C_{33} - 2C_{23} > 0$ $C_{11} + C_{22} + C_{33} + 2(C_{12} + C_{13} + C_{23}) > 0$
$C_{22}(C_{33}C_{55} - C^2_{35}) + 2C_{23}C_{25}C_{35} - C^2_{23}C_{55} - C^2_{25}C_{33} > 0$,
$2[C_{15}C_{25}(C_{33}C_{12} - C_{13}C_{23}) + C_{15}C_{35}(C_{22}C_{13} - C_{12}C_{23}) + C_{25}C_{35}(C_{11}C_{23} - C_{12}C_{13})] - [C^2_{15}(C_{22}C_{33} - C^2_{23}) + C^2_{25}(C_{11}C_{33} - C^2_{13}) + C^2_{35}(C_{11}C_{22} - C^2_{12})] + gC_{55} > 0$,
With $g = C_{11}C_{22}C_{33} - C_{11}C^2_{23} - C_{22}C^2_{13} - C_{33}C^2_{12} + 2C_{12}C_{13}C_{23}$ (2)

As can be seen from Table 1 that both Pnma and $P2_1/m$ phase is mechanically stable. In order to investigate mechanical properties of phases, other crucial parameters have been calculated using elastic constants and presented in Table 2. Bulk modulus of $LiBeH_3$ was found to be 54 GPa in this study which is in a good agreement with ref.[11] (59.82 GPa) and ref.[7] (68.17 GPa). There is no data found in literature to compare bulk modulus of $P2_1/m$ phase of $LiBeH_3$.

Table 1. The obtained elastic constants (GPa) of phases of $LiBeH_3$.

Phases	C_{11}	C_{12}	C_{13}	C_{15}	C_{22}	C_{23}	C_{25}	C_{33}	C_{35}	C_{44}	C_{46}	C_{55}	C_{66}	Refs.
Pnma	96.41	38.13	32.41	-	100.05	27.73	-	93.78	-	52.34	-	36.46	60.65	This study
$P2_1/m$	685.49	252.96	414.79	58.11	757.95	297.67	-4.72	680.11	-83.74	238.18	-8.01	113.94	217.97	This study

Table 2. The calculated Bulk modulus (*B*,GPa), Shear modulus *G* (GPa), Young's modulus *E* (GPa) , *B/G and G/B* ratios, and Poisson's ratios (σ) of phases of $LiBeH_3$.

Phases	B	G	E	B/G	G/B	σ	Refs.
Pnma	54.00	41.17	98.49	1.31	0.76	0.196	This study
$P2_1/m$	449.75	162.65	435.47	2.77	0.36	0.339	This study

DOI: http://dx.doi.org/10.32571/ijct.1190931 E-ISSN: 2602-277X

Brittleness and ductility of $LiBeH_3$ was examined using B/G, G/B and Cauchy pressures. It was stated that a B/G ratio higher than 1.75 indicates ductility and a B/G ratio lower than 1.75 indicates brittleness.[30,31] In addition, Pettifor[32] stated that Cauchy pressure can also provide information about ductility/brittleness and bonding characteristics. Negative Cauchy pressure implies brittleness and directional angular or covalent bondingwhereas positive Cauchy pressure indicates ductility and predominance of ionic bonding characteristics. For an orthorhombic structure, Cauchy pressure is C_{23}-C_{44} for (100) plane, C_{13}-C_{55} for (010) plane and C_{12}-C_{66}) for (001) plane.[33] Pnma phase of $LiBeH_3$ has a B/G ratio of 1.31 which lower than 1.75, thus Pnma phase of $LiBeH_3$ is brittle. Cauchy pressures are -24.61 for (100) plane, -4.05 for (010) plane and -22.52 for (001) plane. The negative values of Cauchy pressures also suggest brittleness and angular/covalent nature. On the other hand, $P2_1/m$ phase of $LiBeH_3$ shows ductile nature since its B/G ratio is higher than 1.75. Cauchy pressures for $P2_1/m$ phase is calculated similar to Pnma phase.[34] It is found as 59.49 GPa for (100) plane, 300.85 GPa for (010) plane and 34.99 GPa for (001) plane. The positive values of Cauchy pressure confirm ductile nature of $P2_1/m$ phase of $LiBeH_3$.

Frantsevich et al.[35] also stated that Poisson's ratio (σ) can be used to determine ductility and brittleness of materials by the ratio of 0.26. If the Poisson's ratio is less than 0.26, the material is brittle, if it is higher than 0.26, it is classified as ductile. By evaluating, Poisson's ratios of phases, it can be confirmed that Pnma phase of $LiBeH_3$ is brittle and $P2_1/m$ phase of $LiBeH_3$ is ductile.
Shear modulus (G) of materials describe materials response against shape change. Young modulus (E) gives information about stiffness. By comparing two phases, it is seen that $P2_1/m$ phase will show higher resistance towards shape change and stiffer compared to Pnma phase.

In addition to polycrystal elastic constants, Vickers hardness and melting point of $LiBeH_3$ is also computed. Vickers hardness is obtained from $H_V^G = 0.1769G-2.899$ and $H_V^E = 0.0608E$ relation and melting point is computed using $Tm = 354 + 4.5 (2C_{11}+C_{33})/3$ relation.[36,37] From our calculations, $H_V^G = 4.38$ GPa and $H_V^E = 5.98$ GPa are obtained for Pnma phase. Both values are less than 10 GPa, thus Pnma phase of $LiBeH_3$ cannot be classified as a hard material. The melting point of Pnma phase of $LiBeH_3$ is obtained as 783.9 K. For $P2_1/m$ phase of $LiBeH_3$, $H_V^G = 25.87$ GPa and $H_V^E = 26.47$ GPa are obtained. It is seen that $P2_1/m$ phase of $LiBeH_3$ is a hard material. The melting point is computed as 3430 K for $P2_1/m$ phase.

3.3 Electronic properties

In order to investigate electronic properties of phases, the electronic band structures and partial and total density of states have been computed and presented in Figure 5 and Figure 6 for both phases. 0 eV was determined as Fermi energy level. As can be seen from Figures that band gaps are present for both phases. Pnma phase has 2.058 eV band gap whereas $P2_1/m$ phase has 3 eV band gap. The band gap seems to increase with pressure. H-1s states seem to contribute to the valence band for both phases. Be-2s states seem to contribute to the conduction band along with H-1s states.

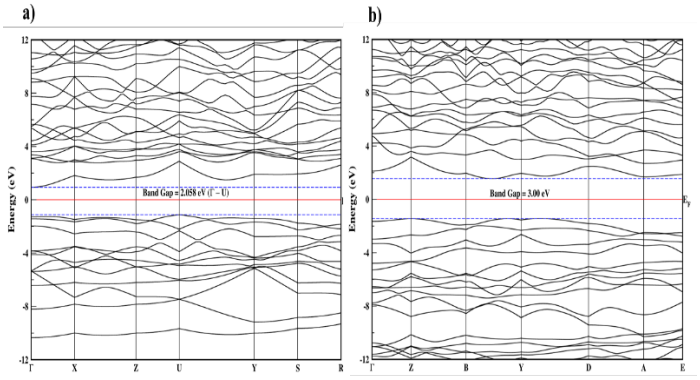

Figure 5. The calculated electronic band structures of $LiBeH_3$ at 0 GPa and at 270 GPa.

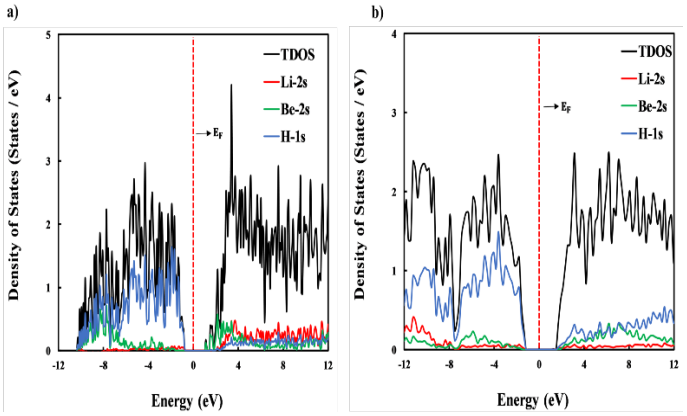

Figure 6. The partial and total DOS of $LiBeH_3$ at 0 GPa and at 270 GPa

4. CONCLUSION

This study investigated the structural, mechanical and electronic properties of $LiBeH_3$ under pressure. A phase transition from Pnma phase to $P2_1/m$ phase was observed at 34 GPa. The elastic constants evaluation depicted that both phases are mechanically stable. The B/G ratio, Cauchy pressure and Poisson's ratio of Pnma phase implied that Pnma phase of $LiBeH_3$ is brittle which might require extra attention when handling it. On the other hand, $P2_1/m$ phase was found to be ductile. The electronic band structure of phases showed band gap, indicating that both phases of $LiBeH_3$ is insulating.

Conflict of interests

I declares that there is no a conflict of interest with any institute, person, company, etc.

DOI: http://dx.doi.org/10.32571/ijct.1190931 E-ISSN: 2602-277X

References

1. Ajanovic, A.; Sayer, M.; Haas, R., The economics and the environmental benignity of different colors of hydrogen. *Int. J. Hydrogen Energy* **2022,** *47* (57), 24136-24154.

2. Dawood, F.; Anda, M.; Shafiullah, G. M., Hydrogen production for energy: An overview. *Int. J. Hydrogen Energy* **2020,** *45* (7), 3847-3869.

3. Andersson, J.; Grönkvist, S., Large-scale storage of hydrogen. *Int. J. Hydrogen Energy* **2019,** *44* (23), 11901-11919.

4. Wolverton, C.; Ozoliņš, V.; Asta, M., Hydrogen in aluminum: First-principles calculations of structure and thermodynamics. *PhRvB* **2004,** *69* (14), 144109.

5. Züttel, A., Materials for hydrogen storage. *Mater. Today* **2003,** *6* (9), 24-33.

6. Andreasen, A., Hydrogenation properties of Mg–Al alloys. *Int. J. Hydrogen Energy* **2008,** *33* (24), 7489-7497.

7. Rehmat, B.; Rafiq, M. A.; Javed, Y.; Irshad, Z.; Ahmed, N.; Mirza, S. M., Elastic properties of perovskite-type hydrides $LiBeH_3$ and $NaBeH_3$ for hydrogen storage. *Int. J. Hydrogen Energy* **2017,** *42* (15), 10038-10046.

8. Reshak, A. H., Photocatalytic water splitting solar-to-hydrogen energy conversion: Perovskite-type hydride $XBeH_3$ (X=Li or Na) as active photocatalysts. *J. Catal.* **2017,** *351*, 119-129.

9. Xiao-Jiao, S.; Zhi, H.; Yan-Ming, M.; Tian, C.; Bing-Bing, L.; Guang-Tian, Z., Electronic structure and optical properties of $LiXH_3$ and $XLiH_3$ (X= Be, B or C). *Chinese Physics B* **2008,** *17* (6), 2222-2228.

10. Santhosh, M.; Rajeswarapalanichamy, R.; Priyanga, G. S.; Kanagaprabha, S.; Murugan, A.; Iyakutti, K., A first principles study of structural stability, electronic structure and mechanical properties of $ABeH_3$ (A = Li, Na). **2015,** *1665* (1), 090015.

11. Vajeeston, P.; Ravindran, P.; Fjellvåg, H., Structural Phase Stability Studies on $MBeH_3$ (M = Li, Na, K, Rb, Cs) from Density Functional Calculations. *Inorg. Chem.* **2008,** *47* (2), 508-514.

12. Ordejón, P.; Artacho, E.; Soler, J. M., Self-consistent order-N density-functional calculations for very large systems. *PhRvB* **1996,** *53* (16), R10441.

13. Perdew, J. P.; Burke, K.; Ernzerhof, M., Generalized Gradient Approximation Made Simple. *Phys. Rev. Lett.* **1996,** *77* (18), 3865-3868.

14. Yamcicier, C.; Merdan, Z.; Kurkcu, C., Investigation of the structural and electronic properties of CdS under high pressure: an ab initio study. *Can. J. Phys.* **2017,** *96* (2), 216-224.

15. Kürkçü, C.; Selgin, A.; Merdan, Z.; Yamçiçier, Ç.; Öztürk, H., Investigation of structural and electronic properties of β-HgS: Molecular dynamics simulations. *ChJPh* **2018,** *56* (3), 783-792.

16. Durandurdu, M., Orthorhombic intermediate phases for the wurtzite-to-rocksalt phase transformation of CdSe: An ab initio constant pressure study. *Chem. Phys.* **2010,** *369* (2-3), 55-58.

17. Kürkçü, C.; Merdan, Z.; Öztürk, H., Theoretical calculations of high-pressure phases of NiF_2: An ab initio constant-pressure study. *Russian Journal of Physical Chemistry A* **2016,** *90* (13), 2550-2555.

18. Kürkçü, C.; Merdan, Z.; Öztürk, H., Pressure-induced phase transitions and structural properties of CoF_2: An ab-initio molecular dynamics study. *Solid State Communications* **2016,** *231*, 17-25.

19. Al, S.; Kurkcu, C.; Yamcicier, C., Structural evolution, mechanical, electronic and vibrational properties of high capacity hydrogen storage TiH_4. *Int. J. Hydrogen Energy* **2020,** *45* (55), 30783-30791.

20. Bougherara, K.; Litimein, F.; Khenata, R.; Uçgun, E.; Ocak, H.; Uğur, Ş.; Uğur, G.; Reshak, A. H.; Soyalp, F.; Omran, S. B., Structural, elastic, electronic and optical properties of Cu_3TMSe_4 (TM= V, Nb and Ta) sulvanite compounds via first-principles calculations. *J Science of Advanced Materials* **2013,** *5* (1), 97-106.

21. Benzoudji, F.; Abid, O. M.; Seddik, T.; Yakoubi, A.; Khenata, R.; Meradji, H.; Uğur, G.; Uğur, S.; Ocak, H. Y., Insight into the structural, elastic, electronic, thermoelectric, thermodynamic and optical properties of MRhSb (M= Ti, Zr, Hf) half-Heuslers from ab initio calculations. *J Chinese Journal of Physics* **2019,** *59*, 434-448.

22. Li, P.; Zhang, J.; Ma, S.; Zhang, Y.; Jin, H.; Mao, S., First-principles investigations on structural stability, elastic and electronic properties of Co_7M_6 (M= W, Mo, Nb) μ phases. *MoSim* **2019,** *45* (9), 752-758.

23. Subhan, F.; Azam, S.; Khan, G.; Irfan, M.; Muhammad, S.; Al-Sehemi, A. G.; Naqib, S. H.; Khenata, R.; Khan, S.; Kityk, I. V.; Amin, B., Elastic and optoelectronic properties of $CaTa_2O_6$ compounds:

DOI: http://dx.doi.org/10.32571/ijct.1190931 E-ISSN: 2602-277X

Cubic and orthorhombic phases. *J. Alloys Compd.* **2019,** *785*, 232-239.

24. Ali, I. O. A.; Joubert, D. P.; Suleiman, M. S. H., A theoretical investigation of structural, mechanical, electronic and thermoelectric properties of orthorhombic $CH_3NH_3PbI_3$. *The European Physical Journal B* **2018,** *91* (10), 263.

25. Rahmani, R.; Amrani, B.; Driss Khodja, K.; Boukhachem, A.; Aubert, P., Systematic study of elastic, electronic, and magnetic properties of lanthanum cobaltite oxide. *Journal of Computational Electronics* **2018,** *17* (3), 920-925.

26. Liu, Q.-J.; Liu, F.-S.; Liu, Z.-T., Structural, Mechanical, and Electronic Properties of Monoclinic $N_2H_5N_3$ Under Pressure. *BrJPh* **2015,** *45* (4), 399-403.

27. Edrees, S. J.; Shukur, M. M.; Obeid, M. M., First-principle analysis of the structural, mechanical, optical and electronic properties of wollastonite monoclinic polymorph. *Computational Condensed Matter* **2018,** *14*, 20-26.

28. Weck, P. F.; Kim, E.; Buck, E. C., On the mechanical stability of uranyl peroxide hydrates: implications for nuclear fuel degradation. *RSC Advances* **2015,** *5* (96), 79090-79097.

29. Nan-Xi, M.; Chun-Ying, P.; Chao-Zheng, H.; Fei-Wu, Z.; Cheng, L.; Zhi-Wen, L.; Da-Wei, Z., Mechanical and thermodynamic properties of the monoclinic and orthorhombic phases of SiC_2N_4 under high pressure from first principles. *Chinese Physics B* **2014,** *23* (12), 127101.

30. Arıkan, N.; Örnek, O.; Charifi, Z.; Baaziz, H.; Uğur, Ş.; Uğur, G., A first-principle study of Os-based compounds: Electronic structure and vibrational properties. *J Journal of Physics Chemistry of Solids* **2016,** *96*, 121-127.

31. Al, S., Investigations of Physical Properties of $XTiH_3$ and Implications for Solid State Hydrogen Storage. In *Zeitschrift für Naturforschung A*, 2019; Vol. 74, p 1023.

32. Pettifor, D., Theoretical predictions of structure and related properties of intermetallics. *J Materials Science and Technology* **1992,** *8* (4), 345-349.

33. Liu, L.; Wu, X.; Wang, R.; Nie, X.; He, Y.; Zou, X., First-principles investigations on structural and elastic properties of orthorhombic TiAl under pressure. *Crystals* **2017,** *7* (4), 111.

34. Ran, Z.; Zou, C.; Wei, Z.; Wang, H., VELAS: An open-source toolbox for visualization and analysis of elastic anisotropy. *Comput. Phys. Commun.* **2022**, 108540.

35.I.N. Frantsevich, F. F. V., S.A. Bokuta, *Elastic constants and elastic moduli of metals and insulators*. Naukova Dumka: Kiev, 1983.

36. Wang, S.-L.; Pan, Y., Insight into the structures, melting points, and mechanical properties of $NbSi_2$ from first-principles calculations. **2019,** *102* (8), 4822-4834.

37. Chen, H.; Yang, L.; Long, J., First-principles investigation of the elastic, Vickers hardness and thermodynamic properties of Al–Cu intermetallic compounds. *Superlattices Microstruct.* **2015,** *79*, 156-165.

DOI: http://dx.doi.org/10.32571/ijct.1170911 **E-ISSN: 2602-277X**

International Journal of Chemistry and Technology

http://dergipark.org.tr/ijct

Research Article

A Schiff base molecule based on phenanthrene: structural characterisation and DNA binding capabilities

Ayşegül KÖSE

Department of Property Protection and Safety, Elbistan Vocational School, Kahramanmaras Istiklal University, Kahramanmaras, Türkiye

Received: 4 September 2022; Revised: 4 October 2022; Accepted: 27 October 2022

*Corresponding author e-mail: aysegul.kose@istiklal.edu.tr

Citation: Köse, A. *Int. J. Chem. Technol.* **2022**, 6 (2), 135-141.

ABSTRACT

A new phenanthren based Schiff base compound (**PBS**) was synthesized by the condensation reaction of phenanthrene-9-carbaldehyde and 4-aminophenol. The structure of the compound was characterized by FTIR, $^{1}H(^{13}C)$ NMR and elementel analysis. Through a single crystal X-ray diffraction investigation, the compound's crystal structure was identified. The X-ray crystallographic data revealed that the phenanthrene and phenol rings are approximately perpendicular with respect to each other. Molecules in the structure are connected to one another by phenol-imine hydrogen bonds [O1-H·····N1] forming supramolecular hydrogen bond chains. Moreover, the phenanthrene fused ring system are involved in π-π stacking interactions with the same sections of the adjacent molecules (head to tail manner). The double-stranded fish sperm DNA (dsFS-DNA) binding properties of the compound was investigated by spectrophotometric, fluorimetric and viscosity methods. According to the spectral data, the interacts of the compound with DNA in groove binding mode with a binding constant (K_b: 4.6 ×10^4 M^{-1}). The fact that the viscosity of the dsFS-DNA did not significantly change when the compound PBS was present suggesting non-intercalative binding of the compound with DNA.

Keywords: Phenanthrene, azomethine, XRD structure, DNA interaction.

Fenantren bazlı bir Schiff bazı bileşiğinin yapısal karakterizasyonu ve DNA bağlama özellikleri

ÖZ

Fenantren-9-karbaldehit ve 4-aminofenolün kondenzasyon reaksiyonu ile fenantren bazlı yeni bir Schiff baz bileşiği (PBS) sentezlenmiştir. Bileşiğin yapısı FTIR, $^{1}H(^{13}C)$ NMR ve elementel analizi ile karakterize edildi. Bileşiğin kristal yapısı, tek kristal X-ışını kırınım deneyi ile belirlendi. X-ışını kristalografik verileri, fenantren ve fenol halkalarının birbirine göre yaklaşık olarak dik olduğunu ortaya çıkardı. Yapıda moleküller, moleküller arası fenol-imin hidrojen bağları [O1-H·····N1] ile bağlanır ve supramoleküler hidrojen bağ zincirleri oluşturur. Ayrıca fenantren halka sistemi, komşu moleküllerin aynı bölümleri ile π-π istifleme etkil (baş-kuruk) etkileşimlerinde yer alır. Bileşiğin çift sarmallı balık sperm DNA'sına (dsFS-DNA) bağlanma özellikleri spektrofotometrik, florimetrik ve viskosimetrik yöntemlerle araştırılmıştır. Spektral veriler, bileşiğin, önemli bağlanma sabiti (K_b: 4.6 x 10^4 M^{-1}) ile oluk bağlanma modunda DNA ile etkileşime girdiğini göstermiştir. Bileşik PBS'nin varlığında, dsFS-DNA'nın viskozitesi önemli bir değişiklik gözlenmemesi, bileşiğin dsFS-DNA ile interkalatif olmayan bağlanma modunda etkileşime girdiğini göstermektedir.

Anahtar Kelimeler: Fenantren, Schiff bazı, kristal yapı, DNA bağlama özellikleri.

1. INTRODUCTION

We still deal with problems and the inefficiency of current medications despite the availability of numerous cancer treatment agents.[1] It is extremely difficult to find possible new chemotherapeutics with increased efficacy and fewer adverse effects.[2,3] One of the most key aspects for therapeutic discovery in the battle against cancer is DNA.[4,5] DNA intercalating compounds are anticipated to reversibly bind DNA and interfere with crucial cancer cell processes like transcription and replication.[6] DNA intercalating substances frequently have polar properties that allow hydrogen bonding interactions with nucleic acids, as well as planar polycyclic aromatic rings (like

DOI: http://dx.doi.org/10.32571/ijct.1170911 E-ISSN: 2602-277X

anthracene and phenanthrene) that aid in the compound's ability to settle between base pairs of DNA.[7,8]

Schiff bases are a basic category of organic compounds and can be prepared from the reaction of aldehyde or ketones with primary amines.[9] Numerous biological activities, such as those against cancer, bacteria, malaria, viruses, and fungi, are present in Schiff base compounds.[10–12] In this study, a Schiff base compound labelled as PBS (Figure 1) containing phenanthrene group was synthesized. It was aimed to provide a dual functionality consisting of hydrophilic hydroxyl groups and planar phenanthrene group in the synthesized compound. The synthesized compound was expected to show a high affinity for the hydrophobic and hydrophilic regions of the DNA molecule. FTIR, NMR, and elemental analysis techniques were used to characterize the generated Schiff base compound's molecular structure. Additionally, the compound's single crystals were formed, and a single crystal X-ray diffraction investigation revealed its structural structure. UV-Vis absorption, florescence, and viscosity experiments were used to assess the produced substance's DNA binding capabilities.

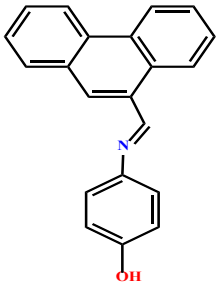

Figure 1. Structure of the phenanthrene-Schiff base compound

2. MATERIALS AND METHODS

2.1. Chemicals

All reagents (4-aminophenol and phenanthrene-9-carbaldehyde) and solvents used in the synthesis were purchased from companies and used as received.

2.2. Physical measurements

Using an LECO CHNS 932, elemental analyses (C, H, and N) were carried out. Using KBr disc (4000-400 cm^1), FTIR spectra were acquired using a Perkin Elmer Spectrum 400 FT-IR spectrophotometer. A Perkin Elmer Lambda 45 spectrophotometer was used to record the compounds' absorption spectra in DMSO solution (10^{-5} M). TMS was employed as the internal standard while 1H/13C NMR spectra in CDCl3 were collected on a Bruker 400 MHz equipment. On a Bruker APEX 2 CCD diffractometer, single crystal X-ray diffraction data for the molecular compound phenanthrene Schiff-based were obtained using Mo- K radiation (= 0.71073) at 293(2) K. Data reduction was done using Bruker SAINT.[13] Using Olex2,[14] SHELXT was used to solve and SHELXL to refine the structure.[15,16] The structure of compound PBS was determined using the direct technique and all of the reflections on F2. The carbon and oxygen hydrogen atoms were positioned correctly using a riding model.

2.3. Synthesis of [(E)-4-((phenanthren-9-ylmethylene)amino)phenol] (PSB)

Absolute ethanol (20 mL) was used to dissolve phenanthrene-9-carbaldehyde (2 mmol), which then underwent a 10-minute reflux process. To the refluxing solution, 4-aminophenol (2 mmol) in absolute ethanol (10 mL) was added. The clear, yellow reaction mixture was then refluxed for an additional four hours and cooled to room temperature. Yellow-colored precipitates that formed after cooling were filtered and air dried.

Chemical Formula: $C_{21}H_{15}NO$. Molecular weight: 297.36 g/mol. Yield: 82%. Colour: Yellow. FTIR (ATR, cm^{-1}) 3005, 2915, 1607, 1503, 1442, 1367, 1273, 1232, 1105, 968, 913, 815, 735, 716, 573, 519. Elemental analyses found (calculated for $C_{21}H_{15}NO$) %: C, 84.73(84.82); H, 4.86(5.08); N, 4.66(4.71). ^{1}H NMR ($CDCl_3$, ppm): 9.65 (b, OH, 1H), 8.80 and 8.76 (d, $CH_{phenanthrene}$, 2H), 8.51 (s, CH=N, 1H), 8.38 (s, $CH_{phenanthrene}$, 1H), 8.17-7.60 (m, $CH_{phenanthrene}$, 6H), 7.30(d, CH_{phenol}, 2H), 6.98(d, CH_{phenol}, 2H). ^{13}C NMR: 162.3(CH=N), 157.3, 144.2, 134.2, 133.8, 132.8, 132.5, 131.0, 130.2, 128.7, 127.3, 126.8, 126.2, 124.2, 123.5, 122.6, 118.3, 116.4.

2.4. DNA binding studies

2.4.1. Absorption spectral measurements

The interactions between double-stranded fish sperm DNA (dsFS-DNA) and synthesized Schiff base compound (PBS) were investigated by UV-Vis spectroscopic titrations according to our previous studies.[17,18] For this, the The substance (PBS) had a UV-Vis absorption spectrum alteration in DMSO (2.0 10-5 M), containing Tris-HCl buffer, pH = 7.0) with increasing amount of double-stranded fish sperm DNA (dsFS-DNA) were recorded in the range of 240-600 nm range. The absorption spectral change of the compound was examined to be able to examine the binding properties of the compound with DNA. Using the Benesi-Hildebrand equation (1), [dsDNA]/(εa–εf) versus [dsDNA] a linear association was seen when the data was plotted.

$$[dsDNA]/(\varepsilon a-\varepsilon f)=[dsDNA]/(\varepsilon b-\varepsilon f)+1/K_b(\varepsilon b-\varepsilon f) \quad (1)$$

DOI: http://dx.doi.org/10.32571/ijct.1170911 E-ISSN: 2602-277X

where f is a compound's extinction coefficient in its free form, b is a compound's extinction coefficient in its fully bound form, [dsDNA] is a compound's concentration in base pairs, and a represents the apparent extinction coefficient calculated from Aobds/[Ligands or complexes]: K_b is the binding constant which was calculated from the slope of the line drawn between [dsDNA]/(εa – εf) and [dsDNA].

2.4.2. Competitive binding studies

Ethidium bromide (EB) is a flat molecule and DNA intercalating agent. EB shows weak emissive in its free form, yet its emission intensity dramatically increases when it is attached to DNA.[19,20] When there are competitive intercalating agent, EB complex's DNA emission intensity decreases (emission quenching) due to the displacement of EB from DNA-EB complex. Most of the time, competitive binding via intercalation is blamed for the DNA-EB complex's emission intensity quenching. In our study, dsFS-DNA (75 µM) solution was treated with EB (5 µM) in Tris-HCl buffer and then increasing amount of the Schiff base compound (0-30 µM in DMSO) were added. The solutions' emission spectra were then measured between 560-760 nm (l_{exc}: 526 nm). The decrease of the emission intensity was examined and the putting out constants (K_{sv}) was obtained from the Stern-Volmer equation (2).

$$F_0/F = 1 + K_{SV}[Q] \quad (2)$$

When there is no Schiff base complex present, F0: DNA-EB emission intensity, *F*: emission intensity of DNA-EB in the presence of the Schiff base compound and [Q]: the total concentration of the Schiff base compound.

2.4.3. Viscosity measurements

Binds to DNA interaction of the compound (PBS) was also studied by measurement of viscosity. Rising amounts of the Schiff-based molecule and the dsFS-DNA solution's viscosity was recorded on an Ostwald viscometer at 25 ± 0.1 °C. The relative viscosity for dsFS-DNA in absence (h_0) and presence (h) of the synthesized compounds was obtained.[21] The relative viscosity $(h/h_0)^{1/3}$ versus 1/R were then plotted. where R: concentration of dsFS-DNA/concentration of the Schiff base compound (PBS).

3. RESULTS AND DISCUSSION

The condensation reaction was used in this study to create a new Schiff base compound with a high yield and purity from phenanthrene-9-carbaldehyde and 4-aminophenol. FTIR, NMR and micro analyses (C, H and N) were used to elucidate the compound's structure. The experimental elemental analysis results are in good agreement with the theoretical estimates of the suggested compound's structure, supporting the sample's purity. The FTIR spectrum of the compound was obtained and the spectroscopic data are provided in the experimental part. In the spectrum of the compound, a broad band 3000-3100 cm^{-1} can be assigned to the phenolic group n(O-H) stretching's. The relatively weak peaks at around 2900 cm^{-1} are due to the n(C-H) stretching's. The imine bond n(C=N) stretching's was observed at 1607 cm^{-1} as relatively sharp peak.[22,23] The emergence of imine bond stretching's in the FTIR spectrum provides evidence that the Schiff base complex has formed. In Figure 1, the compound's FTIR spectrum is presented.

In order to further investigate the structure of the compound, The compound's $^1H(^{13}C)$ NMR spectra were collected in $CDCl_3$ and the NMR data with peak assignments are displayed in the experimental part. In the ^1H NMR spectrum of the compound, a broad peak at 9.65 ppm is due to the phenolic proton.[24] Two doublet peaks at 8.80 and 8.76 ppm are assigned to the phenanthrene protons. The imine bond proton of the compound is shown as a singlet peak at 8.51 ppm.[25] Multiplet and overlapped peaks at 8.17-7.60 ppm are due to the phenanthrene protons. In the spectrum of the compound, two doublet peaks at 7.30 and 6.98 ppm are due to the phenolic C-H protons. The integration values of proton signals support the compound's suggested structure. The ^{13}C NMR spectrum of the compound shows a peak at 162.3 ppm which is attributed to the imine bond carbon atom. The remaining carbon atom signals are displayed between 157.3 and 116.4 ppm. The compound's NMR spectra showed that the sample contains no major organic impurities.

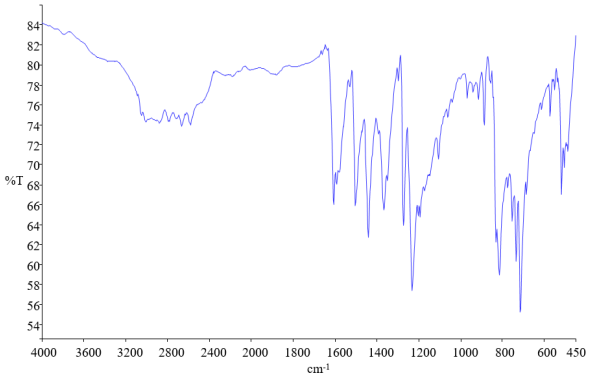

Figure 2. FTIR spectrum of the phenanthrene-Schiff base compound (PBS)

3.1.Crystal structure of the phenanthrene-Schiff base compound (PBS)

Re-crystallization of ethanol solution of the compound produced single crystals of the compound. By using a single crystal XRD investigation, the compound's crystal structure was identified. The compound's X-ray

DOI: http://dx.doi.org/10.32571/ijct.1170911 E-ISSN: 2602-277X

crystallographic information is provided in Table 1. The monoclinic unit cell and P21/n space group were used to solve the structure of the phenanthrene-Schiff base complex with the final refinement value of 0.0421(R_1). The thermal ellipsoid plot of the structure is displayed in Figure 3a In the structure of the compound, phenanthrene and phenol rings are linked by an imine bond (C=N) linkage. The C7-N1 imine bond distance is 1.2715(19) Å showing a characteristic imine bond distance. In the structure, the phenanthrene and phenol rings are almost perpendicular with respect to each other with the dihedral angle of 79.49º. In the structure of the compound, the phenolic group of a molecule makes an intermolecular hydrogen bond [O1-H·····N1] with the imine nitrogen atom of a neighbouring molecule under symmetry operation of -1/2+x,3/2-y,1/2+z. The phenol-imine intermolecular hydrogen bond contacts form a hydrogen bond chain as shown in Figure 3b. The compound's crystal structure was also further stabilized by anticipated stacking interactions π stacking contacts. The flat surface of the phenanthrene fused ring system allows the π-stacking interactions with the neighbouring molecules. Molecules are linked by phenanthroline-phenanthroline head to tail π-π stacking interactions along the *a* axis as shown in Figure 3c.

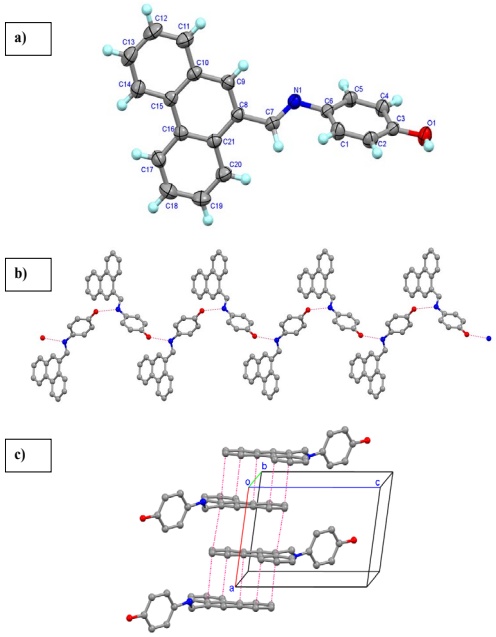

Figure 3 a) Thermal ellipsoid plot (50% probability) of the compound (PBS) with atom numbering. b) hydrogen bond contacts. c) Packing plot showing π-π stacking interactions.

Table 1. X-ray crystallographic data for the compound (PBS)

Empirical formula	$C_{21}H_{15}NO$	β/°	98.455(3)
Formula weight	297.34	γ/°	90
Temperature/K	293(2)	Volume/Å^3	1485.43(8)
Crystal system	Monoclinic	Z	4
Space group	$P2_1/n$	Reflections collected	4714
a/Å	7.1024(2)	Independent reflections	2925 [R_{int} = 0.0155, R_{sigma} = 0.0317]
b/Å	20.9464(6)	Final R indexes [I>=2σ (I)]	R_1 = 0.0421, wR_2 = 0.0970
c/Å	10.0945(3)	Final R indexes [all data]	R_1 = 0.0550, wR_2 = 0.1087
α/°	90		

3.2. Electronic absorption properties

In DMSO solution (10^{-5} M), UV-Vis absorption characteristics of the compound were examined. The absorption spectrum of the compound was taken in the range of 240-640 nm. In the spectrum shown in Figure 4, two absorption bands were observed at 240-440 nm range. The first and more intense peak was observed at 250-290 nm range (l_{max}: 260 nm). The relatively broader absorption band was seen at 300-430 nm range (l_{max}: 364 nm). The absorption bands in the UV-Vis spectrum can be assigned to the π-π* electronic transition due to the π-electrons in the structure of the compound.

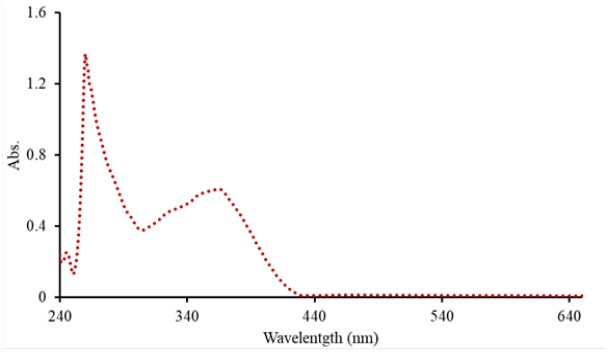

Figure 4. Absorption spectrum of the compound in DMSO (10^{-5} M).

DOI: http://dx.doi.org/10.32571/ijct.1170911 E-ISSN: 2602-277X

3.3. DNA binding studies

DNA is the main target for the most chemotherapy agents of cancer. A huge number of compounds have prepared for the targeting of DNA.[26] To ascertain the impact of the DNA targeting of new drug candidates, the interactions/binding between the drug candidate molecule and DNA should be investigated.[27] The DNA binding agents bind to DNA covalent and non-covalent interactions and the latter one is focus of the many DNA targeting studies.[28] Intercalation between base pairs, groove bonding, and electrostatic interactions are examples of non-covalent interactions between DNA and binding substances.[28,29] The dsFS-DNA (fish sperm double-stranded DNA) binding properties of the phenanthrene based Schiff base compound (PBS) was investigated by UV-Vis absorption measurements. UV-Vis absorption spectra of the compound (PBS) in DMSO: TRIS–HCl buffer solution (2.0 ×10-5 M) were recorded in presence of incremental addition of dsFS-DNA (100-1000 µl, 1.78 × 10−4 M). UV-Vis absorption spectral change of the compound in the presence of PBS is shown in Figure 5.

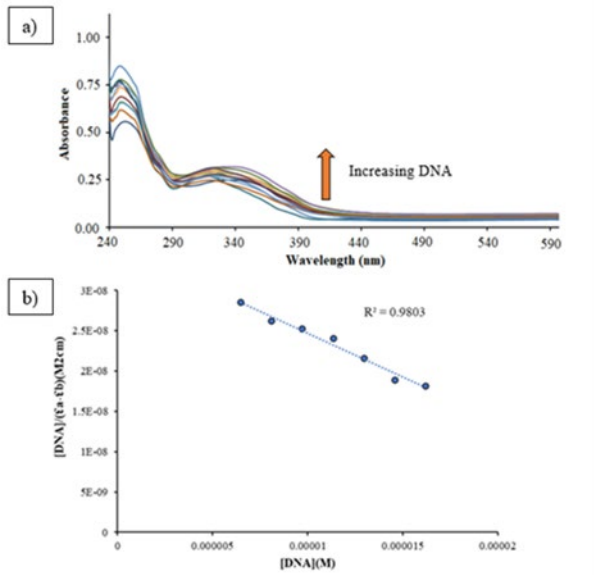

Figure 5. a) Absorption spectra of PSB, in 2 mM Tris–HCl/2 mM NaCl buffer at pH 7.0 in the presence of incremental the addition of dsFS-DNA. b) Plot of [DNA]/Ɛa–Ɛf) vs. [DNA] for the titration of PBS with dsFS-DNA (0-1000 µM).

The compound PBS showed two absorption bands in the range of 240-440 nm. In the presence of DNA, the first absorption band at 240-290 nm range did not show considerable red or blue shift yet the absorption values increased with the gradual addition of DNA (hyperchromic effect). Addition of DNA causes noticeable change in the absorption band at 290-400 nm range. The presence of DNA resulted in a sight red shift accompanied by higher absorption values (hyperchromic effect). The spectral change of the compound PBS in the presence of DNA is indicative of the interactions between the compound and DNA. Using the absorption band at 290-400 nm range, binding constant (Kb) was found to be 4.6 ×104 M-1 from the linear plot [dsDNA]/(εa–εf) versus [dsDNA] (Figure. 5). DNA binding constant of the compound Kb falls within the range of groove binding agents.[30]

Ethidium bromide (EB) are used as a probe of DNA secondary structure and it intercalates into the double-stranded DNA.[31] Although free EB shows weak fluorescence properties in the range of 560-760 nm (lexc: 526 nm), the insertion of EB into DNA base pair causes dramatic increase in the emission intensity.[32] In the presence of a competitive compound, DNA binding competition is expected. The DNA binding competition can visualize by measuring the emission spectra of DNA-EB complex. The emission of the DNA-EB complex is usually quenched in the presence of a competitor molecule. The DNA-EB complex's emission band is being quenched and this is often assigned to the replacement EB form DNA-EB with the competitor molecule, the excited state energy transfer, or the conformational change of DNA. The emission spectra of the DNA-EB complex [dsFS-DNA: 75 µM), EB: 5 µM in Tris-HCl buffer] recorded in the presence of increasing amount of the Schiff base compound (PBS) (0-30 µM in DMSO). It was observed that the emission band of DNA-EB complex at 560-760 nm (lexc: 526 nm) was gradually quenched by the addition of the Schiff base compound. By using the Stern-Volmer equation, Io/I versus [PBS] plot was drawn (Figure 6) and linearity was observed. From slope of this plot, quenching constant (Ksv) was found to be 2.42 × 104 M-1. The obtained Ksv suggests non-intercalative binding interactions between the synthesized compound and DNA.

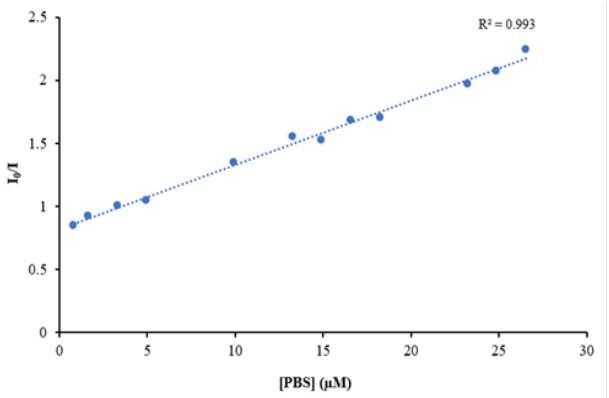

Figure 5. Stern-Volmer plot (I_o/I versus [PBS]) of fluorescence titrations of DNA-EB complex HDSB with PBS. (λ_{exc}: 526 nm).

The interaction between the synthesized phenanthrene based Schiff base compound (PBS) and DNA was further examined by viscosity measurements. When an

DOI: http://dx.doi.org/10.32571/ijct.1170911 E-ISSN: 2602-277X

intercalation agent is applied, viscosity of the DNA solution rises. The DNA length and viscosity are increased when an intercalating molecule binds to the spaces between DNA base pairs. Viscosity of dsFS-DNA solution (50 mM) in the presence of incremental addition of PBS (keeping DNA concentration constant) was recorded and the relative viscosity of dsFS-DNA is shown in Figure 7.

The presence of various concentration of PBS did not cause dramatic change in the viscosity of dsFS-DNA which suggests the non-intercalative binding mode between PBS and dsFS-DNA.[21]

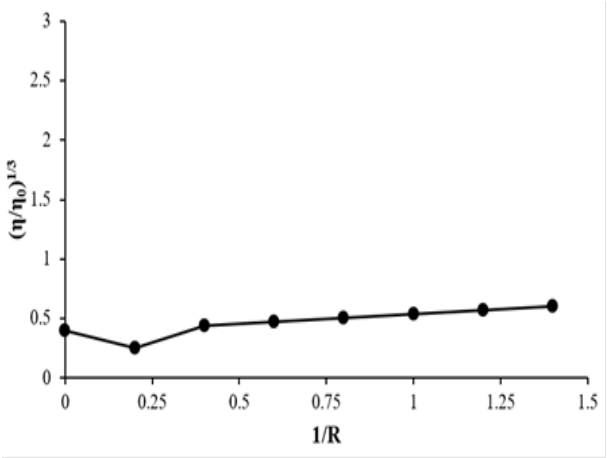

Figure 6. The relative viscosity change of dsFS-DNA (50 µM) with various concentration of the Schiff base compound.

4. CONCLUSIONS

A new phenanthrene based Schiff base compound (PSB) was prepared and its structure was characterized. The compound's crystal structure was clarified by a single crystal XRD investigation. Crystal structure of the compound was stabilised by intermolecular hydrogen bond contacts and π-π stackings. The DNA binding properties of the compound was investigated by spectrophotometric, fluorimetric and viscosity methods. The UV-Vis spectrometric data revealed that the compound has considerable binding affinity to DNA with binding constant (K_b) of 4.6×10^4 M^{-1}. The spectral and viscosity data showed that the compound interacts with double strand DNA *via* non-intercalative groove binding mode.

Conflict of interests

I declares that there is no a conflict of interest with any institute, person, company, etc.

Appendix A. Supplementary data

The cif file for single crystal XRD data was deposited to Cambridge Crystallographic Data Centre with CCDC number of 2194269.

REFERENCES

1. Zhang, Z.; Zhou, L.; Xie, N.; Nice, E. C.; Zhang, T.; Cui, Y.; Huang, C. Signal Transduct Target Ther **2020**, 5, 113.

2. Zhong, L.; Li, Y.; Xiong, L.; Wang, W.; Wu, M.; Yuan, T.; Yang, W.; Tian, C.; Miao, Z.; Wang, T.; Yang, S. Signal Transduct Target Ther **2021**, 6, 201.

3. Sun, D.; Gao, W.; Hu, H.; Zhou, S. Acta Pharm Sin B **2022**, 12, 3049–3062.

4. Palchaudhuri, R.; Hergenrother, P. J. Curr Opin Biotechnol **2007**, 18, 497–503.
5. Cheung-Ong, K.; Giaever, G.; Nislow, C. Chem Biol **2013**, 20, 648–659.

6. Nial J. Wheate; Craig R. Brodie; J. Grant Collins; Sharon Kemp; Janice R. Aldrich-Wright. Mini-Reviews Med Chem **2007**, 7, 627–648.

7. Bandyopadhyay, D.; Granados, J. C.; Short, J. D.; Banik, B. K. Oncol Lett **2012**, 3, 45–49.

8. Ferguson, L. R.; Denny, W. A. Mutat Res Mol Mech Mutagen **2007**, 623, 14–23.

9. da Silva, C. M.; da Silva, D. L.; Modolo, L. V.; Alves, R. B.; de Resende, M. A.; Martins, C. V. B.; de Fátima, Â. J Adv Res **2011**, 2, 1–8.

10. Omidi, S.; Kakanejadifard, A. RSC Adv **2020**, 10, 30186–30202.

11. Przybylski, P.; Huczynski, A.; Pyta, K.; Brzezinski, B.; Bartl, F. Curr Org Chem **2009**, 13, 124–148.

12. Ceramella, J.; Iacopetta, D.; Catalano, A.; Cirillo, F.; Lappano, R.; Sinicropi, M. S. Antibiotics **2022**, 11, 191.

13. Bruker. APEX2 and SAINT Bruker AXS Inc; 1998.

14. Dolomanov, O. V.; Bourhis, L. J.; Gildea, R. J.; Howard, J. A. K.; Puschmann, H. J Appl Crystallogr **2009**, 42, 339–341.

15. Sheldrick, G. M. Acta Crystallogr Sect A Found Crystallogr **2015**, 71, 3–8.

16. Sheldrick, G. M. Acta Crystallogr Sect C Struct Chem **2015**, 71, 3–8.

17.Şenel, P.; Agar, S.; Sayin, V. O.; Altay, F.; Yurtsever, M.; Gölcü, A. J Pharm Biomed Anal **2020**, 179, 112994.

18.Sherwani, I. A. H. A.; Köse, A.; Güngör, Ö.; Kırpık, H.; Güngör, S. A.; Köse, M. Appl Organomet Chem **2022**, 36, 1–17.

19.Husain, M. A.; Ishqi, H. M.; Rehman, S. U.; Sarwar, T.;

DOI: http://dx.doi.org/10.32571/ijct.1170911 E-ISSN: 2602-277X

Afrin, S.; Rahman, Y.; Tabish, M. New J Chem **2017**, 41, 14924–14935.

20.Nyarko, E.; Hanada, N.; Habib, A.; Tabata, M. Inorganica Chim Acta **2004**, 357, 739–745.

21.Maiti, S. K.; Kalita, M.; Singh, A.; Deka, J.; Barman, P. Polyhedron **2020**, 184, 114559.

22.Singh, G.; Pawan; Singh, A.; Shilpy; Diksha; Suman; Sharma, G.; Sahoo, S. C.; Kaur, A. J Mol Struct **2021**, 1229, 129618.

23. Premkumar, M.; Vijayan, P.; Venkatachalam, G. J Organomet Chem **2019**, 902, 120964.

24. Jiang, Z.; Tan, M. L.; Taheri, M.; Yan, Q.; Tsuzuki, T.; Gardiner, M. G.; Diggle, B.; Connal, L. A. Angew Chemie **2020**, 132, 7115–7122.

25. Kulaksizoğlu, S.; Gökçe, C.; Güp, R. Turkish J Chem **2012**, 717–733.

26. Christian, M.; Cermak, T.; Doyle, E. L.; Schmidt, C.; Zhang, F.; Hummel, A.; Bogdanove, A. J.; Voytas, D. F. Genetics **2010**, 186, 757–761.

27. Sheng, J.; Gan, J.; Huang, Z. Med Res Rev **2013**, 33, 1119–1173.

28. Rehman, S. U.; Sarwar, T.; Husain, M. A.; Ishqi, H. M.; Tabish, M. Arch Biochem Biophys **2015**, 576, 49–60.

29. Strekowski, L.; Wilson, B. Mutat Res Mol Mech Mutagen **2007**, 623, 3–13.

30. Shi, J. H.; Chen, J.; Wang, J.; Zhu, Y. Y. Spectrochim Acta - Part A Mol Biomol Spectrosc **2015**, 136, 443–450.

31. Banerjee, A.; Majumder, P.; Sanyal, S.; Singh, J.; Jana, K.; Das, C.; Dasgupta, D. FEBS Open Bio **2014**, 4, 251–259.

32. Shobha Devi, C.; Anil Kumar, D.; Singh, S. S.; Gabra, N.; Deepika, N.; Kumar, Y. P.; Satyanarayana, S. Eur J Med Chem **2013**, 64, 410–421.

DOI: http://dx.doi.org/10.32571/ijct.1187754 E-ISSN: 2602-277X

International Journal of Chemistry and Technology

http://dergipark.org.tr/ijct

Research Article

Cytotoxic, apoptotic, and necrotic effects of silver nanoparticles biosynthesized using *Origanum majorana* extract

Ramazan ERENLER[1,2*], Esmanur GEÇER[2], Büşra MORAN BOZER[3]

[1]*Research Laboratory Practice and Research Center, Igdir University, 76000 Igdir, Türkiye*

[2]*Department of Chemistry, Faculty of Arts and Sciences, Tokat Gaziosmanpasa University, 60240 Tokat, Türkiye*

[3]*Scientific Technical Research and Application Center, Hitit University, Corum, Türkiye,*

Received: 12 October 2022; Revised: 3 November 2022; Accepted: 8 November 2022

*Corresponding author e-mail: rerenler@gmail.com

Citation: Erenler, R.; Geçer, E.; Moran Bozer, B. O. *Int. J. Chem. Technol.* **2022**, 6 (2), 142-146.

ABSTRACT

Nanotechnology has gained great interest due to its widespread application. Anticancer activity of *Origanum majorana* extract and silver nanoparticles was investigated by MTT assay using human pancreatic adenocarcinoma cell lines (Capan-1), mouse normal fibroblast cell lines (L929), and human colon adenocarcinoma cell line (Caco-2). AgNPs@Om exhibited the excellent cytotoxic effect on Capan-1 cell lines with the cell viability of 29.17% and 25.70%, 22.49%, 21.16% at 1.0, 0.5, 0.25, 0.125 µg/mL respectively. However, the extract was determined to show moderate activity. A considerable fall in the viable cell number in Caco-2 cell lines was observed after the treatment of AgNPs@Om. The viable cells of Caco-2 cell lines were detected as 32.0% at 1.0 µg/mL with the treatment of nanoparticles. Yet, the viable Caco-2 cells were determined as 48.2% with the treatment of *O. majorana* extract. Both extract and nanoparticles had no impact on the viability of non-tumor cells (L929). Moreover, nanoparticles induced apoptosis. Consequently, AgNPs@Om may be a promising anticancer drug candidate.

Keywords: Silver nanoparticles, natural products, *Origanum majorana*, anticancer activity.

Origanum majorana özütü kullanarak gümüş nanoparçacıkların sitotoksik, apoptotik ve nekrotik etkileri

ÖZ

Nanoteknoloji, yaygın uygulaması nedeniyle son zamanlarda büyük ilgi görmektedir. *Origanum majorana* özütü ve gümüş nanopartiküllerin antikanser aktivitesi, insan pankreas adenokarsinoma hücre hatları (Capan-1), fare normal fibroblast hücre hatları (L929) ve insan kolon adenokarsinom hücre hatları (Caco-2) kullanılarak MTT metodu ile araştırıldı. AgNPs@Om, sırasıyla 1.0, 0.5, 0.25, 0.125 µg/mL'de %29.17 ve %25.70, %22.49, %21.16 hücre canlılığı ile Capan-1 hücre hatları üzerinde mükemmel sitotoksik etki sergiledi. Ancak ekstraktın orta düzeyde aktivite gösterdiği belirlendi. AgNPs@Om etkileştirilmesinden sonra Caco-2 hücre hatlarındaki canlı hücrelerin sayısında önemli bir azalma gözlendi. Caco-2 hücre hatlarının canlı hücreleri, nanopartiküllerin etkisi ile 1.0 µg/mL'de %32.0 olarak tespit edildi. Ancak *O. majorana* özütü ile muamele edildiğinde canlı Caco-2 hücreleri %48.2 olarak belirlendi. Hem ekstrakt hem de nanopartiküller, tümör olmayan hücrelerin (L929) canlılığı üzerinde önemli bir etkiye sahip değildir. Ayrıca, nanopartiküller apoptozu indükledi. Sonuç olarak, AgNPs@Om umut verici bir antikanser ilaç adayı olabilir.

Anahtar Kelimeler: Gümüş nanopartikül, doğal ürünler, *Origanum majorana*, antikanser aktivite.

1. INTRODUCTION

Medicinal plants have been employed for therapeutic purposes since ancient times.[1-5] These plants reveal a large spectrum of biological activities owing to their bioactive compound contents.[6-8] The discovery of spectroscopy in the 19th century led to natural products becoming the focus of science.[9-12] Secondary metabolites are substances synthesized by plants that have many functions such as protecting them against enemies. These compounds show a wide variety of interactions on the plant itself and other living organisms.[13-14] Because of

DOI: http://dx.doi.org/10.32571/ijct.1187754 E-ISSN: 2602-277X

acting as reducing and stabilizing agents, plant secondary metabolites have been used in the green approach for the synthesis of nanoparticles.[15]

Nanoparticles can be synthesized from nano to micron sizes and have many applications, including bioseparation and biocatalysts with optical, magnetic, electrical, and magnetic field strengths, thanks to their superior properties.[16] The most important advantages of metal nanoparticles are their relatively large surface area compared to their size and their unique properties.[17] Moreover, low cost, ease of use, and high stability are other advantages of metal nanoparticles.[18] In addition, the fact that metal nanoparticles do not have any toxic effects on the environment creates the ideal environment for the use of these nanoparticles.[19] It is accepted by the scientific world that metal oxide nanoparticles have antimicrobial effects, and it is reported that the greatest effect on agents causing the infection is obtained by silver nanoparticles.[20]
While nanoparticles are smaller in size than human cells, they are the same size as biological macromolecules such as receptors and enzymes. Therefore, nanoparticles can be used as probes by conjugating them with peptides, antibodies, or nucleic acids of the same size.[21] Thus, molecular changes and cellular movements related to pathological regions can be observed. These probes provide high sensitivity, stability, and absorption coefficient over a wide spectral range.[22]

Cancer is an illness described by the unrestrained increase and proliferation of abnormal cells in the body and the killing of normal cells and frequently causing death and it is one of the most serious and terrible diseases in the world.[23] Chemotherapy, radiation, and surgical treatments are among the traditional therapeutic strategies used in cancer treatment. These therapies have several limitations, such as high dose requirements, non-specific toxicity, and multidrug resistance. Besides, drugs used in chemotherapy have poor water solubility and have a high incidence of side effects. In addition, chemotherapy drugs cause significant damage to healthy tissues, causing adverse reactions. Therefore, current studies are now focused on safer and more effective treatment of cancer. In this sense, nanotechnology may be the solution to overcome these limitations of conventional chemotherapy. For this reason, the development of anticancer drugs produced from nanoparticles obtained from plants is of great importance.[24]

Origanum genus includes aromatic and medicinal plant species that are used effectively in food, traditional medicine, and the pharmaceutical industry.[25-26] This genus is also well known for its essential oils that are used in the food, cosmetic and pharmaceutical sectors.[27-28] *Origanum majorana* L., a species belonging to the *Origanum* genus of the Lamiaceae family, is a perennial medicinal plant called sweet marjoram.[29]

In this study, silver nanoparticles were synthesized from *Origanum majorana* L. and cytotoxic, apoptotic, and necrotic effects were investigated using Capan-1, Caco-2, and L929 cell lines.

2. MATERIALS AND METHODS

2.1 Chemicals

L-glutamine, trypsin-EDTA, and FBS were purchased from Merck (Darmstadt, Germany). Human pancreatic adenocarcinoma cell lines (Capan-1), mouse normal fibroblast cell lines (L929), and human colon adenocarcinoma cell line (Caco-2) were supplied from Kırıkkale University.

2.2 Synthesis of nanoparticles

Origanum majorana was utilized for silver nanoparticle synthesis. The spectroscopic studies such as X-ray diffraction, Ultraviolet-visible, Fourier-transform infrared as well as Scanning electron microscope revealed the formation of silver nanoparticles. The experimental procedure and spectral data as well as the antioxidant activity of green synthesized AgNPs@Om were reported previously.[30]

2.3 Cell culture

Human pancreatic adenocarcinoma cell lines (Capan-1), mouse normal fibroblast cell lines (L929), and human colon adenocarcinoma cell lines (Caco-2) were used for anticancer activity. Cells were incubated in DMEM-F12 or RPMI culture medium containing 1% antibiotic and 10% FCS in flasks in a carbon dioxide oven at 37 °C.

The medium was changed at 2-day intervals until the cells reach enough. After the cultures reach a certain number, they were removed with trypsin and inoculated into well plates (5.000-10.000 cells/well). When cells reach a certain number, media containing serum and antibiotics were replaced with media containing serum and antibiotics. It was then used to determine necrotic, apoptotic, and cytotoxic activities.[31]

2.4 Cytotoxicity assay

Capan-1, Caco-2, and L929 were inoculated into 96 well plates, with 10.000 cells per well. Substances of varying amounts were added to the cells and incubated for 24 hours. Afterward, *Origanum majorana* and AgNPs@Om (1.0, 0.5, 0.25, 0.125 and 0.0625 mg/mL) were added to the well and incubated for 24 h. Latex and media rubber was used for respectively positive and negative control. The media was incubated at 37°C for 2.5 hours after being replaced with 50 µL MTT solution (1.0 mg/mL). A new solution of MTT in isopropanol (100 µL) was then added in place of the MTT solution.

DOI: http://dx.doi.org/10.32571/ijct.1187754 E-ISSN: 2602-277X

The control cell viability was accepted as 100%. Cell viability was assessed by ELISA at 570 nm and calculated with the formula (1)

$$\text{Cell viability } \% = [Ax/Ay] \times 100 \quad (1)$$

Ax is the sample of optical density, Ay is the control.[32-34]

2.5 Apoptotic and necrotic analysis

Fluorescent staining was performed after the cells prepared as mentioned above interact with Capan-1 cells, Caco-2 cells, and L929 cells at different rates. In this way, apoptosis and necrosis were determined. During staining, cytoplasmic RNA is destroyed by treating cells with ribonuclease A (Sigma R-500) for staining only DNA. Hoechst (33342) staining stains the nuclei of cells blue. Despite staining whole cells, apoptotic cells appear brighter and nuclear homogeneity is lost. In this way, true apoptotic cells are differentiated from normal cells. The other dye used in dual staining is Propidium Iodide (PI). It shows necrosis by staining the DNA red. PI does not pass through the membranes of normal cells but only passes through the membranes of cells with damaged or dead cells, indicating necrotic cells. Cells that were only treated with the drug and affected with drug and inhibitor co-administered complexes will be removed after 24 hours and staining will be performed.

The painting process was carried as briefly, Capan-1 cells, Caco-2 cells, and L929 cells (15×10^3 per well) were cultivated in DMEM with L-glutamine supplemented with 10% fetal bovine serum, 1% penicillin-streptomycin for 24 h, 5% CO_2 atmosphere, and at 37 °C, in a 48-well plate.[35] Different concentrations of AgNPs@Om (50-500 µg/mL) were treated for 24 hours. Then, detached and attached cells were collected and stained with Hoechst dye (33342), PI, and DNAse free-RNAse for 20 minutes at room temperature after washing with phosphate-buffered saline (PBS). The control group included Capan-1 cells, Caco-2 cells, and L929 cells treated with cell medium alone.

2.6 Statistical analysis

GraphPad Prism (8.0.1), Tukey's multiple comparison test, and the one-way ANOVA test were used for statistical analysis, and results were expressed as mean values ± SDs of three independent trials ($P < 0.05$).

3. RESULTS AND DISCUSSION

3.1 Cytotoxic effect

In this study, the cytotoxic effect of the extract and silver nanoparticles using Capan-1, Caco-2, and L929 were investigated by the MTT test. Table 1 shows the cytotoxic effect of *Origanum majorana*-mediated synthesized silver nanoparticles on Capan-1, Caco-2, and L929 cell lines. Cell viability of the Capan-1 cell lines treated with the nanoparticles and extract was determined as 29.17% and 69.35% at 1.0 µg/mL respectively. However, the cell viability decreased after the treatment of nanoparticles at 0.5 µg/mL, treatment of extract caused the increase of the cell viability at the same concentration (0.5 µg/mL). The Capan-1 cell lines' viability decreased with the decrease in concentration. Nevertheless, treatment of extract with Capan-1 cell lines increased the cell viability. In Caco-2 cell lines, nanoparticles were observed to have a significant effect on these cell lines. The cell viability was observed at 0.5 mg/mL as 27.91% after the treatment of AgNPs@Om. At the same concentration, the treatment with extract resulted in cell viability of 53.19%.

The concentration decrease caused an increase in cell viability. Concerning the L929 cell lines, cell viability was determined as 93.7% after the treatment with AgNPs@Om at 1.0 mg/mL, extract treatment resulted in the cell viability of 78.2%. Both extract and nanoparticles caused the increase in cell viability. According to this result, it was concluded that nanoparticles were more effective than the extract at a concentration of 1.0 µg/mL.

Table 1. Cytotoxic effect of AgNPs@Om and extract on cell lines. Data are shown as % viable cells, different letters indicate the significant difference in the same column ($P < 0.05$).

Concentration (mg/mL)	AgNPs@Om			Extract		
	Capan-1	Caco-2	L929	Capan-1	Caco-2	L929
1	29.17±3.6^{c}	31.95±2.7^{c}	93.70±4.4^{a}	69.35±3.4^{a}	48.16±2.1^{a}	78.15±5.3^{a}
0.5	25.70±5.9^{b}	27.92±2.6^{a}	101.75±3.1^{c}	76.11±5.4^{b}	53.19±24.1^{b}	120.69±7.2^{b}
0.25	22.49±1.9^{a}	28.69±2.9^{b}	96.91±2.0^{b}	89.39±4.5^{c}	69.85±2.8^{c}	122.72±7.8^{bc}
0.125	21.16±1.4^{a}	34.07±3.9^{d}	101.27±1.8^{c}	131.31±1.1^{d}	73.60±2.0^{d}	121.97±8.4^{b}

DOI: http://dx.doi.org/10.32571/ijct.1187754 E-ISSN: 2602-277X

3.2 Apoptotic and necrotic cells analysis

In many physiological situations, apoptosis, or programmed cell death, plays an important role in controlling cell number. Many human tumours have impaired apoptosis, implying that apoptotic function disruption contributes significantly to the transformation of a normal cell into a tumour cell. Apoptosis is also a major contributor to chemotherapy-induced tumour cell death.[36] The apoptotic and necrotic index of silver nanoparticles on Capan-1, Caco-2, and L929 cell lines is shown in Table 2. The cell death pathway was confirmed using the double staining method. The apoptotic index was found to be higher than the necrotic index in all cell lines, indicating that cell death occurred via apoptosis. The fluorescent dye Hoechst (33342) in the double staining solution binds to DNA, giving the cell nucleus its blue colour.

Table 2. Apoptotic index and necrotic index of AgNPs@Om on Capan-1, Caco-2, and L929 cell lines at different concentrations (mg/mL).

Concentration (1 mg/mL)	**AgNPs@Om**			**Extract**		
	Capan-1	**Caco-2**	**L929**	**Capan-1**	**Caco-2**	**L929**
% Apoptosis	15,30±1,40[b]	21,50±2,30[b]	8,40±0,70[b]	35,20±2,40[b]	35,20± 1,80[b]	0
% Necrosis	4,40±0,50[a]	4,20±1,30[a]	0,50±0,01[a]	8,20±0,40[a]	12,60± 2,30[a]	0

Apoptotic cell nuclei were distinguished from other nuclei by their blue color, which was caused by the deformation, brightening, and distortion of their borders. PI dyed the necrotic cell nuclei, which appeared red under fluorescent light (Figure 1). The morphological change was not observed in the control groups' cell nuclei. Nonetheless, apoptotic cell nuclei were stained with a blue fluorescence when compared to non-apoptotic cells.

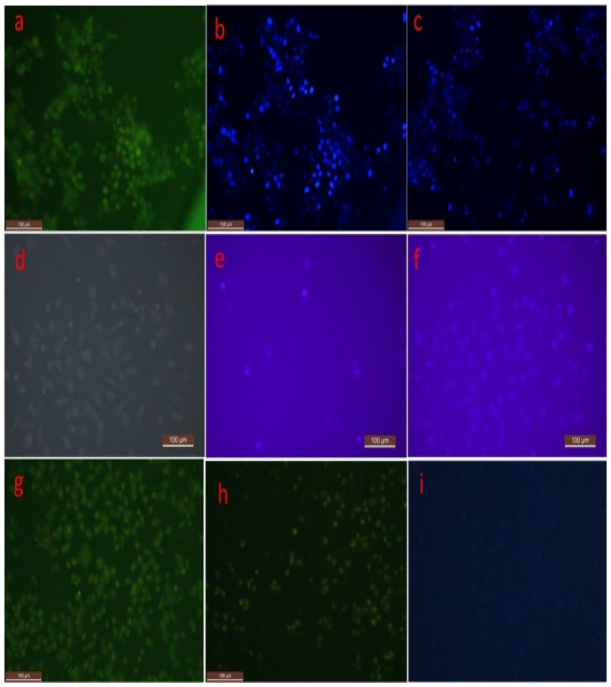

Figure 1. Fluorescence inverted microscopy image of Caco-2, Capan-1, L929 cells treated with extract and silver nanoparticles, a: control, Caco-2, b: Caco-2, extract, DAPI, c: Caco-2, AgNPs, DAPI, d: Capan-1, control, e: Capan-1, extract, DAPI, f: Capan-1, AgNPs, DAPI, g: L929, extract, FITCH, h: L929, AgNPs, FITCH, i: L929 control.

4. CONCLUSION

The synthesized silver nanoparticles from *Origanum majorana* revealed an excellent antiproliferative effect on the corresponding cell lines (Capan-1, Caco-2).

Furthermore, AgNPs@Om induced the cells to apoptosis. Cytotoxic effects of extract and AgNPs@Om were investigated. The percent viability of cell lines was calculated by comparison of absorbance values of control cells. AgNPs@Om did not reveal significant inhibition on L929 cell lines (normal cells). Moreover, observation of the apoptosis pathway in both cell lines after treatment of nanoparticles revealed that the nanoparticles could be a drug candidate. A key mechanism by which cytotoxic drugs kill tumor cells is the activation of apoptosis pathways.

Conflict of Interest

The authors declare that there is no conflict of interest with any person, institution, company, etc.

REFERENCES

1. Topçu, G.; Erenler, R.; Çakmak, O.; Johansson, C. B.; Çelik, C.; Chai, H.-B.; Pezzuto, J. M. *Phytochemistry* **1999,** 50 (7), 1195-1199.

2. Elmastas, M.; Ozturk, L.; Gokce, I.; Erenler, R.; Aboul-Enein, H. Y. *Anal. Lett.* **2004,** 37 (9), 1859-1869.

3. Demirtas, I.; Erenler, R.; Elmastas, M.; Goktasoglu, A. *Food Chem.* **2013,** 136 (1), 34-40.

DOI: http://dx.doi.org/10.32571/ijct.1187754 **E-ISSN: 2602-277X**

4. Erenler, R.; Yilmaz, S.; Aksit, H.; Sen, O.; Genc, N.; Elmastas, M.; Demirtas, I. *Rec. Nat. Prod.* **2014,** 8 (1), 32-36.

5. Kaya, G.; Karakaya, R.; Tilgel, E.; Sandikci, M.; Yucel, E.; Cicek, G.; Kayir, O.; Aksit, H.; Telci, I.; Guzel, A. *J. New Results Sci.* **2014,** 7 (7), 1-6.

6. Türkmen, N.; Öz, A.; Sönmez, A.; Erol, T.; Gülümser, D.; Yurdakul, B.; Kayır, Ö.; Elmastas, M.; Erenler, R. *J. New Results Sci.* **2014,** 6 (6), 27-31.

7. Saidi, A.; Hambaba, L.; Kucuk, B.; Cacan, E.; Erenler, R. *Curr. Bioact. Compd.* **2022,** 18 (3), 72-83.

8. Koysu, P.; Genc, N.; Elmastas, M.; Aksit, H.; Erenler, R. *Nat. Prod. Res.* **2019,** 33 (24), 3592-3595.

9. Erenler, R.; Telci, I.; Ulutas, M.; Demirtas, I.; Gul, F.; Elmastas, M.; Kayir, O. *J. Food Biochem.* **2015,** 39 (5), 622-630.

10. Dede, E.; Genc, N.; Elmastas, M.; Aksit, H.; Erenler, R. *Nat. Prod. J.* **2019,** 9 (3), 238-243.

11. Erenler, R.; Nusret, G.; Elmastaş, M.; Eminağaoğlu, Ö. *Turk. J. Biodiv.* **2019,** 2 (1), 13-17.

12. Nusret, G.; Elmastas, M.; Telci, I.; Erenler, R. *Int. J. Chem. Technol.* **2020,** 4 (2), 179-184.

13. Aydin, A.; Erenler, R.; Yılmaz, B.; Tekin, Ş. *J. Turk. Chem. Soc., Sec A: Chem* **2016,** 3 (3), 217-228.

14. Elmastas, M.; Erenler, R.; Isnac, B.; Aksit, H.; Sen, O.; Genc, N.; Demirtas, I. *Nat. Prod. Res.* **2016,** 30 (3), 299-304.

15. Gecer, E. N. *J. Inorg. Organomet. Polym. Mater.* **2021,** 31 (11), 4402-4409.

16. Gecer, E. N.; Erenler, R.; Temiz, C.; Genc, N.; Yildiz, I. *Particul. Sci. Technol.* **2021,** 40 (1), 50-57.

17. Genc, N. *Particul. Sci. Technol.* **2021,** 39 (5), 562-568.

18. Genc, N.; Yildiz, I.; Chaoui, R.; Erenler, R.; Temiz, C.; Elmastas, M. *Inorg. Nano-Met. Chem.* **2021,** 51 (3), 411-419.

19. Burlacu, E.; Tanase, C.; Coman, N.-A.; Berta, L. *Molecules* **2019,** 24 (23), 4354.

20. de Souza, T. A. J.; Souza, L. R. R.; Franchi, L. P. *Ecotox. Environ. Safe.* **2019,** 171, 691-700.

21. El-Seedi, H. R.; El-Shabasy, R. M.; Khalifa, S. A.; Saeed, A.; Shah, A.; Shah, R.; Iftikhar, F. J.; Abdel-Daim, M. M.; Omri, A.; Hajrahand, N. H. *RSC Adv.* **2019,** 9 (42), 24539-24559.

22. Faraz, A.; Faizan, M.; Sami, F.; Siddiqui, H.; Pichtel, J.; Hayat, S. *IET Nanobiotech.* **2019,** 13 (4), 345-352.

23. Ökten, S.; Çakmak, O.; Erenler, R.; Yüce, Ö.; Tekin, S. *Turk. J. Chem.* **2013,** 37 (6), 896-908.

24. G Ravelo, A.; Estévez-Braun, A.; Chávez-Orellana, H.; Pérez-Sacau, E.; Mesa-Siverio, D. *Curr. Top. Med. Chem.* **2004,** 4 (2), 241-265.

25. Erenler, R.; Meral, B.; Sen, O.; Elmastas, M.; Aydin, A.; Eminagaoglu, O.; Topcu, G. *Pharm. Biol.* **2017,** 55 (1), 1646-1653.

26. Elmastas, M.; Celik, S. M.; Genc, N.; Aksit, H.; Erenler, R.; Gulcin, İ. *Int. J. Food Prop.* **2018,** 21 (1), 374-384.

27. Erenler, R.; Demirtas, I.; Karan, T.; Gul, F.; Kayir, O.; Karakoc, O. C. *Trends Phytochem. Res.* **2018,** 2 (2), 91-96.

28. Karan, T.; Simsek, S.; Yildiz, I.; Erenler, R. *Int. J. Sec. Metabol.* **2018,** 5 (2), 87-93.

29. Erenler, R.; Sen, O.; Aksit, H.; Demirtas, I.; Yaglioglu, A. S.; Elmastas, M.; Telci, İ. *J. Sci. Food Agr.* **2016,** 96 (3), 822-836.

30. Erenler, R.; Dag, B. *Inorg. Nano-Met. Chem.* **2022,** 52 (4), 485-492.

31. Sahin Yaglioglu, A.; Akdulum, B.; Erenler, R.; Demirtas, I.; Telci, I.; Tekin, S. *Med. Chem. Res.* **2013,** 22 (6), 2946-2953.

32. Erenler, R.; Pabuccu, K.; Yaglioglu, A. S.; Demirtas, I.; Gul, F. *Z. Naturforsch. C* **2016,** 71 (3-4), 87-92.

33. Erenler, R.; Sen, O.; Yaglioglu, A. S.; Demirtas, I. *Comb. Chem. High. T. Scr.* **2016,** 19 (1), 66-72.

34. Erenler, R.; Sen, O.; Yildiz, I.; Aydın, A. *Rec. Nat. Prod.* **2016,** 10 (6), 766-770.

35. Karan, T.; Erenler, R.; Bozer, B. M. *Z. Naturforsch. C* **2022**.

36. Hu, W.; Kavanagh, J. J. *Lancet Oncol.* **2003,** 4 (12), 721-729.

DOI: http://dx.doi.org/10.32571/ijct.1170566 **E-ISSN: 2602-277X**

International Journal of Chemistry and Technology

http://dergipark.org.tr/ijct

Research Article

Contributions to the fauna of Türkiye geometridae

Mürşit Ömür KOYUNCU[1*], Vedat GÖRMEZ[2], Murat KÜTÜK[3]

[1*]*Department of Veterinary, Araban Vocational School, Gaziantep University, 27650, Gaziantep, Türkiye*

[2] *Department of Vegetable and Animal Production, Islahiye Vocational School, Gaziantep University ,27800, Gaziantep, Türkiye*

[3]*Biology Department of Biology, Faculty of Science and Arts Gaziantep University, 27310 Gaziantep, Türkiye*

Received: 3 September 2022; Revised: 18 December 2022; Accepted: 20 December 2022

*Corresponding author e-mail: mursitkoyuncu@hotmail.com

Citation: Koyuncu, M. Ö.; Görmez, V.; Kütük, M. *Int. J. Chem. Technol.* **2022**, 6 (2), 147-153.

ABSTRACT

The Geometridae is one of the most populous families in terms of the number of species in the order Lepidoptera. It is known to have more than 23.000 species worldwide. Geometridae species cause damage to forest trees, but it has been reported that they also cause damage to cultivated plants in studies. This research was carried out in Türkiye's Central Black Sea Region (Amasya, Çorum, Ordu, Samsun, Sinop, Tokat, and Yozgat) in 2017 and 2018 years. Adult specimens of Geometridae were collected using an insect net and a light trap in the study region. Obtained specimens were prepared according to standard museum methods for butterflies and prepared genitalia structures. As a result of the study, five subfamilies (Ennominae, Geometrinae, Larentiinae, Orthostixinae, Sterrhinae), 36 genera, and 48 species were determined. Also in this paper, the examined materials and adult photographs of the species are given. This study provides new information about the zoogeographic distribution of Geometridae species identified in the research area.

Keywords: Geometridae, fauna, lepidoptera, Türkiye.

Türkiye Geometridae faunasına katkılar

ÖZ

Geometridae, Lepidoptera takımının tür sayısı bakımından kalabalık familyalarından biridir. Dünyada 23.000' den fazla türü olduğu bilinmektedir. Geometridae türleri orman ağaçlarında zarar yapmaktadır ancak yapılan çalışmalarda kültür bitkilerinde de zarar yaptığı bildirilmiştir. Bu çalışma 2017 ve 2018 yıllarında Türkiye'nin orta Karadeniz bölgesinde (Amasya, Çorum, Ordu, Samsun, Sinop, Tokat, Yozgat) yapılmıştır. Çalışmada ergin Geometridae örnekleri atrap ve ışık tuzağı kullanılarak toplanmıştır. Elde edilen örnekler kelebekler için standart müze yöntemlerine göre hazırlanmış ve genital yapılar hazırlanmıştır. Çalışmanın sonucunda beş alt familya (Ennominae, Geometrinae, Larentiinae, Orthostixinae, Sterrhinae), 36 cins ve 48 tür tespit edilmiştir. Ayrıca bu makalede, türlere ait incelenen materyaller ve ergin fotoğrafları verilmiştir. Bu çalışma, araştırma bölgesinde tespit edilen Geometridae türlerinin zoocoğrafik yayılışı hakkında yeni bilgileri sunmaktadır.

Anahtar kelimeler: Geometridae, fauna, lepidoptera, Türkiye

1. INTRODUCTION

Geometridae is one of the crowded moth families of the order Lepidoptera. Eggs are generally laid under the leaves of the host plant by adult female species. Geometridae larvae are generally polyphagous and cause damage to forest trees. However, in recent studies, it has been reported that it also damages cultivated plants (almond, olive, citrus, corn, sorghum).[1] Species spend the pupal stage in the soil and then emerges as an adult. Adults feed on water and pollen, which benefit pollination due to feeding behavior.

Geometridae adults and larvae adapt well to their natural environments like soil, sand, tree trunks, and branches. Species have some different coloration called cryptic coloration and their situation benefits hiding from natural enemies in their habitats. The larvae remain motionless until the danger has passed.

Geometridae species are distributed in different habitats. It has been observed that some species distribute at above 2000 m in the Black Sea region of Türkiye.[2] Geometridae

DOI: http://dx.doi.org/10.32571/ijct.1170566 E-ISSN: 2602-277X

species are generally active at night (nocturnal), and some species are active during the day (diurnal).

In recent years, studies have been conducted in different regions of Türkiye related to the family Geometridae. Some previous studies on moths in the Black Sea region are as follows.[3-12] According to[13] 687 species of Geometridae are distributed in Türkiye. *Eupithecia nemrutica* (Seven, Mironov & Akın, 2019) as a new species reported from the Adıyaman province of Türkiye.[14] *Protorhoe centralisata* (Staudinger, 1892) as a new record reported from Batman province of Türkiye.[15] *Perigune jordanaria* (Staudinger, 1901) as a new record reported from Batman province of Türkiye.[16] *Kresnaia beschkovi* (Ganev, 1987) as a new record reported from Batman province of Türkiye.[17] Also *Gnophos chorista* Wehrli, 1939 as a new record reported from Batman province of Türkiye[18] Thus, 692 Geometridae species reported up to date from Türkiye.

2. MATERIALS AND METHODS

In this study, Geometridae adults were collected from Amasya, Çorum, Ordu, Samsun, Sinop, Tokat and Yozgat provinces (Figure 1) in 2017-2018. Geometridae specimens were collected by using insect trap and light trap. Obtained specimens were killed in ethyl acetate killing jars and stored in falcon tubes with label information for each sample. For diagnosis preparation of Geometridae specimens, dry samples need to be relaxed first. Relaxing method was used to relax dry samples.[19] Each sample was prepared according to standard museum methods and labelled for diagnosis. Than specimens were diagnosed to literatures.[20-28]

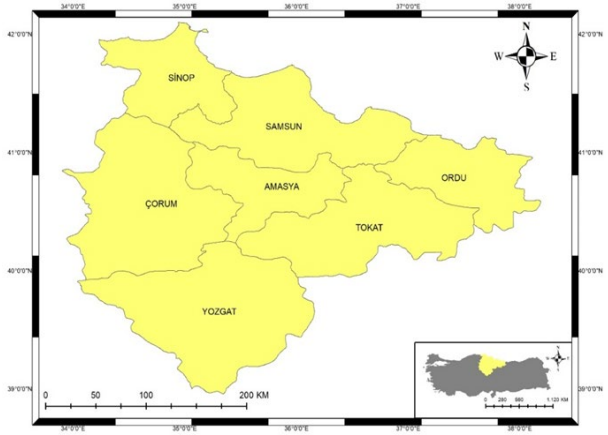

Figure 1. Research area of collected specimens.

3. RESULTS AND DISCUSSION

3.1 Results

This study provide some new faunistic information about Geometridae fauna of Türkiye. As a result of the study, five subfamilies (Ennominae, Geometrinae, Larentiinae, Orthostixinae, Sterrhinae), 36 genera, and 48 species were determined. The identified species are presented below in alphabetical order.

Alcis repandata (Linnaeus, 1758); Figure B-1

Material examined: 4 ♂♂, **Ordu**, Gölköy, Center, 40° 38' N, 37° 36' E, 1130 m, 29.06.2017.

Aplasta ononaria (Fuessly, 1783); Figure B-2

Material examined: 2 ♂♂, **Samsun**, Havza, Çelikalan, 41° 12' N, 35° 51' E, 639 m, 29.07.2017. 2 ♂♂, **Tokat**, Zile, Emirören, 40° 18' N, 35° 58' E, 810 m, 29.06.2017.

Aplocera efformata (Guenée, 1858); Figure B-3

Material examined: 2 ♂♂, **Sinop**, Boyabat, Koçak, 41° 36' N, 34° 38' E, 350 m, 16.06.2017.

Asthena albulata (Hufnagel, 1767); Figure B-4

Material examined: 1 ♂, **Ordu**, Center, Karaca, 41° 00' N, 37° 37' E, 48 m, 30.06.2017. 1 ♂, **Samsun**, Bafra, Esençay, 41° 18' N, 35° 50' E, 223 m, 29.07.2017; 1 ♂, Havza, Çelikalan, 41° 12' N, 35° 51' E, 639 m, 29.07.2017.

Camptogramma bilineata (Linnaeus, 1758); Figure B-5

Material examined: 1 ♀, **Amasya**, Gümüşhacıköy, Sekü, 40° 57' N, 36° 06' E, 809 m, 22.06.2018. 8 ♂♂, 2 ♀♀, **Çorum**, Boğazkale, Hattuşa, 40° 10' N, 34° 37' E, 1070 m, 25.07.2017; 1 ♂, Oğuzlar, Ağaççamı, 40° 48' N, 34° 40' E, 991 m, 22.06.2018; 3 ♂♂, 2 ♀♀, Bayat, Kunduzlu, 40° 45' N, 34° 14' E, 1321 m, 22.06.2018. 4 ♂♂, **Sinop**, Boyabat, Koçak, 41° 36' N, 34° 38' E, 350 m, 16.06.2017; Ayancık, Gökçesakızı, 41° 39' N, 34° 38' E, 640 m, 21.06.2018. 8 ♂♂, **Yozgat**, Center, Kalınbük, 39° 56' N, 34° 42' E, 1215 m, 19.06.2018.

Coenotephria ablutaria (Boisduval, 1840); Figure B-6

Material examined: 3 ♂♂, **Sinop**, Durağan, Çayağzı, 41° 26' N, 35° 08' E, 612 m, 28.07.2017.

Costaconvexa polygrammata (Borkhausen, 1794); Figure B-7

Material examined: 1 ♂, **Sinop**, Boyabat, Koçak, 41° 36' N, 34° 38' E, 350 m, 16.06.2017.

Cyclophora linearia (Hübner, 1799); Figure B-8

Material examined: 3 ♂♂, 1 ♀, **Samsun**, Havza, Çelikalan, 41° 12' N, 35° 51' E, 639 m, 29.07.2017.

Cabera exanthemata (Scopoli, 1763); Figure B-9

Material examined: 4 ♂♂, **Çorum**, İskilip, Başmakçı, 40° 43' N, 34° 35' E, 857 m, 27.07.2017.

Cabera pusaria (Linnaeus, 1758); Figure B-10

Material examined: 1 ♂, **Amasya**, Gümüşhacıköy, Sekü, 40° 57' N, 36° 06' E, 809 m, 27.07.2017. 4 ♂♂, 3 ♀♀, **Çorum**, Bayat, Kunduzlu, 40° 45' N, 34° 14' E, 1321 m, 31.07.2017; 2 ♂♂, Boğazkale, Hattuşa, 40° 01' N, 34° 37' E, 1019 m, 16.08.2017. 2 ♂♂, **Ordu**, Mesudiye, Gölköy, 40° 36' N, 37° 37' E, 1580 m, 29.06.2017; 1 ♂,

DOI: http://dx.doi.org/10.32571/ijct.1170566 E-ISSN: 2602-277X

Gölköy, Center, 40° 38' N, 37° 36' E, 1130 m, 29.06.2017; Gölköy, Döşek, 40° 45' N, 37° 37' E, 1129 m, 30.06.2017.

Chiasmia clathrata (Linnaeus, 1758); Figure B-11

Material examined: 2 ♂♂, **Ordu**, Mesudiye, Gölköy, 40° 36' N, 37° 37' E, 1580 m, 29.06.2017.

Dicrognophos sartata (Treitschke, 1827); Figure B-12

Material examined: 4 ♂♂, **Sinop**, Boyabat, Koçak, 41° 36' N, 34° 38' E, 350 m, 16.06.2017; 2 ♂♂, Durağan, Çayağzı, 41° 26' N, 35° 08' E, 612 m, 28.07.2017.

Eilicrinia cordiaria (Hübner, 1790); Figure B-13

Material examined: 1 ♂, **Yozgat**, Center, Evci, 39° 51' N, 34° 42' E, 1192 m, 19.06.2018.

Ematurga atomaria (Linnaeus, 1758); Figure B-14

Material examined: 1 ♂, **Amasya**, Taşova, Karabük, 40° 43' N, 36° 09' E, 267 m, 19.08.2017. 1 ♂, **Çorum**, Bayat, Kunduzlu, 40° 45' N, 34° 14' "E, 1321 m, 16.08.2017. 2 ♂♂, **Yozgat**, Sarıkaya, Bağlıca, 39° 35' N, 35° 15' E, 1118 m, 28.06.2017.

Heliomata glarearia (Denis & Schiffermüller, 1775); Figure B-15

Material examined: 1 ♂, **Ordu**, Mesudiye, Aşağısuma, 40° 28' N, 37° 42' E, 1430 m, 29.06.2017. 2 ♂♂, 2 ♀♀, **Sinop**, Boyabat, Koçak, 41° 36' N, 34° 38' E, 350 m, 16.06.2017. 1 ♂, **Yozgat**, Center, Tayıp, 39° 50' N, 34° 42' E, 1209 m, 19.06.2018.

Eupithecia breviculata (Donzel, 1837); Figure B-16

Material examined: 1 ♂, **Samsun**, Bafra, Kabaçukur, 41° 19' N, 35° 50' E, 123 m, 18.08.2017. 2 ♂♂, **Sinop**, Boyabat, Koçak, 41° 36' N, 34° 38' E, 350 m, 16.06.2017.

Eupithecia ericeata (Rambur, 1833); Figure B-17

Material examined: 1 ♂, **Çorum**, Bayat, Karatepe, 40° 44' N, 34° 12' E, 1681 m, 22.06.2018.

Eupithecia subfuscata (Haworth, 1809); Figure B-18

Material examined: 1 ♂, 1 ♀, **Ordu**, Mesudiye, Gölköy, 40° 36' N, 37° 37' E, 1580 m, 29.06.2017.

Horisme tersata (Denis & Schiffermüller, 1775); Figure B-19

Material examined: 2 ♀♀, **Tokat**, Niksar, Mutluca, 40° 25' N, 37° 07' E, 436 m, 18.05.2017.

Hydriomena impluviata (Denis & Schiffermüller, 1775); Figure B-20

Material examined: 1 ♂, **Ordu**, Gölköy, Center, 40° 38' N, 37° 36' E, 1130 m, 29.06.2017.

Hylaea fasciaria (Linnaeus, 1758); Figure B-21

Material examined: 3 ♂♂, **Çorum**, Bayat, Kunduzlu, 40° 45' N, 34° 15' E, 1605 m, 26.07.2017.

Hypomecis punctinalis (Scopoli, 1763); Figure B-22

Material examined: 7 ♂♂, **Tokat**, Niksar, Mutluca, 40° 25' N, 37° 07' E, 436 m, 18.05.2017.

Idaea aversata (Linnaeus, 1758); Figure B-23

Material examined: 3 ♂♂, **Çorum**, Bayat, Kunduzlu, 40° 45' N, 34° 15' E, 1605 m, 26.07.2017; 1 ♀, Bayat, Kunduzlu, 40° 45' N, 34° 14' E, 1321 m, 31.07.2017.

Idaea filicata (Hübner, 1799); Figure B-24

Material examined: 1 ♂, **Samsun**, Havza, Çelikalan, 41° 12' N, 35° 51' E, 639 m, 29.07.2017. 2 ♂♂, **Sinop**, Durağan, Center, 41° 23' N, 35° 16' E, 1140 m, 28.07.2017.

Idaea ochrata (Scopoli, 1763); Figure B-25

Material examined: 4 ♂♂, 2 ♀♀, **Çorum**, Mecitözü, İbek, 40° 22' N, 35° 03' E, 870 m, 1.07.2017. 8 ♂♂, **Yozgat**, Center, Büyükincirli, 39° 37' N, 34° 55' E, 1028 m, 19.06.2018.

Idaea politaria (Hübner, 1799); Figure B-26

Material examined: 1 ♂, **Çorum**, Uğurludağ, Kumçeltiği, 40° 34' N, 34° 30' E, 784 m, 1.07.2017; 1 ♀, İskilip, Başmakçı, 40° 43' N, 34° 35' E, 857 m, 27.07.2017; 1 ♂, Center, Konak, 40° 38' N, 35° 11' E, 980 m, 28.07.2017. 1 ♂, **Ordu**, Center, Karaca, 41° 00' N, 37° 37' E, 48 m, 30.06.2017. **Samsun**, Bafra, Kabaçukur, 41° 19' N, 35° 50' E, 123 m, 18.08.2017; 1 ♂, Kavak, Akbelen, 41° 09' N, 35° 53' E, 910 m, 18.08.2017; 6 ♂♂, Samsun, Havza, Ortaklar, 41° 00' N, 35° 34' E, 830 m, 21.06.2018. 3 ♂♂, **Sinop**, Boyabat, Koçak, 41° 36' N, 34° 38' E, 350 m, 16.06.2017.

Idaea rufaria (Hübner, 1799); Figure B-27

Material examined: 1 ♂, **Samsun**, Havza, Çelikalan, 41° 12' N, 35° 51' E, 639 m, 29.07.2017.1 ♂, **Sinop**, Durağan, Center, 41° 23' N, 35° 16' E, 1140 m, 28.07.2017.

Isturgia arenacearia (Denis & Schiffermüller, 1775); Figure B-28

Material examined: 3 ♂♂, **Samsun**, Vezirköprü, Güldere, 41° 17' N, 35° 55' E, 630 m, 29.07.2017.

Ligdia adustata (Denis & Schiffermüller, 1775); Figure B-29

Material examined: 1 ♂, **Yozgat**, Center, Kalınbük, 39° 56' N, 34° 42' E, 1215 m, 19.06.2018.

Lomaspilis bithynica Wehrli, 1939; Figure B-30

Material examined: 2 ♂♂, **Çorum**, Bayat, Kunduzlu, 40° 45' N, 34° 14' E, 1321 m, 22.06.2018.

Lythria cruentaria (Hufnagel, 1767); Figure B-31

Material examined: 1 ♂, **Amasya**, Gümüşhacıköy, Sekü, 40° 57' N, 36° 06' E, 809 m, 30.07.2017; 3 ♂♂, Taşova, Karabük, 40° 43' N, 36° 09' E, 267 m, 19.08.2017. 1 ♂,

DOI: http://dx.doi.org/10.32571/ijct.1170566 E-ISSN: 2602-277X

Çorum, Sungurlu, Kamışlı, 40° 07' N, 34° 28' E, 1000 m, 2.07.2017; 4 ♂♂, Sungurlu, Tuğcu, 40° 11' N, 34° 19' E, 796 m, 19.06.2018. 4 ♂♂, **Samsun**, Havza, Boyalı, 41° 13' N, 35° 52' E, 770 m, 29.07.2017; 3 ♂♂, Ladik, İbi, 40° 58' N, 35° 54' E, 779 m, 30.07.2017. 1 ♀,

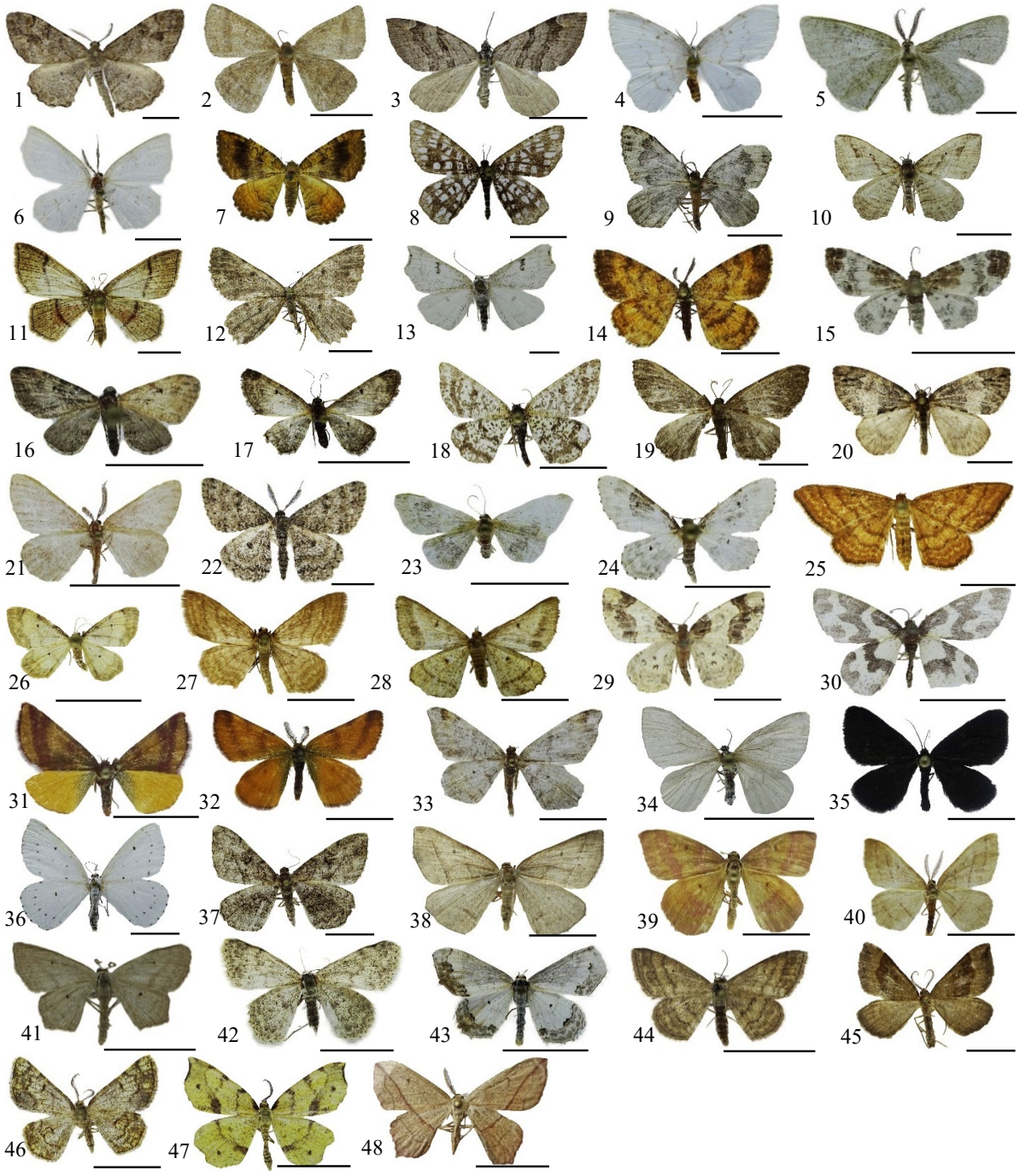

Figure 2. Adult of Geometridae species: 1. *Alcis repandata*, 2. *Aplasta ononaria*, 3. *Aplocera efformata*, 4. *Asthena albulata*, 5. *Cabera exanthemata*, 6. *C. pusaria*, 7. *Camptogramma bilineata*, 8. *Chiasmia clathrata*, 9. *Coenotephria ablutaria*, 10. *Costaconvexa polygrammata*, 11. *Cyclophora linearia*, 12. *Dicrognophos sartata*, 13. *Eilicrinia cordiaria*, 14. *Ematurga atomaria*, 15. *Eupithecia breviculata*, 16. *E. ericeata*, 17. *E. subfuscata*, 18. *Heliomata glarearia*, 19. *Horisme tersata*, 20. *Hydriomena impluviata*, 21. *Hylaea fasciaria*, 22. *Hypomecis punctinalis*, 23. *Idaea aversata*, 24. *I. filicata*, 25. *I. ochrata*, 26. *I. politaria*, 27. *I. rufaria*, 28. *Isturgia arenacearia*, 29. *Ligdia adustata*, 30. *Lomaspilis bithynica*, 31. *Lythria cruentaria*, 32. *L. purpuraria*, 33. *Macaria alternata*, 34. *Minoa murinata*, 35. *Odezia atrata*, 36. *Orthostixis cribraria*, 37. *Peribatodes rhomboidaria*, 38. *Petrophora chlorosata*, 39. *Rhodostrophia discopunctata*, 40. *R. vibicaria*, 41. *Scopula flaccidaria*, 42. *S. marginepunctata*, *43. S. ornata*, *44. S. turbulentaria*, 45. *Scotopteryx chenopodiata*, 46. *Stegania dilectaria*, 47. *Therapis flavicaria*, 48. *Timandra comae.* (Scale: 1cm).

DOI: http://dx.doi.org/10.32571/ijct.1170566 E-ISSN: 2602-277X

Yozgat, Sarıkaya, Yeşilkışla, 39° 24' N, 35° 21' E, 1220 m, 28.06.2017; 1 ♀, Sarıkaya, Bağlıca, 39° 35' N, 35° 15' E, 1118 m, 28.06.2017.

Lythria purpuraria (Linnaeus, 1758); Figure B-32

Material examined: 2 ♂♂, **Amasya**, Taşova, Karabük, 40° 43' N, 36° 09' E, 267 m, 19.08.2017. 1 ♂, **Sinop**, Durağan, Çayağzı, 41° 26' N, 35° 08' E, 612 m, 28.07.2017. 2 ♂♂, **Tokat**, Pazar, Center, 40° 17' N, 36° 19' E, 552 m, 18.05.2017.

Macaria alternata (Denis & Schiffermüller, 1775) Figure B-33

Material examined: 1 ♂, **Çorum**, Bayat, Kunduzlu, 40° 45' N, 34° 15' E, 1605 m, 26.07.2017.

Minoa murinata (Scopoli, 1763); Figure B-34

Material examined: 2 ♂♂, **Sinop**, Ayancık, Gökçukur, 41° 39' N, 34° 40' E, 866 m, 17.08.2017.

Odezia atrata (Linnaeus, 1758); Figure B-35

Material examined: 7 ♂♂, **Tokat**, Almus, Bakımlı, 40° 37' N, 36° 80' E, 826 m, 17.05.2017.

Orthostixis cribraria (Hübner, 1799); Figure B-36

Material examined: 5 ♂♂, **Çorum**, Bayat, Kunduzlu, 40° 45' N, 34° 14' E, 1360 m, 26.07.2017; 1 ♂, Center, Konak, 40° 38' N, 35° 11' E, 980 m, 28.07.2017; 7 ♂♂, 2 ♂♂, Bayat, Kunduzlu, 40° 45' N, 34° 14' E, 1321 m, 31.07.2017.

Peribatodes rhomboidaria (Denis & Schiffermüller, 1775); Figure B-37

Material examined: 1 ♂, **Samsun**, Vezirköprü, Güldere, 41° 17' N, 35° 55' E, 630 m, 29.07.2017. 3 ♂♂, **Sinop**, Boyabat, Koçak, 41° 36' N, 34° 38' E, 350 m, 16.06.2017.

Petrophora chlorosata (Scopoli, 1763); Figure B-38

Material examined: 1 ♂, **Ordu**, Akkuş, Center, 40° 48' N, 37° 00' E, 1310 m, 30.06.2017. 1 ♂, **Yozgat**, Sarıkaya, Yeşilkışla, 39° 24' N, 35° 21' E, 1220 m, 28.06.2017.

Rhodostrophia discopunctata Amsel, 1935; Figure B-39

Material examined: 1 ♂, **Çorum**, Dodurga, Yeniköy, 40° 51' N, 34° 42' E, 977 m, 22.06.2018. 5 ♂♂, **Sinop**, Boyabat, Koçak, 41° 36' N, 34° 38' E, 350 m, 16.06.2017. 1 ♂, **Yozgat**, Sarıkaya, Yeşilkışla, 39° 24' N, 35° 21' E, 1220 m, 28.06.2017; 1 ♀, Center, Büyükincirli, 39° 37' N, 34° 55' E, 1028 m, 19.06.2018; 1 ♀, Center, Tayıp, 39° 50' N, 34° 42' E, 1209 m, 19.06.2018; 1 ♂, Center, Evci, 39° 51' N, 34° 42' E, 1192 m, 19.06.2018.

Rhodostrophia vibicaria (Clerck, 1759); Figure B-40

Material examined: 1 ♀, **Çorum**, Bayat, Kunduzlu, 40° 45' N, 34° 14' E, 1360 m, 26.07.2017; 2 ♂♂, Dodurga, Yeniköy, 40° 51' N, 34° 42' E, 977 m, 22.06.2018; 1 ♂, İskilip, Asarcık, 40° 44' N, 34° 34' E, 1071 m, 22.06.2018; 1 ♂, Bayat, Kunduzlu, 40° 45' N, 34° 14' E, 1321 m, 22.06.2018.

Scopula flaccidaria (Zeller, 1852); Figure B-41

Material examined: 3 ♂♂, **Samsun**, Tekkeköy, Ovabaşı, 41° 12' N, 36° 30' E, 3 m, 18.08.2017.

Scopula marginepunctata (Goeze, 1781); Figure B-42

Material examined: 1 ♂, **Sinop**, Boyabat, Koçak, 41° 36' N, 34° 38' E, 350 m, 16.06.2017.

Scopula ornata (Scopoli, 1763); Figure B-43

Material examined: 1 ♂, **Sinop**, Boyabat, Koçak, 41° 36' N, 34° 38' E, 350 m, 16.06.2017; 1 ♂, Erfelek, Hasandere, 41° 52' 55"N, 34° 56' 42"E, 346 m, 17.08.2017.

Scopula turbulentaria (Staudinger, 1870); Figure B-44

Material examined: 2 ♂♂, 1 ♀, **Sinop**, Boyabat, Gökçeağaçsakızı, 41° 38' N, 34° 36' E, 459 m, 21.06.2018.

Scotopteryx chenopodiata (Linnaeus, 1758); Figure B-45

Material examined: 2 ♂♂, **Çorum**, Bayat, Kunduzlu, 40° 45' N, 34° 14' E, 1360 m, 26.07.2017; 4 ♂♂, Bayat, Kunduzlu, 40° 45' N, 34° 15' E, 1605 m, 26.07.2017.

Stegania dilectaria (Hübner, 1790); Figure B-46

Material examined: 2 ♂♂, 1 ♀, **Çorum**, Boğazkale, Hattuşa, 40° 01' N, 34° 37' E, 1019 m, 16.08.2017.

Therapis flavicaria (Denis & Schiffermüller, 1775); Figure B-47

Material examined: 1 ♂, **Ordu**, Gölköy, Center, 40° 38' N, 37° 36' E, 1130 m, 29.06.2017.

Timandra comae A. Schmidt, 1931; Figure B-48

Material examined: 2 ♂♂, **Çorum**, Boğazkale, Hattuşa, 40° 01' N, 34° 37' E, 1019 m, 16.08.2017. 2 ♂♂, **Samsun**, Havza, Dereköy, 41° 06' N, 35° 42' E, 564 m, 29.07.2017; 1 ♂, Tekkeköy, Ovabaşı, 41° 12' N, 36° 30' E, 3 m, 18.08.2017.

3.2 Discussion

692 species of Geometridae were identified in Türkiye. According to,[13] 199 from Amasya, 2 from Çorum, 87 from Ordu, 13 from Samsun, 23 from Sinop, 41 from Tokat, and 3 from Yozgat Geometridae species were reported. In this paper, 5 species of Geometridae were determined and 3 of them were recorded for the first time in Amasya province; 18 species of Geometridae were determined and 18 of them were recorded for the first time in Çorum province; 10 species of Geometridae were determined and 7 of them were recorded for the first time in Ordu province; 12 species of Geometridae were

DOI: http://dx.doi.org/10.32571/ijct.1170566 E-ISSN: 2602-277X

Geometridae species / Provinces	Species count before this study	Determined species in this study	New record for provinces	Species count after this study
Amasya	199	5	3	202
Çorum	2	18	18	20
Ordu	87	10	7	94
Samsun	13	12	11	24
Sinop	23	16	14	37
Tokat	41	5	3	44
Yozgat	3	9	9	12

Table 1. Distribution of Geometridae species in provinces.

determined and 11 of them were recorded for the first time in Samsun province; 16 species of Geometridae were determined and 14 of them were recorded for the first time in Sinop province; 5 species of Geometridae were determined and 3 of them were recorded for the first time in Tokat province; 9 species of Geometridae were determined and 9 of them were recorded for the first time in Yozgat province (Table 1).

Conflict of interests

Authors declare that there is no a conflict of interest with any person, institute, company, etc.

REFERENCES

1. Kaçar, G.; Özdemir, M. *Plant Prot Bull*. **2015**, 55(4), 255-264.

2. Can Cengiz, F. *MKU. J. Agric. Sci.* **2011**, 16 (1): 11-18.

3. Hakyemez, A. *J. Fac. For. Istanbul U.*, *Seri A*, **1994a**, 44: 111-133.

4. Hakyemez, A. *J. Fac. For. Istanbul U., Seri B*, **1994b**, 44: 123-130.

5. Akbulut, S.; Yüksel, B.; Keten, A. *Turk. J. Zool*., **2003**, 27: 257-268.

6. Özdemir, M. *Cent. ent. Stud., Priamus*, **2007**, vol. 7-94s.

7. Çakan, G.; Okyar, Z. *Turk. Entomo.l Derg-Tu.*, **2007**, 31: 47-62.

8. Can, F. *Turk. J. Zool*., **2008**, 32 351-358.

9. Okyar, Z.; Yurtseven, S.; Aktaç, N.; Çakan, G. *North-West J. Zool.*, **2009**, l. 5, No. 1, 104-120

10. Okyar, Z. *J. Kansas Entomol. Soc.*, **2010**, 83(3), 193-200.

11. Özdemir, M. *Plant Prot Bull*., **2016**, 56(2): 209 -225.

12. Özdemir, M. *Entomofauna*, **2019**, 40 (2): 391-417.

13. Koçak, A. Ö.; Kemal, M. *Cent. ent.Stud., Priamus*, **2018**, 8,1-487.

14. Seven, E.; Mironov, V.; Akın, K. *Zootaxa*, **2019a**, 4668 (3), 443–447.

15. Seven, E. *Acta Biologica Turcica*, **2019b**, 32 (3): 123-127.

16. Seven, E.; Hausmann, A.; Aykal, A. *Zool. Middle. Eas.*, **2021a**, 65-72.

17. Seven, E. *J. Entomol. Res. Soc.*, **2021b**, 23(2), 153-156.

18. Aykal, A.; Seven E. *Trakya Univ. J. Nat. Sci.*, **2022**, 23(1): 81-94.

19. Koyuncu, M.Ö.; Kütük, M. *KSU J. Agric Nat*., **2022**, 25 (1): 127-132.

20. Hausmann, A. The Geometrid Moths of Europe, Volume 1. Apollo Books, Stenstrup, Denmark, 2001.

21. Mironov, V. The Geometrid Moths of Europe, Volume. 4. Apollo Books, Stenstrup, Denmark, 2003.

22. Hausmann, A. The Geometrid Moths of Europe. Volume 2. Apollo Books, Stenstrup, Denmark , 2004.

23. Hausmann, A.; Viidalepp, J. The Geometrid Moths of Europe. Volume 3. Apollo Books, Stenstrup, Denmark, 2012.

DOI: http://dx.doi.org/10.32571/ijct.1170566 **E-ISSN: 2602-277X**

24. Skou, P.; Sihvonen, P. The Geometrid Moths of Europe. Volume 5. Apollo Books, Stenstrup, Denmark, 2015.

25. Leraut, P. Moths of Europa Geometridae Volume II, 2009.

26. Redondo, V.; Gastón, F.J.; Gimeno, R. Geometridae Ibericae. Apollo Books, Stenstrup, Denmark, 2009.

27. Müller, B., Erlacher, S.; Hausmann, A.; Rajaei, H.; Sihvonen, P.; Skou, P.. The Geometrid Moths of Europe.Volume 6. Apollo Books, Stenstrup, Denmark, 2019.

28. Koyuncu, M.Ö.; Kütük, M. *Fresenius Environ. Bull*., **2021**.30(6), 7309-7320.

DOI: http://dx.doi.org/10.32571/ijct.1194667 E-ISSN: 2602-277X

International Journal of Chemistry and Technology

http://dergipark.org.tr/ijct

Research Article

Attachment of idarubicin to glutaraldehyde-coated magnetic nanoparticle and investigation of its effect in HL-60 cell line

Hasan ULUSAL[1*], Fatma ULUSAL[2], Mehmet Akif BOZDAYI[1], Bilgehan GÜZEL[3], Seyithan TAYSI[1], Mehmet TARAKÇIOĞLU[1]

[1] *Department of Medical Biochemistry, Faculty of Medicine, Gaziantep University, 27310, Gaziantep, Türkiye*
[2] *Department of Chemistry and Chemical Processing Technologies, Tarsus University, 33100, Mersin, Türkiye*
[3] *Department of Chemistry, Faculty of Arts and Sciences, Cukurova University, 01330, Adana, Türkiye*

Received: 26 October 2022; Revised: 1 November 2022; Accepted: 30 November 2022

* Corresponding author e-mail: hasan_ulusal@hotmail.com

Citation: Ulusal, H.; Ulusal, F.; Bozdayı, M. A.; Güzel, B.; Taysı, S.; Tarakçıoğlu, M. *Int. J. Chem. Technol.* **2022**,6 (2), 154-163.

ABSTRACT

Idarubicin is a chemotherapeutic drug frequently used to treat breast cancer and acute leukemia. This study aimed to immobilize idarubicin on glutaraldehyde (GA)-coated magnetic nanoparticles (MNP-GA) to prepare a drug with high stability and low toxicity. We prefreed MNPS because of their easy synthesis, low cost, and non-toxicity. In the study, magnetite (Fe3O4) nanoparticles were prepared, coated with glutaraldehyde, characterization processes were performed with Fourier transform infrared spectroscopy (FT-IR), X-ray diffraction pattern (XRD), and Conventional transmission electron microscopy (C-TEM) methods, and idarubicin (IDA) was bound. The cytotoxic effects of idarubicin-bound MNP-GA and free idarubicin on HL-60 cell lines were determined by MTT and ATP tests, and IC50 values were calculated. Flow cytometry was used to evaluate apoptosis status, and the expression of MDR1, Puma, NOXA, BAX, Survivin, and BCL-2 genes were measured by the polymerase chain reaction (PCR). It was found that the IC50 decreased between 5 and 7 times with the use of MNP. In PCR tests, the expressions of apoptotic genes increased, while the expressions of MDR1 and anti-apoptotic genes were decreased in the use of MNP. Apoptosis was found to be increased in flow cytometry measurements. The use of MNP systems has reduced drug resistance since it provides controlled release of the drug and prevents its exit from the cell due to its structure.

Keywords: Acute promyelocytic leukemia, glutaraldehyde, HL-60 cell line, ıdarubicin, magnetic nanoparticles.

Glutaraldehit kaplı manyetik nanopartiküle idarubisin tutturulması ve HL-60 hücre hattında etkisinin incelenmesi

ÖZ

İdarubisin, meme kanseri ve akut lösemi tedavisinde sıklıkla kullanılan kemoterapötik bir ilaçtır. Bu çalışmada, yüksek stabilite ve düşük toksisiteye sahip bir ilaç hazırlamak için idarubisini glutaraldehit (GA) kaplı manyetik nanopartiküllere (MNP-GA) immobilize edilmesi amaçlanmıştır. Manyetik nanopartiküller kolay sentez edilmesi, düşük maliyetli olması ve toksik olmamasından dolayı tercih edilmiştir. Çalışmada magnetit (Fe3O4) nanoparçacıkları hazırlanmış, glutaraldehit ile kaplanmış, Fourier transform kızılötesi spektroskopisi, X-ışını kırınım deseni ve Konvansiyonel transmisyon elektron mikroskobu yöntemleri ile karakterizasyon işlemleri yapılmış ve idarubisin bağlanmıştır. İdarubisine bağlı MNP-GA ve serbest idarubisinin HL-60 hücre hatları üzerindeki sitotoksik etkileri MTT ve ATP testleri ile belirlendi ve IC50 değerleri hesaplandı. Apoptoz durumu flow sitometrisi ile değerlendirildi ve MDR1, Puma, NOXA, BAX, Survivin ve BCL-2 genlerinin ekspresyonu polimeraz zincir reaksiyonu (PCR) yöntemi ile ölçüldü. MNP kullanımı ile IC50'nin 5 ile 7 kat arasında azaldığı tespit edilmiştir. PCR testlerinde apoptotik genlerin ekspresyonları artarken, MNP kullanımında MDR1 ve anti-apoptotik genlerin ekspresyonları azaldı. Akım sitometri ölçümlerinde apoptoz artışı saptandı. MNP sistemlerinin kullanımı, ilacın kontrollü salınımını sağladığı ve yapısı gereği hücreden çıkışını engellediği için ilaç direncini azaltmıştır.

Anahtar Kelimeler: Akut promyelositik lösemi, glutaraldehit, HL-60 hücre hattı, idarubisin, manyetik nanopartiküller.

DOI: http://dx.doi.org/10.32571/ijct.1194667 E-ISSN: 2602-277X

1. INTRODUCTION

In recent years, magnetic nanoparticles have significant great attention due to their critical applications in catalysis, biocatalysis, biomedicine, biosensor, bio-separation, and magnetic resonance imaging contrast enhancement.[1-3] Magnetic nanoparticles (MNPs) are attractive supports for these areas because of their high surface area/volume ratio and ease of preparation. Magnetic nanoparticles have enormous advantages because they can be easily separated from the reaction medium due to their magnetic properties and are homogeneously dispersed in the solution. In addition, changing the surfaces and polarities of MNPs with chemicals increases their resistance to solutions. Surface modification can be carried out by numerous methods, such as hydrolysis techniques, surfactant-free sonochemical reactions, and sol-gel methods.[4-6] During or following their syntheses, coating agents such as oleic acid, epoxy-thiol group, chitosan, and polymers are used for surface modification.[7-10] In particular, aldehyde groups are used as a binding agent to bind the biomolecule to the support in immobilization applications. Aldehydes are biocompatible molecules and form Schiff bases by binding to amine groups over a wide pH range.

Cancer is defined as reducing or damaging cellular control and normal maturation mechanisms. Its characteristics include heavy cell growth and the ability to spread and metastasize to undifferentiated cells and tissues and adjacent tissues.[11] Cancer-related deaths are the second most common disease after cardiovascular diseases globally and in our country in the last 20 years.[12] It is a social problem due to its high prevalence and high risk of death. Many methods, such as surgery, chemotherapy, immunotherapy, hormone therapy, cell transport therapy, and radiation therapy, are used in cancer treatment, and chemotherapy is one of them.[12]

Anthracyclines are among the most effective anticancer drugs ever developed. Anthracycline's cytotoxicity is generally due to its ability to diffuse across the cell membrane, intercalate between DNA base pairs, and target topoisomerase II.[13] Doxorubicin is one of the earliest anthracyclines and is widely used to treat leukemia, bladder, Hodgkin's lymphoma, and breast cancers. Idarubicin (IDA) is a synthetic analog of daunorubicin and is often used to treat acute promyelocytic leukemia, acute myeloid leukemia, and chronic lymphocytic leukemia. The absence of the methoxy group in the structure of IDA significantly increases lipophilicity, which accelerates cellular uptake and provides higher DNA binding capacity.[14]

Traditional chemotherapy is still questioned due to the lack of therapeutic agents at the tumor site, the inadequacy of chemotherapeutic drugs in aqueous media, rapid clearance, and the lack of cancerous site-selective drugs.[15] The nanoparticle-supported drug is one of the methods that can use as an alternative to chemotherapy. The primary purpose of this method is to increase the effectiveness of chemotherapeutic drugs and minimize the interaction with healthy cells and the side effects of these drugs.

The basic properties of nanoparticles in biotechnology are their nanoscale structure, magnetic properties, and ability to transport active biomolecules in specific tasks. A magnetic nanoparticle consists of a magnetic core, a protective layer, and an organic crosslinking.[16] Glutaraldehyde is the most practical and widely used cross-linker in nanoparticle studies.[17] Sahin et al. attached glutaraldehyde to polyvinyl alcohol-coated MNPs.[18] Zhao et al. bound albumin to amino acid-coated MNPs with the help of glutaraldehyde.[19] In cases where the magnetic nanoparticle is covered with a protective coating material, and an intermediate arm is attached, the particle size becomes larger than desired. So, it makes MNP challenging to enter the cell. In this study, we used glutaraldehyde directly, as a protective coating and cross-linker, without using a protective layer. In this way, the design of nanoparticles has been reduced one step, and the cost has also decreased. The use of glutaraldehyde as a cross-linker and a coating material was applied for the first time in our study. In this respect, our work has been innovative and original, and it is different from other publications using glutaraldehyde-coated nanoparticles.

For this purpose, in this research, magnetite (Fe_3O_4) magnetic nanoparticles were synthesized and coated with glutaraldehyde and finally, IDA was bound. The cytotoxic effect of this complex was investigated on acute promyelocytic leukemia (HL-60) cell line by cell viability analysis. At IC_{50} concentrations, apoptosis status was evaluated by flow cytometry, and expression of MDR1, Puma, NOXA, BAX, Survivin, and BCL-2 genes was measured by polymerase chain reaction (PCR) method.

2. MATERIALS AND METHODS

2.1. Reagents and chemicals

Ferrous sulfate ($FeSO_4.7H_2O$, >99%), ferric chloride ($FeCl_3 \cdot 6H_2O$, 97%), glutaraldehyde, dimethyl sulfoxide (DMSO), sodium hydroxide, and phosphate buffer saline (PBS) were purchased from Sigma-Aldrich. All materials were used without further purification. Gaziantep University Medical Biochemistry Department provided an HL-60 cell line. RPMI 1640 medium and fetal bovine serum were purchased from Capricorn. The spectroscopic techniques listed below characterized the magnetic nanoparticles and compared them with the reported characterizations of similar compounds. Fourier transform infrared spectra of materials were recorded

DOI: http://dx.doi.org/10.32571/ijct.1194667 E-ISSN: 2602-277X

on a Thermo Fourier transform infrared spectroscopy (FT-IR) spectrophotometer; Smart ITR diamond attenuated total reflection (ATR). Elemental analyses (C, N, H) were recorded on a Thermo Scientific Flash 2000, CHNS elemental analyses apparatus. Electronic spectra were obtained on a Perkin Elmer Lambda 25 UV spectrometer. Conventional transmission electron microscopy (C-TEM) spectra were recorded on FEI Tecnai G^2 Spirit BioTwin CTEM, 20-120 kv (contrast transmission electron microscopy). X-ray diffraction (XRD) patterns were recorded on Rigaku Miniflex CuKα, λ=0.154nm.

2.2. Synthesis of magnetic nanoparticles

Glutaraldehyde-coated magnetic nanoparticles were prepared according to co-precipitation method prepared.[7] Briefly, a solution of $FeSO_4.H_2O$ (1.25 g, 7.33 mmol) and $FeCl_3.6H_2O$ (2.34 g, 8.6 mmol) in 100 mL of water at 90 ºC was stirred with a mechanic stirrer for 30 minutes. Next, 12 mL of 0.1 M NaOH solution was added to this solution dropwise at a vigorous stirrer under N_2 atmosphere, and black magnetic nanoparticles were precipitated. Finally, 12 mL of 0.3 M NaOH solution was added to the mixture, and precipitation was finished. It remained under this condition for 30 minutes and turned reddish-brown. It was allowed to cool to room temperature, and the MNPs were washed several times with deionized water until pH reached 7. FT-IR, XRD, and C-TEM characterization analyzes were performed.

2.3. The coating of magnetic nanoparticles by glutaraldehyde

For surface coating and modification with glutaraldehyde, 1.0 g of MNPs was suspended in 100 mL of distilled water by ultrasonication for 30 minutes.[20] Next, 5 g of glutaraldehyde solution (25%, 12.5 mmol the glutaraldehyde/MNP ratio used was determined from the amount of MNP remaining in the water. Glutaraldehyde was added so that as little MNP as possible remained in the water phase.) was added to this mixture under vigorous mechanical stirring. The mixture was stirred and ultrasonicated for 2 hours at room temperature. Over time, a brown foam phase appeared on the mixture. The obtained glutaraldehyde-coated magnetic nanoparticles (MNP-GA) were washed with distilled water and acetone and then dried in an oven at 50 °C. FT-IR, XRD and C-TEM characterization analyzes of these materials were performed.

2.4. Idarubicin immobilization

Prepared MNP-GA material was weighed per well with the final concentration of 2 mg/mL and added to a 24-well plate. IDA solutions have dissolved in DMSO at different concentrations (10.0; 5.0; 1.0; 0.5; 0.1 and 0.01 µM). Samples for each concentration were prepared in triplicate, and the results were averaged. Besides, only MNP-GA and PBS were placed in three wells to observe the toxic effect of synthesized supports. Initially, the absorbance of each IDA solution was measured at a wavelength of 412 nm in a UV-Vis Spectrophotometer (BioTek, Synergy H1 microplate reader) to calculate the percent IDA retention. The prepared plates were mixed horizontally at 600 rpm for 24 hours. After 24 hours, unbound IDA was separated by magnetic decantation, absorbance was measured at 412 nm wavelength, and the percent retention of IDA was calculated. Finally, it was washed two times with PBS solution to remove impurities of usable purity in the cell culture.

2.5. Investigation of cytotoxic effect of MNP-GA-IDA complex on HL60 cell Line

Firstly, the cell number was optimized according to the cells' incubation time and proliferation potential. 1000 µL of HL60 cell suspension was added to the MNP-GA-IDA complex prepared with $1.0\text{-}1.5*10^5$ cells per well.

To compare the prepared drug with free IDA, 900 µL HL60 cell suspensions were added to 24-well microplates with $1.0\text{-}1.5*10^5$ cells per well. 100 µL of IDA was added to the cell suspensions at a final concentration of 10.0; 5.0; 1.0; 0.5; 0.1 and 0.01 µM. Each prepared sample was applied in 3 replicates. In addition, the only cell suspension was added to three wells as the negative control, and MNP-GA without IDA was added to investigate the toxic effect of MNP-GA. Three plates were prepared for the incubation period of 24, 48, and 72 hours. The same procedure was performed twice, one for MTT cytotoxicity analysis and the other for ATP cell viability assay analysis.

2.6. MTT cytotoxicity analysis

MTT viability assay was used to determine cell viability in HL-60 cells. Prepared plates were incubated at 37 °C for 24, 48, and 72 hours in a carbon dioxide incubator. After incubation, 5 mg/mL MTT solution was added to all wells and incubated for 4 hours. Then, the cell culture medium in the wells was carefully removed and 1000 µL of DMSO was added to each well and mixed for 10 minutes to dissolve the violet crystals.

The intensity of the purple color formed during MTT analysis is directly related to cell viability. The absorbance of the plates was measured using a plate reader set to 570 nm. The viability of the cells used as a negative control was considered 100 % and the percentage of viability of the drug-treated cells was

DOI: http://dx.doi.org/10.32571/ijct.1194667 E-ISSN: 2602-277X

calculated. Consequently, the IC_{50} concentration was calculated from the concentration-dependent curve of cell proliferation.

2.7. ATP cell viability analysis

The CellTiter-Glo Luminescent Cell Viability Assay was utilized to determine cell viability in HL-60 cells. Cells were treated with different concentrations of MNP-GA-IDA complex and free IDA. After 24 h, 48 h, and 72 h incubation at 37 °C, 100 µL of assay reagent was added to each well. It was incubated on an orbital shaker for 2 minutes to induce cell lysis. The luminescent signals were determined by a luminometer (Synergy H1 Multi-Mode Reader, BioTek Instruments; Winooski, VT, USA). IC_{50} values of incubation times (24, 48, and 72 h) were calculated separately for complex and free IDA. All experiments were repeated three times.

2.8. Determination of apoptotic cells by flow cytometry method

Annexin V is a member of the annexin family of intracellular proteins that bind to phosphatidylserine (PS) in a calcium-dependent manner. PS is typically found in the portions of the plasma membrane facing the cytoplasm- in healthy cells. However, during early apoptosis, the membrane asymmetry is lost, and PS migrates to the outer portions. The fluorochrome-labeled Annexin V can then target and identify apoptotic cells specifically. IC_{50} values obtained from MTT and ATP cytotoxicity tests were used to measure the level of apoptosis. Commercial Annexin V Apoptosis Kit (Biolegend 640932, USA) containing Annexin V and Propidium Iodide (PI) dyes was used to detect apoptosis for MNP-GA-IDA and free IDA.

2.9. Measuring gene expressions

In this study, to examine the effect of magnetic nanoparticles, the expressions of multidrug resistance 1 gene (MDR1), the expressions of apoptotic (Puma, NOXA, and BAX) and anti-apoptotic (Survivin and BCL-2) genes, and β-actin gene as control were measured by PCR method.

Solutions corresponding to the IC_{50} values found in MTT and ATP cytotoxicity tests for MNP-GA-IDA and free IDA were prepared and added to the wells to measure gene expressions. $1x10^5$ cells of HL-60 were added to each well and subjected to incubation times of 24, 48, and 72 hours. At the end of the incubation period, the liquid portion of each well was removed and centrifuged at 10000 g for 15 minutes. Then, RNA isolation (Macharey-Nagel NucleoSpin®RNA, 740955.50, Germany), cDNA synthesis from mRNA (Thermo Fischer Scientific, High-Capacity cDNA Reverse Transcription Kit, Cat No: 4374966, USA), and measurement of gene expressions (Go Taq qPCR ® Master Mix, ProMega, USA) by Real-Time PCR (QIAGEN, Germany) was performed according to commercial kit protocols.

3. RESULTS AND DISCUSSION

3.1. Characterization of modified magnetic nanoparticles

Various solvents such as water, ethanol, methanol, and acetone were tried as solvents during the coating of MNPs with glutaraldehyde. However, when organic solvents were used, it was observed that the glutaraldehyde coating was less than water and could not be identified in the characterization. On the other hand, in the experiments where water was used as a solvent, it was observed that the coating was achieved when the foam formed on the surface of the mixture was separated and analyzed after a while.

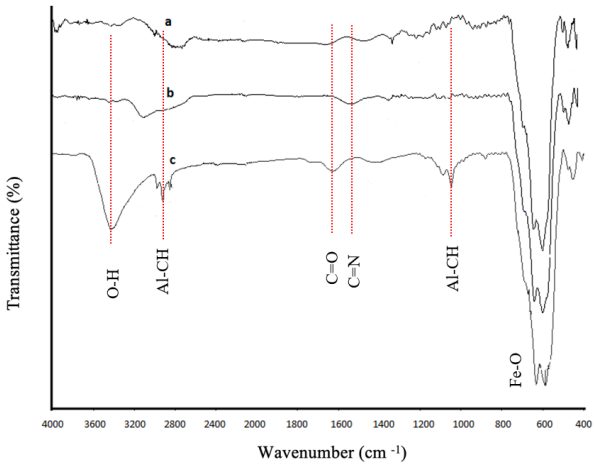

Figure 1. FT-IR spectra of (a): MNPs, (b): MNP-GA, and (c): MNP-GA-IDA.

The characterization of magnetic nanomaterials was verified by FT-IR, C-TEM), XRD, ICP-OES, and UV-Vis. Figure 1 shows the FT-IR spectra of MNPs (a), MNP-GA (b), and MNP-GA-IDA (c). The characteristic peak for Fe-O was observed at 541 cm^{-1} for two materials. A strong O-H band about 3400-3450 cm^{-1} was observed in both MNP-GA and MNP-GA-IDA, indicating that –OH groups cover the surface of Fe_3O_4 nanoparticles. The intensity of this bond increased after immobilization due to the presence of –OH groups in hemoglobin. C-H aliphatic bands of IDA were observed at 2900 and 1051 cm^{-1}. The peaks observed at 1633 cm^{-1} indicate the presence of C=O bands of the aldehyde group of IDA and glutaraldehyde. C=N band observed at 1524 cm^{-1} refers to the Schiff base formed between hemoglobin and MNP-GA.[9]

DOI: http://dx.doi.org/10.32571/ijct.1194667 E-ISSN: 2602-277X

Figure 2 shows the XRD patterns of MNPs (a) and MNP-GA (b) nanocomposites. Fe_3O_4 characteristic peaks were observed for both samples with the indices ((220), (311), (400), (422), (511), and (440)). These peaks refer to spinel structure (JCPDS card number is 65-3107). The primary diameter of the magnetic nanoparticles was calculated as 20 nm and 24.8 nm for MNPs and MNP-GA, respectively, using the peak of (311) from the Scherrer formula. These data show that the surface modification did not change the crystal structure and size of Fe_3O_4, suggesting that the immobilization occurred only on the particle surface.

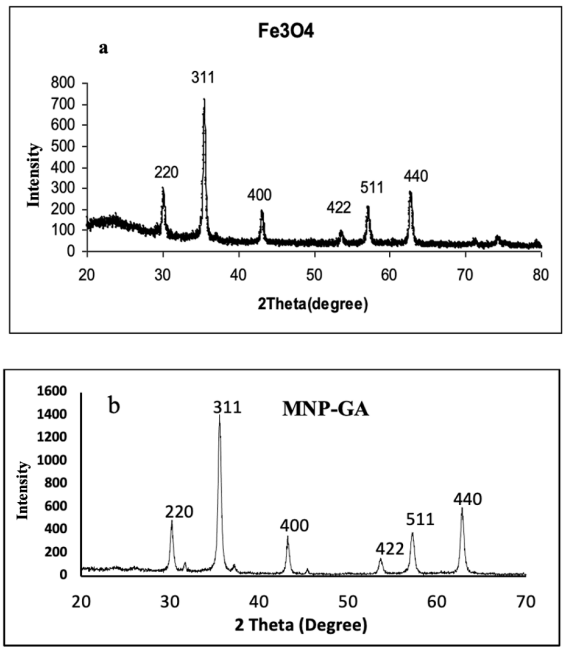

Figure 2. XRD spectra of (a): Magnetic Nanoparticles, (b): Magnetic Nanoparticles-Glutaraldehyde.

Contrast transmission electron microscopy images of MNP, MNP-GA, and MNP-GA-IDA are shown in Figure 3. The dark black colored spots in the middle indicated the magnetic nanoparticles, and the lighter outer image indicated the coated organic material. Most nanoparticles are spherical, and the average particle size was calculated as 21.0±2.5 nm (200 counted particles), 23.8±3.1 nm (364 counted particles), and 30.8±6.0 (172 counted particles) for MNPs, MNP-GA, MNP-GA-IDA, respectively. It is clear that MNP-GA does not agglomerate and is well-dispersed, meaning that the glutaraldehyde coating prevents the agglomeration of particles. The C-TEM image of MNP-GA-IDA shows that the coating thickness is 2-6 nm, and there are two layers on the surface of spherical-shaped magnetic nanoparticles. The first of these layers is glutaraldehyde, while the other layer shows IDA. When the MNP-GA and MNP-GA-IDA images are compared, surface difference is remarkable. It can be seen from the C-TEM images that the IDA is attached to the support material. It was observed that the agglomeration amount of the particles increased after the IDA coating. According to all analysis results, it was understood that MNP was synthesized correctly and in desired sizes.

Table 1. Atomic composition of nanomaterials.

Material	Fe %	O %	C %	% N
MNP	72.36	27.64	-	-
MNP-GA	69.42	25.92	1.96	-
MNP-GA-IDA	66.32	27.84	3.27	2.57

C: Carbon, Fe: Iron, GA: Glutaraldehyde, IDA: Idarubicin, MNP: Magnetic nanoparticles, N: Nitrogen, O: Oxygen,

The atomic composition of the prepared nanomaterials is given in Table 1. According to the ICP-OES results, the amount of Fe atoms in MNP-GA-IDA decreases compared to MNPs while the amount of C atoms increases. Although MNP and MNP-GA materials do not contain nitrogen atoms, MNP-GA-IDA obtained by binding IDA is expected to contain nitrogen. Energy-dispersive X-ray spectroscopy analysis showed that the nitrogen content was 2.57%. The increase in carbon and nitrogen amounts when the iron level decreases indicate that glutaraldehyde is coated on the MNP surface, and IDA is immobilized to MNP-GA.

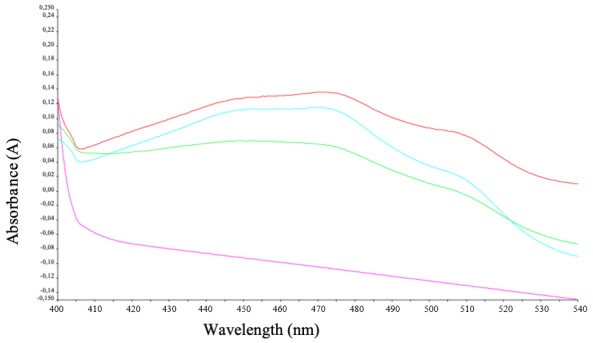

Figure 4. UV-Vis spectra of IDA. Red peak freshly prepared idarubicin solution, the blue curve is MNP-free IDA solution prepared in PBS and subjected to the same procedures as in the idarubicin binding assays, green curve remaining solution from MNP-GA binding and the purple curve represents the absorption spectra of the PBS solution.

The UV-Vis spectrum is shown in Figure 4. Red peak freshly prepared IDA solution, the blue curve is MNP-free IDA solution prepared in PBS and subjected to the same procedures as in the IDA binding assays, the green curve remaining solution from MNP-GA binding, and the purple curve represents the absorption spectra of the PBS solution. When the spectra were compared, IDA alone degraded at room temperature as expected. The decrease in peak intensity indicates the immobilization of IDA to MNP-GA. Two characteristic peaks appear at 447 nm and 471 nm from the UV-Vis spectrum of MNP-GA-IDA,

DOI: http://dx.doi.org/10.32571/ijct.1194667 E-ISSN: 2602-277X

indicating that IDA retains its structure after immobilization. The wavelength at which substances absorb is in the blue region. The complementary color of blue is orange. The color of the idarubicin solution is also orange. In this region, n-π* and π-π transitions are seen. These transitions are due to the benzene ring in idarubicin.[21] Evidence of the stability of the glutaraldehyde-coated MNP material is given in Figure 4. Accordingly, the absence of peaks of pure GA in the presence of MNP-GA indicates that GA remains on the MNP surface.[22]

Coating with glutaraldehyde was performed to maintain the magnetic nanoparticles' stability, prevent agglomeration and bind the drug. Glutaraldehyde is an aldehyde containing a carbonyl group at both ends. This way, one terminal can be connected to the magnetic nanoparticle, while the other terminal can be connected to IDA by forming a Schiff base. C-TEM images show that agglomeration is low, and aspherical grain structure is formed (Figure 3).

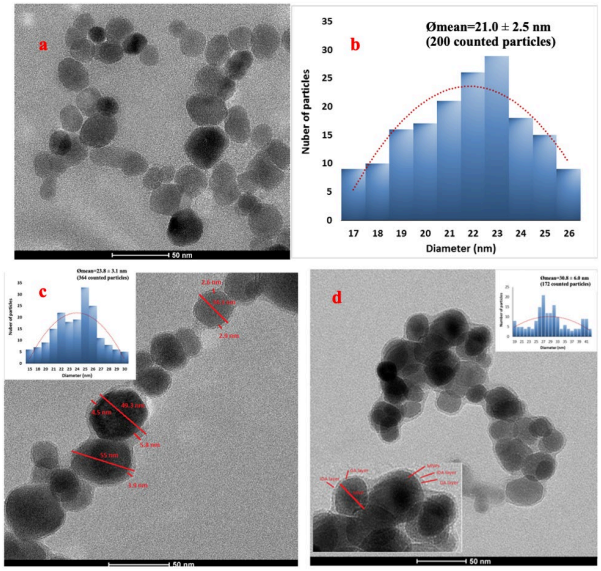

Figure 3. (a): C-TEM image of MNPS, (b): particle size distribution of MNPs, (c): C-TEM image and particle size distribution of MNP-GA, and (d): C-TEM image and particle size distribution of MNP-GA-IDA.

IDA was attached to the magnetic nanoparticles for which characterization processes were performed. IDA-linked constructs were checked by FT-IR analysis. The characteristic C=N stretching peaks seen in the FT-IR spectrum indicate binding of the IDA (Figure 1).

3.2. Cytotoxicity analysis findings

MTT assay was performed to determine the cytotoxic effects of different concentrations of free IDA and MNP-GA-IDA on the HL60 acute promyelocytic leukemia cell line. From the concentration-dependent cell proliferation curve, the concentration at which 50% of the cells were viable (IC_{50}) was calculated from the data obtained from the MTT assay. Living cells reduce tetrazolium to purple-colored formazan crystals by mitochondrial reductase activity. First, DMSO is added to dissolve the formazan crystals in the reaction medium, and then the viability analysis is completed by measuring the optical density of the chromogen at 570 nm. According to the result obtained from the analysis, a positive correlation was observed between the amount of absorbance and the number of viable cells. The IC_{50} values of both the IDA and MNP-GA-IDA complex calculated at 24, 48 and 72 hours from the MTT test are given in Table 2.

Table 2. IC_{50} values of MNP-GA-IDA and free idarubicin in the HL-60 cell line

		IC_{50} (µM)		
		24 h (mean ± SD)	48 h (mean ± SD)	72 h (mean ± SD)
IDA	MTT	3,106 ± 0.179	0,834 ± 0.061	0,319 ± 0.035
	ATP	3,303 ± 0.148	0,819 ± 0.015	0,298 ± 0.059
MNP-GA-IDA	MTT	0,439 ± 0.054	0,094 ± 0.012	0,076 ± 0.010
	ATP	0,441 ± 0.057	0,098 ± 0.019	0,068 ± 0.007

GA: Glutaraldehyde, IDA: Idarubicin, MNP: Magnetic nanoparticles

The basic principle of luminescence ATP cell viability test; recombinant luciferase enzyme oxidizes luciferin to oxyluciferin in the presence of ATP and molecular oxygen. At the same time, the luminescence radiation level and the amount of ATP are parallel. Therefore, as cytotoxicity increases in the ATP cell viability test, the luminescent radiation decreases, and the measured optical density decreases. The luminescence ATP cell viability assay was used to calculate the concentration (IC_{50}) at which 50% of the cells were viable from the concentration-dependent cell proliferation curve. The IC_{50} values of both the IDA and MNP-GA-IDA complex calculated at 24, 48 and 72 hours from the ATP test are given in Table 2. When the results were examined, it was determined that the IC_{50} values in the MNP-GA-IDA complex were between 5 and 8 times lower than in the free IDA application.

3.3. Apoptosis findings

Apoptotic cells are divided into early and late apoptotic cells. In cases where the cell membrane remains intact and only PS is released, it is classified as an early apoptotic cell, and when the plasma membrane becomes permeable, it is classified as a late apoptotic cell, known as secondary necrotic. The direct exposure of healthy living cells to trauma, such as extreme heat, mechanical and chemical attacks, and exposure to excessive toxic drugs, cause necrotic cell formation as the membrane completely breaks down.[23] A flow cytometry device determined apoptosis status for MNP-GA-IDA and free IDA. In Figure 5, the LL region represents viable cells, the UL and UR regions represent apoptotic cells, and the LR region represents necrotic cells. In the development of an effective drug, the cells should be recruited at

DOI: http://dx.doi.org/10.32571/ijct.1194667 E-ISSN: 2602-277X

apoptotic sites. When Figure 5 is examined, it is seen that the control cells are mostly alive. When the MNP-GA-IDA complex is applied, the cells begin to accumulate in the apoptotic regions, and the cells do not go into necrosis. This shows that the MNP-GA-IDA complex kills cells not by necrotizing but by stimulating the apoptotic pathway.

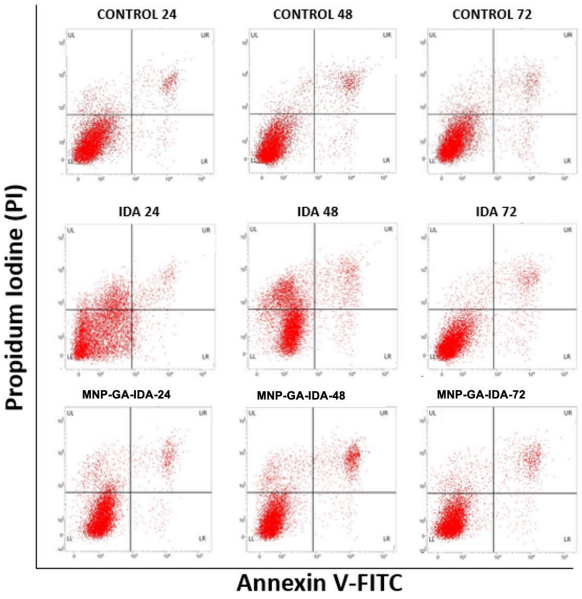

Figure 5. Apoptosis findings of control, idarubicin and Magnetic Nanoparticles-Glutaraldehyde-idarubicin (LL: Live cell, UL: Early apoptotic cell, UR: Late apoptotic cell, LR: Necrotic cell).

3.4. Gene Expressions Findings

To examine changes in cell apoptosis, the expressions of multidrug resistance 1 gene (MDR1) in HL-60 cell line, apoptotic (Puma, NOXA, and BAX) and anti-apoptotic (Survivin and BCL-2) genes, and β-actin gene as control were measured. Gene expressions were analyzed in duplicate and averaged.

$2^{-\Delta\Delta Ct}$ (coefficient of variation relative to control gene) values for each gene are given in Table 3. Expressions of genes belonging to the control group were accepted as 1. Expressions of genes belonging to MNP-GA-IDA and free IDA groups were given compared to the control group. When the results are examined, it is seen that while the expressions of apoptotic genes increase, the expressions of anti-apoptotic genes decrease in MNP-GA-IDA application. It is also seen that MDR1 expressions are severely decreased. In particular, a 6- and 10-fold increase was observed in apoptotic NOXA gene expressions at the end of 48 and 72 hours, while there was a decrease of more than 50% in the expressions of anti-apoptotic and MDR1 genes. These results show that the drug administered with the nanoparticle complex kills cancerous cells at lower doses by increasing cell apoptosis and reducing multidrug resistance.

In this study, magnetic nanoparticles were used to prevent the development of multidrug resistance and reduce the toxic effect of IDA on healthy tissues by reducing the effective dose.

The cytotoxic effects of magnetic nanoparticles loaded with IDA on the HL-60 cell line were investigated. When the results obtained from MTT and ATP cytotoxicity tests are examined (Table 2), it is seen that the IC_{50} values in the IDA immobilized MNP-GA structure is decreased compared to pure IDA. A decrease in the effective dose (IC_{50}) indicates an increase in the cytotoxic effect. These results show that the synthesized IDA-loaded magnetic nanoparticles increased the cytotoxic effect. The primary purpose of this study was to give the patient a lower concentration that would have the same effect due to the toxic effects of the drug given during chemotherapy. There may be many reasons for the decrease in the effective dose of the drug. These; maybe because the magnetic nanoparticle facilitated the drug uptake into the cell, increased the stability of the drug, increased the half-life with the gradual release of the drug, and decreased drug resistance. There are no magnetic nanoparticle studies in the literature to reduce the effective dose of IDA in the HL-60 cell line. When studies with different drugs or cells are examined, Gunduz et al. attached IDA to nanoparticles coated with polyethylene glycol. They found IC_{50} values two times lower than free IDA in the MCF-7 cell line.[15]

Our study found that MDR1 gene expressions in the MNP-GA-IDA system were decreased compared to the free IDA molecule. Thus the drug resistance in the cell decreased, and the drug became more effective than the free IDA molecule. In their study, Cheng et al. found that drug resistance decreased in the use of drugs loaded with magnetic nanoparticles in resistant K562 cells.[24] In addition, Zhao et al. found that the using magnetic chitosan nanoparticles in glioblastoma cell lines downregulated MDR1 gene expressions.[25]

On the other hand, magnetic nanoparticles enter the cell by endocytosis due to their size.[26] Gupta et al. stated that the ideal particle size for drug delivery should be between 10-100 nm. In this way, the drug will be freed from being catabolized by the reticuloendothelial system (RES).[27] In the XRD and C-TEM analyses performed in this study, particle sizes were smaller than 50 nm. In this way, our drug-loaded magnetic nanoparticles can remain in the cell. Furthermore, nanoparticles entering the cell provide a gradual release of the drug. In this way, it is ensured that the drug has a continuous cytotoxic effect in the cell. Furthermore, as the gradual release of the drug by the MNP enables the drug to get rid of P-

DOI: http://dx.doi.org/10.32571/ijct.1194667 E-ISSN: 2602-277X

glycoprotein-mediated drug pumps, drug resistance in the cell also decreases.[26]

Table 3. $2^{-\Delta\Delta Ct}$ values of genes.

		PUMA (mean ± SD)	BAX (mean ± SD)	NOXA (mean ± SD)	Survivin (mean ± SD)	BCL-2 (mean ± SD)	MDR1 (mean ± SD)
Control	24h	1,00	1,00	1,00	1,00	1,00	1,00
	48h	1,00	1,00	1,00	1,00	1,00	1,00
	72h	1,00	1,00	1,00	1,00	1,00	1,00
IDA	24h	0,80 ± 0,10	0,99 ± 0,11	1,34 ± 0,21	0,91 ± 0,08	0,53 ± 0,10	0,81 ± 0,08
	48h	0,89 ± 0,09	3,23 ± 0,45	1,92 ± 0,18	0,90 ± 0,14	0,75 ± 0,09	0,61 ± 0,03
	72h	1,32 ± 0,08	2,09 ± 0,18	2,07 ± 0,24	0,95 ± 0,11	0,74 ± 0,05	0,71 ± 0,06
MNP-GA-IDA	24h	1,93 ± 0,32	1,15 ± 0,09	2,88 ± 0,46	0,56 ± 0,07	0,65 ± 0,08	0,62 ± 0,04
	48h	1,46 ± 0,22	2,22 ± 0,31	6,08 ± 0,54	0,55 ± 0,08	0,92 ± 0,12	0,55 ± 0,08
	72h	1,39 ± 0,24	4,48 ± 0,72	10,85 ± 1,23	0,51 ± 0,04	0,61 ± 0,06	0,41 ± 0,06

GA: Glutaraldehyde, IDA: Idarubicin, MNP: Magnetic nanoparticles,

When the multi-drug resistance gene expressions are examined (Table 3), it is seen that the expressions in MNP structures are decreased compared to the control cells. These findings support the cytotoxicity findings and show that IDA-loaded MNP structures reduce drug resistance. Decreased drug resistance allows the drug to act at lower concentrations.

One of the reasons for the development of drug resistance is the disruption of the apoptosis mechanism. Apoptosis is regular and tightly controlled programmed cell death. The molecular mechanism of drug-induced apoptosis is associated with a mitochondrial dysfunction characterized by increased mitochondrial membrane permeability and the release of cytochrome C from the mitochondria.[28] When the expressions of apoptotic and anti-apoptotic genes were examined, it was found that the expressions of apoptotic genes increased, and the expressions of anti-apoptotic genes decreased (Table 3).

When the flow cytometry results were examined (Figure 5), it was observed that MNP-GA loaded with IDA did not lead to necrosis of the cells in 24, 48, and 72 hours incubations. Our results show that our MNP systems do not cause necrotic effects. Therefore, it is desired that the drug selected as a cancer drug has an apoptotic effect on the cell. Especially drugs that lead the cell to late apoptosis are preferred because they kill the cell gradually.

In summary, our results show that the use of nanoparticle structure significantly reduces the effective dose of the drug. It was seen that the MNP-GA-IDA structure was most effective at the 72nd hour, according to all results. Further, it was observed that the expressions of MDR1 and anti-apoptotic genes decreased, and the expressions of apoptotic genes increased despite the use of lower doses of drugs. In addition, it was seen from the Annexin V results that the MNP structure was not necrotic. Therefore, reducing the drug dose will reduce the patient's drug exposure, thus reducing the side effects. In addition, reducing the use of drugs will provide significant economic savings.

Considering all these results, it is seen that MNP drug delivery systems have many advantages over free drugs. These; (i) Free drugs between 10-100 nm are eliminated and excreted due to their small size, while drug-loaded MNPs can remain in circulation due to their size around 20-50 nm,[29] (ii) since drug-loaded MNP has lower IC_{50} values than free drug, side effects may decrease[29] (iii) drug-loaded MNPs can quickly enter vessels and are easily targeted to cancer cells[30] (iv) since drugs bind to MNPs, they are less affected by environmental conditions and have higher stability than free drug.[30]

4. CONCLUSIONS

In the present research, idarubicin was successfully immobilized after Fe_3O_4 magnetic nanoparticles were prepared using the precipitation method, and then coated with glutaraldehyde. It is clear that the nanoparticle has been synthesized and has the desired dimensions from the FT-IR, XRD, and C-TEM testing results. The MNP-GA-IDA complex was administered to HL-60 cells, and the change in cytotoxicity against free idarubicin was measured using MTT and ATP assays. Idarubicin complexed with the nanoparticle had 5 to 7 times lower IC50 values. Furthermore, it was demonstrated that the MNP-GA-IDA complex increased the expression of

DOI: http://dx.doi.org/10.32571/ijct.1194667 E-ISSN: 2602-277X

apoptotic genes compared to free idarubicin and decreased the expressions of anti-apoptotic genes and the MDR1 gene. Consequently, it has been ascertained that the utilization of MNP systems decreases the effective dose of the drug, stimulates apoptosis, and reduces the prevalence of resistance to multiple drugs. Since our study is the first magnetic nanoparticle study to reduce the effective dose of IDA in the HL-60 cell line and the first study to directly link drugs with GA, a cross-linker, without using any organic preservatives, it will be a reference and guide for future research.

ACKNOWLEDGEMENTS

Dr. Hasan Ulusal has received research grants from the Scientific and Technological Research Council of Türkiye (TÜBİTAK) (BIDEB 2211-E domestic graduate scholarship program). Dr. Fatma Ulusal has received research grants from TÜBİTAK (BIDEB 2218 postdoctoral research fellowship program). This study was funded by the Management Unit of Scientific Research Projects of Gaziantep University (BAP project no: TF.DT.19.54 and TF.19.52). These are gratefully acknowledged.

Conflict of interests

The authors declare that there is no conflict of interest.

REFERENCES

1. 26. Chawla, S.; Pundir, C. S. *Biosens Bioelectron* **2011,** *26* (8), 3438-3443.
2. Luo, S.; Zheng, X.; Xu, H.; Mi, X.; Zhang, L.; Cheng, J.-P. *Adv Synth Catal* **2007,** *349* (16), 2431-2434.
3. Zheng, M.; Zhang, S.; Ma, G.; Wang, P. *J Biotechnol* **2011,** *154* (4), 274-280.
4. Ghanbari, D.; Salavati-Niasari, M.; Ghasemi-Kooch, M. *J Ind Eng Chem* **2014,** *20* (6), 3970-3974.
5. Lu, Y.; Yin, Y.; Mayers, B. T.; Xia, Y. *Nano Lett* **2002,** *2* (3), 183-186.
6. Waseem, M.; Munsif, S.; Rashid, U.; Imad ud, D. *Appl Nanosci* **2014,** *4* (5), 643-648.
7. Jadhav, N. V.; Prasad, A. I.; Kumar, A.; Mishra, R.; Dhara, S.; Babu, K. R.; Prajapat, C. L.; Misra, N. L.; Ningthoujam, R. S.; Pandey, B. N.; Vatsa, R. K. *Colloids Surf B Biointerfaces* **2013,** *108*, 158-168.
8. Mahmood, I.; Ahmad, I.; Chen, G.; Huizhou, L. *Biochem Eng J* **2013,** *73*, 72-79.
9. Tang, T.; Fan, H.; Ai, S.; Han, R.; Qiu, Y. *Chemosphere* **2011,** *83* (3), 255-264.
10. Zhou, H.; Li, W.; Shou, Q.; Gao, H.; Xu, P.; Deng, F.; Liu, H. *Chinese J Chem Eng* **2012,** *20* (1), 146-151.
11. Lubbe, A. S.; Alexiou, C.; Bergemann, C. *J Surg Res* **2001,** *95* (2), 200-6.
12. Ferlay, J.; Soerjomataram, I.; Dikshit, R.; Eser, S.; Mathers, C.; Rebelo, M.; Parkin, D. M.; Forman, D.; Bray, F. *Int J Cancer* **2015,** *136* (5), E359-86.
13. Ma, P.; Dong, X.; Swadley, C. L.; Gupte, A.; Leggas, M.; Ledebur, H. C.; Mumper, R. J. *J Biomed Nanotechnol* **2009,** *5* (2), 151-61.
14. Ma, P.; Mumper, R. J. *Nano Today* **2013,** *8* (3), 313-331.
15. Gunduz, U.; Keskin, T.; Tansik, G.; Mutlu, P.; Yalcin, S.; Unsoy, G.; Yakar, A.; Khodadust, R.; Gunduz, G. *Biomed Pharmacother* **2014,** *68* (6), 729-36.
16. McBain, S. C.; Yiu, H. H.; Dobson, J. *Int J Nanomedicine* **2008**, 3 (2), 169-80.
17. Pinto, R. V.; Gomes, P. S.; Fernandes, M. H.; Costa, M. E. V.; Almeida, M. M. *Mater Sci Eng C Mater Biol Appl* **2020**, 109, 110557.
18. Sahin, S.; Ozmen, I. *J Pharm Biomed Anal* **2020**, 184, 113195.
19. Zhao, L.; Yang, B.; Dai, X.; Wang, X.; Gao, F.; Zhang, X.; Tang, J. *J Nanosci Nanotechnol* **2010**, 10 (11), 7117-20.
20. Danafar, H.; Sharafi, A.; Askarlou, S.; Manjili, H. K. *Drug Res (Stuttg)* **2017**, 67 (12), 698-704.
21. Barbey, C.; Bouchemal, N.; Retailleau, P.; Dupont, N.; Spadavecchia, J. *ACS Omega* **2021**, 6 (2), 1235-1245.
22. Matei, A.; Puscas, C.; Patrascu, I.; Lehene, M.; Ziebro, J.; Scurtu, F.; Baia, M.; Porumb, D.; Totos, R.; Silaghi-Dumitrescu, R. *Int J Mol Sci* **2020**, 21 (9).
23. Poon, I. K.; Hulett, M. D.; Parish, C. R. *Cell Death Differ* **2010**, 17 (3), 381-97.
24. Cheng, J.; Cheng, L.; Chen, B.; Xia, G.; Gao, C.; Song, H.; Bao, W.; Guo, Q.; Zhang, H.; Wang, X. *Int J Nanomedicine* **2012**, 7, 2843-52.
25. Zhao, P.; Wang, H.; Gao, H.; Li, C.; Zhang, Y. *Neurol Res* **2013**, 35 (8), 821-8.

DOI: http://dx.doi.org/10.32571/ijct.1194667 **E-ISSN: 2602-277X**

26. Fang, C.; Kievit, F. M.; Veiseh, O.; Stephen, Z. R.; Wang, T.; Lee, D.; Ellenbogen, R. G.; Zhang, M. *J Control Release* **2012**, 162 (1), 233-41.

27. Gupta, A. K.; Gupta, M. *Biomaterials* **2005**, 26 (18), 3995-4021.

28. Kim, R.; Emi, M.; Tanabe, K.; Toge, T. *Cancer* **2004**, 101 (11), 2491-502.

29. Attari, E.; Nosrati, H.; Danafar, H.; Kheiri Manjili, H. *J Biomed Mater Res A* **2019**, 107 (11), 2492-2500.

30. Tarantash, M.; Nosrati, H.; Kheiri Manjili, H.; Baradar Khoshfetrat, A. *Drug Dev Ind Pharm* **2018**, 44 (11), 1895-1903.

DOI: http://dx.doi.org/10.32571/ijct.1187768 **E-ISSN: 2602-277X**

International Journal of Chemistry and Technology

http://dergipark.org.tr/ijct

Research Article

The comparison of chemical content and bioactive capacity of domestic and import *Hypericum perforatum* aqueous extracts

Sarmad MARAH[1], Ibrahim DEMIRTAS[2], Tevfik OZEN[1*]

Ondokuz Mayıs University, Science Faculty, Department of Chemistry, Samsun, Türkiye

Igdir University, Faculty of Science and Art, Department of Biochemistry, Igdır, Türkiye

Received: 12 October 2022; Revised: 7 December 2022; Accepted: 8 December 2022

*Corresponding author e-mail: tevfikoz@omu.edu.tr

Citation: Marah, S.; Demirtas, I.; Ozen, T. *Int. J. Chem. Technol.* **2022**, 6 (2), 164-169

ABSTRACT

Hypericum perforatum, known as St. John's Wort and most used ethnaformacolgically, belongs to the *Hypericaceae* family. In this work, we aimed to evaluate the antioxidant, antimicrobial, DNA protective activities, and enzyme inhibitor properties of domestic and import *H. perforatum* aqueous extracts. The total phenolic and flavonoid contents were also determined for both samples. Results exhibited a high phenolic content for Domestic *H. perforatum* aqueous extract (DHPE) and Import *H. perforatum* aqueous extract (IHPE) samples. Meanwhile, inhibition activity levels for α-glucosidase were remarkable, the IC_{50} value of DHPE was 16.35±0.07 µg/mL, and the IC_{50} value of IHPE was 15.05±1.36 µg/mL, both samples demonstrated almost twice of the standard inhibitor effect (IC_{50}: 30.62±2.07 µg/mL). Moreover, the inhibition activity of both samples against α-amylase was more effective than acarbose. The antibacterial results were as follows; the highest MIC value detected by IHPE was 64 µg/mL against *B. cereus*. In addition, IHPE was shown to be more effective than the domestic sample against all microorganisms. Furthermore, DHPE exhibited good protective activity from oxidative H_2O_2-induced DNA damage. Both tested samples had an abundance of phenolic content and were high in inhibitory activity against diabetic enzymes. Generally, bioactivity tests' results appeared quite effective for both samples compared to the standards.

Keywords: *H. perforatum*, aqueous extract, phytochemical content, bioactivity.

Yerli ve ithal *Hypericum perforatum* sulu ekstraktlarının kimyasal içeriği ve biyoaktif kapasitesinin karşılaştırılması

ÖZ

Sarı kantaron olarak bilinen ve etnaformakoljik olarak en çok kullanılan *Hypericum perforatum*, Hypericaceae familyasına ait bir bitkidir. Bu çalışmada yerli ve ithal *H. perforatum* sulu ekstraktlarının antioksidan, antimikrobiyal, DNA koruyucu aktiviteleri ve enzim inhibitör özelliklerini değerlendirmeyi amaçladık. Her iki örnek için de toplam fenolik ve flavonoid içerikleri belirlendi. Analiz sonuçları, Yerli *H. perforatum* sulu özüt (DHPE) ve İthal H. perforatum sulu özüt (IHPE) numuneleri için yüksek fenolik içerikti. Numunelerin diyabetle ilgili temel enzimlere karşı inhibisyon aktivitesi seviyeleri çarpıcıydı; α-glukosidaza gelince, DHPE'nin IC_{50} değeri 16.35±0.07 µg/mL idi ve IHPE'nin IC_{50} değeri 15.05±1.36 µg/mL idi, bu da sırasıyla enzimin standart inhibitörünün etkinliğinin neredeyse iki katını temsil ediyor. Özellikle, DHPE'nin α-amilaz ve α-glukosidaz üzerindeki inhibisyon aktivitelerinin akarboza göre daha etkili olduğu belirlendi (IC_{50}: 30.62±2.07 µg/mL). Antibakteriyel test şu şekildeydi; en yüksek MİK değeri IHPE tarafından *B. cereus'a* karşı 64 µg/mL olarak tespit edildi. Ayrıca, IHPE yerli örnekten daha etkiliydi. DHPE, oksidatif H_2O_2 ile indüklenen DNA hasarından iyi koruyucu aktivite sergiledi. Sonuç olarak, test edilen her iki numune de bol miktarda fenolik içeriğe sahipti ve diyabetik enzimlere karşı inhibitör aktivitelerinde yüksekti. Ayrıca, diğer biyoaktivite testleri, standartlara göre oldukça etkili olduğu gözlendi.

Anahtar Kelimeler: *H. perforatum*, sulu ekstrakt, fitokimyasal içerik, biyoaktivite.

DOI: http://dx.doi.org/10.32571/ijct.1187768 E-ISSN: 2602-277X

1. INTRODUCTION

Hypericum perforatum is an enduring species distributed worldwide, also recognized as St. John's wort. It is classified under folk medicines due to its curative abilities for many diseases. The Cherokee, Iroquois, and Montagnais all left behind records of using *H. perforatum*. All of these tribes appeared to have utilized the kinds as a febrifuge or cough remedy, but the Cherokee employed it extensively. The use of the herb's distilled oil as a treatment for cuts and bruises was one of the first, most popular, and widespread pharmacological uses of this plant in Europe after the 16th century.[1] *H. perforatum* contains many bioactive molecules with various pharmacologic effects, such as antioxidant activity.[2] Due to the rising need for raw materials as a source of organic bioactive compounds, this plant species has drawn a lot of attention recently.[3] It has naturalized many regions, most notably North America and Australia. It is indigenous to Europe, West Asia, North Africa, Madeira, and the Azores. The plant can infiltrate meadows, disturbed places, dirt roads, the sides of roads and highways, and sparse woodlands and spreads quickly through runners or prolific seed production. *H. perforatum* is currently one of the world's most widely used medicinal plants due to the rapid rise in the consumption of goods derived from it in recent years.[4] In previous studies, plants' importance has been evaluated for their biological and chemical properties and their use in treating infectious diseases. *H. perforatum* contains many bioactive molecules with various pharmacologic effects, such as antioxidant activity.[2] Due to ecological considerations, genetic differences within the species, cutting time, sample preparation and processing, and storage circumstances like light exposure, these constituents' concentrations frequently change. Buds, flowers, and the tips of twigs contain concentrated amounts of significant bioactive substances. Regardless of this diversity, it is understood that about 20% of the plant extract is made up of bioactive substances.[5-7] Recent interest has evaluated its antimicrobial activity against several bacterial and fungal strains.[1]

The plant has many therapeutic uses, including treating burns, eczema, psychiatric disorders, intestinal illnesses, and skin wounds.[8] In addition, its extract's chemical compositions have various pharmaceutic attributes that are related to anti-inflammatory, antiviral, antitumor, and wound-healing activities.[3] In this study, using total phenol and flavonoid content testing, we attempted to create a comprehensive picture of the bioactive chemical components for both *H. perforatum* extracts. Additionally, the number of biological activities is investigated as antioxidant, antibacterial, and DNA-protective activities, in addition to determining the inhibitory effects of the extracts for the enzymes connected to diabetes, α–glucosidase and α–amylase.

2. MATERIALS AND METHODS

2.1. Reagents and solutions

The domestic (D) and import (I) samples of *H. perforatum* (HP) were provided by ERSAG Company (Denizli, Türkiye). DHP and IHP aqueous extracts (aerial parts) were obtained using the extraction method as follows. 10 kg of DHP and IHP were placed in a heat-resistant net inside the extraction device and mixed with 50 L of distilled water at 80 degrees for 2 hours in a particular-made extraction system. After that, the liquid part was removed from the extraction mixture using the vacuum pump. The next step was applying the spray-drying to produce the dark brown dry extract powder (1 kg, 10%). Then, dried samples of DHP and IHP aqueous extracts (E) were obtained and stored at -20 ºC.

2.2. Analysis of chemical content

Analysis of total phenol content (TPC) was obtained using the Folin & Ciocalteu method.[9] The entire total flavonoid content (TFC) was estimated using the aluminum chloride method with slight modification.[10]

2.3. Determination of antioxidant capacity

We have applied three theories known and widely used in the literature to determine the antioxidant capacity of the samples. Firstly, the ammonium molybdenum method was applied to detect the total antioxidant activity of samples, based on forming green phosphate/Mo (V) complex within 695 nm.[11,12] Then, the free radical scavenging capacities for samples were spectrophotometrically evaluated using 1,1-diphenyl-2-picryl-hydrazyl ($DPPH^{\bullet}$)[13] and 2,2'-Azino-bis(3-ethylbenzothiazoline-6-sulfonic acid) ($ABTS^{\bullet+}$).[14]

2.4. Determination of antimicrobial capacity

The antimicrobial effect of samples was detected using six different bacteria gram-positive (*Staphylococcus aureus*; ATCC 25213, *Enterococcus faecalis*; ATCC 29212, and *Bacillus cereus*; CCM 99) and gram-negative (*Pseudomonas aeruginosa*; ATCC 15442, *Klebsiella pneumoniae*; ATCC 10031 and *Escherichia coli*; ATCC 25922). Samples and standard antibiotics were prepared with a concentration of 8.192 mg/mL, and the microdilution method was applied to find the minimum inhibition concentration (MIC).[15] Samples were diluted by mixing with cationic MHB medium (Mueller Hinton II Broth + $CaCl_2$ + $MgCl_2$) in a sterile 96-well plate. Then, 10 µL of 0.5 McFarland bacterial solution was added to each well. After that, the plates were incubated at + 4 °C followed by incubation at 37 °C (*B. cereus* incubation at 30 °C) for 120 minutes. MIC has been read after 16-18 hours of incubation.

DOI: http://dx.doi.org/10.32571/ijct.1187768 E-ISSN: 2602-277X

2.5. Inhibition of α–amylase and α–glucosidase

α-amylase inhibition activity of samples was determined spectrophotometrically depending on the hydrolysis of starch in an acidic medium.[16] α-glucosidase inhibition also was determined spectrophotometrically by measuring the formation of yellow-colored p-nitrophenol.[17, 18].

2.6. DNA protective activity

DNA protection activity of samples was determined using the agarose gel electrophoresis method.[19] The experiment was applied by preparing a mixture of 4 µL of glycerol, 5 µL of the sample, 3 µL of pBR322 plasmid DNA (172 ng/µL), and 1 µL of 30 % H_2O_2. The mixture was submitted to UV for 5. Then 2 µL of bromophenol blue was added, and the mixture was loaded to the 1.5 % agarose gel wells (1X TBE buffer + 2 µL ethidium bromide). Then electrophoresis was applied for 120 minutes at 90 volts. Finally, the % DNA protection activity was determined using the ImageJ program.

2.7. Statistical analysis

Experimental data were recorded using Microsoft Excel and statistically analyzed by SPSS 22.0. Data like survival rate, hatchability, and malformation rate parameters were analyzed using the one-way analysis of variance (ANOVA) test and Tukey test when the variance data were homogeneous. A rank sum test was used for graded data such as urine analysis indexes. P values lower than 0.05 were considered significant.

3. RESULTS AND DISCUSSION

3.1. Total phenolics and total flavonoids

The chemical composition analysis was performed to detect the total phenol and flavonoid content, as Gallic acid for phenolics and quercetin for flavonoids. Results revealed that DHPE with 155 mg GAE/g extract had more phenolics content than the other sample, which also was not far from this number, 142 mg GAE/g extract. While the flavonoid content of IHPE came in first place in quantity with 46 mg QE/g extract, as shown (Table 1). This highly content may be behind the vast bioactive effects of these samples. In order to compare our results with literature data, we found that in another study that the total phenolic content of five extracts of *H. perforatum* in different parts using two solvents (EtOH–water and water) was between 191 ± 5 to 257 ± 4 mg of gallic acid/g of dry extract for the organic extracts and between 162 ± 3 to 228 ± 2 mg of gallic acid/g of dry extract for the water extracts, however, our DHPE and IHPE samples have a 155 and 142 mg GAE/g extract, respectively, which is almost the same range with this study results from.[20] In addition, in another study, total

Table 1. Chemical contents for *H. perforatum* extracts

Sample	[a]Total phenol content (TPC)	[b]Total flavonoid content (TFC)
DHPE	155.87±0.83	35.66±0.03
IHPE	142.96±0.76	46.02±0.67

[a]TPC: mg gallic acid equivalent/g extract
[b]TFC: mg quercetin equivalent/g extract
DHPE: Domestic *H. perforatum* aquous extract
IHPE: Import *H. perforatum* aquous extract

phenolic and flavonoid content of Turkish *H. perforatum* extracts (ethanol, methanol, and water) were determined to have the highest phenolic content as gallic acid equivalent (355.01 ± 0.43 mg/g ethanol extract). In comparison, the ethyl acetate extract had the highest quantity of total flavonoids as quercetin equivalent (167.37 ± 0.88 mg/g methanol extract). However, both phenolic and flavonoid contents were lower than our aqueous extract contents.[21] The phytochemical analysis of methanol extract of aerial parts of *H. perforatum* showed that the total phenolics content was (21.90 ± 0.9 mg/g sample) and the total flavonoids content was (17.10 ± 0.02 mg/g sample). These results confirm that our tested samples both the phenolic and flavonoid content of the extracts are high relative to their peers.[22] Furthermore, *H. perforatum* methanol aerial part extract showed a total phenolic content of 15.01 ± 1.54 mg/g and total flavonoids of 4.67 ± 0.22 mg/g, and both contents were lower than our plant contents.[23]

3.2. Antioxidant activity

The results showed that the antioxidant activity of both samples was very close to the standard antioxidants in general. Further, DHPE showed a higher effect than E vitamin and almost was same to BHA as IC_{50} value 72.68±0.41 µg/mL for the total antioxidant test. Furthermore, both samples give nearly the same activity for the DPPH$^{\bullet}$ sacavenging test as IC_{50} value of 4.35±0.24 µg/mL for DHPE and 4.63±1.27 µg/mL for IHPE. Also, there was a slight difference in the IC_{50} value with the standard antioxidants. For the last antioxidant test, both samples had higher effects than the E vitamin, Table 2.

Table 2. Antioxidant acttivity results for *H. perforatum* extracts.

Sample	Total antioxidant	DPPH$^{\bullet}$ scavenging	ABTS$^{\bullet+}$ scavenging
DHPE	72.68±0.41^{a}	4.35±0.24^{a}	16.16±2.05^{b}
IHPE	110.05±0.15^{c}	4.63±1.27^{a}	9.14±0.28^{a}
BHA	72.49±2.59^{a}	3.41±0.16^{a}	8.93±0.82^{a}
Vitamin E	86.025±0.40^{b}	4.05±0.32^{a}	19.50±0.83^{b}

Note: Data are means of three repetitions ± standard deviation (SD), variance analysis: $p<0.05$
IC_{50} value, µg/mL: DPPH$^{\bullet}$, ABTS$^{\bullet+}$
$A_{0.5}$ value, µg/mL: Total antioxidant
DHPE: Domestic *H. perforatum* aquous extract
IHPE: Import *H. perforatum* aquous extract

By comparing what we found to other literature research, we found that the radical scavenging activity of both extracts was higher than the methanolic extracts of *H.*

DOI: http://dx.doi.org/10.32571/ijct.1187768 E-ISSN: 2602-277X

perforatum, which gave an IC_{50} value of 8.7± 0.23 µg/mL against DPPH.[24] Also, in another study, where they determined a high flavonoid content for *H. perforatum* ethanol extract, the DPPH· scavenging test results were IC_{50} value of 10.63 µg/mL, lower than our aqueous extract.[25] Another research investigated the antioxidant properties of Turkish *H. perforatum* species and found that ethyl acetate, methanol, and water extracts are lower than gallic acid as a standard antioxidant; however, our extracts give an activity almost the same as the standards.[21] In another study, the DPPH· scavenging activity of *H. perforatum*' raw extract was IC_{50} of 10.63 µg/mL, which is almost half the scavenging activity value of our extracts.[25]

3.3. α–glucosidase and α–amylase inhibitory effect

The α-glucosidase is one of the critical enzymes of the human digestive system, located in the small intestine. Its role is to process and break down complex carbohydrates into small, simple, and absorbable carbohydrates. Inhibiting this enzyme represents a solid solution to delaying glucose absorption and preventing the postprandial rise in blood glucose levels, which may prohibit the development of diabetes. Table 3 clarifies the α–glucosidase inhibition activity of HPE samples and the acarbose. IHPE exhibited the highest inhibition activity with an IC_{50} value of 15.05±1.36 µg/mL; however, both samples showed an inhibition activity higher than the standard inhibitor, which gave an IC_{50} value of 30.62±2.07 µg/mL. Because of its capacity to break down polysaccharide molecules, α-amylase is also considered one of the most important enzymes of the human digestive system, so it also may prohibit the development of diabetes. Results show that (IHPE) has the highest inhibition effect, with an IC_{50} value of 22.24±1.79 µg/mL; this effect was better than the inhibition effect of both (IHPE) and acarbose, Table 3

Table 3. Enzyme inhibition acttivity results for *H. perferatum* extracts.

Sample	α-Glucosidase	α-Amylase
DHPE	16.35±0.07[a]	22.24±1.79[a]
IHPE	15.05±1.36[a]	54.35±0.35[b]
Acarbose	30.62±2.07[b]	59.01±1.04[b]

Note: Data are means of three repetitions ± standard deviation (SD), variance analysis: $p<0.05$
IC_{50} value (µg/mL): α-Glucosidase, α-Amylase
DHPE: Domestic *H. perferatum* aquous extract
IHPE: Import *H. perferatum* aquous extract

Moreover, in the literature review that we had done, we found that α-amylase and α-glucosidase inhibition activity for the roots, non-flower shoots, and flower shoots methanolic extracts of *H. perforatum* were lower than acarbose inhibition for α-glucosidase and lower than half the value of acarbose inhibition for the α-amylase enzyme, on the other hand, our extracts were higher in their inhibition activity than acarbose for both enzymes.[26] In another study, the inhibition activity of *H. perforatum* water-alcoholic extract against α-amylase and α-glucosidase enzymes was found to be lower than acarbose (reference inhibitor); by comparing these results to our result, we conclude that *H. perforatum* aqueous extract was more effective against both enzymes.[27]

3.4. Determination of antimicrobial capacity

The antibacterial potential of *H. perforatum* samples differed when tested against three-gram positive and three-gram negative bacteria, including *K. pneumoniae, P. aeruginosa, E. coli,* and *B. cereus, E. faecalis,* and *S. aureus*. *H. perforatum* sample antibacterial activities were represented as Minimum Inhibitory Concentration (MIC, g/mL) and MIC values in Table 4.

Table 4. Antimicrobial capacity results for *H. perforatum* extracts and antibiotics.

Samples	Gram-staining-negative		
	E. coli	***P. aeruginosa***	***K. pneumoniae***
DHPE	4096	4096	4096
IHPE	256	1024	1024
Amoxicillin	>1024	>1024	>1024
Tetracycline	4	8	8
Samples	**Gram-staining-positive**		
	E. faecalis	***B. cereus***	***S. aureus***
DHPE	4096	2048	4096
IHPE	1024	64	512
Amoxicillin	>1024	0.5<	>1024
Tetracycline	4	0.5<	4

DHPE: Domestic *H. perferatum* aquous extract
IHPE: Import *H. perferatum* aquous extract

The highest antibacterial activity was IHPE against *B. cereus* bacteria, with a MIC value of 64 µg/mL. However, IHPE has shown low antibacterial activity against almost all bacteria, with a MIC value of 2048 µg/mL against *B. cereus* and 2096 µg/mL against the other bacteria. Also, we used Amoxicillin and Tetracycline as positive control in our research; the results showed that IHPE was nearest in its activity to Amoxicillin; on the other hand, Tetracycline was higher than both samples and Amoxicillin. Moreover, in the literature review that we had done, *H. perforatum* extracts had shown a significant effect on *S. aureus.*[28] Another study found that the gram-positive bacterial strains were more sensitive to the methanolic extract of *H. perforatum* in their minimum inhibitory concentration than gram-negative bacterial strains.[22]

3.5. DNA protective activity

DNA protection capability for the *H. perforatum* samples was performed using the plasmid DNA derived from pBR322 in the presence of ultraviolet and hydrogen peroxide. The addition of *H. perforatum* samples to the reaction mix prohibits modification of the formation of line DNA. It helps to protect the native formation of DNA (Figure 1, a-b). Our results showed that IHPE had the highest effect on protecting the DNA supercoiled and

DOI: http://dx.doi.org/10.32571/ijct.1187768 E-ISSN: 2602-277X

open-circular forms compared to the other tested samples and the quercetin (as a positive control too). However, IHPE gave a 30.31 protection percentage, IHPE gave a 60.01 protection percentage, and quercetin gave a 41.31 protection percentage for the supercoiled form. On the other hand, for the open-circular, the protection percentages were 25.78 for the IHPE, 57.33 for IHPE, and 47.85 for the quercetin. In the previous study made by,[29] they also tested the DNA protection activity for water and ethanol extracts of the *H. perforatum*; it has been proven beyond a doubt that all *H. perforatum* extracts have the ability to offer DNA protection potentials against UV rays when hydrogen peroxide is present. *H. perforatum* seed, flower, fruit methanol, and water extracts exhibit substantial DNA protection activity. However, our extracts also exhibit a high protection activity for plasmid DNA forms.[30]

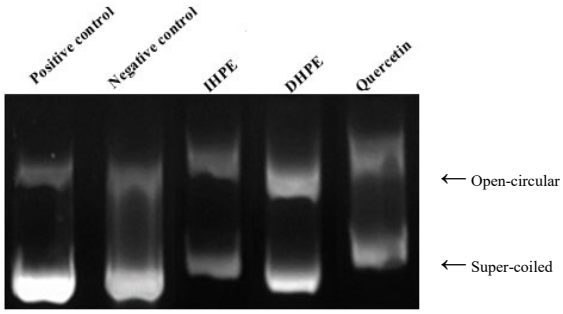

Lane 1: plasmid DNA as a positive control,
Lane 2: plasmid DNA with H_2O_2 and UV as a negative control,
Lane 3: plasmid DNA + H_2O_2 + UV + IHPE (Import *H. perforatum* aquous extract)
Lane 4: plasmid DNA + H_2O_2 + UV + DHPE (Domestic *H. perforatum* aquous extract)
Lane 5: plasmid DNA + H_2O_2 + UV + Quercetin

(a) Agarose gel electrophoresis image

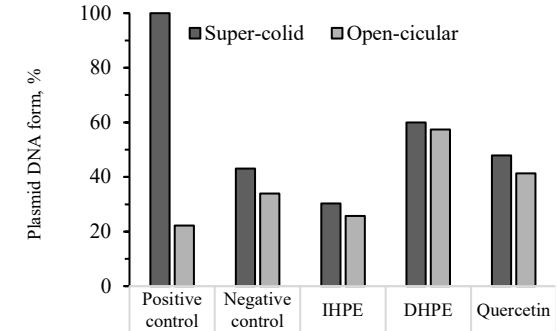

	Positive control	Negative control	IHPE	DHPE	Quercetin
Super-colid	100,000	43,058	30,310	60,010	47,850
Open-cicular	22,178	33,913	25,780	57,330	41,310

(b) Comparing chart of % density of the open-circular and supercoiled forms of plasmid DNA.

DHPE: Domestic *H. perforatum* aquous extract
IHPE: Import *H. perforatum* aquous extract

Figure 1. DNA damage protection potential results for *H. perforatum* samples.

CONCLUSION

This work represents a cohesive academic base of standard biologic activities for Turkish *H. perforatum* extract for further pharmacological investigation and application. In addition to matching the test results of the domestic extract with the reference materials, we also tested imported *H. perforatum* extract to compare the bioactivity of both extracts. However, we have observed the reflection of the high phenolic content for the domestic extract on the different biological activity as an antioxidant and the inhibitory effect of key enzymes linked to type 2 diabetes mellitus (α-amylase and α-glucosidase), which could be a clue to the existence of potential antidiabetic contents. On the other hand, the imported extract showed a high ability to protect the DNA structure and high antibacterial activity compared to the domestic extract and the reference materials. This is evidence of the difference in the environment of plants in changing the chemical composition.

ACKNOWLEDGEMENTS

We thank the ERSAG company group for providing the *H. perforatum* extracts. Also, we would like to express our gratitude to the institutions concerned. This work was supported by Ondokuz Mayis University-BAP with the project numbered PYO.FEN.1904.20.003.

Conflict of interests

I declare that there is no a conflict of interest with any person, institute, company, etc.

REFERENCES

1. Saddiqe, Z., I. Naeem, and A. Maimoona, *J. Ethnopharmacol.*, **2010**. 131(3): p. 511-521.

2. Oliveira, A.I., et al., *Front. Plant Sci.*, **2016**. 7: p. 1004.

3. Nahrstedt, A. and V. Butterweck, *J. Nat. Prod.*, **2010**. 73(5): p. 1015-1021.

4. Wills, R.B., K. Bone, and M. Morgan, *Nutr. Res. Rev.*, **2000**. 13(1): p. 47-77.

5. Linde, K., *Complement. Med. Res.*, **2009**. 16(3): p. 146-155.

6. Wurglics, M. and M. Schubert-Zsilavecz, *Clin. Pharmacokinet.*, **2006**. 45(5): p. 449-468.

7. Patocka, J., *J. Appl. Biomed.*, **2003**. 1(2): p. 61-70.

8. Butterweck, V., *CNS Drugs*, **2003**. 17(8): p. 539-562.

9. Golmakani, E., et al., *J. Supercrit Fluid*, **2014**. 95: p. 318-324.

DOI: http://dx.doi.org/10.32571/ijct.1187768 E-ISSN: 2602-277X

10. Chang, C.-C., et al., *J. Food Drug Anal.*, **2002**. 10(3).

11. Prieto, P., M. Pineda, and M. Aguilar, *Anal. Biochem.*, **1999**. 269(2): p. 337-341.

12. Mohamed, R., M. Pineda, and M. Aguilar, *J. Food Sci.*, **2007**. 72(1): p. S059-S063.

13. Blois, M.S., *Nature*, **1958**. 181(4617): p. 1199-1200.

14. Re, R., et al., *Free Radic Biol Med*, **1999**. 26(9-10): p. 1231-1237.

15. Andrews, J.M., *J. Antimicrob. Chemother.*, **2001**. 48(suppl_1): p. 5-16.

16. Ercan, P. and S.N. El, *Food Chem.*, **2016**. 205: p. 163-169.

17. Mayur, B., et al., *J. Med. Plant Res.*, **2010**. 4(15): p. 1547-1553.

18. Sancheti, S., S. Sancheti, and S.-Y. Seo, *Pak. J. Pharm. Sci.*, **2010**. 23(2).

19. Sevgi, K., B. Tepe, and C. Sarikurkcu, *Food Chem Toxicol*, **2015**. 77: p. 12-21.

20. Gioti, E.M., et al., *Food Chem.*, **2009**. 117(3): p. 398-404.

21. Altun, M.L., et al., *Ind Crop Prod*, **2013**. 43: p. 87-92.

22. Nawchoo, I.A., et al., *Asian J Plant Sci*, **2012**. 2(4): p. 414-420.

23. Kalogeropoulos, N., et al., *LWT-FOOD SCI TECHNOL*, **2010**. 43(6): p. 882-889.

24. Heinrich, M., et al., *Chem. Biodivers.*, **2017**. 14(8): p. e1700100.

25. Zou, Y., Y. Lu, and D. Wei, *J. Agric. Food Chem.*, **2004**. 52(16): p. 5032-5039.

26. Tusevski, O., et al., *S. Afr. J. Bot.*, **2018**. 117: p. 301-310.

27. Kladar, N., et al., *Evid. Based Complement. Alternat. Med.*, **2017**. 2017.

28. Bahmani, M., et al., *Mini Rev. Med. Chem.*, **2019**. 19(11): p. 923-932.

29. Sekeroglu, N., et al., *Indian J Pharm Educ Res*, **2017**. 51(2): p. 1-7.

30. Aktepe, N., et al., *Medicine*, **2022**. 11(2): p. 784-8

DOI: http://dx.doi.org/10.32571/ijct.1199221 E-ISSN: 2602-277X

International Journal of Chemistry and Technology

http://dergipark.org.tr/ijct

Research Article

The investigation of the effect of chalcones with benzoic acid on xanthine oxidase activity

Bedriye Seda KURŞUN AKTAR[1], Şevki ADEM[2], Emine Elçin ORUÇ-EMRE[3]

[1] *Malatya Turgut Özal University, Yeşilyurt Vocational School, Department of Hair Care and Beauty Services, Malatya, Türkiye*

[2] *Çankırı Karatekin University, Faculty of Sciences, Department of Chemistry, 18100 Çankırı, Türkiye*

[3] *Gaziantep University, Faculty of Art and Sciences, Department of Chemistry, Gaziantep, 27410, Türkiye*

Received: 3 November 2022; Revised: 5 December 2022; Accepted: 14 Aralık 2022

*Corresponding author e-mail: sedakursun@windowslive.com

Citation: Kurşun, Aktar, B. S.; Adem, Ş.; Oruç-Emre, E. E. *Int. J. Chem. Technol.* **2022**, 6 (2), 170-175.

ABSTRACT

Inhibitors of xanthine oxidase (XO) are effective and most major therapeutic drugs for the management of gout. Chalcone compounds are important in terms of biological activity and have great importance in enzyme studies in recent years. In the presented study, the effects of some chalcones on the enzyme were tested in vitro by the spectrophotometric method. Compounds showed an inhibitory effect between 7.21±0.07 and 13.78±0.13 µM IC50 values. The conformations and interactions of the compounds in the active site of the enzyme were determined by the molecular docking method using Molegro Virtual Docker software. Molecular modeling studies show that the B ring of chalcones has a significant contribution to the inhibition effect on the XO enzyme. The presented study suggests that chalcones may be a potential inhibitory group for XO.

Keywords: Chalcone, xanthine oxidase inhibitor, molecular docking.

Benzoik asitli kalkonlarin ksantin oksidaz inhibitörü üzerine etkisinin incelenmesi

ÖZ

Ksantin oksidaz (XO) inhibitörleri, gut tedavisinde çok önemli ve etkili terapötik ilaçlardır. Kalkon bileşikleri biyolojik aktivite açısından önemli olup, son yıllarda enzim çalışmalarında da büyük bir öneme sahiptir. Yapılan çalışmada, bazı kalkonların enzim üzerindeki etkileri spektrofotometrik yöntemlerle in vitro olarak test edildi. Bileşikler, 7.21±0.07 ve 13.78±0.13 uM IC50 değerleri arasında bir inhibitör etki gösterdi. Enzimin aktif bölgesindeki bileşiklerin konformasyonları ve etkileşimleri Molegro Virtual Docker yazılımı kullanılarak moleküler yerleştirme yöntemi ile belirlendi. Moleküler modelleme çalışmaları, kalkonların B halkasının, XO enzimi üzerindeki inhibisyon etkisine önemli bir katkısı olduğunu göstermektedir. Yapılan çalışma sonucunda, kalkonların XO için potansiyel bir inhibitör grup olabileceğini düşündürmektedir.

Anahtar kelimeler: Kalkon, ksantin oksidaz inhibitörü, molecular docking.

1. INTRODUCTION

Compounds with α-β unsaturated ketone structure containing 1,3-diarylprop-2-en-1-one structure are called chalcone. Chalcones can be isolated both naturally and synthetically. Chalcones show very different biological activities. In recent years, research on enzyme inhibition of chalcones has become very important. The chalcones have inhibitory effects against enzymes such as xanthine oxidase,[1] protein tyrosine kinase,[2] quinone reductase,[3] tyrosinase,[4] mammalian alpha-amylase[5], monoamine oxidase,[6] pyruvate kinase M2 (PKM2),[7] carbonic anhydrase I (CAI),[7] heme oxygenase,[8] carbonic anhydrase II (CAII),[7] aldose reductase, acetylcholinesterase (AChE),[9] α-amylase and α-glucosidase,[10] butyrylcholinesterase (BChE).[9] Xanthine oxidase inhibitor reduces uric acid production in humans and inhibits xanthine oxidase. Xanthine oxidase (XO) is a type of enzyme that is a form of xanthine oxidoreductase and produces reactive oxygen species. XO catalyzes the oxidation of hypoxanthine to xanthine and catalyzes the oxidation of xanthine to uric acid.

DOI: http://dx.doi.org/10.32571/ijct.1199221 E-ISSN: 2602-277X

Xanthine oxidase is used for the treatment of hyperuricemia and gout, as it is an enzyme responsible for the catabolism of purines and their conversion to uric acid. The XO inhibitor drug, which has been used commercially for many years, is the purine analog called allopurinol.[11] However, new drug candidates were needed because of the many side effects of allopurinol such as hypersensitivity, gastrointestinal problems, and renal toxicity. Because XO inhibitors, especially in the treatment of gout and hyperuricemia; It has also been associated with diabetes, hypertension, and other cardiovascular diseases.

2. MATERIALS AND METHODS

Materials

Enzyme, substrate, inhibitor and other reagents used in enzyme activity studies were purchased from Sigma-Aldrich. Structures of the analysed compounds 1,[12] 2,[12] 3,[13] 4,[13] and 5[12] are given in Table 1.

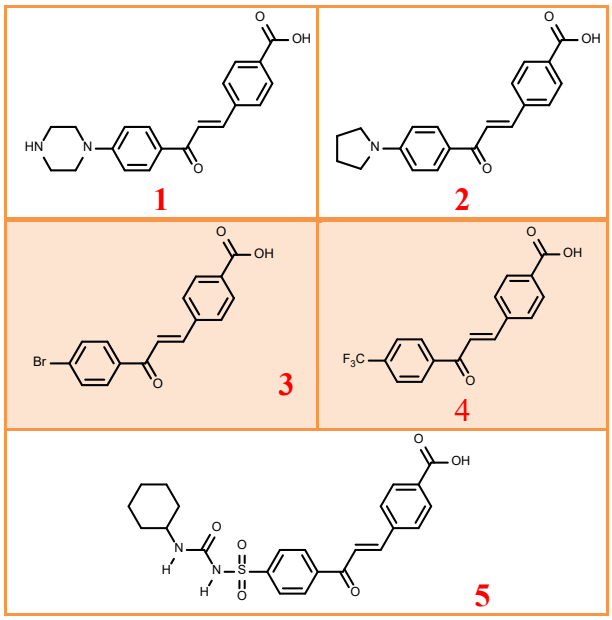

Table 1 The structures of the analysed compounds (1-5).

2.1. Inhibitory effects of Xanthine oxidase by Chalcones

The Xanthine oxidase inhibition experiment was performed according to the slightly changed methods in the previous reports.[14] Desired concentrations of enzyme and substrate were arranged by potassium phosphate buffer (pH 7.5, 50 mM), and the tested compounds were dissolved in DMSO at 1 mg/mL, then diluted with pure water ten times.

The enzyme solution (10 µL), 500 mM potassium phosphate buffer (50 µL), and different concentrations of chalcones (100 µL), and were added to the 96-well plate and incubated at 37 °C for 15 min. Then, hypoxanthine as substrate (60 µL, 3 mM) was added to each well and allowed to be incubated at 37 °C for 20 min. Finally, the alteration in the absorbance within 7 minutes was measured at 295 nm by using a multiple-reader spectrophotometer. Allopurinol was used as a positive control. The percent inhibition of xanthine oxidase activity was computed by comparing the inhibitor absorbance values with the control value without an inhibitor. IC_{50} values were obtained from the curve of concentration plots of molecules versus % activity.

2.2. Molecular Docking

Molecular docking was accomplished by the MolegroVirtual Docker for enzyme ligand docking.[15] The XO crystal structures (PDB IDs. 3NVY/ Quercetin, 7D6O/ Oxypurinol (www.rcsb.org/structure/7D6O), 3NRZ/Hypoxanthine, 3NVW/ Guanine) were retrieved from RCSB Protein Data Bank.[16-18] The XO structures were optimized in the Protein Preparation tool to obtain the chemically proper configuration by repairing structural errors in amino acids. Inhibitor structures were modeled in ChemDraw, and optimized and prepared three-dimensional (3D) sdf structure using the MarvinSketch. The docking site was described as the area occupied by the co-crystal ligands plus a 13 Å wide zone in its immediate proximity, yielding a docking region that was wide enough to set each of the docked chalcones. The docking operation was repeated 10 times for each compound. The best poses were visualized and analysed using Discovery Studio 2021 Client program (v17.2, Accelrys, San Diego, CA).

3. RESULTS AND DISCUSSION

3.1. Biological Activity

Xanthine oxidase inhibitors use as a drug to treat hyperuricemia and gout disease.[19,20] XO inhibitors from many different groups have been reported in the literature.[21] The derivatives of some chalcones were reported as strong xanthine oxidase inhibitors.[22-24] In this study, we tested some chalcones to determine their inhibitor potentials against this enzyme activity at 1-25 µM concentrations. Also, we performed docking studies to predict the accuracy of binding poses of compounds with enzyme active sites. Results tabulated in Table 2.

As shown in Table 2, among the chalcone compounds examined here compounds **1** and **2** had the greatest effect with 7.21±0.07 and 7.54±0.09 µM IC_{50} values, respectively. Compounds **3**, **4**, and **5** showed a strong inhibitory effect on XO, and the IC_{50} of these compounds were 8.82± 0.12, 9.80± 0.10, and 13.78± 0.13 µM , respectively (Figure 1). Allopurinol was used as a control to compare, its IC_{50} values were determined as 6.18± 0.10. The compounds demonstrated an inhibition effect against the enzyme at values very close to the standard.

DOI: http://dx.doi.org/10.32571/ijct.1199221 E-ISSN: 2602-277X

The name of compounds/Molecular Weight (g/mol)	IC_{50} values µM	PDB ID and References ligands							
		3NVY/ Quercetin		7D6O/ Oxypurinol		3NRZ/Hypoxanthine		3NVW/ Guanine	
		MolDock Score	LE	MolDock Score	LE	MolDock Score	LE	MolDock Score	LE
1 /335.376	7.21±0.07	-142.45	-5.70	-176.96	-7.08	-176.21	-7.05	-179.97	-7.20
2 /320.362	7.54±0.09	-145.96	-6.08	-181.03	-7.54	-173.23	-7.22	-179.63	-7.48
3 /330.153	8.82± 0.12	-151.53	-7.58	-155.09	-7.75	-152.52	-7.63	-155.03	-7.75
4 /319.255	9.80± 0.10	-162.30	-7.06	-170.20	-7.40	-168.54	-7.33	-168.16	-7.31
5 /434.337	13.78± 0.13	-170.70	-5.33	-217.79	-6.81	-210.66	-6.58	-224.05	-7.00
Resolution		2.00 Å		1.99 Å		1.80 Å		1.60 Å	

Table 2 The results obtained from in vitro and in silico studies against xanthine oxidase.

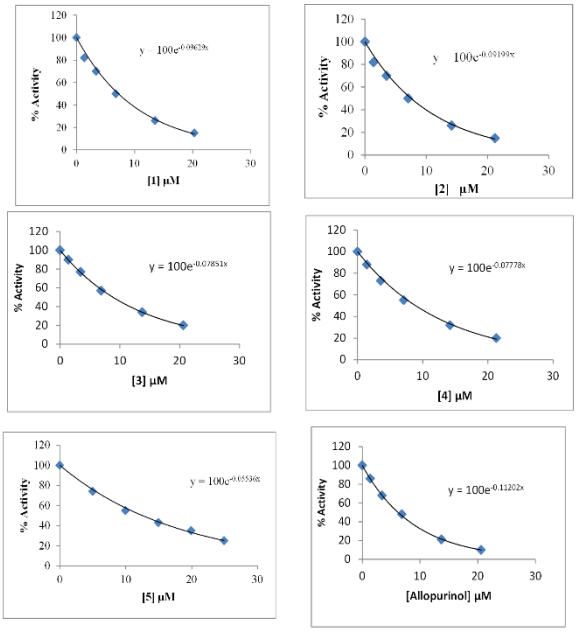

Figure 1 Inhibition rate graphs of chalcones on xanthine oxidase activity *in vitro*.

In order to further analyse the conformation and orientation between compounds, and xanthine oxidase, molecular docking was performed using MolegroVirtual Docker software. First, to evaluate the binding patterns of some substrates and inhibitors to the active site of the enzyme, interactions in their crystal structures were visualized with the Discovery Studio 2021 Client program (Figure 2). Then, the co-crystalline ligands were placed in the centers of the grids, and docking was performed against the active region. As seen in Table 2, the results of the others are similar, except for the crystal structure to which the quercetin ligand is attached. Docking results with the crystal structure 3NVW with the best resolution were selected for detailed interaction analysis. Figure 3 shows the docking site, the conformations of active site amino acids and ligands, and the overlap of ligands. The tested compounds displayed similar binding diagrams due to the parallel orientations of the ligands. The docking score of compounds **1**, **2**, **3**, **4**, and **5** are -176.21, -173.23, -152.52, -168.54 and -210.66 MolDock Score. When the *in vitro* and in silico results are evaluated together, there is a difference between the experimental results of compound **5** and the in silico results. It may be normal for it to have a higher MolDock Score because it has a higher molecular weight and contains more functional groups. However, another factor in evaluating the docking results is the Ligand Efficiency value obtained by the ratio of the docking score to the number of heavy atoms in the molecule. When the results are evaluated according to this value, it is seen that the in silico results generally support the in vitro results.

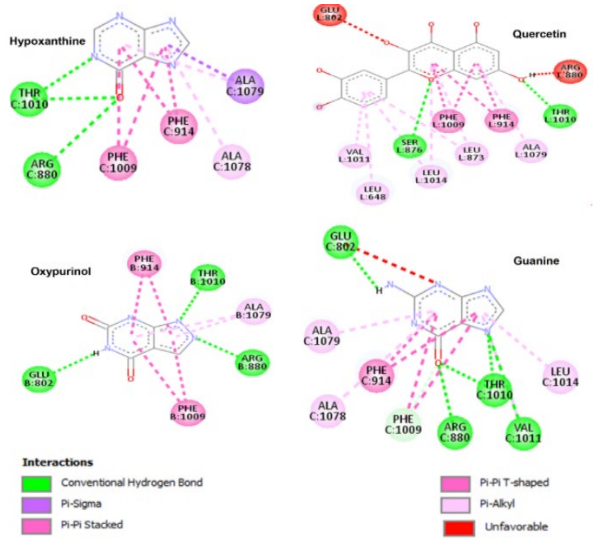

Figure 2. Dimensional view of the interaction diagrams of reference ligands with xanthine oxidase.

DOI: http://dx.doi.org/10.32571/ijct.1199221 E-ISSN: 2602-277X

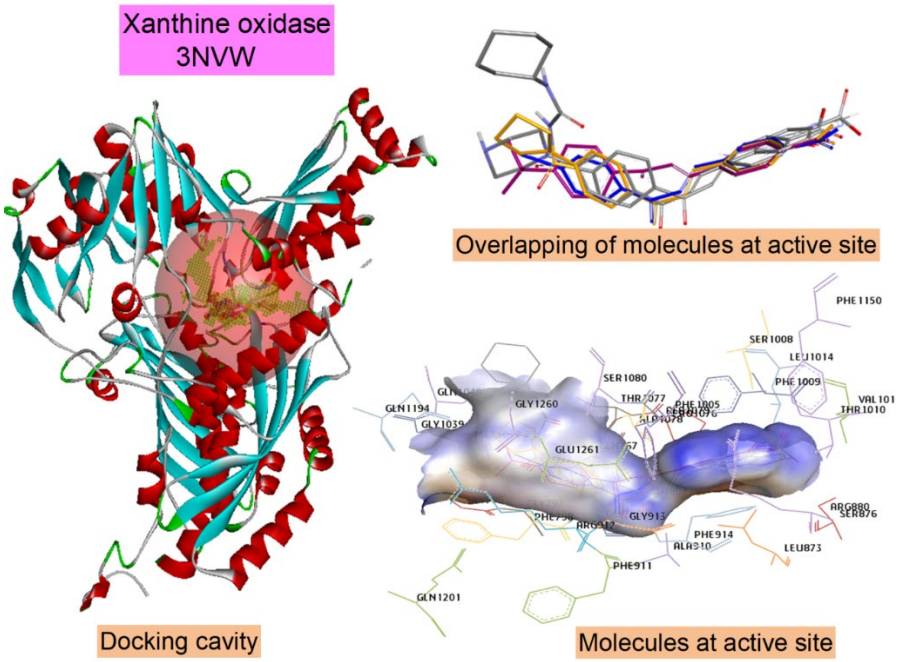

Figure 3 The cavity (active site) of xanthine oxidase, ligands with amino acid residues at the active site, and overlapping of chalcones.

It is observed that compound **1** formed hydrogen bonding with THR1010 amino acid. GLY799 formed a carbon-hydrogen bond with the O of propenal on the chalcone. On the other hand, the sulfur atom present in Methionine1038 residue interacted with the A ring of chalcone to form a Pi-Sulfur interaction. MET1038, ALA 1078, and ARG912 residues performed Alkyl interactions with cyclic structures on the Pi-fur molecule (Figure 4).

The oxygen of carboxylic acid moiety in the B ring of ligand **2** could form three hydrogen bonds with the backbone donor hydrogen bond of Thr1010, the side chain donor hydrogen bond of Arg880 and the side chain donor hydrogen bond of Thr1010. This compound formed the hydrophobic interactions with ALA1079, ALA1078, PHE914, ARG912 and MET1038 via piperazine and benzene groups (Figure 5).

The compound **3** established interactions with residues MET1038, ARG912, GLY799 PHE914, ARG880, THR1010, ALA1079, ALA1078, and PHE914. The carboxyl substituent of the B ring formed hydrogen bonds with ARG880 and THR1010. Benzene groups of compound Br-Far showed hydrophobic interactions with

ARG912, PHE914, ALA1079, and ALA1078. Also, a Pi-Sulfur interaction between MET1038 and A ring was observed. Brome moiety established an alkyl interaction with MET1038.

As seen in Figure, ARG880, THR1010 and GLU802 residues play a vital role in the binding of the substrate and inhibitors to the active pocket of the XO enzyme. The carboxyl group attached to the B benzene ring of the molecules makes strong hydrogen bonds with ARG880 and THR1010 in the enzyme's active site. Also, modifications to other parts of the molecule did not strongly affect the inhibitory potential of the molecule towards the enzyme. The inhibition effect of hydroxylated chalcones against the enzyme was tested previously. The article reported that molecules without the -OH group on the B ring did not affect the enzyme activity. The -OH groups in various positions on the B ring enhanced the inhibition effect of the molecules against the enzyme.[22] Similar results are seen in the results of another study. Also, the addition of -OCH-substituted groups on the B ring reduced or eliminated the effect of the molecules on the enzyme activity.[23-25]

The previously reported studies and the data obtained in this study may be said to be one of the main fragments of the B ring in the inhibition of the XO enzyme by chalcone-type molecules. In addition, heterocyclic structures participate in Pi-Pi Stached and Pi-Pi T-Tshaped hydroboical interactions. PHE914 and PHE1009 are the most important amino acid residues contributing to such interactions. Similar to the substrate and inhibitors, PHE1009, ALA1079, and PHE914 were evaluated to be the vital residues in the molecular interaction between chalcones and xanthine oxidase.

DOI: http://dx.doi.org/10.32571/ijct.1199221 E-ISSN: 2602-277X

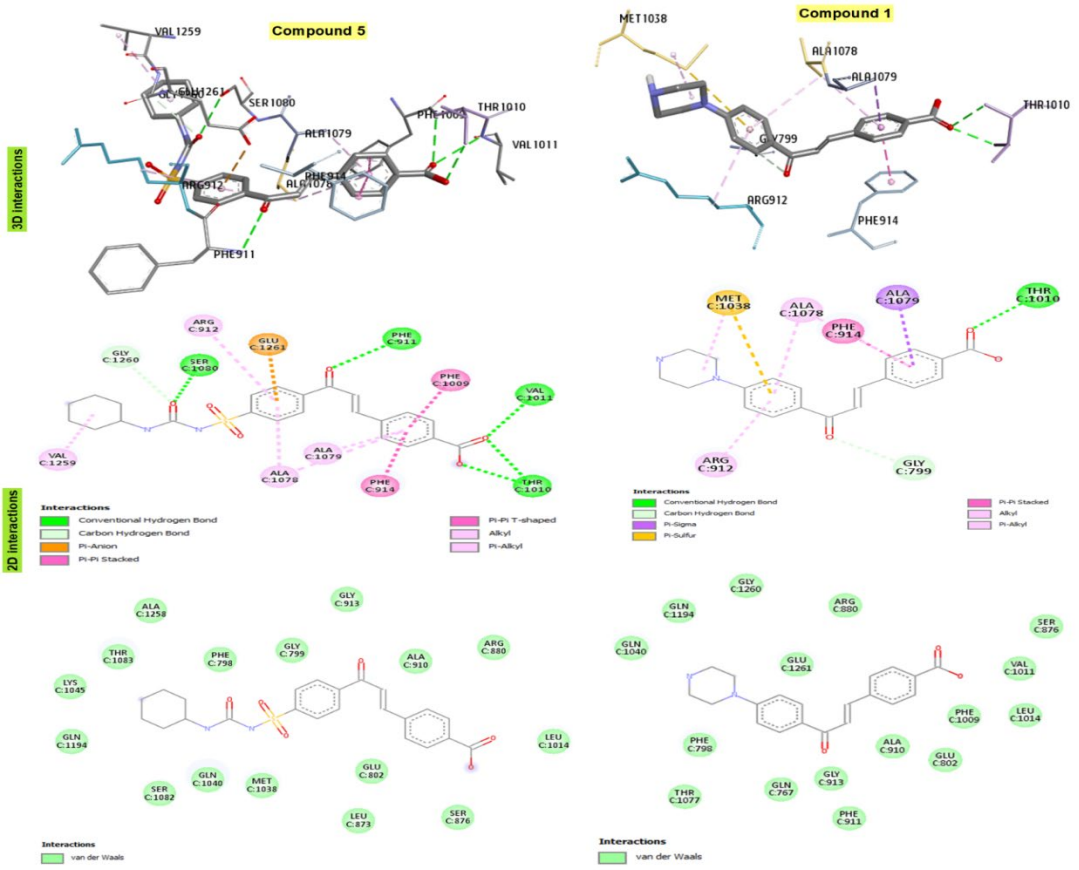

Figure 4 Three and two-dimensional view of the interaction diagram of chalcones with xanthine oxidase.

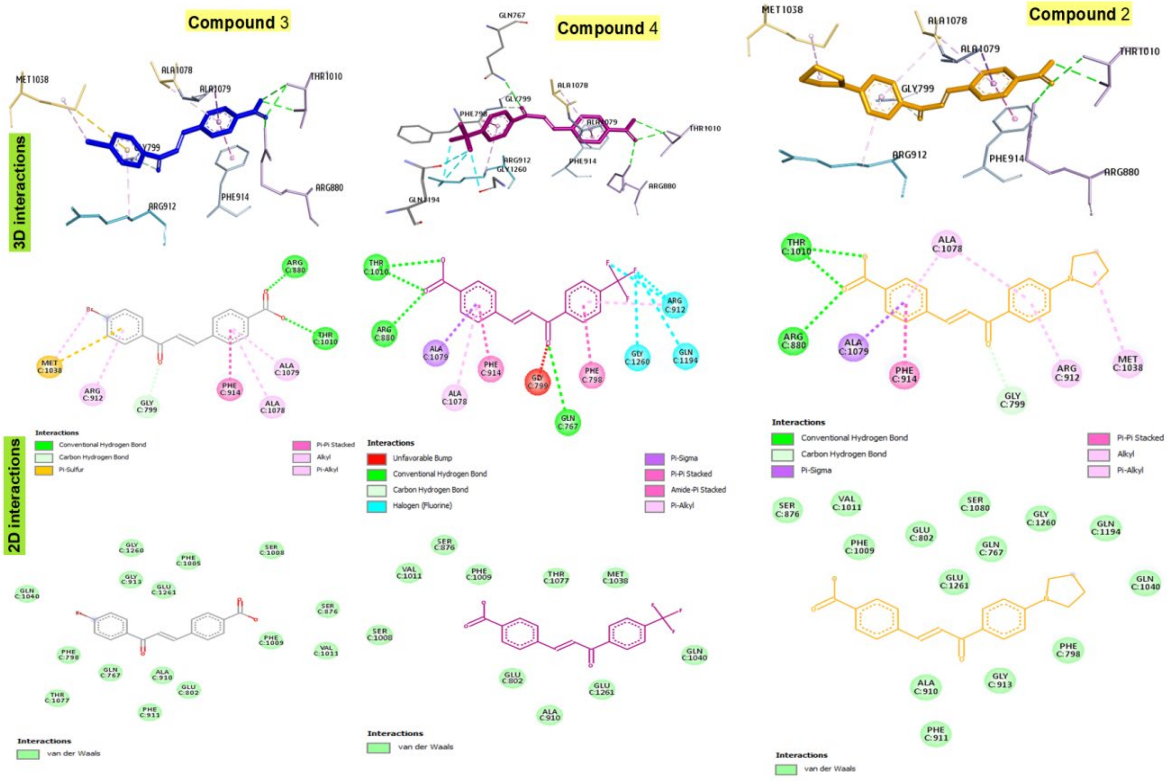

Figure 5 Three and two-dimensional view of the interaction diagrams of chalcones with xanthine oxidase.

DOI: http://dx.doi.org/10.32571/ijct.1199221 E-ISSN: 2602-277X

4. CONCLUSIONS

Some chalcone evaluated their xanthine oxidase inhibitor activity. Compounds 1 and 2 had the greatest effect with 7.21±0.07 and 7.54±0.09 µM IC50 values, respectively.

Conflict of interests

I declares that there is no a conflict of interest with any person, institute, company, etc.

REFERENCES

1. Burmaoglu, S.; Ozcan, S.; Balcioglu, S.; Gencel, M.; Noma, S. A. A.; Essiz, S.; Ateş, B.; Algul, O. Bioorg. Chem. **2019**, 91, 103149.

2. Nerya, O.; Musa, R.; Khatib, S.; Tamir, S.; & Vaya, J. Phytochemistry, **2004**, 65(10), 1389- 1395.

3. Miranda, C. L.; Aponso, G. L. M.; Stevens, J. F.; Deinzer, M. L.; Buhler, D. R. Cancer Lett. **2000**, 149(1-2), 21-29.

4. Chaves, O. A.; Barros, L. S.; Oliveira, M. C.; Sant'Anna, C. M. R.; Ferreira, A. B.; Silva, F. A.; Sobrinho, D.C.; Netto-Ferreira, J. C. J. Fluor. Chem. **2017**, 199, 30-38.

5. Najafian, M.; Ebrahim-Habibi, A.; Hezareh, N.; Yaghmaei, P.; Parivar, K.; Larijani, B. Mol. Biol. Rep. **2011**, 38(3), 1617-1620.

6. Chimenti, F.; Fioravanti, R.; Bolasco, A.; Chimenti, P.; Secci, D.; Rossi, F.; Yanez, M.; Orallo, F.; Ortuso, F.; Alcaro, S. J. Med. Chem. **2009**, 52(9), 2818-2824.

7. Aktar, B. S. K.; Oruç-Emre, E. E.; Demirtaş, İ.; Yağlıoğlu, A. Ş.; İyidoğan, A. K.; Güler, Ç.; Adem, Ş. Turk. J. Chem. **2018**, 42(2), 482-492.

8. Lee, S.H.; Seo, G.S.; Kim, H.S.; Woo, S.W.; Ko, G.; Sohn, D.H. Biochem. Pharmacol. **2006**, 72(10), 1322-1333.

9. Kurşun-Aktar, B. S.; Sıcak, Y.; Tok Taşkın, T.; Oruç-Emre, E. E.; Şahin-Yağlıoğlu, A.; Karaküçük-İyidoğan, A.; Öztürk, M.; Demirtaş, İ. J. Mol. Struct. **2020**, 1211, 128059.

10. Mphahlele, M. J.; Zamisa, S. J.; & El-Gogary, T. M. J. Mol. Struct. **2021**, 1245, 131090.

11. Ardan, T.; Kovačeva, J.; Čejková, J. Acta histochemica, **2004**,106(1), 69-75.

12. Aktar, B.S.K.; Sıcak, Y.; Oruç-Emre, E.E. Int. J. Chem. Technol. **2022**,6(1), 7-14.

13. Tao, X. X.; Duan, Y. T.; Chen, L. W.; Tang, D. J.; Yang, M. R.; Wang, P. F.; Xu, C.; Zhu, H. L. Bioorg. Med. Chem Lett. **2016**, 677-683.

14. Wang, Y.; Zhang, S.; Zhang, Y.; Yao, F.; Zhao, G.; Wang, J.; Liu, L.; Yang, Y.; Li, X.; Sun, Y.; Hu, Y.; Bai, Z.; Wang, P.; Li, R.; Xu, X. ACS Food Sci. Technol. **2021**, 1: 2182-91.

15. Thomsen, R.; Christensen, M. H. J. Med. Chem. **2006**, 49(11), 3315-3321.

16. Cao, H.; Hall, J.; Hille, R. Biochemistry. **2014**, 53(3), 533-541.

17. Cao, H.; Pauff, J. M.; Hille, R. J. Biol. Chem. **2010**, 285(36), 28044-28053.

18. Cao, H.; Pauff, J. M.; Hille, R. J. Nat. Prod. **2014**, 77(7), 1693-1699.

19. Borges, F.; Fernandes, E.; Roleira, F. Curr. Med. Chem. **2002**, 9(2), 195-217.

20. Pacher, P.A L.; Nivorozhkin, A.; Szabó, C. Pharmacol. Rev. **2006**, 58(1), 87-114.

21. Kaur, G.; Singh, A.; Arora, G.; Monga, A.; Jassal, A. K.; Uppal, J.; Bendi, P. M. S.; Bora, K. S. Chem. Biol. Drug Des. **2022**, 100(3), 443-468.

22. Hofmann, E.; Webster, J.; Do, T.; Kline, R.; Snider, L., Hauser, Q.; Higginbottom, G.; Campbell, A.; Ma, L.; Paula, S. Bioorg. Med. Chem. **2016**, 24(4), 578-587.

23. Bui, T. H.; Nguyen, N. T.; Dang, P. H.; Nguyen, H. X.; Nguyen, M. T. T. SpringerPlus. **2016**, 5(1), 1-8.

24. Niu, Y.; Zhu, H.; Liu, J.; Fan, H.; Sun, L.; Lu, W.; Liu, X.; Li, L. Chem.-Biol. Interact. **2011**, 189(3), 161-166.

25. Choi, W.; Villegas, V.; Istre, H.; Heppler, B.; Gonzalez, N.; Brusman, N.; Snider, L.; Hogle, E.; Tucker, J.; Oñate, A.; Oñate, S.; Ma, Li.; Paula, S. **2019**, Bioorg.Chem. 86, 686-695.